Eur. Phys. J. Plus (2026) 141:582
https://doi.org/10.1140/epjp/s13360-026-07661-1

THE EUROPEAN
PHYSICAL JOURNAL PLUS

Review

Nuclear physics midterm plan in Italy: detector developments

Paolo Cardarelli[52], **Roberto Catalano**[2], **Manuela Cavallaro**[2], **Stefano Corradetti**[4], **Alessia Di Pietro**[2], **Franco Galtarossa**[22], **Andrea Gottardo**[4], **Marcello Lunardon**[12,22], **Cristian Massimi**[38,39,a], **Rosario Nania**[38], **Gabriele Pasquali**[9,14], **Silvia Pisano**[1,40,b], **Walter Raniero**[4], **Alessandro Scordo**[1], **Leonello Servoli**[11], **Luis Acosta**[2,84], **Marco Agnolin**[20,24], **Clementina Agodi**[2], **Vitor A. P. Aguiar**[70], **Andrei Alexandrov**[13], **Simone Amaducci**[2], **Lucio Anderlini**[9], **Alberto Andrighetto**[4], **Alberto Arzenton**[4], **Luis Humberto Avanzi**[71], **Oscar Azzolini**[4], **Lucia Baldesi**[9,14], **Michele Ballan**[4], **Laura Bandiera**[52], **Sandro Barlini**[9,14], **Giuseppe Battistoni**[3], **Roberto Bedogni**[1], **Nicola Belcari**[58,59], **Luca Bellan**[4], **Marco Bellini**[15], **Giovanna Benzoni**[3], **Anna Bergamaschi**[47], **Davide Bersani**[58], **Stefano Bertoldo**[4,12], **Andreas Best**[13,20], **Manuele Bettelli**[46], **Lisa Biasetto**[75], **Maria Giuseppina Bisogni**[58,59], **Michael Block**[5,66], **Giacomo Borghi**[3,24], **Marcello Borri**[48], **Angela Bracco**[3,17], **Luca Brombal**[64,65], **Mara Bruzzi**[9,14], **Manuel Caamaño**[16], **Alessandro Calamida**[1], **Daniela Calvo**[56], **Alberto Camaiani**[9,14], **Franco Camera**[3,17], **Matteo Campostrini**[4], **Stefano Capra**[3,17], **Francesco Cappuzzello**[2,23], **Diana Carbone**[2], **Giuseppe Cardella**[18], **Marco Carminati**[3,24], **Pietro Carra**[58,59], **Chiara Carraro**[4,12], **Sara Maria Carturan**[4,12], **Giovanni Casini**[9], **Salvo Rita Cavallaro**[2], **Francesca Cavanna**[56], **Lisa Centofante**[4], **Piergiorgio Cerello**[56], **Efraín Chávez Lomelí**[69], **Eliane de Fátima Chinaglia**[71], **Caterina Ciampi**[19], **Esther Ciarrocchi**[58,59], **Mario Ciocca**[62], **Roberto Cirio**[56,57], **Giuseppe A. P. Cirrone**[2], **Sara Cisternino**[4], **Gerardo Claps**[1,45], **Francesco Collamati**[41], **Paolo Colombo**[75], **Michele Comunian**[4], **Lorenzo Corradi**[4], **Michele Costa**[2], **K. M. Costa**[71], **Fabio Celso Luigi Crespi**[3,17], **Gabriele Croci**[3], **Giacomo De Angelis**[4], **Mario De Cesare**[13,73,74], **Lucia De Dominicis**[4,12], **Angelica De Gregorio**[41,43], **Clément Delafosse**[72], **Franck Delaunay**[28], **Giovanni De Lellis**[13,20], **Davide De Salvador**[4,12], **Timo Dickel**[5,67], **Antonia Di Crescenzo**[13,20], **François Didierjean**[55], **Antonino Di Leva**[13,20], **Antonio Di Nitto**[13,20], **Davide Di Vita**[3,24], **Lorenzo Domenichetti**[21], **Yunsheng Dong**[3], **Gilbert Duchêne**[55], **Mourad El Idrissi**[4], **Juan Esposito**[4], **Riccardo Faccini**[6,41], **Alessia Fantini**[29,30], **Veronica Ferrero**[56,57], **Michel Filliger**[55], **Paolo Finocchiaro**[2], **Enrico Fioretto**[4], **Elisa Fiorina**[56], **Carlo Fiorini**[3,24], **Massimiliano Fiorini**[37,52], **Maria Fisichella**[2], **Giorgia Franchin**[75], **Gaia Franciosini**[41,43], **Giuliana Galati**[42,82], **Elisa Maria Gandolfo**[13,20], **Fabio Gargano**[82], **Elena Geraci**[18,23], **Andrea Giachero**[49,50], **Simona Giordanengo**[56], **Mauro Giovannini**[68,76], **Piero Giubilato**[12,22], **Alain Goasduff**[4], **Giovanni Luca Guardo**[2], **Mariacristina Guarrera**[2], **Marcilei Aparecida Guazzelli**[71], **Chiara Guazzoni**[3,24], **Arcadio Huerta Hernández**[69], **Herbert Hess**[53], **Calem Hoffman**[7], **Gianluca Imbriani**[13,20], **Keida Kanxheri**[11,25], **Benjamin Kay**[7], **Giorgio Keppel**[4], **Alisa Kotliarenko**[4,37], **Aafke Kraan**[58], **Alma Kurmanova**[2], **Marco La Cognata**[2], **Stefano Lagomarsino**[9], **Livio Lamia**[2,23,26], **Gaetano Lanzalone**[2,27], **Dario Lattuada**[2,27], **Adele Lauria** [13,20], **Nicolas Le Neindre**[28], **Silvia Leoni**[3,17], **Giordano Lilli**[4], **Ivano Lombardo**[18,23], **Massimo Loriggiola**[4], **Lorenzo Loriggiola**[4], **Gianluigi Maggioni**[4,12], **Concettina Maiolino**[2], **Carlo Mancini-Terracciano**[6,41], **Alberto Manfreda**[13], **Alice Manna**[38,39], **Mattia Manzolaro**[4], **Michela Marafini**[40,43], **Tommaso Marchi**[4], **Naomi Marchini**[9], **Daniel José Marín Lámbarri**[69], **Ismael Martel**[8], **Guido Martín Hernández**[44], **Petra Martini**[52,83], **Nunzia Simona Martorana**[18], **David Mascali**[2], **Antonio Massara**[2], **Pierfrancesco Mastinu**[4], **Francesca Mastrotto**[78], **Sueli Hatsumi Masunaga**[71], **Adrien Matta**[28], **Ilaria Mattei**[3], **Mario Nicola Mazziotta**[82], **Enrico Mazzoni**[58], **Nilberto Heder Medina**[70], **Mauro Menichelli**[11], **Marco Miliucci**[1,51], **Benedicte Millon**[3], **Riccardo Mirabelli**[6,41], **Martina Moglioni**[58,59], **Vincenzo Monaco**[56,57], **Alberto Monetti**[4], **Giovanna Montagnoli**[12,22], **Maria Cristina Montesi**[13,81], **Sandra Moretto**[12,22], **Silvio Morganti**[41], **Cristina Morone**[29,30], **Matteo Morrocchi**[58,59], **Luca Morselli**[4], **Liliana Mou**[4], **Mohamad Moukaddam**[26], **Annamaria Muio**[2], **Silvia Muraro**[3], **Elizabeth Musacchio-Gonzalez**[4], **Adriana Nannini**[9], **Daniel R. Napoli**[4], **Enrico Napolitani**[12], **Eugenia Naselli**[2], **Jose Roberto Brandão Oliveira**[70], **Pietro Ottanelli**[9], **Emanuele Vincenzo Pagano**[2], **Lucio Pancheri**[34], **Julien Pancin**[19], **Luciano Pandola**[2], **Giovanni Passaleva**[9], **Santi Passarello**[2], **Vincenzo Patera**[41,43], **Francesco Pennazio**[56], **Giancarlo Pepponi**[31], **Giada Petringa**[2], **Silvia Piantelli**[9], **Federico Pinna**[56], **Felix Pino**[12], **Rosario Gianluca Pizzone** [2,23], **Gaetano Elio Poma**[4], **Michela Prest**[50,54], **Gianfranco Prete**[4], **Nicoletta Protti**[60,61], **Chiara Provenzano**[32,33], **Alberto Pullia**[3,17], **Marco Pullia**[62], **Salvatore Pulvirenti**[2], **Gaia Pupillo**[4], **Alberto Quaranta**[34,35], **Luciano Ramello**[56,63], **David Rapagnani**[13,20], **Nicola Realdon**[78], **Alessandra Retico**[58], **Riccardo Ridolfi**[38,39], **Valentino Rigato**[4], **Fabio Risitano**[18,36], **Francesca Rizzo**[2,23], **Marco Rocchini**[9], **Stefano Romano**[2,23], **Davide Rosso**[4], **Valeria Rosso**[58,59], **Antonio Domenico Russo**[2], **Luigi Russo**[1], **Paolo Russotto**[2], **Roberto Sacchi**[56,57], **Alessandro Saltarelli**[10,11], **T. M. Santarelli**[71], **Domenico Santonocito**[2], **Roberto Baginski Batista Santos**[71], **Alessio Sarti**[41,43], **Daniele Scarpa**[4], **Christoph Scheidenberger**[5], **Gabriele Sciacca**[4], **Silvio Sciortino**[9,14], **Diletta Sciti**[79], **Adalberto Sciubba**[41,43], **Giacomo Secci**[3,17], **Matúš Sedlák**[4], **Francesca Servadei**[79], **Francesco Sgarbossa**[4,12], **Marie-Hélène Sigward**[55], **Luca Silvestrin**[12], **Laura Silvestroni**[79], **Elena Solfaroli Camillocci**[85], **Alessandro Spatafora**[2], **Roberto Spighi**[38], **Eleuterio Spiriti**[1], **Giancarlo Sportelli**[58,59], **Alberto Stefanini**[4], **Antonella Tamburrino**[1,40], **Marianna Testa**[1], **Giacomo Ticchi**[3,24], **Gemma Tinti**[1], **Valery Tioukov**[13], **Davide Tomasella**[12], **Francesco Tommasino**[35], **Domenico Torresi**[2], **Marco Toppi**[41,43], **Giacomo Traini**[41], **Antonio Trigilio**[41,43], **Salvatore Tudisco**[2], **Aurora Tumino**[2,27], **Giacomo Ubaldi**[38,39],

Martina Ursino[2], **Simone Valdrè**[9], **Hesiquio Vargas Hernández**[69], **José Javier Valiente Dobón**[4], **Emanuele Vardaci**[13,20], **Elisa Vettorato**[4,78], **Anna Vignati**[56,57], **Mauro Villa**[38,39], **Roberto Gleason Villagrán**[69], **Ilenia Viola**[77], **Oliver Wieland**[3], **Jeffery Wyss**[80], **Alice Zanini**[75], **Irene Zanon**[4], **Roberto Zarrella**[38,39], **Luca Zoli**[79]

[1] Laboratori Nazionali di Frascati, Istituto Nazionale di Fisica Nucleare, Via E. Fermi 54, 00044 Frascati, Italy
[2] Laboratori Nazionali del Sud, Istituto Nazionale di Fisica Nucleare, Via S. Sofia 62, 95123 Catania, Italy
[3] Sezione di Milano, Istituto Nazionale di Fisica Nucleare, Via G. Celoria 16, 20133 Milano, Italy
[4] Laboratori Nazionali di Legnaro, Istituto Nazionale di Fisica Nucleare, Viale dell'Università 2, 35020 Legnaro, Italy
[5] GSI Helmholtzzentrum für Schwerionenforschung GmbH, Planckstr. 1, 64291 Darmstadt, Germany
[6] Dipartimento di Fisica, "Sapienza" - Università di Roma, Piazzale Aldo Moro 5, 00185 Roma, Italy
[7] Argonne National Lab., S. Cass Avenue, Lemont, IL 60439, USA
[8] Departamento de Física Aplicada, Universidad de Huelva, Avenida de las Fuerzas Armadas, 21071 Huelva, Spain
[9] Sezione di Firenze, Istituto Nazionale di Fisica Nucleare, Via Sansone 1, 50019 Sesto Fiorentino, Italy
[10] Dipartimento di Fisica, Università di Camerino, Via Madonna delle Carceri, 9B, 62032 Camerino, MC, Italy
[11] Sezione di Perugia, Istituto Nazionale di Fisica Nucleare, Via A. Pascoli, 06123 Perugia, Italy
[12] Dipartimento di Fisica e Astronomia "Galileo Galilei", Università di Padova, Via Marzolo, 9B, 35131 Padova, Italy
[13] Istituto Nazionale di Fisica Nucleare, Sezione di Napoli, Napoli, Italy
[14] Dipartimento di Fisica e Astronomia, Università di Firenze, 50019 Sesto Fiorentino, Italy
[15] Istituto Nazionale di Ottica, Consiglio Nazionale delle Ricerche, 50019 Sesto Fiorentino, Italy
[16] IGFAE, Universidade de Santiago de Compostela, 15706 Santiago de Compostela, Spain
[17] Dipartimento di Fisica, Università degli Studi di Milano, Via Celoria 16, 20133 Milano, Italy
[18] Sezione di Catania, Istituto Nazionale di Fisica Nucleare, Via S. Sofia 64, 95123 Catania, Italy
[19] GANIL, CNRS/IN2P3, CEA/DRF, bd Henri Becquerel, 14076 Caen, France
[20] Dipartimento di Fisica "Ettore Pancini", Università di Napoli "Federico II", Via Cintia, 80126 Napoli, Italy
[21] Institut Laue-Langevin, Avenue des Martyrs, 71, 38042 Grenoble, France
[22] Sezione di Padova, Istituto Nazionale di Fisica Nucleare, Via Marzolo, 8, Padova, Italy
[23] Dipartimento di Fisica e Astronomia "Ettore Majorana", Università degli Studi di Catania, Via S. Sofia 64, 95123 Catania, Italy
[24] Dipartimento di Elettronica, Informazione e Bioingegneria, Politecnico di Milano, Piazza L. Da Vinci 32, 20133 Milano, Italy
[25] Dipartimento di Fisica e Geologia, Università di Perugia, 06123 Perugia, Italy
[26] Centro Siciliano di Fisica Nucleare e Struttura della Materia, Via S. Sofia 64, 95123 Catania, Italy
[27] Università di Enna "Kore", Piazza dell'Università, 94100 Enna, Italy
[28] ENSICAEN, UNICAEN, CNRS/IN2P3, LPC Caen, Normandie Université, 14000 Caen, France
[29] Dipartimento di Fisica, Università di Roma Tor Vergata, Via della Ricerca Scientifica, 1, 00133 Roma, Italy
[30] Sezione di Tor Vergata, Istituto Nazionale di Fisica Nucleare, Via della Ricerca Scientifica, 1, 00133 Roma, Italy
[31] Center for Sensors and Devices, Fondazione Bruno Kessler, Via Sommarive, 18, 38123 Povo, TN, Italy
[32] Sezione di Lecce, Istituto Nazionale di Fisica Nucleare, Via Provinciale per Arnesano, 73100 Lecce, Italy
[33] Dipartimento di Ingegneria dell'Innovazione, Università del Salento, Via per Monteroni, 73100 Lecce, Italy
[34] Dipartimento di Ingegneria Industriale, Università di Trento, Via Sommarive, 9, 38123 Povo, TN, Italy
[35] Trento Institute of Fundamental Physics and Applications, Istituto Nazionale di Fisica Nucleare, Via Sommarive, 14, 38123 Povo, TN, Italy
[36] Dipartimento di Scienze Matematiche e Informatiche, Scienze Fisiche e Scienze della Terra, Università di Messina, Viale Ferdinando Stagno d'Alcontres, 31, 98166 Messina, Italy
[37] Department of Physics and Earth Science, University of Ferrara, Via Saragat 1, 44122 Ferrara, Italy
[38] Sezione di Bologna, Istituto Nazionale di Fisica Nucleare, Viale C. Berti Pichat 6/2, 40127 Bologna, Italy
[39] Dipartimento di Fisica e Astronomia, Università di Bologna, Viale Berti Pichat 6/2, 40127 Bologna, Italy
[40] Museo Storico della Fisica e Centro Studi e Ricerche "E. Fermi", Via Panisperna 89/A, 00184 Roma, Italy
[41] Sezione di Roma, Istituto Nazionale di Fisica Nucleare, Piazzale Aldo Moro 5, 00185 Roma, Italy
[42] Dipartimento di Fisica, Università di Bari, Via Giovanni Amendola, 70125 Bari, Italy
[43] Department of Basic and Applied Sciences for Engineering (SBAI), Sapienza University of Rome, Via Antonio Scarpa 14, 00161 Rome, Italy
[44] Centro de Aplicaciones Tecnológicas y Desarrollo Nuclear, 502 Calle 30, La Habana, Cuba
[45] Fusion and Nuclear Safety Department, C. R. Frascati, Energia Nucleare Energie Alternative (ENEA), Via Enrico Fermi 45, 00044 Roma, Italy
[46] Istituto Materiali per l'Elettronica e il Magnetismo, Consiglio Nazionale delle Ricerche, Parco Area delle Scienze 37/A, 43124 Parma, Italy
[47] Paul Scherrer Institut, Forschungsstrasse 111, 5232 Villigen, Switzerland
[48] Daresbury Laboratory, Science and Technology Facilities Council (STFC), Keckwick Lane, Daresbury WA4 4AD, UK
[49] Dipartimento di Fisica, Università di Milano-Bicocca, Piazza delle Scienza 3, 20126 Milano, Italy
[50] Sezione di Milano Bicocca, Istituto Nazionale di Fisica Nucleare, Piazza delle Scienza 3, 20126 Milano, Italy
[51] Italian Space Agency, Via del Politecnico snc, 00133 Rome, Italy
[52] Sezione di Ferrara, Istituto Nazionale di Fisica Nucleare, Via Saragat 1, 44122 Ferrara, Italy
[53] Institut für Kernphysik, University of Cologne, Zülpicher Str. 77, 50937 Köln, Germany
[54] Dipartimento di Fisica, Università degli Studi dell'Insubria, Via Valleggio 11, 22100 Como, Italy
[55] IPHC, CNRS/IN2P3, Université de Strasbourg, Rue du Loess 23, 67037 Strasbourg - Cedex 2, France
[56] Sezione di Torino, Istituto Nazionale di Fisica Nucleare, Via P. Giuria 1, 10125 Torino, Italy
[57] Dipartimento di Fisica, Università di Torino, Via P. Giuria 1, 10125 Torino, Italy
[58] Sezione di Pisa, Istituto Nazionale di Fisica Nucleare, Largo B. Pontecorvo 3, 56127 Pisa, Italy
[59] Dipartimento di Fisica, Università di Pisa, Largo B. Pontecorvo 3, 56127 Pisa, Italy
[60] Dipartimento di Fisica, Università di Pavia, Via A. Bassi 6, 27100 Pavia, Italy
[61] Sezione di Pavia, Istituto Nazionale di Fisica Nucleare, Via A. Bassi 6, Pavia, PV, Italy
[62] Centro Nazionale di Adroterapia Oncologica, Strada Campeggi, 27100 Pavia, Italy
[63] Dipartimento per lo Sviluppo Sostenibile e la Transizione Ecologica, University of Piemonte Orientale, Piazza S.Eusebio, 5, 13100 Vercelli, Italy
[64] Sezione di Trieste, Istituto Nazionale di Fisica Nucleare, Via A. Valerio 2, 34127 Trieste, Italy
[65] Dipartimento di Fisica, Università degli Studi di Trieste, Via A. Valerio 2, 34127 Trieste, Italy

[66] Department of Chemistry, Helmholtz Institute Mainz, University of Mainz, 55099 Mainz, Germany
[67] Physikalisches Institut, Justus-Liebig-Universität Gießen, 35392 Gießen, Germany
[68] Dipartimento di Chimica e Chimica Industriale, Università di Genova, Via Dodecaneso, 31, 16146 Genova, Italy
[69] Instituto de Física, Universidad Nacional Autónoma de México, Apartado Postal 20-364, 04510 Ciudad de México, México
[70] Instituto de Física, Universidade de São Paulo, Rua do Matão 1371, São Paulo 05508-090, Brasil
[71] São Bernardo do Campo, Centro Universitário da FEI, Av. Humberto de Alencar Castelo Branco 3972-B - Assunção, São Bernardo do Campo, SP 09850-901, Brasil
[72] CNRS/IN2P3, IJCLab, Université Paris-Saclay, 15 rue Georges Clémenceau, 91405 Orsay, France
[73] Dipartimento di Metodologie e Tecnologie per le Osservazioni e Misure, Centro Italiano Ricerche Aerospaziali, Via Maiorise, 81043 Capua, Italy
[74] Dipartimento di Matematica e Fisica, Università degli Studi della Campania, Viale Lincoln 5, 81100 Caserta, Italy
[75] Dipartimento di Ingegneria Industriale, Università degli Studi di Padova, Via Marzolo 9, 35131 Padova, Italy
[76] Sezione di Genova, Istituto Nazionale di Fisica Nucleare, Via Dodecaneso 33, 16146 Genova, Italy
[77] Istitute of Nanotechnology, Soft and Living Matter Laboratory, Consiglio Nazionale delle Ricerche, Sapienza University, P. le A. Moro 54, 00185 Rome, Italy
[78] Dipartimento di Scienze del Farmaco, Università degli Studi di Padova, Via Marzolo 5, 35131 Padova, Italy
[79] Istituto di Scienza, Tecnologia e Sostenibilità per lo Sviluppo dei Materiali Ceramici, Consiglio Nazionale delle Ricerche, Via Granarolo 64, 48018 Faenza, Italy
[80] Dipartimento di Ingegneria civile e meccanica, Università degli Studi di Cassino e del Lazio Meridionale, Via Gaetano di Biasio 43, 03043 Cassino, Italy
[81] Dipartimento di Scienze Chimiche, Università di Napoli “Federico II”, Via Cintia, 80126 Napoli, Italy
[82] Sezione di Bari, Istituto Nazionale di Fisica Nucleare, Via E. Orabona 4, 70125 Bari, Italy
[83] Dipartimento di Scienze dell’Ambiente e della Prevenzione, Università di Ferrara, Via L. Borsari, 46, 44121 Ferrara, Italia
[84] Instituto de Estructura de la Materia, Consejo Superior de Investigaciones Científicas, C/Serrano, 113 bis, 119, 121 y 123, 28006 Madrid, España
[85] Centro Nazionale per la Protezione dalle Radiazioni e Fisica Computazionale, Istituto Superiore di Sanità, Viale Regina Elena, 299, 00161 Roma, Italy

Received: 8 January 2026 / Accepted: 7 April 2026

Abstract The INFN Laboratori Nazionali di Frascati was established in 1954 to host an electro-synchrotron, the first particle accelerator built in Italy, and since then played a crucial role in the field of nuclear and particle physics and for the development of acceleration and detection technologies. Within this historical tradition, a workshop was organized at LNF in the framework of the Nuclear Physics Mid Term Plan Italy, an initiative of the Nuclear Physics Division of the Istituto Nazionale di Fisica Nucleare, to discuss the detection techniques employed in nuclear physics and to identify the open issues to be addressed to realize the scientific programs of the experiments foreseen in a midterm perspective. The present report summarizes the outcome of the discussions.

Abbreviations

ASIC	Application Specific Integrated Circuit
AGATA	Advanced GAmma Tracking Array
AGC	Automatic Gain Control
CCD	Charge Coupled Device
CMOS	Complementary Metal–Oxide Semiconductor
CSP	Charge Sensitive Preamplifiers
CT	Computed Tomography
DAFNE	Double Annular Factory for Nice Experiments
DAQ	Data acquisition
ECR	Electron Cyclotron Resonance
ENC	Equivalent Noise Charge
ESRF	European Synchrotron Radiation Facility
e-XTP	Enhanced X-ray Timing and Polarimetry
FBK	Fondazione Bruno Kessler
FPT	Flexible Plasma Trap
FWHM	Full Width Half Maximum
GPD	Gas Pixel Detector
HAPG	Highly Annealed Pyrolytic Graphite
HDR	High Dynamic Range
HPGe	High-Purity Germanium

---

[a] e-mail: Cristian.Massimi@bo.infn.it (corresponding author)

[b] e-mail: silvia.pisano@lnf.infn.it (corresponding author)

HPLF	High Power Laser Facility
iLGAD	Inverted Low Gain Avalanche Detector
IXPE	Imaging X-ray Polarimetry Explorer
INFN	Istituto Nazionale di Fisica Nucleare
IPHC	Institut Pluridisciplinaire Hubert Curien
LNF	Laboratori Nazionali di Frascati
LNL	Laboratori Nazionali di Legnaro
LNS	Laboratori Nazionali del Sud
MITIQO	Monitoraggio In situ di Tossicità, Indicazione geografica e Qualità di Olio d'oliva e vino
MLD	Monolayer Doping
N3G	Next Generation Germanium Gamma Detectors
OREO	Oriented Calorimeter project
PANDORA	Plasma for Astrophysics, Nuclear Decay Observation and Radiation for Archaeometry
PMT	Photomultipliers tubes
PLS	Pulsed Laser Melting
PSI	Paul Scherrer Institut
R[NONSPACE	&D] Research and Development
RN agents	Radiological and Nuclear agents
SIDDHARTA-2	Silicon Drift Detectors for Hadronic Atom Research by Timing Application
SIPMs	Silicon Photomultipliers
SNR	Signal-to-Noise Ratio
SPAD	Single-Photon Avalanche Diode
SPECT	Single-Photon Emission Computed Tomography
SPhC	Single-Photon Counted
SQUID	Superconducting Quantum Interference Device
STFC	Science and Technology Facilities Council
TASTE	Transportable and Agile Spectrometer for metal Trace in Edible liquids
TES	Transition Edge Sensors
TID	Total Ionizing Dose
UKRI	UK Research and Innovation
UNIPD	Università degli Studi di Padova
VOXES	High resolution VOn hamos X-ray spectrometer using HAPG for Extended Sources
X-FEL	X-ray Free Electron Laser
XRF	X-ray Fluorescence

1 Executive summary

Nuclear physics has been progressing in the last decades thanks to the introduction of new theoretical tools better describing the nuclear and elementary degrees of freedom playing a role in the macroscopic properties of hadrons and nuclei, and to the strong developments of new experimental techniques. The search for processes more and more rare boosted considerable efforts in the preparation of new beam types (for example, the radioactive ions beams, RIBs), new targets more adequate to the increased luminosity and new ways to measure the characteristics and kinematic quantities of particles and nuclei involved in the collisions.

The Third Scientific Commission of INFN deals with the experiments devoted to nuclear studies, both in national and international facilities (see webpage https://web.infn.it/csn3/index.php/it/). The energy characterizing the collisions spans from the meV to the TeV of the LHC at CERN, with very different experimental approaches. This demands continuous developments of new and improved detection techniques able to reveal particles and radiation over a wide energy interval and exploiting different energy loss or light production mechanisms.

A report on the midterm perspective for nuclear physics in Italian laboratories, i.e., covering a time span from five to ten years, cannot then proceed without considering the perspective on detector developments that will play a crucial role in the realization and design of the experiments during the next years. It will be focused on the low-to-medium energy domain that is the one characterizing the main activities that will be carried out in Italian laboratories. Detector developments for the realization of physics program devoted to ultra-relativistic heavy-ion collisions will not be covered.

The present paper is part of the series "Nuclear Physics Mid Term Plan in Italy" and complements the works dedicated to the activities at the Italian Laboratori Nazionali di Legnaro [1], Laboratori Nazionali del Sud [2], Laboratori Nazionali del Gran Sasso [3] and Laboratori Nazionali di Frascati [4] that described the scientific program foreseen in the next years at the Italian laboratories of the Italian "Istituto Nazionale di Fisica Nucleare" (INFN). The goal and the structure of this series have been already discussed in the introductory paper [5]. The LNF session of the workshop comprised six working groups, focused, respectively, to the charged particle detectors, the neutron detectors, the γ and X-rays detectors, the detectors for medical application, the target development for nuclear physics and future facilities at the INFN Laboratori Nazionali di Legnaro and Laboratori Nazionali del Sud. The initiative bringing to the present publication follows the previous INFN Nuclear Physics Division joint works on nuclear astrophysics [6] and on particle identification techniques [7].

1.1 Charged particle detectors

Charged particle detectors have a widespread use in nuclear physics experiments and applications. In nuclear reaction studies, the detection and identification of the outgoing nuclear fragments and of the heavy remnants of the colliding nuclei is mandatory for a meaningful comparison with the predictions of the different theoretical models. Moreover, charged particle detectors find application as beam diagnostics and dosimeters, e.g., in radiotherapy with charge particle beams. The wide range of possible applications requires a large variety of different detector technologies, to adapt to specific requirements as diverse as large geometric efficiency, large radiation hardness, fast response, etc.

When the beam intensity is relatively weak, an extended acceptance (needed to cope with the low reaction rate) can be reached by using the same material both as a target and as a detector. This is the basic principle of the so-called active targets (ATs). ATs are mostly gas-based detectors where the nuclear reaction under study takes place between the beam particles and the nuclei of the gas itself. Each charged reaction product produces an ionization track in the gas. A superimposed electric field makes the electrons drift toward a segmented xy-plane anode so that a projection of each track on the xy-plane is obtained, including the information about the ionization density along the track. The third coordinate of each track segment is obtained from the time needed by the electrons, drifting at a constant velocity, to reach the anode. From the ionization density profile, it is possible both to identify the emitted fragments and to estimate their kinetic energy (see Sect. 3.1 for more details).

ATs are relatively slow devices, not well suited for large beam intensities, which instead call for fast-response and radiation-hard detectors. In that respect, semiconductor detectors based on silicon carbide (SiC) promise better performance, even better than legacy silicon detectors. SiC can be used to produce both p-n junction and Schottky diodes. Compared to silicon, its larger bandgap and larger energy threshold for the production of lattice defects make SiC more suited for use at large fluence such as in experiments with high-intensity beams, in-plasma studies or as beam diagnostics (see Sect. 3.2 for details).

In view of using SiC detectors in nuclear physics experiments, the extension to SiC of the fragment identification techniques already successfully applied to silicon detectors is also underway. One of these techniques is pulse shape discrimination (PSD), based on the time evolution of the current induced in the detector by the collected electron–hole pairs. PSD studies in SiC have still to reach their maturity, though promising results have already been obtained (see Sects. 3.2.4 and 3.3). Monolithic multi-detector structures can also be obtained on a single SiC crystal, allowing for the realization of compact detector “telescopes,” exploiting the well-known ΔE-E technique to identify the impinging fragments (see Sect. 3.2.3). Both PSD and the ΔE-E technique have a lower threshold in energy for identification. Moreover, mass (i.e., isotopic) identification is only achievable up to a given atomic number (in silicon, $Z \sim 20$ for PSD and $Z \sim 25$ for ΔE-E).

For the detection of heavier ions at energies of few MeV/u magnetic and time-of-flight (ToF) spectrometers are instead necessary in order to provide ion identification through the combined measurement of position, ToF, energy loss and total energy or of some of these observables. Studies of transfer reactions, fusion-fission dynamics at Coulomb barrier energies and nuclear structure have strongly benefited from the use of such devices. In Sect. 3.4, developments for few selected spectrometers belonging to research lines of INFN will be presented. With the advent of the SPES project at LNL, which is foreseen to deliver radioactive ion beams in the forthcoming years, it will be necessary to characterize the incoming beam (purity, rate, etc.) and to measure the reaction products with dedicated detectors placed at zero degrees. This is particularly important for reactions where at least one of the reaction products has a strongly forward-focused kinematics, such as, to mention some, direct reactions in inverse kinematics, compound-nucleus reactions and Coulomb excitation reactions. Dedicated detectors should be designed to provide ToF, energy and scattering angle measurements of the beam-like ions. The main challenge is represented by limited rate capability of existing technologies. Taking inspiration from existing detectors at current RIB facilities, possible solutions suited for the energies, masses and physics opportunities specific of INFN-LNL and, in particular, of SPES will be outlined in Sect. 3.5.

Besides the use of zero-degree detectors, the study of direct transfer reactions with SPES beams in inverse kinematics will strongly benefit from the use of highly segmented silicon detector arrays for the detection of the light target-like recoils. One of these detectors is currently being designed within the GRIT collaboration, of which INFN is member. The main challenges are represented by the mechanical integration, the electronic processing of a huge number of signals and the use of pulse shape analysis to identify the light reaction products. Moreover, the coincidence between highly segmented Si detectors and γ-ray tracking arrays will also allow to extend the studies of sub-barrier fusion reactions to lower cross sections, important for the determination of reaction rates of astrophysical interest. Possibilities and developments related to these detectors will be presented in Sect. 3.6.

The search for new technologies or the evolution of the ones already known is ongoing. Three of them in different stages and capable of tackling different problems are presented here. The first one is the use of the emulsion technology in the ions detection. The passive nature of these devices dictates a reduced amount of recorded particles, but this is more than compensated by the extreme precision in the determination of the track parameters, including energy loss per track segment, allowing very precise measurements as proved by the FOOT experiment. Besides new development will reduce the size of the grains of the films allowing to gain almost

Table 1 Proposed upgrades and developments for the WG1 (charged particle detectors)

Tag	Description	Notes and critical issues	Exp. time	Phase
DET-ATa0	New field cage at LNL	Fully funded (CSN3)	2024	A
DET-ATa1	New pad plane at LNL	Fully funded (CSN3)	2026-2027	B
DET-ATa2	Resident AT at SPES	Beam line needed up to AT	2026-2027	B
DET-ATb0	Pure gas mult. and readout	From scratch	2025-	B
DET-ATc0	2nd level trig w/CNN	Need new FEE	>2027	C
DET-SICa0	Thick SiC detectors	Need for lower doping, characterization	2025	A
DET-SICa1	Pixelated SiC det.	Need low defect density, study of mech. mounting	2025	A
DET-SICa2	Fast timing FEE	Components availability issue	2025	A
DET-SICb0	Monolithic SiC ΔE-E	R&D of moderator	2026	B
DET-SICb1	SiC-based neutron det.	Buried electrode realization, high input capacitance FEE	2026	B
DET-SICb2	Study of PSA in SiC	Experiment approved at LNS, need CS beams	2027	B
DET-SPEa0	Integration of PRISMA second arm	Mechanical adaptation of the current scattering chamber	2025-2026	A
DET-SPEa1	TOSCA high rate and Z identification	Preliminary in-beam tests at GSI	2025	A
DET-SPEb0	New PRISMA focal plane detector	Commissioned, mechanical modifications required	2026-2027	B
DET-SPEb1	TOSCA large size	To be designed and funded	2026-2027	B
DET-SPEc0	DSSD array at PRISMA target position for fission studies	To be designed and funded	>2029	C
DET-ZDDb0	Development of a RIB tracker system	Realization of two MCP detectors with emissive-foil	2028-2029	B
DET-ZDDc0	Identification of evaporation residues at 0° with exotic beams	Design and realization of a multi-sampling IC	2028-2030	C
DET-ZDDc1	Position-sensitive fast IC with delay lines	Feasibility to be studied	2029-2031	C
DET-SSDa0	System for fast-reset signals	Design of a dedicated back-end firmware	2025-2026	A
DET-SSDb0	Multiplexing to speed up the readout	New version of a low-dead-time analog memory	2026-2027	B
DET-SSDc0	AC-coupled detectors	Re-design of ASIC boards and detectors	2029-2030	C
DET-3DDa0	Precision Timing (<100 ps)	Increase in detector area	2024-2025	B
DET-EMUa0	Precision passive tracking	Production site	2024	A
DET-ASIHa0	Radiation-resistant device	Need R&D for single particle detection	2026	C

As described in Ref. [5], the proposed projects are labeled as Phase A if feasible in a two-year perspective, Phase B in case small upgrade/additions to the present technologies are needed and Phase C when important R&Ds are required. Details are given in Sect. 3

a factor ten in spatial resolution. The technique and current developments will be presented in Sect. 3.7. The second one is the development of a radiation hard detector using diamond as substrate with the production of graphitic conductive paths on the surface and the bulk of the material to obtain electrodes and conductive lines allowing an all-carbon radiation hard device. Such device, with the suitable readout electronic has been developed and tested by the TIMESPOT collaboration reaching a time resolution between 50 and 100 ps on the passage of a single particle. These results will be described in Sect. 3.8. The third one is the development of devices made of amorphous silicon, hydrogenated to reduce the number of dangling bonds and obtain a ionizing radiation detector. The material is by itself extremely radiation hard due to its disordered structure, and it could be produced as thin films (1-30 micrometers thickness) in many different patterns, over quite wide area (6 inch wafers) and using many different substrates, including plastic ones. The HASPIDE project is developing several type of devices that could be used as beam diagnostic, possibly in transmission mode, in different environments. The single-ion detection is one of the next developments. All results and plans will be described in Sect. 3.9.

All of the aforementioned developments require man-power, funds, time and intense R&D work. Table 1 presents a synthetic summary of the present state of these researches and of the main steps to be taken in the immediate future.

1.2 Neutron detectors

Neutron detectors are an essential tool for the development of several research fields, namely nuclear, particle and astroparticle physics as well as radiotherapy and radiation protection. In this review, several neutron detection systems are described, with a focus on the ongoing developments and possible upgrades to be implemented in the next years.

Neutrons cannot directly ionize, and therefore, their detection is based on nuclear reactions and the detection of charged particle or electromagnetic radiation originating from neutron-induced reactions. To date, well-established neutron detectors work as counters, measuring the number of interactions in a detector, or as spectrometers, providing data on the energy distribution of the incident radiation. More in details, counter detectors can be operated as spectrometers when used in combination with the time-of-flight technique. This is possible when the neutron source position is known, i.e., in fixed-target experiments. A prerequisite for these kind of detectors is the ability to distinguish signals originating from different particles, in particular the neutron/γ discrimination capability. In addition, the TOF technique requires excellent time resolution and therefore organic—either plastic or liquid—scintillators are typically employed. The exploited nuclear reaction in organic scintillators is the neutron–proton elastic scattering, consequently these detectors are sensitive to fast neutrons. In this field, current developments are ongoing for NARCOS (Sect. 4.1.1) and NEDA (Sect. 4.1.2), segmented large-area detectors to be used in the near future in both heavy-ions and radioactive ion-beam facilities [1, 2] for nuclear physics experiments far from the valley of β stability. Depending on the nuclear reaction to be studied, the neutron energy region of interest can span form a few hundreds of keV to MeV neutrons. The novelty of NARCOS is the possibility to retrieve the neutron interaction point in the detector. In addition, it is conceived to work simultaneously as charged particle and uncharged particle detector. The advantage of NEDA is the very small detection threshold and the large area covered. It was conceived as a neutron counter to be used in combination with other detection systems, as, for example, AGATA.

For similar applications including the study of neutron delayed emission in beta decays, innovative materials for neutron detection have been proposed. For instance, the CLYC scintillator has a relatively high neutron detection efficiency and can measure the neutron energy with good energy resolution without using the TOF technique. The advantage is that the detector can be positioned close to the target, thus covering a large solid angle with a relatively small volume.

Other ongoing detector developments are related to MeV-neutron detectors for the measurement of nuclear reaction cross sections of interest for nuclear astrophysics. For instance, SHADES exploits the combination of plastic scintillators and ^{3}He tubes with the aim of controlling the neutron detection efficiency of the system (Sect. 4.1.3). In a few years, SHADES will become operational and start the measurement campaign at LUNA [3]. Another example is the VALAR project (Sect. 4.1.4), related to neutron diagnostic in laser–matter interaction [2].

Neutron beam detectors are widely used in TOF facilities (Sect. 4.2). They are used to characterize and monitor neutron beams with energies from meV to GeV. Several neutron-induced reactions are commonly used to cover this large neutron-energy interval, namely ^{6}Li(n,α), ^{10}B(n,α), ^{12}C(n,n) and ^{235}U(n,f) in addition to neutron–proton elastic scattering. In contrast to the neutron detectors mentioned above, these kind of detectors have much lower neutron efficiency (some orders of magnitude) and good n/γ discrimination capability. (In most cases they are insensitive to γ rays.) Similarly to neutron detectors for applications, the advancements are related to the adoption of cutting-edge and possibly radiation-hardness charged particle detectors properly coupled with neutron converters (Li, B, C, H, U) and the preparation of thin, homogeneous and stable layers of these converting materials. It is worth mentioning that several small-group application-based initiatives are ongoing.

Finally, the neutron's direction cannot be determined by any detector that is currently operational. Nevertheless, there is a number of pioneering ongoing projects aiming at reconstructing the neutron momentum of fast neutrons (e.g., MONDO, RIPTIDE). The working principle is to use 2-body nuclear reactions to retrieve the energy and direction of the impinging neutron.

1.3 X-ray and gamma detectors

X-ray detectors are rapidly evolving in the latest years, reaching impressive performances in terms of energy and position resolution, imaging and rate capabilities. In this review, several of these radiation detectors are presented, with particular emphasis on their possible future applications in nuclear physics. Proceeding in increasing order of detectable energy range, for soft X-rays ($E <$ 10 keV) a very interesting technology is represented by Gas Pixel Detectors (GPDs), having the unique capability to measure the linear polarization of the incoming photons [8]; also, the energy and the impact point of the X-ray on the detector can be inferred, allowing for simultaneous imaging and spectroscopy. Such detectors are used, for example, for the investigation of the neutron stars' equation of states, where "exotic" states and phases of matters such as nuclear superfluids, hyperons and deconfined quarks are most likely formed. For energies up to 20 keV, charge coupled devices (CCDs) are still widely used in several fields, in particular for imaging purposes coupled with X-ray optical elements. For example, the pinhole CCD system developed by the PANDORA collaboration [9] will be able to perform high-resolution spatially resolved X-ray spectrometry with several applications also in nuclear physics, like the measurement for the first time of β-decays in laboratory plasmas [10]. In this direction, a dedicated test bench, named FPT (Flexible Plasma Trap) [11], will be used at Laboratori Nazionali del Sud (LNS) for R&D on diagnostics and detectors. Going to higher energies, CZT detectors are presently experiencing a huge technological boost, providing very impressive energy resolutions at room temperatures (2 keV @122 keV[12], 5.1 keV @660 keV[13]), large detection efficiency (>98% @60 keV with 1-mm-thick detector) and good time resolution ($\sim$50 ns) [14]. These characteristics increased their appealing as X-ray detectors from 30-40 up to 300 keV allowing their applications in several fields, including nuclear physics, where the recent advancements in dynamic range and energy resolution of CZT detectors enable their implementation in experimental apparatus, like that of the SIDDHARTA-2 experiment at LNF (Laboratori Nazionali di Frascati), searching for X-ray transitions emitted from kaonic atoms. CZT detectors will allow, in the near future, to perform measurements using targets of aluminum, lead, sulfur or carbon in the 40-300 keV range [15]. Similar dynamic range and even better energy resolutions (at cryogenic temperatures) can be reached also with high-purity germanium (HPGe) detectors, which are also commonly used for radiation detection. These semiconductor devices can be also used as strip detectors for position measurements like the XH cryogenic detector system developed at UKRI-STFC Daresbury Laboratory in Daresbury (UK) [16, 17] and now commercially available. A complete different philosophy is instead that of the hybrid pixel detectors, where different materials are used to match different energy ranges; in these detectors the sensor is separated from the readout electronics, where the signal is digitized. A wide energy range detection is also possible with Transition Edge Sensors (TES) showing, at the cost of the necessity of very delicate cryogenic systems able to reach temperatures as low as a few mK, impressive energy resolving powers of $E/\Delta E > 10^3$ [18]. Among the several applications of these high-resolution devices, the HOLMES collaboration, led by INFN, will assess the neutrino mass by study the electron capture of the 163-holmium by implanting this radioactive isotope into gold absorbers coupled to TESs [19, 20]. Similar resolutions but with limited energy ranges can be also achieved with the cheaper and easier to handle technique of Bragg spectroscopy, one of the most established X-ray spectroscopy methods. Even if this technique has been usually limited to detect photons from very small (almost point-like) source, the VOXES (high-resolution VOn hamos X-ray spectrometer using HAPG for Extended Sources) collaboration at the INFN Laboratories of Frascati (LNF) exploited the unique properties of Highly Annealed Pyrolytic Graphite (HAPG) mosaic crystals to develop a high-resolution X-ray spectrometer able to reach few eV resolution and sub-eV precision measurements of photons emitted from millimetric targets [21]. Other possible applications range from fundamental physics, synchrotron radiation and X-FEL applications, to the agrifood sector where, as an example, information about the quality of edible liquids could be provided through the detection of the shift of the typical fluorescence lines of metals induced by oxidation mechanisms.

Gamma-ray detectors find applications in various fields, including nuclear physics, high-energy physics and astroparticle physics. In nuclear physics, solid-state and scintillator detectors are commonly utilized. For gamma-ray spectroscopy, exemplified by projects like AGATA [22] and GALILEO, high-purity germanium (HPGe) detectors with exceptional energy resolution are employed to conduct nuclear experiments. Significant technological advancements have been made in the past decade, particularly with segmented detectors like AGATA. Notably, a new, versatile encapsulation for germanium crystals has been developed [23]. This innovative version allows for multiple openings and closings, facilitated by a special elastic seal. The capsule can be efficiently pumped to high vacuum during annealing treatment, enhancing the likelihood of restoring neutron-damaged crystals. At IPHC, HPGe crystals undergo a meticulous 2D scanning process using a focused ^{137}Cs source [24]. This procedure aims to reveal any damage to the crystalline structure. Such characterization is vital for assessing crystal quality both before and after nuclear experiments, providing valuable insights into the integrity of the material. A groundbreaking technology, known as pulsed laser melting (PLM), has been developed through the N3G project in recent years, revolutionizing the creation of contacts/junctions on HPGe crystals and subsequent segmentation [25]. This innovative method has enabled the fabrication of a thin junction with a dimension of less than 200 nm [26], thereby minimizing the dead layers within the volume of HPGe crystals. The HPGe doping process, facilitated by PLM technology, can be achieved through a thin coating using PVD techniques [27] or MLD techniques [28]. The PLM process on HPGe crystals represents a departure from conventional doping diffusion methods, preserving the high purity of the germanium bulk [29]. Additionally, a new front-end electronic system for coaxial detectors, featuring cryogenic flexible cabling and ASIC electronics housed within a gamma cryostat, is currently being developed by the INFN group in Milan. In addition, there has been significant progress in the detection of fast gamma rays through the development of a $LaBr_3 : Cr : Sr$ scintillator. The research on this gamma detector, particularly focusing on the silicon photomultiplier (SiPM), is advancing to enhance gamma detection capabilities. The robust electronics in gamma-ray detectors have undergone substantial development. A notable achievement is the 3” SiPM on the $LaBr_3 : Cr : Sr$ scintillator with new AGC electronics, covering a broad energy range of gamma rays up to 25 MeV [30]. The PANDORA experiment, designed to detect the beta decay of selected radioisotopes in a plasma trap [31], will incorporate an array of 14 HPGe GASP gamma-ray detectors from the GALILEO experiment. The electronic pre-amplification of these GASP detectors has been modified to accommodate high counting rates, reaching up to 50 kHz [32]. In the field of astrophysics, substantial contributions have been made in recent decades. Large-area telescopes like FERMI-GLAST and DAMPE calorimeters for high-energy gamma rays in the GeV range have been developed to study dark matter and gravitational wave events in space [33, 34]. The silicon trackers in these telescopes were developed by INFN of Bari, with testing and calibration of the calorimeter conducted at SPS at CERN, covering a wide energy range from a few GeV up to 200 GeV. In high-energy particle physics, the OREO project aims to develop a highly compact electromagnetic calorimeter with inorganic scintillator crystals [35]. While the primary focus is on nuclear/hadronic physics, the applications could be extend to industrial and medical branches.

1.4 Detectors for medical applications

The fields of nuclear and fundamental physics have long been at the forefront of technological innovation, developing advanced technologies and sophisticated instrumentation, in particular concerning radiation detectors with cutting-edge performance characteristics.

Radiation detection plays a fundamental role in the biomedical field, enabling the measurement, monitoring and characterization of radiation exposure, both for diagnostic and therapeutic purposes. The ability to accurately detect and quantify radiation is critical in many biomedical areas such as radiation therapy, nuclear medicine, radiobiology and X-ray imaging. As a result, the development of sophisticated radiation detectors tailored to meet the specific requirements of very diverse applications in the biomedical field has become paramount.

Sometimes it is the technological innovation of novel detectors that opens up new possibilities for specific applications. In other cases, new diagnostic or therapeutic techniques require the development of appropriate new detection technologies to meet unprecedented measurement requirements.

Many challenges are associated with the technological transfer from fundamental physics research to medical radiation detectors. These challenges encompass not only the technical aspects, such as adapting detector designs and optimizing performance parameters, but also the need for collaboration between experts from different fields and the consideration of regulatory frameworks concerning the development and testing of medical devices. For this reason, many multidisciplinary initiatives have been funded and promoted by INFN or have involved INFN researchers in collaboration with national and international research institutions.

Given the wide range of radiation type, detector requirements and specifications across different applications, a general discussion encompassing all technology transfer initiatives would be complex and not very profitable. To provide a more focused analysis, we approached the work by identifying three main categories:

- Treatment monitoring and optimization;
- Dosimetry, quality assurance and radiotherapy;
- X-ray and nuclear medicine imaging.

In the first section (Sect. 6.1), we will give an overview of some of the most important INFN projects aimed at the charged particles treatment monitoring and optimization and we will discuss recent solutions the community is currently developing regarding dose delivery systems, online range verification and target fragmentation. Both the standard delivery approach and the novel delivery technique based on the use of ultra-high dose-rate electrons and protons (FLASH Radiotherapy, FRT), which requires the development of a new generation of detectors able to overcome the limitations of conventional ionization chambers, will be considered. Innovative dose verification systems for Boron Neutron Capture Therapy (BNCT) cell-selectivity exploitation will be discussed as well.

The second category (Sect. 6.2), "Dosimetry, quality assurance and radiotherapy," deals with new challenges on (a) Flash Radiotherapy, from modeling to monitoring and dosimetry; (b) Microdosimetry, using gas detectors (TEPC and mini-TEPC) and diamond detectors; and (c) New devices for dosimetric purposes, with the new Silicon Carbide and Amorphous Silicon technologies and pixelated diamond devices.

Finally, in the "X-ray and nuclear medicine imaging" section 6.3, some of the recent and ongoing initiatives regarding detectors for medical imaging are discussed. In the field of radiography, the two major innovations reported concern the development of perovskite X-ray imaging detectors and hybrid detectors having photon-counting and spectral capabilities. In the field of nuclear medicine imaging are discussed the development of gamma detectors for the measurement of the internal activity distribution in patients undergoing targeted radionuclide therapy and β detectors for radio-guided surgery with β-emitting radiotracers and microscopy imaging by contact.

1.5 Target developments for nuclear physics

Targets represent extremely important components in nuclear physics experiments with accelerators, either for experimental activities in fundamental science or for applications such as the production of radioisotopes or neutrons. In case of nuclear physics experiments, targets are usually composed of either thin films of specific isotopic species deposited on substrates, self-sustaining foils or gases. Targets for the production of radioisotopes or neutrons are usually exposed to high power deposition from the primary beam. Their design must therefore be accurate so as to satisfy strict requirements in terms of power dissipation, mechanical properties or material microstructures, to maximize production without incurring in failure. In the main text, recent advances on innovative target design, production and characterization at INFN are reported, divided in two sections: targets for nuclear physics experiments (Sect. 7.1) and targets for new production facilities (Sect. 7.2).

As far as the targets for nuclear physics experiments are concerned, it is important to underline that in any experimental study with accelerated beams, the choice of a proper target is a crucial issue, as important as the choice of the impinging beam and of the detection systems. A careful production and characterization procedure of the target foils must therefore be one of the main objectives in the preparation of an experiment. At INFN, the main target laboratories are located at LNS and LNL and have decades-long experience in the production of targets for nuclear physics experiments. An overview of the activities related to the target manufacturing and characterization at INFN is given.

The development of innovative targets is a key aspect also for any new production facility. Regardless of the specific species of interest to produce (radioactive ion beams, radioisotopes for medicine, neutrons, etc.), the availability of efficient, high power targets is fundamental to fulfill the needs of experimental users. This need emerges from the necessity of pushing the impinging beam intensity as high as possible, in order to maximize the yield of the desired products, without undergoing failure of the target. This is in most cases related to the capability of the target material, or of the targetry in general, to efficiently dissipate heat to minimize

Table 2 Summary table on the ongoing activities at Italian laboratories for target development, with critical aspects and expected timeline

Target	Comment/description	Critical items/challenges for R&D	Exp. time
LUNA-jet target	Supersonic gas jet target for LUNA	Ionization Hydrogen handling	TBD
LUNA-solid targets	Solid targets for LUNA	Purity, reduction of contaminants (F, D2)	2023
CTADIR	Cryogenic targets at LNL	Structural integrity of target windows under irradiation	2023
NUMEN-target	Thin isotopic cryotargets for NUMEN high-intensity beams	Operation in a harsh radiation environment Availability of isotopically enriched materials Thickness and uniformity	2025
SPES-target	Production target of the SPES ISOL facility at LNL	High power commissioning for 3D targets	2024
ISOLPHARM-target	Secondary target for the ISOLPHARM project at LNL	Compatibility with different radioisotope beams	2025
LARAMED-target	Targets for direct production of medical radioisotopes at LNL	High power irradiation at LNL Availability of isotopically enriched materials	2025
NEPIR-target	Targets for neutrons at LNL	Safety and radioprotection (beryllium)	2025
FRAISE-target	Target for FRAISE facility at LNS	High power commissioning	2024

thermal induced stresses. An extensive research and development program is currently being carried out at INFN regarding this topic. An overview of these activities is given in the main text. Table 2 presents a synthetic summary of the present state of these researches and of the main challenges in the immediate future.

The importance of the developments of target for nuclear physics is demonstrated by the number of large-scale European projects, collecting the community of users in different sub-fields related to nuclear physics. Presently at least in three of such projects a task is specifically devoted to targets.

In the EURO-LABS project, a subtask dedicated to targets is part of “Access to Research Infrastructure for Nuclear Physics - Service Improvements” activity. The main goal of the subtask is to gather the community of European “nuclear target makers” having specific expertise in the field of target manufacturing and characterization, both for nuclear and applied physics purposes. The planned activities are the study of existing and novel materials, the improvement of current and development of novel fabrication techniques, the target characterization procedures and the sharing of knowledge among the community.

In the ChETEC INFRA project, a task is dedicated to solid targets for nuclear astrophysics. Within this task, named STAR (Solid Targets for Astrophysics Research), the collaboration wants to develop, test and make protocols of special solid targets complying with the requirements of the experimental studies of nuclear reactions of astrophysical interest—namely purity, enrichment, composition, thickness and stability when hit by an ion beam.

In the project PRISMAP—The European medical radionuclides program, a task is devoted to target design and characterization for medical radionuclides production. Targets for radionuclide production always require specific attentions during the design phase, especially for target materials and cooling technologies. In particular, the intensity of the primary beam impinging on the target is usually increased as much as possible in order to maximize the radionuclide production. This tendency induces the optimization of high-performance cooling systems based on thermal conduction, convection and radiation. Moreover, target materials must guarantee specific microstructures and thermophysical properties.

1.6 New facilities at LNF, LNL and LNS

The INFN Laboratori Nazionali di Legnaro (LNL) (Sect. 8.1) and Laboratori Nazionali del Sud (LNS) (Sect. 8.2) are undergoing major accelerator developments to deliver exotic beams as well as high-intensity stable beams. New experimental facilities are being proposed and designed for the implementation of the associated nuclear physics program, with a possible realization in the midterm period. Concerning facilities for stable beams, the working group concentrated on refurbished mass spectrometers MAGNEX and PRISMA and complementary detectors like G-NUMEN or GALILEO-III for improved heavy-ion tracking and reaction kinematics reconstruction, also considering the need to withstand the high counting rate from accelerator refurbishments. For unstable beams, both from ISOL (LNL) and in-flight (LNS) techniques, the working group elaborated projects for facilities for ground-state property studies and for nuclear spectroscopy of the shell structure and reactions at low and intermediate energies. The former will foresee setups for the study of the global products of β decay, for high-resolution mass spectroscopy and for laser and nuclear magnetic and quadrupole resonance studies. The latter will rely on large-scale facilities combining different setups for γ-rays, ions and neutron detection and spectrometry. Large solid-angle coverage γ-ray arrays like G-NUMEN or GALILEO-III will be coupled to high-granularity silicon arrays or superconducting solenoids to study with electromagnetic and nuclear probes direct reactions with exotic beams. The development of superconducting ring recoil spectrometers and accumulation rings for heavy ions is also envisaged, to fully exploit the physics opportunities provided by exotic beams. For nuclear astrophysics studies, the development of several detector arrays is ongoing or foreseen, both for the detection of charged particles and neutrons, these last being emitted after β-decay. The installation of a β-decay station is also foreseen. Two new facilities are going to be constructed at LNS: PANDORA, a new concept plasma-based facility and the laser facility I-LUCE. These two facilities will allow to exploit new opportunities in multidisciplinary studies, nuclear physics, nuclear astrophysics and applications.

2 Introduction

The INFN Laboratori Nazionali di Frascati (LNF) played a crucial role in the history of nuclear and particle physics. It was established in 1954 to host an electro-synchrotron, the first particle accelerator built in Italy, and give birth, under the guidance of Bruno Touschek, to the design and the realization of the first electron–positron collider AdA (*Anello di Accumulazione* in Italian, i.e., “storage ring”), proving the feasibility of the approach that eventually turned out to be highly strategic in the development of particle physics. In the decades after, it hosted the project ADONE that confirmed the observation of the J/ψ after its discovery at the Stanford Linear Accelerator Center and Brookhaven National Laboratory. Nowadays, a new e^+e^- machine is operational, DAΦNE, the *Double Annular Factory for Nice Experiments*, that carried out an important physics program in the study of CP violation in the kaon sector and in the understanding strong interactions in the strange sector through the production of kaonic atoms. In parallel to the operation of the experiments, LNF was always very active in the research and development of detection techniques, contributing to the design and the construction of many detectors for nuclear and particle physics experiments worldwide. Within the workshop series [5], it has then been decided to elect the Frascati National Laboratory as the natural host for the session devoted to the detection techniques. The program was articulated in 6 working groups, each covering one of the main aspects of nuclear and particle experimental physics. The various working groups gathered the expertise of the Italian research groups and laboratories connected with the INFN Third Scientific Commission devoted to nuclear physics experiments. In particular, working groups from 1 to 3 discussed the status of the art and the perspective for the detection of charged particles, neutrons and photons (in the gamma and X-ray energy regime); working group 4 reported about the application of the above-mentioned technologies for medical applications, while working group 5 illustrated the development of targets for nuclear physics. Working group 6 discussed possible, future measurements at the INFN Laboratori Nazionali di Frascati, Laboratori Nazionali di Legnaro and Laboratori Nazionali del Sud.

3 Charged particle detectors

This section presents the ongoing R&D work on charged particle detectors in two different contexts: (i) experiments at radioactive ion-beam (RIB) facilities, where the need for large geometric efficiency, to cope with the relatively weak beam intensity, motivates the design of active target (AT) detectors (Sect. 3.1); (ii) experiments with large beam intensities, which instead require fast-response and radiation-hard detectors, like those based on silicon carbide (SiC) (Sect. 3.2). Apart from developing radiation-hard semiconductor detectors based on SiC, one would also like to apply to SiC the same particle identification techniques so successfully implemented with silicon detectors, like pulse shape discrimination (PSD) (see Sects. 3.2.4 and 3.3) and the ΔE-E technique, possibly applied to compact monolithic multi-detectors (see Sect. 3.2.3).

It is worth noting that for heavy fragments PSD and ΔE-E techniques cannot be exploited and they should be replaced by magnetic and TOF spectrometers. Therefore, an intense R&D work is planned. In Sect. 3.4, developments for few selected spectrometers belonging to research lines of INFN will be presented.

With the advent of the SPES project at LNL, for many experiments employing radioactive ion beams (RIBs), it will be necessary to characterize the incoming beam (purity, rate, etc.) and to measure the reaction products with dedicated detectors placed at zero degrees. This is particularly important for reactions where at least one of the products has a strongly forward-focused kinematics, such as in the case of direct reactions in inverse kinematics, compound-nucleus reactions and Coulomb excitation reactions. Such detectors should be able to measure ToF, energy and scattering angle of ions close to the beam direction (see Sect. 3.5). For the specific case of direct transfer reactions, the use of arrays of highly segmented silicon detectors coupled with state-of-the-art γ-ray arrays will have unparalleled performance in terms of efficiency and energy resolution. The main challenge is the treatment of a huge number of signals and the mechanical integration in small scattering chambers. The coupling of such detectors (silicon and gamma-ray arrays) will also allow to extend the studies of sub-barrier fusion reactions to lower cross sections, important for the determination of reaction rates of astrophysical interest. Possibilities and developments related to these detectors will be presented in Sect. 3.6.

Finally, the undergoing efforts in the development of several well-established technologies are presented. The first case considered is the use of the emulsion technology in the ions detection (Sect. 3.7). The second is the development of a radiation hard detection using diamond as substrate with the production of graphitic conductive paths on the surface and in the bulk of the material to obtain electrodes and conductive lines allowing an all-carbon radiation hard device as the one developed and tested by the TIMESPOT collaboration (Sect. 3.8). The third one is the development of devices made of amorphous silicon, hydrogenated to reduce the number of dangling bonds and obtain a ionizing radiation detector. The HASPIDE project is developing several type of devices that could be used as beam diagnostic, possibly in transmission mode, in different environments (Sect. 3.9).

3.1 Active target detectors

Gas-based ATs use the same gas as both target and detection medium, thus achieving large geometric efficiency in contexts where a low reaction rate is expected. In particular, Time Projection Chambers (TPC) operated in active target mode [36–40] offer new experimental opportunities in nuclear physics and nuclear astrophysics [41–43], mainly in connection with radioactive ion beams (RIB), where high efficiency and thick targets are needed to compensate the weak beam intensity. In a TPC, each charged reaction product produces an ionization track and a superimposed electric field makes the electrons drift toward a segmented anode so that a projection of each track on the anodic plane is obtained, including the information about the ionization density along the track. The third coordinate of each track segment is obtained from the time needed by the electrons, drifting at a constant velocity, to reach the anode. From the ionization density profile, it is possible both to identify the emitted fragments and to estimate their kinetic energy. As a consequence, TPC offer the possibility to track the incoming beam up to the interaction vertex, to estimate the effective interaction energy as well as to reconstruct the direction of the out-coming tracks with a resolution $\Delta\theta \sim 1^\circ$.

ATs are very versatile detectors. As a matter of fact, they lend themselves to be used in various research fields as, e.g., single-nucleon exchange reactions to investigate the so-called *shell migration* [44, 45] and two-nucleon exchange reactions to investigate the role of pairing correlations in exotic nuclei [46–48], as well as for the search of cluster structure in the light mass region [49]. ATs are also relevant in giant resonance studies, especially for giant monopole resonance via (α,α') and (d,d$'$) [50, 51]. Eventually, ATs are also employed in decay studies [52], two-proton radioactivity [53] and studies of astrophysical interest [54], e.g., (α, n) and (α, p) mainly using a Multi-Sampling Ionization Chamber (MUSIC [55]).

3.1.1 *Toward a hybrid pad plane for pure gasses*

The detection plane, which consists of a micro-pattern gas detector (MPDG), is the core of an AT and allows for the multiplication of the primary electrons, at the same time preserving spatial and collection time information (e.g., Micromegas [56]). However, as the gas medium is in common with the active volume itself, some questions have to be addressed. In fact, though working without a quench gas can easily lend the MPDG to a discharge regime [57], one would like to operate with pure hydrogen and deuterium to perform (d,p) or (p,t) reactions, or pure helium for (α,α').

To date, the most promising solution is exploiting pre-amplification devices on top of the primary MPGD, to extend the maximum achievable gain using hydrogen or other gases [58–61]. For a double Thick Gas Electron Multiplier (THGEM) [58], effective gains of the order of 10^4 have been reached in pure H_2, for pressure ranging from 100 and 300 mbar. Double- and triple-layer multilayer THGEM (M-THGEM) has been tested in different configurations also in pure He [59], obtaining a gain of about 10^6, comparable to the typical gain obtained for a standard He+(10%)CO_2. Eventually, M-THGEM has been also tested using pure CO_2 as a gaseous medium, aiming at performing two-nucleon pick-up reaction using $^{12}C^{18}O_2$[60]. Such devices can work in a stand-alone configuration acting as a new sensor plane for AT [38] or coupled with standard MICROMEGAS in a hybrid configuration [62].

3.1.2 *Space-charge effects and δ-rays detection*

The second key element of an AT is the uniform drift field, typically generated by the so-called field cage. Typical field values range from 100 V/cm up to 1000 V/cm, with typical deviations of a few percent at the active volume border [40]. However, high-charge and/or high-intensity beams can spoil the field homogeneity and uniformity, and in turn, the reconstruction capability of the AT. Space-charge effects have been observed for a K beam with an instantaneous rate as high as 10^4 pps and a mean rate of around 800 pps [63]. A mitigation option to this issue is the introduction of a beam mask, i.e., a cathode–anode system, matching the field inside the active volume, in order to rapidly collect the generated electron-ion pairs, thus suppressing their influence on the drift field [64, 65]. However, the introduction of a beam mask has a drawback: the loss of tracking capability in the region covered by the mask itself. Consequently, the vertex reaction reconstruction needs to rely on the light target ejectile and the nominal beam trajectory where only two products are present in the electric channel.

As the charge and the energy of the incoming beam increase, the δ-ray production also starts to play a significant role. Although δ-ray tracks can be removed during the off-line analysis, the generation of spurious hits affects the TPC trigger rate. An interesting solution has been adopted by the CAT collaboration [66]: a permanent dipole magnet, of about 1 T, has been located, inside the active volume, around the beam axis, thus confining the δ-electrons within its volume. In order to prevent the drift field distortion, the magnet support structure is equipped with a voltage divider that matches the equipotential planes inside the active volume, restraining the track displacement within 1 mm.

3.1.3 *Active target for SPES*

NUCLEX is an Italian collaboration within INFN, studying reaction mechanisms and nuclear structure using charged particles as probes, in an energy regime going from a few MeV/nucleon to ∼50 MeV/nucleon (see, e.g., [67–73]).

NUCLEX is now in the process of developing ATS (AT for SPES), a TPC based on the concept of the ACTAR-TPC demonstrator [74] but with significant improvements, to provide LNL with an active target for RIB studies. Also, in this case the main limitations are mainly related to the beam intensity and stopping power: both can generate space-charge effects within the TPC. In this respect, ATs will be equipped with a sliding-seal chamber and a rotating platform to match the beam intensity delivered by SPES with the detector limits ($\leq 10^5$ pps). Moreover, a new detection plane and field cage, responsible for the generation of the drift field, will be realized, with the possibility to realize a hybrid micro-pattern gas detection system to work with pure gas (*i.e.*, without quenchers) and to equip the field cage with an electromagnetic mask to further screen space-charge effects and confine δ-rays generated by the beam. It is worth mentioning the efforts within the NUCLEX collaboration to investigate the possibility of a neural network-based “intelligent” trigger system [75], being able to classify the events depending on different patterns at the detection plane level.

3.2 Silicon carbide detectors

Exposure to high fluxes of radiation is known to cause appreciable deterioration of semiconductor device performance. Generally, in junction detectors, the main evidence of damage is a fluence proportional increase in the leakage current. Loss of energy resolution and of charge collection efficiency are also signs of increasing damage.

Silicon carbide (SiC), a wide bandgap semiconductor, is presently intensively studied, as an alternative to silicon for the production of radiation hard devices [76–79]. SiC can be used to produce both p-n junction and Schottky diodes, and when compared to silicon, its larger bandgap and larger energy threshold for the production of lattice defects make it more suited for use at large fluence such as in experiments with high-intensity beams, in-plasma studies or as beam diagnostics. One application example would be in frontier activities in nuclear and sub-nuclear physics, where one needs to operate at high fluxes of incident particles, e.g., in order to measure cross sections of very rare phenomena [80]. The huge interest in silicon carbide due to its use in the automotive sector is motivating intense R&D in this field. On the other hand, SiC represents a new challenge for detector manufacturing. This motivated ST-microelectronics in Catania to set up a new clean room, to be managed by CNR-IMM institute, in order to produce and test SiC devices. PSD techniques, already developed for silicon detectors, can be also applied successfully to SiC detectors, as demonstrated by the first preliminary studies [81].

SiC detectors are also particularly attractive for laser-driven experiments because SiC devices show large thermal stability and are insensitive to photons in the visible range [82]. Therefore, they could be successfully employed in measuring the cross section of nuclear reactions in laser-induced plasma (see, e.g., Ref. [83] and references therein). A reliable measurement of these cross sections is needed, for instance, in order to understand the nucleosynthesis of nuclei such as ^{26}Al ($T_{1/2} = 7.17 \times 10^5$ y). Aluminum-26 constitutes an early example of multi-messenger astronomy. In fact, it is detected (through the daughter ^{26}Mg) in the earliest formed solids of the Solar System, in Al-rich chondrules called presolar grains found inside meteorites and in the Galactic interstellar medium (through its decay emission line at 1809 keV). Though ^{26}Al is the most robust constraint on nucleosynthesis models, its nucleosynthesis is still uncertain[1] and the study of nuclear cross sections in laser-induced plasma could answer key astrophysical questions, as the plasma effect on the population of the states in ^{26}Al and on its lifetime.

3.2.1 *SiC radiation hardness*

The SiCILIA collaboration (started as a Call in the V scientific commission of INFN) performs systematic studies of the behavior of SiC as a detector material [82]. Within SiCILIA, INFN and IMM-CNR are cooperating in R&D activities on SiC technology, also in view of several new and ambitious INFN projects, e.g., NUMEN [80, 85] and NuReLP [86–88]. Some of the most important results concerning the technological issues and the particle detection applications have been recently published [81, 89, 90].

In recent years, several studies on radiation damage have been conducted by the SiCILIA collaboration to investigate the performance of SiC detector prototypes, also in comparison with more traditional silicon detectors. Damages were induced by different radiation types: electrons, protons, heavy ions, photon and neutrons. Some devices were irradiated by using 5 MeV electrons, up to a total fluence of 10^{13} e/cm^2. No instability or deterioration has been observed. Other devices were irradiated by using 60 MeV protons up to 2 kGy without observing instability or deterioration [91]. Ion beams of ^{16}O (12.5 MeV) and ^{27}Al (24.2 MeV) were also used [92]: SiC p-n junction devices were irradiated up to 10^{12} ions/cm^2, and a reduction of the total charge collection efficiency of about 40 % has been observed without major changes in the resolution. A SiC p-n junction device, 100 μm thick, was irradiated with 14 MeV neutrons, up to a total fluence of 4.45×10^{11} n/cm^2. No instabilities have been observed [93]. Thin silicon carbide membranes were irradiated by a 12.4 KeV photon beam up to 45 GGy without observing instability or deterioration [94].

---

[1] Complications in the relevant nuclear physics behind the net production of ^{26}Al arise from the presence of an isomeric state in ^{26}Al at $E_x = 228$ keV ($T_{1/2} = 6.35$ s, hereafter ^{26}Al^m), see Ref. [84] and references therein.

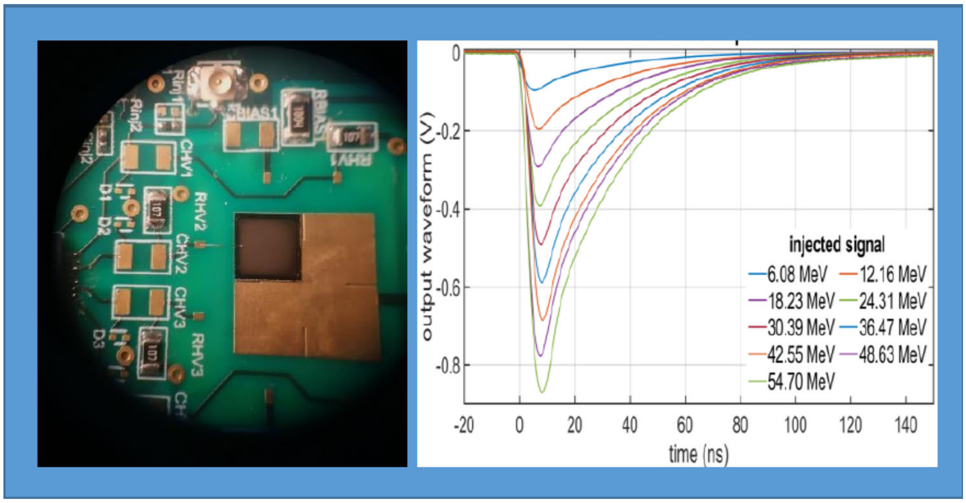

Fig. 1 Left, microscope view of one pad mounted in a prototype mother board. Right, measured waveforms obtained using the operational amplifier (ADA4895)

3.2.2 SiC-based tagging system for fragmentation beams

One of the methods to develop radioactive ion beams (RIBs) is the in-flight fragmentation method coupled to the use of a fragment separator [95]. Nuclei are produced by fragmentation reactions of intermediate energy projectiles on a relatively thin target and they are selected in magnetic rigidity (i.e., their momentum divided by their charge) by a suitable combination of electromagnetic fields. The produced beam is, in most of the cases, a cocktail beam that can be at least partially purified at the cost of some degradation in energy and emittance [96]. The overall beam quality is generally poorer than a standard stable beam, due both to a large emittance (producing a beam spot of few cm diameter or more) and a limited energy resolution (often larger than 2-3 %). A measurement of the beam trajectory is therefore generally needed. When the complete purification of the beam is not possible, an opportune tagging device able to identify, event by event, the beam is also needed. Owing to the intensity of the beam, the tagging system needs to be radiation-hard. In parallel to the construction of the new fragment separator FRAISE at INFN-LNS [97, 98], a new tagging device is being developed, based on silicon carbide pixelated detectors featuring a high-event rate capability and being radiation tolerant—features not available at the required level in the previous instrument [99]. The basic detection unit is designed to measure up to 10^7 pps. The tagging system can identify the RIBs composition using the joint measurement of the energy loss (ΔE, with resolution better than 1 %) of ions passing through the detection unit and the time of flight between two detection units or measured with respect to a reference signal synchronous with the primary beam (bunch) arrival on the production target, like the radiofrequency signal of a cyclotron (a time resolution < 1 ns is needed for charge/mass identification). One also needs to measure the 2D profile of the RIB with the precision required for the characterization of the beam transport properties (about 2-3 mm spatial resolution for most of the cases). The full trajectory reconstruction is made possible by the use of different detectors, see, for instance, Ref. [100]. With this new tagging device, the RIB energy could be measured event by event, with a precision better than 0.5 %. The beam energy will be obtained again thanks to a TOF measurement over a long base of flight between two detection units. In the case of FRAISE, for the beams sent to the 4π CHIMERA detector, we can have a base of flight of at least 15 m (up to 25 m could be possible). With a typical velocity of the RIBs around 10 cm/ns, the overall TOF resolution has to be better than 375 ps, that is, 250 ps for each sensor. This is a demanding goal, feasible but requiring a careful and smart design of each component.

The detector topology will be the one of a pad detector, having a basic segmented structure of 9 pads (about $5 \times 5\,\text{mm}^2$ active area each) arranged in a window-like configuration into a $2.25\,\text{cm}^2$ single die, with a minimum dead layer between neighbor dies of the order of few hundreds μm. This will result in dead zone of about 15 %. Two detection layers of about $6 \times 3\,\text{cm}^2$ will be coupled with a half-pitch shift both in X and in Y and readout in coincidence to partially recover for the dead region around each sensor die, thus allowing the goal of larger efficiencies of the order of 92 %. Figure 1 (left panel) shows a microscope view of one pad mounted in a prototype mother board used for the preliminary test of the system. The detector thickness will be of the order of 100 μm. This is a compromise between the need of a small perturbation on the beam energy, the need to minimize the output node capacitance, as required by the target signal-to-noise ratio, and the request to have a relatively fast collection time for the detected charge.

A dedicated multichannel front end in charge preamplifier configuration with high bandwidth (target rise time below 1 ns), low-noise, high-linearity and compact design is also being implemented, to tackle with all the aforementioned requirements. Particular care will be posed in the choice of the discharge mechanism and of the discharge time constant. In the right panel of Fig. 1, the measured waveforms obtained with one of the tested operational amplifiers (ADA4895) are shown for various values of the injected signal measured as silicon equivalent energy. A fast shaping time is used in order to optimize the time resolution. However, also the energy resolution of the system is good enough. The measured integral-nonlinearity—computed as the maximum deviation from the linear fit up to the considered amplitude—is better than 0.3 % up to 50 MeV deposited energy (silicon equivalent, 108 MeV in SiC). The widespread of deposited energies in the detector, depending on the detected species and on the incident energy, imposes the development of a selectable gain front end or of different front ends targeted to the different energy ranges. An additional challenge is the trade-off among the limited available power budget in view of a real system composed by many channels[2] and other factors like the extremely low noise required to preserve the identification capabilities for thin, high capacitance, detectors and the small amount of deposited charge, due to the relatively large energy needed to produce an electron–hole pair in SiC. The construction of the prototype is ongoing, and preliminary tests are foreseen in the immediate future.

3.2.3 SiC-based monolithic ΔE-E telescope

A common problem in nuclear physics experiments is the charge, Z, identification of the particles emitted in the reaction with very low energy. In general, a two-stage detector telescope technique is adopted. A thin first-stage detector measures the energy loss of the particle, ΔE, and the second-stage detector measures its residual energy, E. Combining the two information, one can identify the particle charge, and in some cases also mass, using the energy loss dependence [7]. Often this is realized by using as a first stage a gas detector whose effective thickness can be simply adjusted by changing the gas pressure. The advantage of gas detectors is their relatively low cost and their resistance to radiation damage. In several cases, semiconductor detectors are preferred for ΔE measurement, especially when very compact structures are needed. Unfortunately, even if large efforts have been put forward on the production of thin detectors [101, 102], they are commercially available only down to 10 μm minimum thickness. They are also quite expensive due to manufacturing difficulties and fragile both from a mechanical and radiation hardness point of view. In some pioneering works [103, 104], detector telescopes having monolithic structures and ΔE with a thickness of about 1 μm have been developed. Inspired by these works and taking into account the latest INFN innovations on silicon carbide (SiC) obtained from the SiCILIA collaboration [81, 82, 93], an innovative monolithic device based on SiC technology with an energy identification threshold of about 0.5 MeV/A is now being developed.

3.2.4 PSD in SiC

The applicability of the ΔE-E method strongly depends on the capability to lower the threshold given by the punch through energy of the impinging particle in the first stage of the telescope. As said, such threshold can be lowered by reducing the thickness of the first stage, and optimal performances could be achieved in this respect by employing monolithic ΔE-E structures with a very thin ΔE stage. However, another viable solution for such limitation can be provided by the application of PSD (pulse shape discrimination) algorithms for the identification of the low-energy particles stopped in the first stage detector. This identification method, successfully used for silicon sensors [105–109], relies on the dependence of the time evolution of the signal induced in a single detector on the ionization density along the track, which in turn depends on the mass, charge and energy of the impinging nuclear fragment.

A preliminary study of the PSD performance of SiC detectors has been carried out in Ref. [81] exploiting the prototypes produced by the SiCILIA collaboration. The sensors were tested in a reverse mounting configuration that in the past has been proved as the most suitable for this kind of application [110]. A good charge identification of the nuclear fragments has been successfully achieved exploiting two different pulse shape related observables, namely the rise time of the charge signal and the maximum of the current signal, the latter obtained from the charge signal through digital differentiation based on a smoothing spline interpolation algorithm. Also, some hints of mass identification for hydrogen and helium isotopes could be found for a lower-biased SiC detector.

The first results of the application of PSD algorithms to SiC detectors are promising; however, PSD studies in silicon carbide are still at a preliminary stage, and the work of Ref. [81] has to be extended. Indeed, an experiment has been proposed and accepted at INFN-LNS: a systematic study of the SiC PSD performance in relation to the applied bias, similar to that of Ref. [109], is foreseen. An evaluation of the PSD identification capability with respect to specific characteristics of the detector (e.g., the doping uniformity or the defect density) would be interesting, as well as a study of the limits of stability of the PSD performance in terms of heavy-ion fluence delivered to the SiC sensors [111], especially in view of their potential application in high-dose rate environments.

3.2.5 SiC+^{6}LiF for neutrons

Silicon carbide's capability to withstand harsh operating conditions makes it an interesting solution also for the development of neutron detection and monitoring systems to be used in those environments characterized by high radiation fluences and/or high temperatures. Such requirements can be found both in experimental applications, such as in zero-degree measurements and diagnostics with high-flux neutron beams [112, 113], but also in technology applications, such as high-level radioactive waste management [114], neutron monitoring systems in nuclear power plants [114, 115] or in the upcoming fusion reactors [116].

A possible solution for the detection of thermal neutrons is instead represented by SiC sensors coupled with a converter layer, such as ^{6}LiF, containing specific isotopes interacting with neutrons with relatively high and well-known cross sections [117, 118]: in particular, the neutron capture reaction ^{6}Li(n,α)^{3}H is a standard for neutron energies from 25 meV to 1 MeV. Some old generation

---

[2] In the realistic case of a 3 × 6 cm^2 active area, needed to cover the full beam area, about 100 channels per detection layer are needed, depending on granularity.

SiC+^{6}LiF detectors have been inspected in the past with promising results [114], but this field could benefit from the new generation SiC devices produced by the SiCILIA project.

In many applications, neutrons must be detected in presence of intense γ backgrounds: in these cases, a desirable characteristic for a neutron detection system is the γ-insensitivity, or alternatively the capability to perform a reliable n/γ discrimination. In a mixed neutron/γ field, if the energy released by γ-rays in the detector is sensibly lower than that released by the charged particles resulting from the neutron reaction with the converter, a simple pulse height threshold can provide an effective n/γ discrimination [119, 120]. More specifically, in the case of a ^{6}Li-based converter, the exploited reaction ^{6}Li(n,α)^{3}H results in the back-to-back emission of a 2.73 MeV triton and a 2.05 MeV α particle. Both products can be used for neutron counting, but the detection of lower-energy α particles can be more affected by the possible γ contamination in the low-side of the spectra. In fact, in a recent work inspecting a SiC+^{6}LiF configuration [121] the authors could exploit only the triton peak for neutron counting and foresaw the study of a *sandwich semiconductor* configuration to separate the α particles from the γ-background. Instead, in Refs. [122, 123], PSA methods have been successfully applied to n/γ discrimination for a CVD diamond detector+^{6}LiF configuration: this is a relatively new application of PSA (at variance with its use in scintillators which has been extensively studied [124]) that could be tested also on similar SiC-based devices. The combination of the characteristics of the SiC detectors with a PSA-based n/γ discrimination could open new possibilities and many technological spin-offs for neutron counting in harsh environments, often characterized by a strong γ-background.

3.2.6 SiC detectors for particle ID in hot, laser-induced plasma

In laser-driven experiments, the large thermal stability and insensitivity to photons in the visible range make SiC detectors an attractive choice [82]. Also, thanks to their radiation hardness, it will be possible to stand the high radiation flux produced in a laser-induced experiment, as well as the high temperatures achieved due to exceptional thermal shock-resistant qualities. We propose an R&D activity which aims at investigating the use of these prototype detectors in laser-driven experiments [125]. In parallel, we will evaluate the possibility to extend pulse shape analysis (PSA) to very low energies (namely few to hundreds keV). Indeed, digital sampling techniques were successfully utilized for PSA experiments outlining the high potential of digital PSA to decrease the lower-energy threshold of the particle identification [126].

After this evaluation and validation phase, SiC-based devices will be employed in studying astrophysically relevant nuclear reactions under conditions close to the astrophysical ones (energy, density and pressure), in particular the plasma effect on the population of the states in ^{26}Al and on its lifetime. This will allow us to reduce the systematic uncertainties often introduced by the extrapolation procedures, to estimate the contribution of nuclear excited states and to characterize the plasma by determining density, temperature and charge states of the constituent ions.

3.2.7 SiC detectors characterization

Thanks to their performances, i.e., high radiation hardness and high energy and time resolution, new generation particle detector systems are assumed to use SiC detectors. It is the case of the NUMEN project [80, 127], which will use large-area SiC detectors as the ΔE stage of the new particle identification (PID) wall of the MAGNEX magnetic spectrometer [128] (see Sect. 8.2.1). State-of-the-art SiC detectors 100 μm thick, 10 μm dead layer, 15.4 × 15.4 mm^2 area including $\approx$ 400 μm edge structure have been already produced to this purpose [129]. Stringent requirements must be satisfied by these devices:

- Thin dead layer to be used in transmission (ΔE measurements);
- Low depletion voltage, since they have to work in low-pressure gas environment;
- Thickness and charge collection uniformity within each detector to guarantee high PID performances;
- Homogeneity among different devices in terms of depletion voltage, thickness, resolution, etc., since 720 SiC detectors will be used to cover the large detection area (154 × 1260 mm^2).

Accurate characterizations of these new devices must be performed to establish to what extent the mentioned requirements are fulfilled and then guide further R&D activity. A first investigation regards how the charge collection efficiency (CCE) behaves in the full active volume and near the edges of the detector. This can be studied using 3D microscopic characterization techniques as the ion beam-induced charge (IBIC) that utilizes focused MeV range accelerated ions to probe charge transport [130, 131]. Using the same IBIC beams or collimated alpha sources at different incident angles, it is possible to measure the dead layer thickness present in the back of the epitaxial layer and study possible channeling effects. Other important properties are the full depletion voltage and the doping concentration value and profile. These can be accessed by the C-V and I-V characteristics measured through a probe station able to reach high-voltage biases (up to about 1.2 kV) [129].

3.3 Pulse shape discrimination in semiconductor detectors

PSD relies on the dependence of the time evolution of the signal induced in a single detector, which in turn depends on the mass, charge and energy of the impinging nuclear fragment. This is due both to the different range for particles having the same energy and different charge and/or mass and to the different ionization densities, in turn due to their different stopping power. For heavy charged particles, in fact, the ionization density is so high that the charges along the track behave like a plasma, shielding the interior of the track from the external electric field. Therefore, the ionization density affects the collection time of the electron–hole pairs through the so-called *plasma time*, i.e., the time needed by the electron–hole column to be eroded by the electric field of the reverse biased junction.

PSD has been studied deeply, in last two decades, especially for silicon junction detectors. For these detectors, a large database of digitized waveforms is now available for many Z, A and energy combinations, thanks, e.g., to the detailed R&D conducted by the FAZIA collaboration [132]. This opens the opportunity to isotopically access the low energy fragments produced in nuclear collisions [69, 133, 134].

3.3.1 Charge collection simulations

For the design of new devices, as those treated in Sect. 3.2.4, and the *a priori* evaluation of their PSD capabilities, realistic microscopic simulation of the charge collection process could be really helpful. For heavy charged particles, the microscopic description should include the electron–hole mutual interaction, in order to reproduce their already mentioned plasma-like behavior. Though there have been sporadic attempts in the past [135–139], with mixed success, this is a line worth following, possibly including also the effects of damage. A deeper understanding of the underlying process, validated by a few dedicated experiments or by comparison with the already available waveform database, could be of great help in our search for the best shape parameters and detector configurations. The simulations could help in clarifying why a fragment must penetrate beyond a given minimum range in order to be identified and the reason why the mass resolution improves for under-depleted detectors.

3.3.2 Combining time of flight and PSD

The energy threshold for identification of fragments could be lowered by a combination of time-of-flight (ToF) measurements and PSD. ToF measurements give the velocity of the fragment and, combined with energy information, the fragment mass. However, it has been shown that the atomic number can also be obtained, by combining ToF measurements and shape related parameters. A preliminary result has been published as Fig. 30 of Ref. [7], showing an energy vs time-of-flight correlation obtained from FAZIA, summed over ~ 80 telescopes for ^{48}Ca+^{12}C at 25 AMeV. Fragments are stopped in the first silicon layer, 300 μm thick, and they are identified up to neon isotopes, both in atomic and mass number, with very good resolution. To get such a good result, all digitizing channels must be carefully synchronized. In fact, all the ADC clocks are synchronized with a custom procedure, reducing clock delay differences down to 10 ps. An innovative aspect of the ToF measurement adopted in FAZIA telescopes is the “start” time mark extraction, as it is obtained from completely identified fragments: from the energy, mass and detection time of any such fragment, the velocity (and therefore the collision time, knowing the flight base) can be easily calculated by reversing the kinetic energy formula. The ToF of a not-identified fragment can be obtained from its own time mark and from the reaction time estimated from identified fragments. Combining ToF and PSD, it is possible to identify light ions penetrating less than 50 μm inside the first telescope layer, i.e., ions which cannot be identified via PSD. This could open the possibility to use FAZIA-like telescopes even at lower energies, like at SPES.

3.4 Spectrometers

Spectrometers are at the forefront for heavy-ion identification at energies of few MeV/u. They can be divided into magnetic spectrometers, which select the ions according to their mass-over-charge ratio (m/q) through a set of magnetic elements, and time-of-flight spectrometers, which have normally simpler designs and distinguish the ions via E-ToF or position-ToF correlations. Studies of nuclear structure and of transfer and fusion-fission dynamics at Coulomb barrier energies have strongly benefited from the use of such devices.

In this section, we will present possible upgrades for the study of reaction dynamics and nuclear structure with spectrometers, employing transfer, fusion and fission reactions. In Sect. 3.4.1, we will focus on proposed upgrades of the large acceptance magnetic spectrometer PRISMA at LNL; in Sect. 3.4.2, we will present possible developments for the ToF spectrometer TOSCA of the FORTE collaboration.

3.4.1 The magnetic spectrometer PRISMA at LNL

Electromagnetic spectrometers are versatile setups aimed at the detection of particles with a wide range of masses and atomic numbers involved in reactions at relatively low bombarding energies ($\sim 5 - 20$ MeV/u). Modern spectrometers combine the use of a series of electromagnetic elements that bend the trajectory of the particles, and a series of position detectors to track the trajectory before and after the magnetic set. In addition, the spectrometer is completed with detectors to measure the energy loss (ΔE) and total energy (E) of the ions. At energies close to the Coulomb barrier, magnetic spectrometers can be used to study processes such as inelastic, transfer, fusion and fission reactions. Among the best examples of this kind are PRISMA at INFN-LNL [140, 141], VAMOS at GANIL [142] and MAGNEX at INFN LNS [128, 143, 144]. They are all equipped with a set of large-size magnetic elements (dipoles and quadrupoles), and all have the possibility to rotate around the target point, allowing a significant angular coverage.

Further developments can be foreseen to improve the performance of PRISMA for the study of multi-nucleon transfer (MNT), fission, quasi-fission or fusion reactions. Possible upgrades can be applied to the detection setup around the target and at the focal plane. These are reviewed in this section and sketched in Fig. 2. Further major upgrades of PRISMA, in particular for the study of transfer reactions with radioactive ion beams, will be discussed in Sect. 8.1.1. In Sect. 8.2.1, the foreseen upgrades of the MAGNEX magnetic spectrometer at LNS are reported.

Full tracking around the target Currently, the scattering angle of the reaction products is measured with a micro-channel plate (MCP) detector placed inside the target chamber upstream of the first magnetic element [145], under the assumption that the reaction occurred at the center of the target. The installation of a second MCP detector, as shown in Fig. 2 left, would allow the determination of position and angle of the scattered particles, achieving a full tracking at the target position. This is particularly important when using extended targets such as gas cells or very heavy beams that can be defocused to limit the density of power released on target.

The study of certain reaction channels, such as transfer-induced fission in inverse kinematics, requires not only the measurement of the scattered beam-like products but also the detection and identification of the recoil target-like particle. Multilayered stripped silicon detectors covering a large solid angle are an efficient solution when the transfer occurs on light target ions ($Z \leq 10$). Commercial annular double-sided strip silicon detectors (DSSSD) or custom ensembles built with trapezoid/wedge-shaped layers can be arranged in fixed configurations to perform ΔE-E measurements for particle identification, as well as the tracking needed to obtain the recoil angle. With these observables, the corresponding partner in the transfer reaction (the fissioning system) can be fully characterized. This allows, for instance, the measurement of the excitation energy of the fissioning system in inelastic and transfer-induced fission reactions [146].

In reactions where the angle between products is too small to allow the detection of one particle in PRISMA and the other one in a detector placed in the target chamber, or when both products are heavy enough, the use of a second arm in kinematic coincidence with PRISMA can be the ideal solution. While it is not possible to build a second full-fledged spectrometer, a reduced version can give enough information to complement that of PRISMA. A detector including a position- and time-sensitive detector (MWPPAC) followed by a Bragg chamber for Z identification has been already built and commissioned [147]. Depending on the distance between this setup and the target position, a rough estimation on the mass of the second product could be obtained, as well as the emission angle and the identification of the atomic number. This was demonstrated in the analysis of the multi-nucleon-transfer reaction ^{130}Te+^{197}Au [148] at 1.07 GeV in inverse kinematics, where a matrix correlating the mass of light and heavy transfer products could be constructed. This matrix allowed to quantify, as a function of the number of transferred neutrons, the contribution of secondary processes, such as neutron evaporation, to the survival probability of the heavy reaction partner. An important upgrade of this second arm would be the possibility to couple it to γ-ray arrays and to rotate it continuously around the target to accommodate as much as possible the folding angle in laboratory of both products. In addition, the geometrical acceptance should be similar to that of PRISMA in order to reduce any loss in statistics when requiring the kinematic coincidence.

In order to house these ancillary setups, the target chamber would need to be redesigned while retaining the rotation capabilities of PRISMA and the coupling to γ-ray spectrometers such as AGATA [149].

Possible upgrades at the focal plane The detector setup at the focal plane of PRISMA consists of a position-sensitive MWPPAC detector [150] that measures the position and ToF of the particle at a fixed distance from the entrance of PRISMA and, together with the reconstruction of the flight path, allows to deduce its magnetic rigidity. Currently, this allows for a relatively accurate identification in mass (up to $A \sim 140$) and atomic charge state. An improved ion trajectory reconstruction, through the use of transport matrices or with a full tracking, where azimuthal and polar angles at the focal plane are measured by means of a second position-sensitive detector placed at the exit of the dipole, can improve the performance of PRISMA in terms of mass (up to $A \sim 200$) and atomic number identification. However, the characteristics of this detector must be compatible with the low energies of the ions normally detected in PRISMA.

Currently, the precision of the energy loss measured along any of the rows of pads in the existing ionization chamber (IC) [150] is somehow affected by the incident angle of the particle, which modifies the effective length of the path traveled by the particle in the chamber. The measurement of the direction of the particle at the focal plane would help remove this effect and obtain the energy loss for the same effective depth for all particles. This could also be achieved by measuring the x and y position of the ions in the IC. The y position can be deduced by measuring the electron drift time while, for the x position, the use of a segmented anode is necessary and would represent a major upgrade of the current IC design.

Besides the developments so far outlined, intrinsic upgrades of the PRISMA detectors can be planned in the next years. For instance, a replacement of the current MWPPAC with a more efficient one for light ions and the use of gases with higher stopping power (C_3F_8) than those normally employed in the IC (CH_4 and CF_4) can increase significantly the limits of detection of PRISMA and make the study of new physics cases possible (see also Ref. [151]), also in view of the forthcoming experimentation with SPES beams.

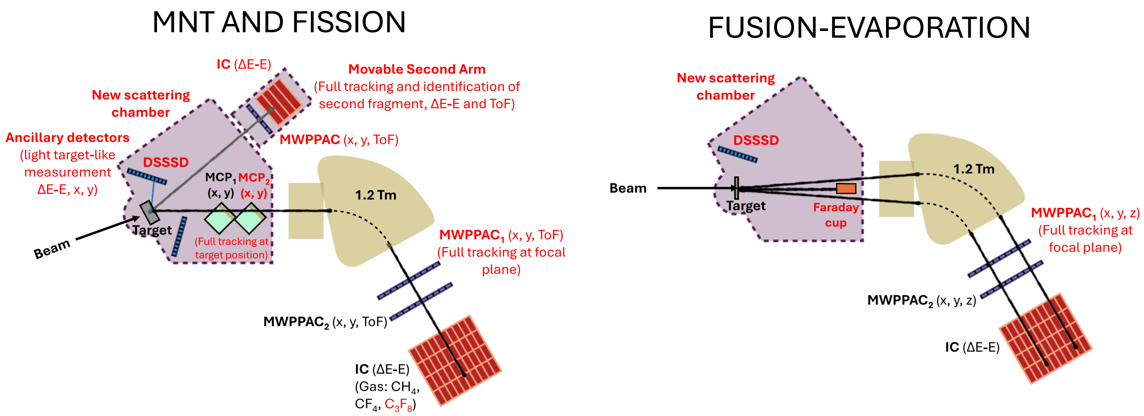

Fig. 2 (Left) Sketch of the upgrades proposed in Sect. 3.4.1 for the PRISMA magnetic spectrometer for MNT and fission studies. (Right) Layout of the PRISMA spectrometer in the zero-degree configuration for fusion-evaporation studies. In both figures, shape and dimensions of the scattering chamber are not meant to be realistic. The items indicated in red represent new upgrades not currently present on the spectrometer

The PRISMA spectrometer at zero degrees for fusion-evaporation studies The magnetic spectrometer PRISMA can be used in vacuum to perform measurements of fusion-evaporation reactions at angles very close to 0°. The beam intensity should not exceed $\sim 10^5$ pps to protect the focal plane detectors. The direct beam will be stopped in a Faraday cup (see Fig. 2 right), while the evaporation residues (ER) produced in the angular range $\theta \simeq 2° - 5°$ will be analyzed by PRISMA and detected at the focal plane. Once again the installation of a second position-sensitive MWPPAC detector (MWPPAC$_1$ in the figure) near the exit of the dipole magnet will allow the full tracking of the ions despite the need of removing the MCP detector presently installed 25 cm downstream of the target.

A further possibility, allowing the use of higher intensity beams, is moving upstream the target position by $1.5 - 2$ meters, and installing in front of PRISMA a Wien filter to separate the beam particles from the ER. Otherwise, the setup may remain the one sketched in Fig. 2 left, with the advantage of including 0° in the range of measurable angles, and the possibility of re-installing the MCP detector in its present position.

This configuration of PRISMA at 0° will allow interesting studies of nuclear structure on the proton-rich side of the nuclear chart, by combining the spectrometer with last-generation γ-ray arrays, both with stable and exotic beams.

3.4.2 The ToF spectrometer TOSCA

The FORTE collaboration has been established to study the role of shell effects in heavy-ion induced reactions aimed at the production of nuclei very rich in neutrons populating the so-called Terra Incognita and for the synthesis of super heavy elements. The processes under scrutiny are: (1) binary-fission modes and ternary fission of heavy and superheavy nuclei; (2) multi-nucleon-transfer reactions populating exotic neutron-rich species in the unknown nuclear chart regions, including those of astrophysical interest. The collaboration operates in several laboratories such as LNL, JYFL and GSI.

A time-of-flight spectrometer coupled, whenever required by the experimental aim, with charged particles, neutrons and gamma-ray detectors, is the main device used to pursue the research program. The basic elements of the ToF spectrometer are two pairs of arms placed on opposite sides with respect to the beam axis centered on the same reaction plane. Each arm is equipped with a start and a stop detectors to measure the velocity vectors of fragments with a spatial and time resolutions of about 1 mm and 180 ps FWHM, respectively. Correlating angles and ToF of both reaction fragments, the primary mass and energy of binary fragments are reconstructed imposing momentum and energy conservation laws [152, 153].

The small dimensions and the versatility of the arms make the ToF spectrometer a portable solution that can be easily integrated in different existing facilities [7, 154–156]. By mounting the arms in different angular configurations, large range of mass asymmetries of the fission fragments can be covered, making it suitable for the investigation of a wide variety of nuclear reactions [157, 158].

A new conceptual modular design of the detector unit acting as start and stop detectors has been recently developed by the FORTE collaboration at Napoli INFN for TOSCA (Time-Of-flight-sub-nano-second Spectrometer for Charged radiation Applications). This new design represents an upgrade of the largely used CORSET setup [152]. TOSCA unit has a triangular trapezoidal shape, as shown in Fig. 3 left. A thin Mylar layer facing the target is mounted orthogonally to a sandwich of two MCPs in chevron configuration assembled with an active area of $70 \times 90\,\text{mm}^2$. These two faces are connected by an oblique plane made of a grid of wires acting as electrostatic mirror. The X and Y coordinates at which the ions cross the conversion foil are reconstructed by combining 4 position signals (X_L, X_R and Y_U, Y_D). In Fig. 3 right, a position matrix obtained with a TOSCA unit irradiated by an alpha-particle source is shown.

The main advantages of TOSCA spectrometer, with respect to previous one belonging to the FORTE collaboration [7], are the modularity, the sensitivity to the position of all the detector units and the low-energy and angular straggling. Small degradation of

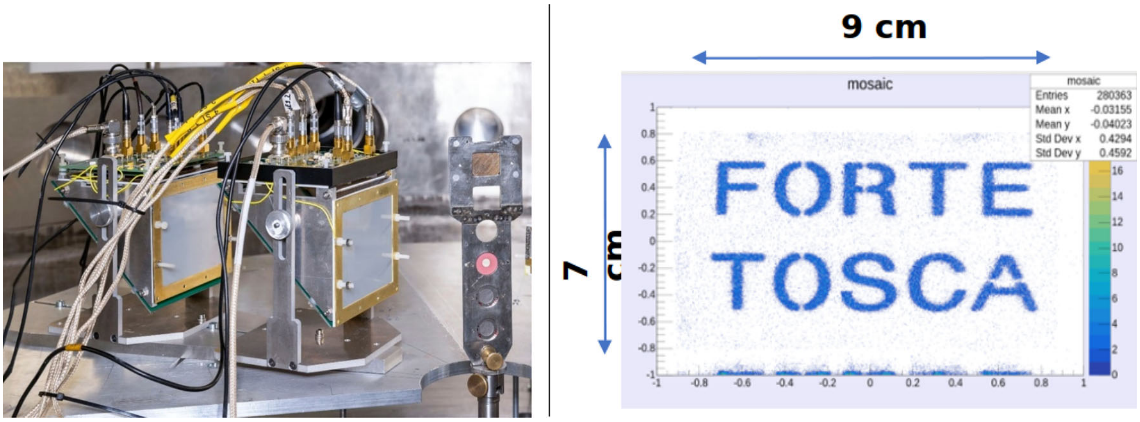

Fig. 3 (Left) A TOSCA arm, made of two units, as mounted inside the Large Scattering Chamber at Accelerator Laboratory of University of Jyväskylä. (Right) Two-dimensional spectrum of coordinates X and Y obtained using an alpha-particle source (^{241}Am) and placing in front of a TOSCA unit a mask with 3-mm-width letters and 1-mm-width lines in O, R and A

the resolutions caused by large beam spot sizes, thanks to measurement of impact positions in both start and stop detectors, and high radiation hardness, thanks to the use of emittive foils instead of direct implantation in the detector, are additional assets of the device. In a test experiment, performed at the Accelerator Laboratory of the Department of Physics (JYFL) of the University of Jyväskylä in May 2022, to study the ^{40}Ar+^{208}Pb reaction at beam energy of 200 MeV, a mass resolution of 3-4 amu was obtained, in line with the state-of-the-art ToF spectrometer.

Typical reaction studies explore the dynamical evolution of the composite system with long lifetimes compatible with those of compound nuclei using different variety of probes [159–162] or need to separate the binary products of fast reactions (e.g., deep inelastic and quasi-fission) from those of fission [163, 164] to get insight on the scission point configuration, e.g., deformation, mass asymmetry and dissipated energy. The direct detection of both fragments of the binary reactions provide valuable information concerning the process kinematics, as the angular, Total Kinetic Energy (TKE) and fragment mass distributions [165, 166]. In this context the mass-TKE distributions represent a very sensitive observable used to study the intensity and nature of nuclear viscosity [157, 167], the competition of different fission modes [168–170] and the production rate of neutron-rich nuclei [153].

Several upgrades of the setup are ongoing, involving the construction of arms with larger angular coverage and solutions aimed at the identification of the atomic mass of fragments and suited for higher intensity and pulsed beams. These solutions take advantage of the use of the modular and passing through TOSCA units and can be realized with the use of multi-ToF arm coupled with ΔE-E telescope array and a new data acquisition system based on sampling electronics for pulsed beams/higher rates.

3.5 Zero-degree detection for RIB delivered by SPES

In forthcoming years, at the SPES facility at LNL, neutron-rich radioactive ion beams (RIBs) of masses A $\sim$ 100 are expected to be re-accelerated at energies of 5-10 MeV/u. In experiments employing RIBs, it is extremely important to characterize the beam composition and to separate the reaction products from the unreacted beam. Mandatory requirements for the detectors used for this aim are the minimization of energy losses in the detectors, the maximization of efficiency and transmission and the capability to sustain beam rates of $\sim 10^5$ pps.

Taking inspiration from existing detectors in ISOL and in-flight RIB facilities, we propose possible solutions and developments suited for the energies, masses and physics opportunities that are specific of INFN-LNL and, in particular, of SPES.

3.5.1 Advanced detection systems for evaporation residues

Unexpected phenomena might show up from studies of fusion reactions with exotic beams; in particular, systematic experimental investigations of the role of transfer in fusion are required. An experimental activity in this field will be made possible by exploiting selected neutron-rich beams produced by the SPES facility. Typical interesting beams are ^{96}Sr, ^{94}Kr and heavier ones like ^{134}Sn, ^{136}Te. All these beams will be provided with intensities in excess of 10^5 pps. The beam quality (stability, energy definition and size of the spot on target) and its purity are essential for fusion experiments below the Coulomb barrier.

The intensity of those beams will allow placing a detector system right along the beam path and detecting the forward-peaked ER distribution with almost 100% efficiency. Obviously, the detectors shall be able to withstand high counting rates and one has to filter out the overwhelming beam-like background.

Figure 4 shows the setup proposed for such experiments. The full detector telescope, including three micro-channel plate (MCP) detectors, can be used at 0° for beam intensities up to $10^4 - 10^5$ pps [171]. For higher intensities, it can be installed downstream of the electrostatic deflector of LNL, or of any other device capable of beam rejection.

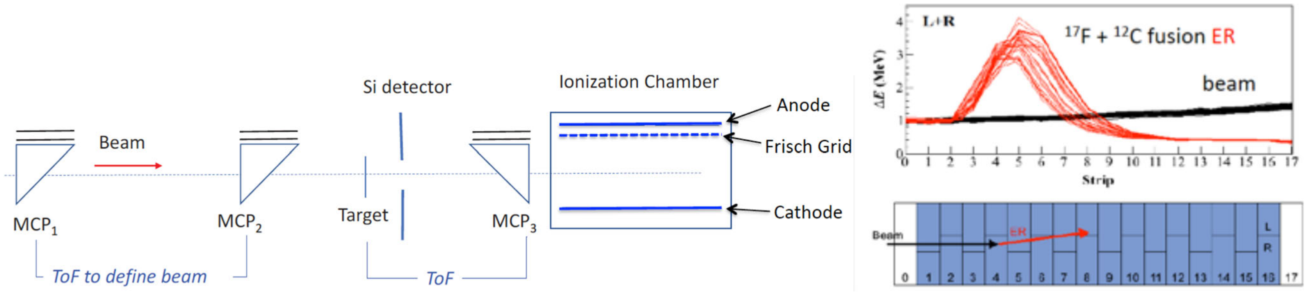

Fig. 4 (Left) Layout of the proposed setup including three micro-channel plates (MCP) detectors, the (external) target, the annular Si detector and the ionization chamber (IC). (Right) Different signals coming from beam particles (black line) and fusion events (red line). Below, the layout of the segmented anode is reported. The figures on the right are taken from Ref. [172]

An ionization chamber with a multi-sampling anode can be used either with stable or exotic beams. The structured anode geometry allows the separation of fusion events from beam particles, getting inspiration from the design of the MUSIC detector [172, 173].

As a complementary tool to the external target depicted in Fig. 4, the IC can work as an active target detector measuring the energy loss of beam ions and fusion-evaporation residues produced in the interaction of the beam with the nuclei of the filling gas. The ER will experience much higher energy loss inside the chamber gas. As a consequence, fusion events will produce a peaked signal in the detector, while beam particles will gradually lose energy throughout the chamber. Being segmented, the chamber will also allow to determine the position where the reaction takes place. Since the beam energy decreases moving forward in the chamber, the fusion excitation function can be measured with a single beam energy.

MCP$_1$ and MCP$_2$ (position-sensitive) will monitor the beam quality, rate and energy and give a timing reference. The ToF between them, together with the ΔE IC signal, will enable rejecting beam contaminants [173]. This is particularly important when using exotic beams at sub-barrier energies. The ToF between MCP$_2$ and MCP$_3$ will select the ER, exploiting their lower velocity with respect to the beam ions crossing the target without interaction. Fusion events will be additionally identified in the IC by ΔE-E measurements. An annular silicon detector installed between the target and MCP$_3$ will detect ER at angles larger than $\sim 4°$. We point out that this setup will be very useful also for fusion studies with the light exotic beams produced by the SPES facility.

3.5.2 Zero-degree detection for direct reactions

Direct transfer reactions, where one or few nucleons are exchanged between projectile and target, represent an extremely powerful tool to study the structure of atomic nuclei and to investigate a large variety of astrophysical scenarios. With the use of RIB, such reactions may be performed in inverse kinematics, with the heavy (radioactive) beam impinging on the light target. For this reason, the energies and masses of the heavy transfer products are very close to those of the beam ions, so the combination of several tracking detectors giving (X,Y,ΔE,E_{tot},ToF) information is needed to distinguish the reaction products from unreacted beam ions and to perform the full event reconstruction. The possible use of a magnetic spectrometer like PRISMA at zero degrees for this kind of reactions will be discussed in Sect. 8.1. Here we shall focus on other types of detectors that could provide the desired information.

The main contribution to the background in the particle and γ-ray spectra is usually provided by fusion-evaporation reactions on C and O atoms present in most standard targets or on the windows of common cryogenic targets. A simple ToF determination of the reaction products is often sufficient to eliminate a large fraction of this background. In some cases the full identification of the reaction products in Z and A is instead necessary to have full control on the reaction dynamics [174].

Even when dealing with ISOL beams, which normally have spot sizes of few mm, the reconstruction of the beam impact position and angle on target can be of extreme importance. This is particularly true if cryogenic targets, which may present significant window deformations [175], are employed. Moreover, the measurement of the impact angle of beam ions on target has important consequences not only on the reaction excitation energy resolution but also on the extraction of transfer angular distributions.

As proposed in Sect. 3.5.1 and shown in Fig. 4, trajectory and impact position reconstruction on target can be obtained with two beam trackers upstream of the target, providing also a ToF measurement for beam identification. A configuration of the tracking detectors with a magnetic field spiralizing the electrons from the emittive foil toward the MCP should be applied in order to maintain a good position resolution ($\sim$ 1 mm). Such detectors could be developed following the design of the entrance detector of PRISMA [145].

The determination of the scattering angle and ToF of the heavy ejectile, correlated with the scattering angle and energy of the light recoil measured in a Si array-like GRIT (see Sect. 3.6.1), can select in a univocal way the reaction kinematics of interest and reduce the background due to other reaction channels, such as fusion-evaporation and break-up. These quantities can be measured placing an additional MCP, with characteristics similar to the beam trackers, after the target.

The energy loss ΔE of the heavy ejectiles can be measured in an IC designed to sustain high beam rates of 10^5 pps. Following the design proposed in Ref. [176], it could consist of several gaps of $\sim$ 2 cm length filled with gas, with alternating cathodes and anodes to reduce the electrons and ions drift time, as depicted in Fig. 5. To reduce the recombination of the ion/electron pairs the cathodes

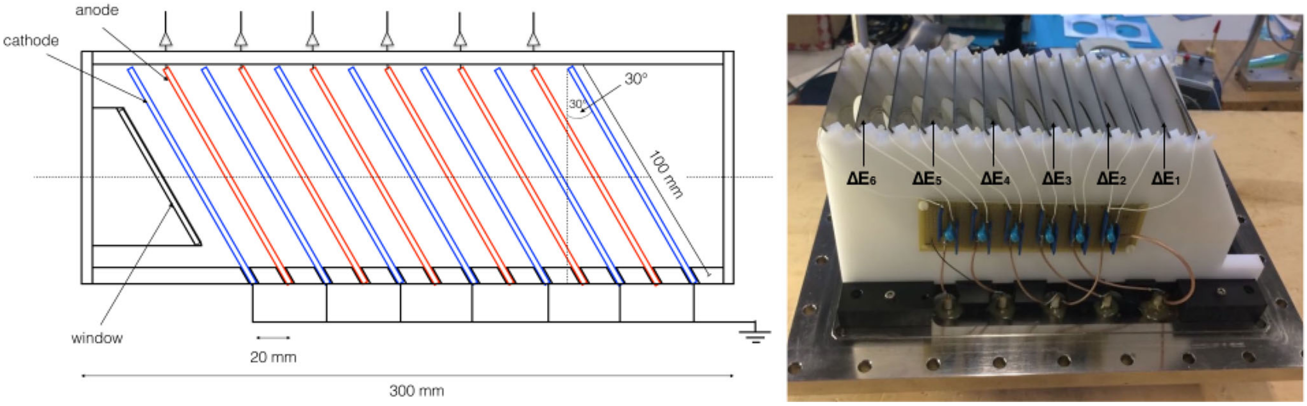

Fig. 5 (Left) Sketch of the tilted-electrode fast ionization chamber. (Right) A photograph of the prototype built at LNL. Taken from Ref. [177]

and anodes of the chambers must be tilted. A prototype has been already built and commissioned with good results at LNL [177]. In this configuration without Frisch grid, the IC signal is influenced by both electrons and positive ions. Charge preamplifiers (PACs) are generally used to have good signal-to-noise (S/N) ratio but the ion current is so low that only the electron current is significantly contributing to the measurement. For this reason, the operating point of this chamber is around 1 V/cm/mbar in isobutane (C_4H_{10}) and even lower in CF_4, to have low electron velocities measurable by a PAC, at the expense of a faster charge collection. A solution to improve the counting rate would be to design a current amplifier with high gain to be able to increase the electric field and remove the ions more rapidly while being able to measure the fast electron current. Moreover, with respect to the existing design described in Ref. [177], an increase in the transmission could be achieved reducing the number of wires of the electrodes and increasing the space between them from 1 to 2 mm.

To minimize the amount of material traversed by the heavy ejectiles, a position reconstruction in the IC could be considered, with anodes composed of electrically isolated wires [178]. Two of these position-sensitive anode grids can be rotated by 90° one with respect to the other to get (X, Y) coordinates. However, the current designs use individual electronics channels with PAC to have a good S/N ratio, but this limits the working points of the IC, as mentioned before. A possible solution, which would require a dedicated study, is the use of delay lines with good current amplifiers.

3.6 Segmented silicon detectors

As anticipated in Sect. 3.5.2, with the advent of the SPES facility at LNL, direct transfer reactions in inverse kinematics with RIB will be widely exploited for the study of a large number of physics cases, from nuclear structure to reaction mechanism and nuclear astrophysics [1]. To cope with the low beam intensities and the kinematic compression due to the inverse kinematics condition, high efficiency and high angular resolutions are needed for the detection of the light recoils [179]. In Sect. 3.6.1 we will describe the main challenges for the design and construction of such an array and its coupling with other detectors, in particular γ-ray arrays.

The coupling of segmented Silicon arrays and γ-ray detectors can find applications also in the study of fusion reactions at extreme sub-barrier energies, in particular for studies of astrophysical interest. The possibilities offered by such coupling will be outlined in Sect. 3.6.2.

3.6.1 GRIT for direct transfer reactions at SPES

GRIT, which stands for Granularity, Resolution, Identification and Transparency, is a project aiming at the construction of a new generation silicon array for the study of exotic nuclei through direct reactions. Achievements made over the last decades with resistive strips array, such as TIARA [180, 181] and T-REX [182], and then by highly segmented silicon arrays, such as MUST2 [183] and SHARC [184], demonstrated the capability of such devices to deliver a large number of observables on a wide range of exotic nuclei. The most relevant observables are transfer differential cross sections, excitation energy of the reaction products and decay branching ratios.

The GRIT concept is based on bringing together the success of different systems: the high-granularity and particle identification capability of MUST2, combined with the ability to measure simultaneously different reaction channel of the MUST2-TIARA combination, as well as the transparency of TIARA, SHARC and T-REX to perform particle-γ coincidences.

To this end, GRIT is designed as a 4π array of double-sided silicon detectors (DSSD). The sphere is paved with a combination of trapezoidal, square and annular detectors. In particular, in the forward hemisphere the detectors are composed of 3 layers to stop energetic light charged particles, while in the backward hemisphere and in the ring at 90° there are 2 layers. The total number of strips to read is approximately 7000. The outer diameter of the silicon array is designed to fit inside the state-of-the-art HPGe tracking array AGATA [149], allowing unmatched resolving power in γ-ray spectroscopy.

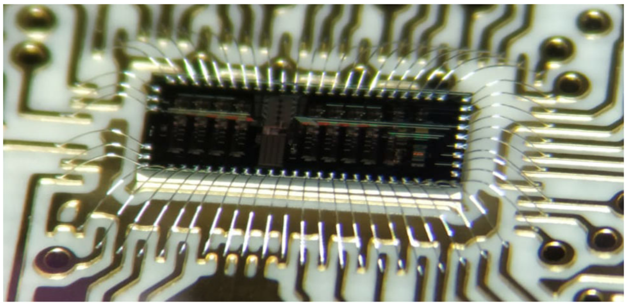

Fig. 6 Microphotograph of the custom-designed ASIC preamplifier developed for the GRIT array

The large inner diameter of the AGATA array allows the positioning of the detector at an increased distance from the target than what was possible with EXOGAM [185] or TIGRESS [186] in the case of TIARA and SHARC, respectively. This results, for the target-like charged particles, in a longer flight path of 165 mm from the target to the detectors, which is normally sufficient to obtain identification of their mass via E-ToF correlation when they stop in the first layer of the telescopes. In addition, the silicon wafers are chosen to be doped by neutron Transmutation Doping (nTD), resulting in a very uniform response across the active area of the detector. This allows the use of Pulse Shape Analysis (PSA) to discriminate, both in charge and mass, particles stopping in the first layer of the telescope [126]. The use of PSA is especially important for the study of neutron-rich nuclei via (d,t) and (d,^{3}He) pick-up reactions, as both concurrent channels produce low-energy $A = 3$ particles [187]. Such technique gives an improved discrimination of low-energy particles than the use of thin detectors and the E-ΔE methodology.

The total requirement of a high granularity, 7000 channels to read with digital electronics, operating under vacuum, remaining mostly transparent to γ-rays and fitting inside AGATA, is of course a major challenge that requires a few technology breakthroughs.

A major one is the design of an analog memory [188, 189] capable of sampling detector signals at 200 MHz with an Effective Number of Bits (ENOB) of at least 10. This memory allows for the sampling of many channels in parallel and the digitalization with a limited number of ADCs placed directly on the Front-End Electronic (FEE). The result is a drastic decrease in the number of electronic components, and a very small number of signals coming out of the chamber. The GRIT collaboration started working toward this goal with the design of the PLAS ASIC, a 32-channel, dead-time-free analog memory. Originally designed by the University of Valencia, two versions have been produced and tested so far. The continuation of the work at LPC Caen is now converging toward the design of a fully functional ASIC, which should be achieved in the coming couple of years.

Another key development for the GRIT array is focused on integrated preamplifiers whose energy range is not limited by the output voltage dynamic range of the circuit. This result is achieved with the so-called Fast-Reset technology [190]. Using a time-over-threshold technique [191], we can perform high-resolution spectroscopy up to an energy that is more than one order of magnitude larger than the natural saturation limit of the preamplifier.

The circuit that implements this technique has been integrated in a custom-designed ASIC preamplifier [192, 193] realized in AMS C35 technology (see Fig. 6) and extensively tested [194, 195]. This ASIC integrates an analog implementation of the time-over-threshold algorithm [196] and is able to produce, for over-threshold signals, analog pulses with amplitude directly proportional to the energy deposited in the detector [197] that are insensitive to baseline fluctuations.

In general, these techniques, aimed at the energy-range extension of the FEE, will be particularly useful for the readout system of the third thick silicon layer. In such detectors the stopping of particles with energy way above 40 MeV, which is the nominal saturation threshold of the ASIC preamplifiers, is foreseen.

This ASIC requires an external discrete 1 GΩ resistor as continuous feedback discharge device. With the goal of maximum miniaturization, research has been carried out on the possibility to substitute such resistor with integrated structures [198]. In particular, the possibility to use integrated polysilicon resistors has been evaluated [199] and an extensive research on the noise produced by such structures has been carried out [200, 201].

Since a high number of channels is foreseen in the GRIT array, the ASIC preamplifier was developed keeping the minimization of the power dissipation as the priority: as a matter of fact, each channel accounts for 11 mW only.

The FEE cooling is realized with selective laser sintering (SLS) 3D printing technology and designed for minimum shadow on AGATA crystals.

The mechanical chamber housing detector, front-end board (FEB) and cooling system is already designed and prototypes cooling block are being tested to validate the performance of the cooling circuit.

The design of the FEB is ongoing and includes power and bias distribution, a pre-amplification stage followed by the analogue memory and digitization via an onboard ADC. Slow control of the electronic and readout of the ADC are carried out by an embedded Complex Programmable Logic Device (CPLD). All data are readout via an LVDS differential pair through Ethernet protocol to the FASTER Back-End Electronics (BEE) outside the chamber. The in-beam commissioning of ASIC preamplifiers is foreseen in a near future.

Possible long-term area of R&D is the use of AC-coupled detectors instead of DC-coupled ones, a technology currently employed mostly for trackers, with decoupling capacitance integrated inside the detector silicon wafer. Such solution allows to save space on the FEE boards while avoiding DC current to flow to the input node of the preamplifiers. Once the GRIT array will be completed, an R&D program to produce and test a telescope using such technology could allow a long-term upgrade of the array.

3.6.2 Gamma-particle coincidences for fusion reaction studies

Heavy-ion fusion reactions are essential to investigate the fundamental problem of quantum tunneling of many-body systems in the presence of intrinsic degrees of freedom. Such reactions are a topic of continuing interest in the study of nuclear reactions. Moreover, the fusion of light systems far below the barrier has much relevance also in the field of astrophysics and the phenomenon of fusion hindrance may have important consequences for stellar evolution.

Experiments for the measurement of very small fusion cross sections can be performed at LNL in the next two years, using the technique of γ-ray charged particle coincidences at the combined setup of AGATA + S1 annular DSSD. The high θ and ϕ resolution of the front and back sides, respectively, of this DSSD detector makes it ideal for the identification of energy groups of evaporated protons and α particles from the compound nucleus (CN), populating discrete states in the residual nuclei. This is especially useful in the study of medium-light systems, where neutron evaporation is not a dominant part of the fusion-evaporation cross section.

The first experiments using this technique were performed at Argonne where Gammasphere [202] was put in coincidence with a compact array of three annular double-sided silicon strip detectors located inside the target chamber, to measure $^{12}\mathrm{C} + ^{12}\mathrm{C}$ fusion at very low energies [203]. Cross sections down to 6 nb were measured.

3.7 Nuclear emulsion films

The detectors based on nuclear emulsion films have contributed to many important achievements and discoveries in fundamental physics. In the recent past, thanks to the advances in high-speed automated scanning and to the development of novel emulsion with grains at the nanometric scale, the emulsion detectors technique has experienced a renewed interest in experiments for Dark Matter search and for studying neutrino physics [204–208]. In nuclear physics, too, nuclear emulsion detector has a strong appeal due to their compact setup integrating the target and the radiation-sensitive region able to provide an high spatial and angular resolution in reconstructing the particles interactions. The FOOT (FragmentatiOn Of Target) experiment is an international project designed to carry out the fragmentation cross-section measurements relevant for Charged Particle Therapy (CPT), a technique based on the use of charged particle beams for the treatment of deep-seated tumors [209]. The experiment aims to measure the target fragmentation induced by proton beams in the human tissues in the energy range relevant for therapeutic applications ($150 - 250\,\mathrm{MeV}$). The micrometric range of generated fragments forces the use of detection techniques based on an inverse kinematic approach to calculate the target fragments production cross section, in which a primary beam (carbon or oxygen) impinges on targets made of carbon and hydrogen-enriched carbon materials (C_2H_4). From their linear combination, the cross section on hydrogen is derived.

FOOT is based on two complementary setups: a magnetic spectrometer, covering a polar angle acceptance up to about 10° with respect to the beam axis, for fragments $Z \geq 3$, and an emulsion spectrometer, to measure light fragments ($Z \leq 3$) up to 70° with respect to the beam axis. The emulsion spectrometer is composed by three different sections, as shown in Fig. 7. The vertexing region, consisting of 30 emulsion films interleaved with layers of target material (C or C_2H_4), is aimed to reconstruct the interaction vertices between the primary ions beam and the target. The charge identification region, composed by 36 emulsion films, identifies the charge of the fragments produced by the interaction. The Momentum Measurement region, consisting in a sequence of about 80 emulsion films and passive materials with increasing stopping power, is dedicated to measure the fragments momentum on the basis of the range and Multiple Coulomb Scattering methods [210]. The combination of these two independent methods for the energy and momentum estimation, in addition to the charge identification performed in the second detector region, opens up the opportunity for isotopic identification of fragments produced in a specific interaction event [211].

Nuclear emulsion films consist of two $70\,\mu$m thick sensitive emulsion layers deposited on both sides of a $210\,\mu$m thick plastic base, resulting in a total thickness of $350\,\mu$m. AgBr crystals, dispersed in the gelatine matrix forming the emulsion layer, are sensitive to ionizing particles and keep memory of their trajectory. Their sensitivity corresponds to 30 grains over a track length of $100\,\mu$m for a Minimum Ionizing Particle (MIP).

The AgBr crystals are sensitized by charged particles crossing the emulsion layers; a chemical development turns the latent image into a sequence of dark silver grains that during the scanning with an automated microscope, are recognized as aligned clusters of dark pixels. A sequence of aligned clusters in different emulsion films allows to reconstruct the particle trajectory inside the detector (see Fig. 8), with an accuracy of about $0.3\,\mu$m in position and 1.2 mrad in angle.

The realized emulsion spectrometers have been exposed to ^{16}O ion beams (200 MeV/n and 400 MeV/n) at the GSI facility in Darmstadt (Germany). Some results of the interaction vertices reconstruction (see Fig. 9) and of the charge identification of the fragments are presented here.

In nuclear emulsions, the process of charge identification is related to the possibility of expand the dynamic range of the emulsion film response by inducing a controlled fading [212–214].

The grain density along particle trajectory is proportional to the particle energy loss over a certain dynamic range: Highly ionizing particles, such as the ion beams and their fragments considered here, induce a saturation effect that is removed by keeping the emulsion films for 24 h, at temperatures above 28°C with a relative humidity higher than 95%.

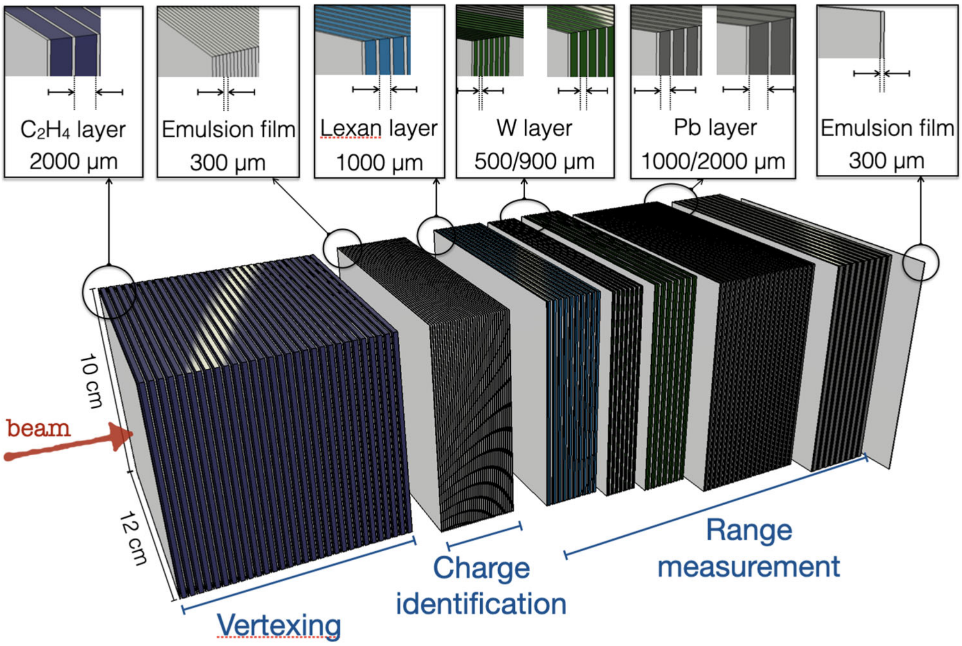

Fig. 7 Scheme of the FOOT emulsion detector

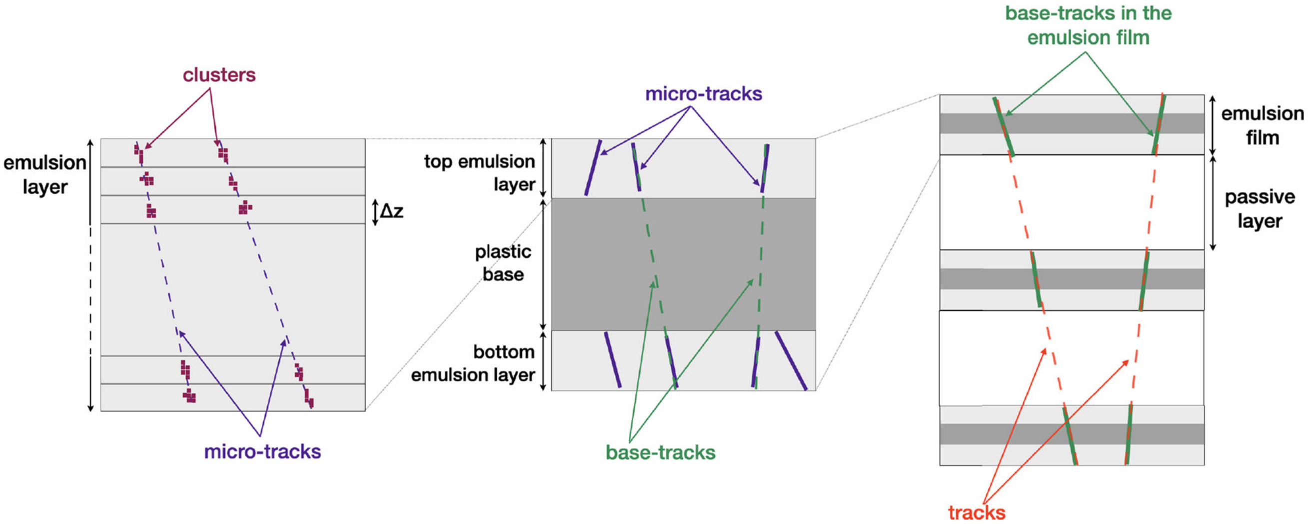

Fig. 8 Schematic drawing of a tracks reconstruction: different tomographic images, grabbed at equally spaced depth levels through the sensitive layer (left), micro-tracks association between two emulsion layers to form a base-tracks (center) and base-tracks association to form a track

For each particle track, a variable named “volume” is defined as the sum of pixel brightness and it is related to the particle ionization. Combining volume variables it is possible to identify the fragments charge on the basis of two interrelating methods: a “cut-based” method to separate cosmic rays and fragments with $Z \leq 2$ and a principal component analysis (PCA) for the identification of fragments with $Z \geq 2$. Table 3 shows how the charge of the produced fragments is distributed [215].

It is under investigation the possibility to use a new generation of nuclear emulsion films, called Nano Imaging Tracker (NIT), whose improved spatial resolution will allow the fragmentation measurement in direct kinematic approach [216, 217]. NIT is emulsions films having grains at the nanometric scale that allow to detect particles tracks lengths shorter than 100 nm. The AgBr crystals are about 40 nm diameter and the average distance between two neighboring ones is about 70 nm.

3.8 Time resolution of diamond detectors with graphite electrodes

Diamond has been studied for decades as an ideal semiconductor to obtain extremely radiation hard radiation detectors. It has been considered for the fabrication of sensors in various fields [218, 219] including experiments in high-energy physics [220], clinical dosimetry [221], detection of neutrons [222] and deep UV radiation [223, 224]. The most interesting characteristics of diamond are: the high saturation velocity and high-charge carrier mobility which make them very suitable for timing detectors [225]; the low dark

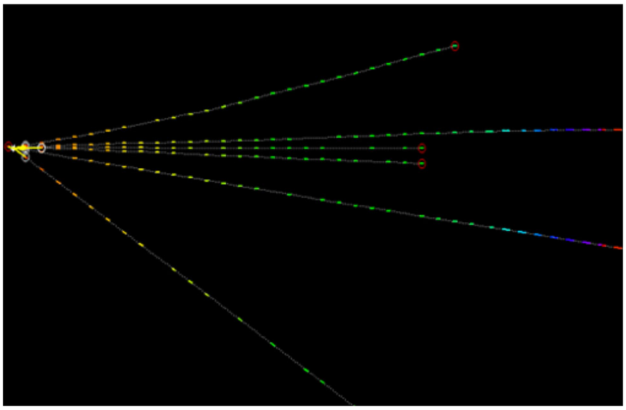

Fig. 9 A typical example of a reconstructed vertex obtained from the interaction of ^{16}O at 200 MeV with C_2H_4target; the colored segments of each fragment track represent the signal registered by the emulsion film

Table 3 Charge identification at 200 MeV/n

Z	Cut-based	PCA	Total	%	Stat. Err. (%)	Syst. Err (%)
1	23754	–	23754	69	0.6	5
2	715	5861	6576	19	1.2	2
3	–	3093	3093	9	1.8	2
> 3	–	1029	1029	3	3.0	1

current ($\sim$ pA/cm^2) and a relatively low dielectric constant that increase the signal-to-noise ratio; the high thermal conductivity and full transparency to visible light which allow to operate them without cooling [226] and light shielding. In addition diamond has been demonstrated to be extremely radiation hard [227, 228]. The main drawbacks of diamond as a detector material are the large bandgap which significantly reduces the amount of charge generated by Minimum Ionizing Particles in diamond with respect to silicon and the difficulty to produce large-size single-crystal samples. Although relatively large samples of polycrystalline diamond can be obtained, the charge collection efficiency can be strongly degraded by crystalline defects, reducing the usefulness of this material as a detector.

In more recent years, micro-fabrication of electrodes by laser graphitization of the crystal bulk [229] enabled the construction of 3D diamond detectors [230–232] that showed excellent detection properties [233] as well as very promising results on radiation hardness [228].

Only very recently, however, 3D diamond detectors were considered and systematically studied for timing applications, within the Timespot[3] collaboration [234]. The 3D geometry, reducing significantly the charge collection path, allows to reach excellent time resolutions making 3D diamond detectors ideal candidates for 4D tracking systems [235] at future accelerators. In addition, the shorter collection path, makes the 3D configuration much more radiation resistant than the planar geometry [228].

3.8.1 Fabrication of 3D diamond sensors

The 3D diamond sensors are built by fabricating conductive electrodes (or *columns*) in the bulk of mono- or polycrystalline chemical vapor deposition (CVD) [236, 237] diamonds. In Refs. [232] and [234] the electrodes were obtained by laser graphitization of the diamond with an 800 nm Ti/Sapphire laser with 50 fs pulses focused inside the bulk of 500μ m-thick single-crystal CVD (scCVD) diamonds. Diamond is transparent to 800 nm light, but a sufficiently high light density can result in multiple-photon interactions causing energy absorption through large-bandgap transitions which induce a phase transition from crystalline to mixed carbon phase including graphite. Sufficiently short pulses prevent annealing of graphite into amorphous carbon which is not conductive. To ensure an optimal laser beam focusing, spherical aberrations due to the high diamond refractive index were corrected with a Spatial Light Modulator (SLM) [232, 238]. According to Refs [239, 240], the generated graphite is concentrated in thin domains embedded in the crystal lattice. Due to this underlying structure, the resistivity of the graphitized electrodes can be rather large which can result in resistances of the order of $10^5 - 10^6\Omega$ for 500 μm-long electrodes. The high resistivity of electrodes immediately deteriorates the timing properties of the sensors because output signals are attenuated and slowed down. Therefore, particular care has to be paid in order to keep the electrode resistance as low as possible for timing applications [241]. Recently, several diamond sensors with 32×32, 55×55 μm pitch pixels were fabricated and bump-bonded to a 28-nm timing ASIC [242, 243] (Fig. 10).

Prototypes of 3D diamond pixel sensors have been tested with electrons from a ^{90}Sr electron source and with 180-GeV pions at CERN's SPS-H8 test beam [241, 244, 245]. The measured time resolution shows a dependence from the signal amplitude fully consistent with the estimated electronics noise of the readout chain. An asymptotic time resolution of $\sim$ 80 ps has been obtained,

---

[3] Timespot is an R&D initiative on 3D solid-state detectors for timing applications funded by Italian National Institute for Nuclear Physics (INFN).

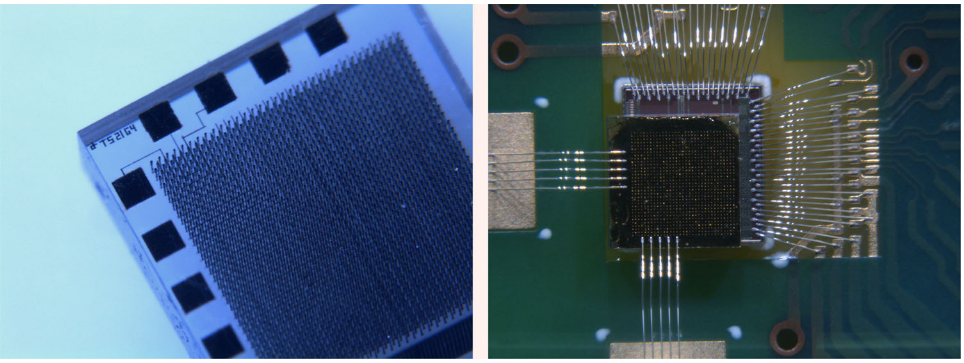

Fig. 10 Left: 32 × 32 pixel sensor fabricated on a 2.3 × 2.3 mm^2 scCVD sample. Right: the same sample bump-bonded to the Timespot chip and wire-bonded to a test board

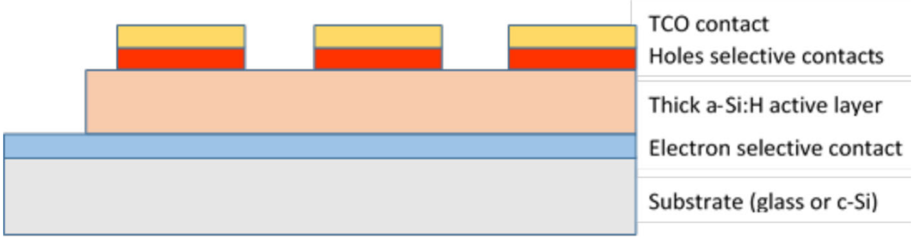

Fig. 11 Conceptual scheme of a-Si:H device with charge selective contacts. Substrate could be different from glass. The thickness of the active layer could be in the range of 1-30 μ while the other layers are typically tens of nm, save the substrate

with a measured efficiency of more than 99%. The behavior of the 3D diamond sensors has been simulated in details obtaining excellent agreement with data [241, 244, 246].

Simulations show that the asymptotic time resolution is limited by the column resistance which with the present technology is difficult to be further reduced below a few tens of kΩ. Another limitation of the 3D diamond sensor fabrication is represented by the time required by the graphitization process which amount to several seconds per column and can hardly be reduced. This represents a major obstacle toward large-scale fabrication of graphitized diamond pixel sensors necessary for the construction of a practical tracker for a high-energy physics experiment.

The very good results obtained so far for Minimum Ionizing Particles points to the possibility to use the detectors also for ion detection due to the higher energy deposition. Specific tests to measure the time resolution in such use case are being considered.

3.9 Hydrogenated amorphous silicon devices.

Hydrogenated amorphous silicon (a-Si:H) has been used since many years in the fabrication of devices related to optoelectronics, such as solar cells, thin-film transistors and other applications [247].

The amorphous silicon is a material highly resistant to ionizing radiation damage due to its intrinsic disordered nature. To obtain a detector grade device it is necessary to reduce the number of dangling bonds inside the material. This is done by introducing hydrogen into the material to passivate dangling bonds to reduce defects and recombination centers. Increasing hydrogen content enlarges the bandgap reducing the background current of the device. The typical value of hydrogen content to obtain a detector grade device is 10-15%. Several methods have been proposed for the preparation of device grade a-Si:H but the PECVD (plasma-enhanced chemical vapor deposition) method is the most widely used due to its capability to consistently prepare uniform, high-quality materials on a large-area substrate [248]. Typical deposition temperature should be confined between 100 °C (to avoid more defective material) and 350 °C (to avoid hydrogen desorption), and normally it is around 200 °C. This range of temperatures allows for the deposition of thin layers of material (few micrometers) on a variety of substrates, among which also thin layers of plastic materials like polyamide [249]. This feature allows the possibility of transmission detectors for different applications: instrumented flange at the vacuum/air separation of charged particle accelerators, transmission detectors for dosimetry of actual dose delivered to patients by clinical beams in radiotherapy, monitoring of radiation fluxes in space applications.

Within the research program of the INFN HASPIDE project several non-optimized devices have been fabricated and tested both with and without ionizing radiation beams. To obtain a working device the choice of the contacts to bias the sensitive volume and readout the signal in current is of fundamental importance. Two types of configuration have been produced: a p-i-n structure, with implantation of doping elements on the two sides of the planar intrinsic material, and a charge selective contact structure where the two contact layers implement a different mobility to select between the two types of charge carriers. This latter configuration is obtained via the deposition of metallic oxides like TiOx for electron selection and MoOx for hole selection [250]. Figure 11 shows a typical device configuration.

Many device configurations are possible: pixels, strips, circle, custom patterns, single or in arrays, with different thickness and area, different contact types. Important properties of such devices are the capability to work at ~ 0 V bias and the sharp definition of the sensitive volume defined by the contact area and the thickness[251].

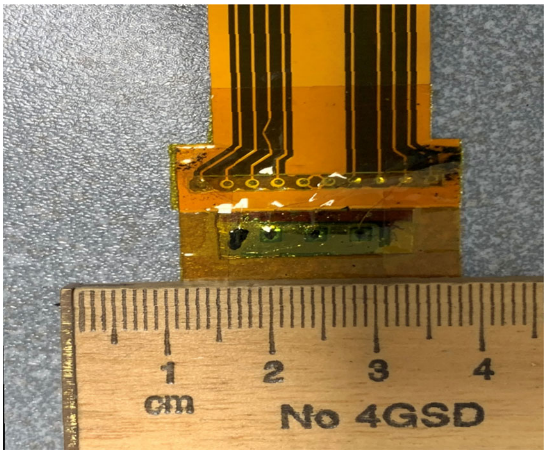

Fig. 12 3 pixel array, $2 \times 2\,\mathrm{mm}^2$ size, 2.5 μm thick, 25 μm kapton substrate, 70 μm thickness of kapton protection tape

Exposed to X-ray from laboratory tubes, electrons or photons from clinical LINACs, protons from adrotherapy accelerators, the linearity of the response with respect to beam flux (or dose rate) is excellent ($R = 0.999$), the sensitivity is of the order of tens of pC/cGy, and the noise is less than 10 pA when read in current mode.

The response of devices from the same production batch are similar within 5-10% both in dark conditions and under external beam irradiation [252]. Finally, the radiation resistance has been verified exposing two devices, one p-i-n diode and the other with charge selective contacts, to the Josef Stefan Institute neutron source up to $5 \times 10^{16}\,\mathrm{n}_{eq}/\mathrm{cm}^2$. The devices recover the same I-V shape after 12 h annealing at 100 °C, while the linearity of the response is preserved both before and after the annealing, but did not fully recover at the values before the neutron irradiation [253].

Some applications that will be developed in the near future will be based on the availability of thin devices with arrays of pixels. Presently some linear arrays (Fig. 12) are already available, $2 \times 2\,\mathrm{mm}^2$ pixel size, embedded in 25+70 μm kapton material. They will be tested not only on clinical beams but also on other types of beams (protons, ions, electrons) with the goal to have an instrumented flange to be used in transmission at the vacuum/air interface.

Further possibilities to use a-Si:H detectors will be single-ion and low-energy proton detection, using a specific radiation-hard front-end readout. Lastly, neutrons could also be detected both with and without a ^{10}B film deposition over the a-Si:H layer.

4 Neutron detectors

Neutron detectors encompass a wide variety of devices, which can be classified based on their detection techniques, the energy spectrum of the neutron radiation or their intended application.

4.1 Organic scintillators for neutron detection

In nuclear physics experiments with fixed target, it is possible to use counter detectors in combination with the time of flight to retrieve the information about the kinetic energy. Either plastic or liquid scintillators are used for their good time resolution. In the following sections, four neutron detectors to be extensively used in experiments with radioactive beams, and/or experiments for nuclear astrophysics are described in details. The energy region of interest is between a few hundreds of keV to about 100 MeV, depending on the nuclear reaction to be studied.

4.1.1 NArCoS

NArCoS (Neutron ARray for COrrelation Studies) [254–259] is a project focused on the realization of a new detector based on stacks of plastic scintillators. The detector offers both high energy and angular resolution and is sensitive to neutrons as well as charged particles within the same detection cell. The kinetic energy of interest ranges from 1 to 100 MeV for neutrons and up to 100 AMeV for charged particles, as expected in nuclear reactions during Fermi energy heavy-ion collisions. The detector is made up of elementary cells, each with dimensions of $3 \times 3 \times 3\,\mathrm{cm}^3$. The material used is the plastic scintillator EJ-276 G (the green-shifted version). This detector can discriminate neutrons from gamma particles using the pulse shaping discrimination technique (and is also capable of discriminating light charged particles) [257, 260]. Each elementary cell is independently read by a matrix of SiPMs, and the signal is acquired through digital electronics. The expected angular resolution for neutrons is about 1° at a distance of 150 cm from the target in the laboratory frame. Neutron energy is deduced using the time-of-flight method. Thanks to the fast response of the organic scintillator serving as the stop reference and in conjunction with an MCP as the start reference, an energy resolution of approximately 6%-8% can be achieved, assuming a time resolution of 500 ps.

In summary, NArCoS is designed as a hodoscope, consisting of clusters, each comprising four elementary cells arranged in a linear configuration, with approximate dimensions of $3 \times 3 \times 12\,\mathrm{cm}^3$. This design choice was made to achieve an optimal balance between granularity, angular resolution and neutron detection efficiency. Using Geant4 simulations, a mean neutron detection efficiency of 25% for one cluster and 33% for a setup of nine clusters was estimated. The prototype will consist of 64 elementary cells (16 clusters) arranged in a cubic geometry (dimensions approximately $12 \times 12 \times 12\,\mathrm{cm}^3$).

The most likely process for detecting neutrons within the plastic scintillator at the energies of interest is neutron–proton elastic scattering, which can be exploited through the proton recoil technique (or, more generally, the nuclear recoil technique). To discriminate signals originating from neutrons, the hodoscope will be coupled with a veto detector for charged particles, most likely a double-sided silicon strip detector.

This neutron detector is designed to operate under vacuum and is also intended to be versatile and modular, allowing reconfiguration of both its mechanical and electronic components. While some work has already been completed, significant efforts are still needed in terms of simulations and experimental tests to achieve the optimal configuration for both mechanical and electronic aspects. The studies conducted so far using Geant4 simulations are promising, but the simulation work needs to be further refined and validated through experiments.

At present, a PRIN (2020H8YFRE) project is ongoing (spanning three years, starting in May 2021 and ending in May 2024) to study a prototype project, with the goal of completing the study by the end of the PRIN. The physical case for which this detector is intended is of paramount importance in the physics of heavy ions at Fermi and intermediate energies. In fact, new facilities for radioactive ion beams under construction worldwide represent a unique opportunity to study nuclear matter under extreme conditions, far from stability.

Much of current nuclear physics knowledge is based on the properties of nuclei close to the line of stability. Extrapolating this knowledge to the region far from stability introduces large uncertainties, and it is now clear that some of the “basic truths” of nuclear physics need to be revisited in the near future. For this reason, the proper detection of neutrons is a crucial goal for the coming years. Neutron detection with high angular and energy resolution will allow exploration of important aspects of nuclear physics, such as in-medium nuclear interactions, the Equation of State of nuclear matter, exotic unbound nuclear states and exotic nuclei—both from structural and dynamical perspectives. Powerful techniques, such as neutron-based correlation functions (intensity interferometry), can also be used, among other examples. These studies have significant implications for nuclear astrophysics, nucleosynthesis processes, neutron stars and play an important role in the emerging field of “multi-messenger astronomy.”

4.1.2 NEDA

The NEutron Detector Array (NEDA) [261] is a neutron detector array of the next generation. It has been constructed as an ancillary detector for use with AGATA (see Sect. 5.2.1 for details), which is a state-of-the-art high-resolution γ-ray spectrometer based on the γ-ray tracking technique [149]. The first implementation of NEDA has been done with AGATA 1π at GANIL [262, 263]. However, other large γ-ray arrays are also foreseen to be coupled to NEDA. Neutron and charged particle detectors provide a good selection of the decay channels that has been demonstrated to be very efficient for the study of neutron-deficient nuclei populated by fusion-evaporation reactions, e.g., for the investigation of nuclei close to the N=Z line. A recent work in this direction made with the detector NEDA can be found in Ref. [264]. NEDA is also a well-suited device for the investigation of exotic nuclei populated with transfer reactions, where the emitted particle is a neutron. A large variety of new radioactive beams will be accessible in the next years for transfer reactions induced by proton- and neutron-rich projectiles from radioactive beam facilities such as HIE-ISOLDE (CERN, Geneva, Switzerland), SPES (INFN-LNL, Italy), SPIRAL2 (Caen, France) and FAIR (Darmstadt, Germany). Neutron detectors based on liquid scintillators that provide neutron-γ identification by pulse shape discrimination and time of flight have been in use for decades. There are a few examples of high-efficiency neutron detectors with high discrimination capabilities between neutrons and γ rays that can be coupled to large γ-ray arrays, such as Neutron Wall [265, 266] Neutron Shell [267] and DESCANT [268].

NEDA is conceptually designed to be a versatile and a highly efficient neutron detector array, with good neutron-γ discrimination capabilities at high counting rates. It will be used as a neutron tagging instrument coupled with large γ-ray arrays at stable and radioactive ion-beam facilities. It will efficiently measure neutrons emitted from outgoing channels in fusion-evaporation and low-energy transfer reactions. The kinematics of particles emitted in these two types of nuclear reactions, fusion-evaporation and transfer, demand very different characteristics from a neutron detector. In the former case, the neutrons have a Maxwellian distribution with a maximum at energies of a few MeV and due to the kinematics of the reaction, they have an angular distribution peaked at forward angles with respect to the beam direction. NEDA has specially been optimized to have large efficiency in such fusion-evaporation reactions, for neutron multiplicities 2 and 3. In transfer reactions, the neutrons can reach energies above 10 MeV and their angular distributions highly depend on the angular momentum transferred, energy of the beam and kinematics of the reaction.

The NEDA front-end electronics is fully digital and uses the Global Trigger and Synchronization system to improve processing capabilities, flexibility and integration with other detector systems, in particular γ-ray arrays such as AGATA. The core of the front-end electronics is the NUMEXO-2 cards that consist of a set of four FADC Mezzanines, each containing four 200 Msample/s digitizers. The motherboards of the cards contain two FPGA units, a Virtex-6 and a Virtex-5, which carry out the pre-processing tasks. The data acquisition system of NEDA in its first implementation with AGATA is based on the NARVAL system.

The NEDA detectors are hexagonal with a cross-section fitting a 5-inch photomultiplier tube with a length of around 20 cm. The active volume of the detector, around 3 ls, is filled with the liquid scintillator EJ-301 (which is equivalent to BC501A). However, the collaboration is still looking for new materials with good neutron-gamma capabilities and better material behavior.

4.1.3 SHADES

In low-energy nuclear physics, the measurement of reaction cross sections at energies far below the Coulomb barrier is often required, for example, as input for astrophysical models [269]. The detection of neutrons provides a significant challenge in this case due to the necessary choice between energy sensitivity (scintillators, time of flight) or efficiency (large moderating counters). The first option is generally not able to reach the desired sensitivities to cover the low energy range of the reactions of interest. In the latter case, the main issues arising are difficulties with efficiency determination and the loss of discriminating power due to the almost nonexistent energy sensitivity. Recent developments are utilizing moderator geometries designed to achieve a quasi-flat, energy-independent detection efficiency [270], but also in these cases it is not possible to discriminate against beam-induced or other backgrounds or to resolve contributions from the population of excited states in the reaction.

The SHADES (Scintillator-^{3}He Array for Deep-underground Experiments on the S-process, ERC-StG 2019 #852016) aims at moving a step forward by constructing a large array of liquid scintillators (EJ-309) and ^{3}He counters. By capture-gating on the counters, it is possible to recover some information on the neutron energy through the signal in the liquid scintillators, where the neutrons have been thermalized. The detector has been constructed and is currently being characterized. First use case will be the measurement of the astrophysically important reaction ^{22}Ne(α, n)^{25}Mg [271], but if the performance is satisfactory the array can be easily employed for other nuclear measurements.

4.1.4 Versatile array for laser-induced astrophysics research (VALAR)

The interaction of ultra-short laser pulses with an expanding gas mixture at controlled temperature and pressure inside a vacuum chamber allows the formation of plasmas with multi-keV temperature alongside strong electromagnetic pulse and X-ray emissions [272, 273]. These energies overlap with the typical temperatures of stellar cores where thermonuclear reactions occur, thus making this paradigm a perfect scenario for nuclear astrophysics research [274]. Indeed, maximizing the laser absorption, the Coulomb dissociation of the molecules result in multi-keV ion acceleration with a nearly isotropic emission (Coulomb explosion) whose interaction with the surrounding plasma triggers nuclear reactions [275–277].

In this framework, the possibility to mimic the stellar conditions by generating a controlled laboratory plasma with thermodynamical status not too different from stellar conditions will open the way for the study of nuclear reactions of outmost importance for nuclear astrophysics such as the deuterium burning, deuterium-tritium, deuterium-^{3}He, proton-lithium, proton-boron, ^{12}C-^{12}C, ^{12}C-^{16}O and ^{16}O-^{16}O fusion reactions [278]. In particular, neutron detection is an essential diagnostic in the area of fusion science. Through the measurement of neutron yields and energy spectrum, one can calculate fusion power, plasma temperature and areal density of the target. Because of its importance in fusion research, many types of neutron detectors and techniques have been developed [279]. Scintillation detectors are one example of the most commonly used neutron detectors in inertial confinement fusion and tokamak experiments, and it can be extended to the nuclear astrophysics approach. In fact, scintillation detectors are well suited for measuring low neutron yields, even if they suffer from saturation under high neutron flux. Also, strong electromagnetic pulse noise or X-rays can severely affect the measurements.

For instance, a table-top short pulse laser system can generate nuclear fusion from explosions of laser-heated deuterium clusters, triggering the DD fusion reaction that generates 2.45 MeV neutrons and 3.02 MeV protons [280]. In this case, a maximum of 10^8-10^9 neutrons per shot in a sub-nanosecond burst is expected, limiting the possibility to use classic silicon detectors due to the presence of high electromagnetic pulse noise and non-single detection of the emerging particles. On the other hand, a liquid/plastic scintillator used in a time-of-flight mode can ensure the possibility of detecting and measuring multiple neutrons [281]. The number of neutrons hitting the detector during a laser shot can be obtained by dividing the measured peak amplitude by the average signal of one neutron obtained during a peculiar calibration procedure.

In Fig. 13, the signals obtained using different kind of scintillators detectors is obtained in a DD fusion experiment. The red line corresponds to a liquid scintillator EJ-309, the green one to an EJ-232Q plastic scintillator, the blue line to a lithium glass detector mainly devoted to thermal neutrons, while the purple one to an EJ-276 G plastic one. It is clearly evident that the plastic scintillators recover faster from the electromagnetic pulse and gamma flash peak, being immediately ready for collecting the neutron peak but on the other hand the signal of the liquid scintillator is far from the saturation point, allowing to a higher neutron flux detection. These preliminary results and tests underline the needs of new investigation in order to evaluate the best detector and array exploitable for study nuclear astrophysics reactions induced by laser–matter interaction.

4.2 Detectors for neutron beams and applications

As mentioned in the previous section, any counter detector can be used in principle as a spectrometer when used in combination with the time-of-flight technique. This detection system is extensively exploited to characterize neutron beams with energy spanning from

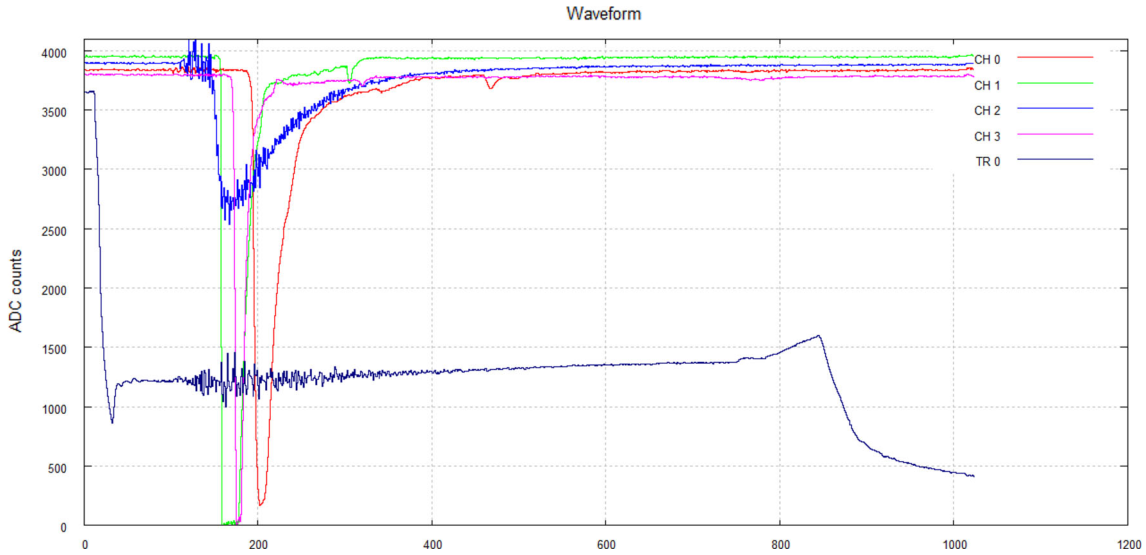

Fig. 13 Neutron TOF detection with different scintillators (see text for details)

meV to GeV. In this subsection, an overview of the detectors currently used in neutron beam facilities and their possible upgrades is presented, together with examples of detectors especially designed for applications.

4.2.1 Neutron beam detectors

Neutron beam facilities and applications have highly specific requirements regarding detector performance. These demands drive continuous innovation and lead to the development of specialized experimental apparatus and techniques. The most accurate measurements of neutron energy are typically achieved using the time-of-flight technique. By measuring the time interval between neutron production and its detection over a precisely known flight path, this method can achieve uncertainties as low as 10^{-4}. This is the case, for example, for the n_TOF facility at CERN, where a set of detectors have been developed to measure the neutron flux from thermal energy 25.3 meV to 1 GeV. All detectors exploit well-known nuclear reactions to convert neutrons into charged particles. By counting the number of reactions as a function of the time of flight, these detectors can reconstruct the neutron flux. In particular, the reactions exploited at n_TOF are the ^{6}Li(n,t), ^{10}B(n,α), ^{235}U(n,f), ^{238}U(n,f) and neutron–proton elastic scattering; each one is defined as a standard on a neutron energy range from the IAEA (International Atomic Energy Agency).

The range from thermal to 1 MeV is covered by the detectors SiMon [282] and SiMon2 [119], which exploits a thin ^{6}LiF foil to convert the neutrons to alphas and a tritons. The reaction products are detected by four off beam silicon detectors, facing the sample with a 45° angle with respect to the beam, with the main advantage of being almost transparent for the neutron beam itself. One of the inconveniences of silicons exposed to intense neutron fields is the sensitivity to radiation damages that can strongly affect the performances of solid-state detectors. In recent years the interest for silicon carbide-based detectors is increasing (see Sect. 3.2 for details), thanks to the possibility to operate in harsh environments, found both in basic research with high-flux neutron beams and in nuclear technology [114]. In fact, silicon carbide is characterized by a good radiation hardness [283], and its wide bandgap (3.26eV) allows for low-noise measurements even at high temperatures (tested up to 700°C [114]). As for other semiconductor-based devices, other advantages lie in their compactness, low power consumption and reasonably low cost. SiC detectors have been tested for fast neutron detection, not showing instabilities up to a 14 MeV neutron fluence of 4.45×10^{11}n cm^{-2} [93], nor polarization effects due to partial charge carriers trapping after irradiation, which instead have been observed in diamond detectors.

For the detection of low energy neutrons, SiC detectors can be coupled with converter foils, e.g., ^{6}LiF. Some examples of SiC+^{6}LiF devices, mostly exploiting old generation, small area SiC detectors, already gave promising results in the past. Some interesting developments for such configuration could be obtained by combining the expertise on this specific configuration gained by some INFN groups using Si detectors, with the output of the INFN-CSN5 SiCILIA project, that in the last years managed to produce state-of-the-art thick and large-area SiC detector devices [82], already successfully tested from multiple points of view [81]. Such studies can be of interest for n_TOF, since SiC+^{6}LiF could be used as neutron monitor for the new experimental area NEAR, characterized by a high neutron flux [284].

The detectors used to measure the n_TOF flux at higher energy are mostly gas detectors exploiting uranium fission and able to work at 0° on the beam. A first gas detector based on the Micromegas technology uses ^{10}B and ^{235}U as neutron converters, covering a range from thermal energy to 150 MeV. The ^{235}U fission is exploited also by an additional gas detector, a calibration ionization chamber, provided by the Physikalisch-Technische Bundesanstalt. A further system relying on fission fragment detection to measure the incident neutron flux is the PPACMon [285]. Therefore, the most suitable samples to choose for use with this detector

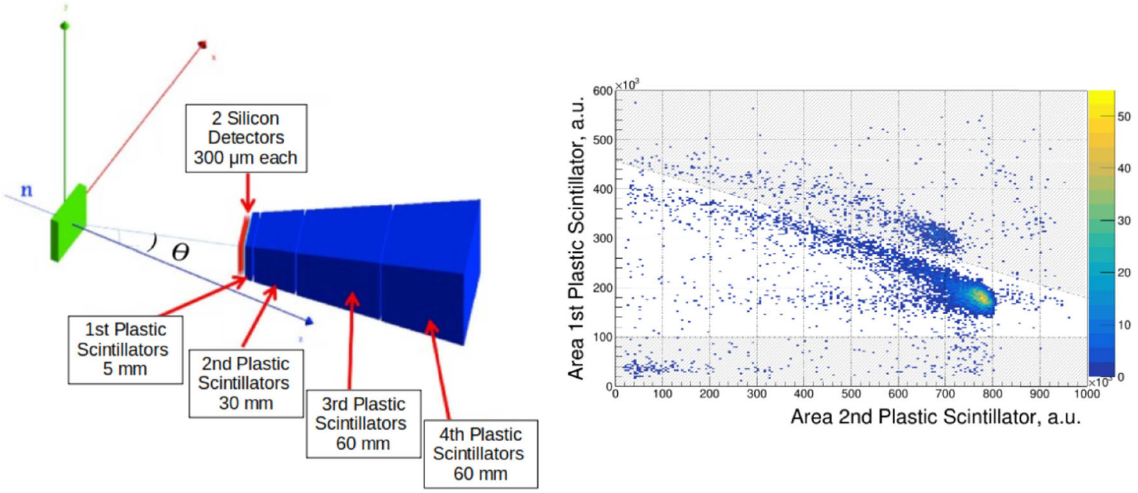

Fig. 14 Drawing of the detector (left) and ΔE-E matrix (right); the dashed lines represent the conditions to select the scattered protons

are ^{235}U and ^{238}U. The PPACMon detector identifies fission events via the coincident signals generated by the two fission fragments emitted back-to-back, thus maximizing the signal-to-noise ratio. This technique coupled with the excellent time resolutions allows PPACMon to work from thermal to few GeV of neutron energy.

To complete the picture, Recoil-Proton Telescopes [286, 287] were developed to measure the neutron flux relative to the neutron–proton scattering reaction. To cover the wide neutron energy range the telescopes are multi-stage, they are composed of two stage of 300 μm thick silicons followed by 4 plastic scintillators of EJ-200 with truncated pyramid shape and increasing thickness from 0.5 to 6 cm. Exploiting the ΔE-E matrices to perform particle identification, it is possible to reconstruct the neutron beam impinging on a polyethylene target in the energy range from a few MeV up to hundreds of MeV. The geometrical drawing of the telescope is reported in the left panel of Fig. 14. The right panel contains the ΔE-E matrix for neutron kinetic energy of 74.8 ± 2.2 MeV, obtained with the coincidences between the first and second scintillators, and the gray area represents the experimental conditions used to distinguish protons from other charge particles. The present detector is partially limited in terms of maximum neutron energy by the low stopping power of the plastic scintillators that constitute the last stages of the telescope, an upgrade with a inorganic scintillator is currently under investigation.

A detector based on scintillator, in this case inorganic, has been developed as well at the Laboratori Nazionali di Legnaro [288]. Such detector employs the reaction ^{10}B(n,α) to convert the neutrons, aiming to detect the 480 keV gamma emitted by the exited ^{7}Li. The ^{10}B is contained in a thick disk that is mechanically coupled to the scintillator. This approach removes any limitations to the concentration of the dopant in the scintillator that might cause inefficiencies in the light collection. In addition, using an assembly allow to estimate the gamma background, repeating the measurement without the ^{10}B disk.

In recent years the interest for Timepix (see Sect. 6.3.1 for details) in the neutron detection fields is growing. Detectors based on Timepix technology have been developed for neutron flux measurement in beam facilities and nuclear fusion reactors, having application also for boron neutron capture therapy.

For fast neutrons, one of the most advanced prototypes is the "Diamondpix", a diamond coupled to a Timepix3 chip. The first prototype has been realized with a polycrystalline CVD (see diamond devices in Sect. 6.2 for details) plate with a thickness of 500 μm and an area of $10 \times 10\,\mathrm{mm}^2$. It has been coupled through the bump-bond technique to the Timepix3 chip that covers an area of $14 \times 14\,\mathrm{mm}^2$ with a matrix of 256×256 pixels, each having an area of $55 \times 55\mu\mathrm{m}^2$ [289]. Timepix3 is controlled through the Kathrine [290] module that can register the time of arrival of particles in time ranges of several hours (data-driven acquisition mode). In order to characterize the new detector, experimental tests have been performed successfully on the FNG facility (ENEA Frascati) with 14 MeV neutrons [291] and, recently, on the CERN n_TOF facility. Results presented in these studies show the potentials of Diamondpix: discrimination capability of fast neutrons from gamma background through morphological analysis, time-of-flight measurements with a time resolution of 1.6 ns and charge measurements on reaction products in diamond. In addition, also a silicon Timepix3 has been proposed for fast neutrons detection; in this case, specific plastic converters have been used to detect the recoil protons. Results of preliminary tests on the FNG facility reported in Fig. 15 show the potentiality of this detector, in particular for identification of recoil protons. For thermal neutrons, some prototypes based on the on Timepix1 [292] deposited with converter materials like B_4C and LiF have been realized. In particular, a study on a Timepix1 with a 1.2 μm LiF layer enriched at 95% with ^{6}Li has been carried out on the thermal neutron source HOTNES (ENEA Frascati) and results show a clear sensitivity to thermal neutrons. Currently, a new Diamondpix is under construction with a monocrystalline CVD diamond to perform accurate spectroscopic measurements on fast neutrons. For thermal neutrons, instead, a Timepix3 with a converting layer of B_4C (enriched at 96% with ^{10}B) will be soon realized to exploit the simultaneous acquisition of charge and time.

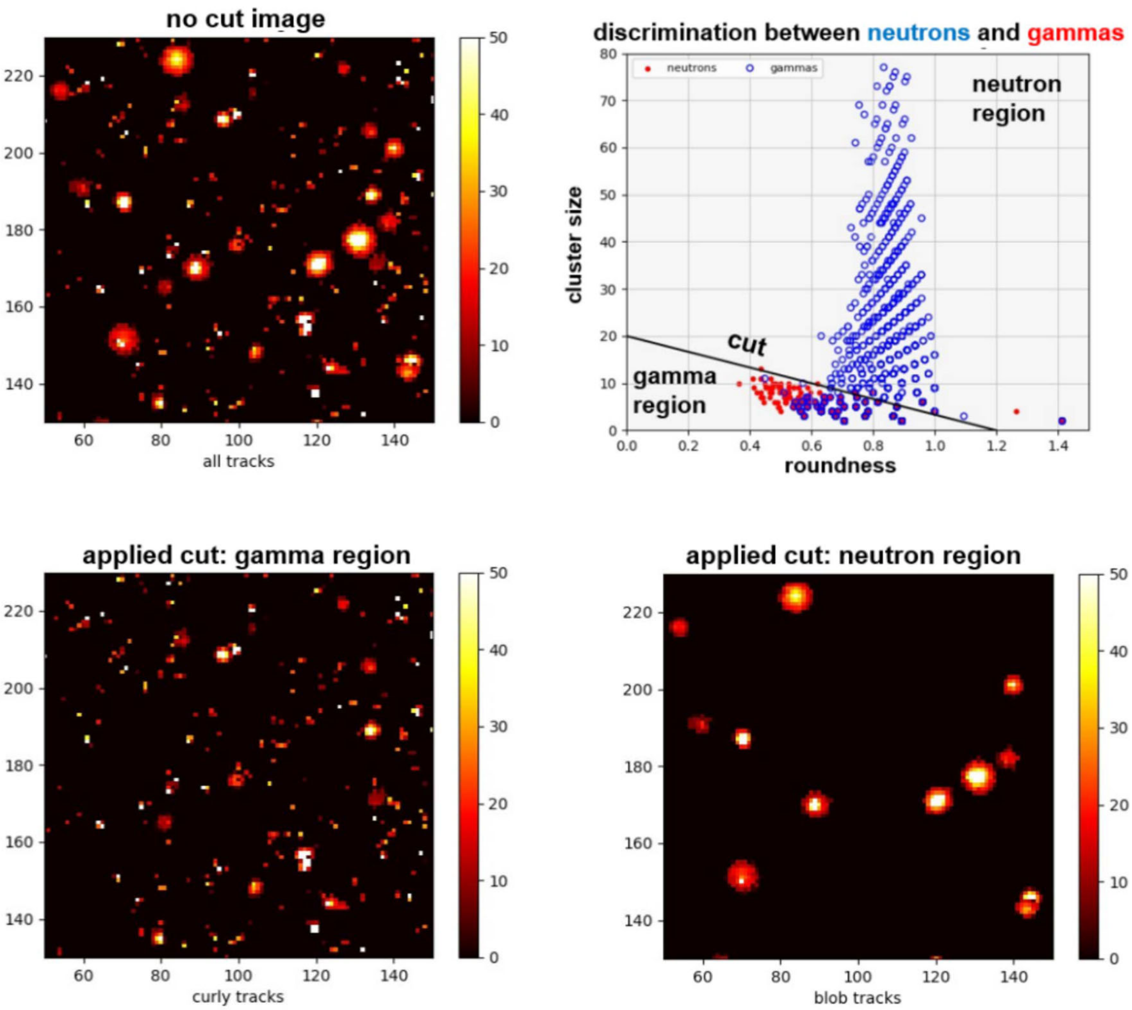

Fig. 15 Neutron/Gamma discrimination based on the track shape for the Timepix3 coupled with a diamond detector

Since ten years, a multi-institutional collaboration between Milano-Bicocca University, ISTP-CNR, INFN and CERN is working to develop GEM detectors optimized for slow neutrons for spallation sources. To detect slow neutrons, GEM detectors are equipped with single boron-cathode converters [293] or with a series of boron lamellas [294]. A recent work shows the development of an innovative GEM detector where the converter is the GEM foil itself. In fact, 1μm of $^{10}B_4C$ has been deposited on both GEM foil surfaces; stacking several boron-coated GEM (BGEM) foils, the number of converted neutrons increases. Different detector configurations have been tested: the first one was coupled with Timepix (Multi-Boron GEMPix detector [295] with 3 BGEM foils of $3 \times 3\,\text{cm}^2$) and the second one with GEMINI (3MBGEM detector with 3 BGEM foils of $10 \times 10\,\text{cm}^2$) electronic readout. Both configurations show a linear increase in the counting rate as the number of boron layers increases. Therefore, it is possible to add several BGEM foils, at least six, to achieve a detection efficiency of 25% for thermal neutrons (Fig. 16).

The LEMRAP laboratory at INFN-LNF is active since more than years in the development of neutron spectrometry and dosimetry techniques [296, 297]. Particularly, here it was firstly conceptualized and prototyped the single moderator neutron spectrometer, able to simultaneously determine all energy components of a neutron field from thermal neutron to GeV. The performance is comparable to that of a traditional Bonner spheres but the operation is in real-time, greatly extending the measurement potentialities. The most recent prototype NCT-WES [298] (Neutron Capture Therapy-Wide Energy Spectrometer) is shown in Fig. 17. The neutron fluence is measured by six thermal-energy neutron detectors, located at different depths along the cylindrical axis of the device. The analysis is complemented by a detailed MCNP6 modeling of the detector to extract the response matrix. Clinical test of the detector for its use for boron neutron capture therapy is currently undergoing [299].

4.2.2 Applications

Many technological applications require the detection of neutrons, from industry to nuclear medicine and nuclear energy production. For the latter, neutron detectors play a fundamental role, with crucial implications for safety and security reasons. Present day

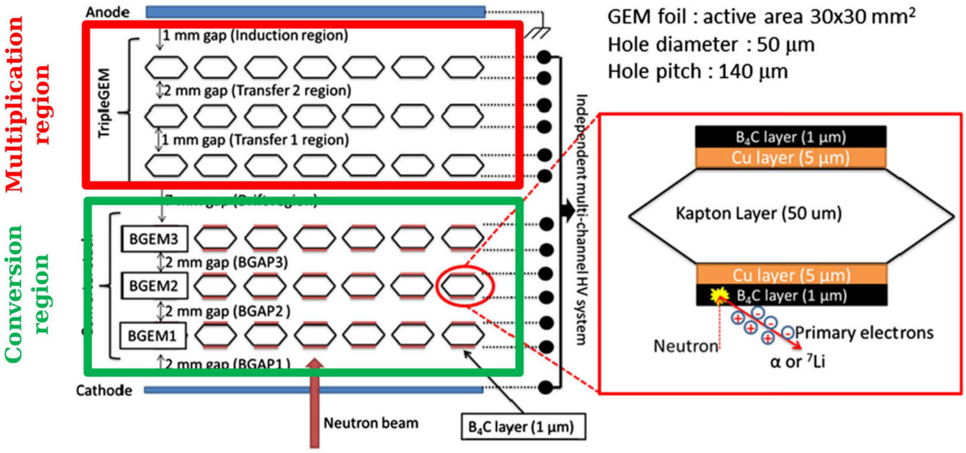

Fig. 16 Structure of a BGEM detector, in the prototype three $^{10}B_4C$ layers were mounted in the conversion region

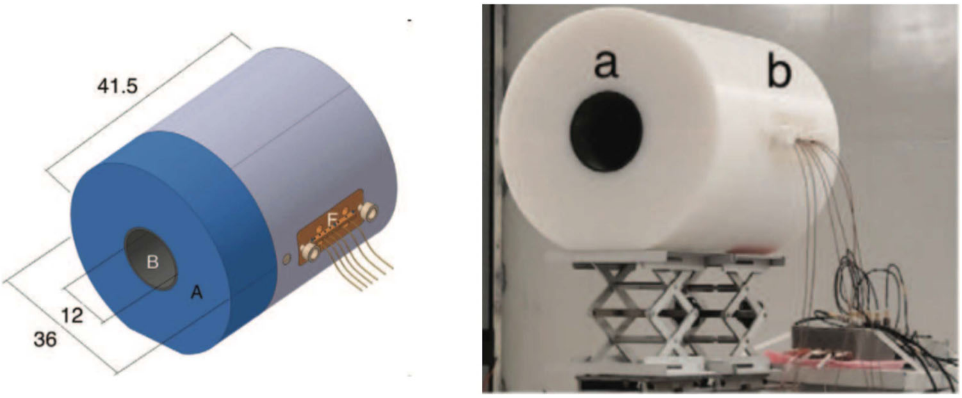

Fig. 17 Left panel: structure of a BGEM detector. Right panel: a prototype with three $^{10}B_4C$ layers mounted in the conversion region

technology heavily relies on ^{3}He detectors, which have great performance in terms of neutron conversion (thermal cross section is 5300 b) and low sensitivity to gamma ray. On the other hand, ^{3}He is artificially produced and its procurement is becoming more and more problematic and expensive. Recently the decline of the ^{3}He gas supply, as well as its increasing price, has triggered international efforts to develop neutron detectors that make use of alternative materials and/or techniques.

In the framework of the MICADO (Measurement and Instrumentation for Cleaning And Decommissioning Operations) EU project, a set of 32 solid-state thermal-energy neutron detectors named SiLiF [120] has been built and characterized in order to monitor nuclear materials contained in radioactive waste drums possibly containing small quantities of actinides, as well as around spent fuel casks in interim storage or during transportation. SiLiF are based on single-pad silicon detector coupled to a thin layer of ^{6}LiF, which upon capture of a low energy neutron produces an alpha particle and a triton that are detected in the silicon. As compared to the well-known thermal neutron detectors, SiLiF technology allows to achieve comparable performances at about one order of magnitude lower prices. SiLiF detectors can provide realistic measurements of the total or thermal neutron flux, respectively, when used with or without polyethylene moderator.

In the context of the INFN BoLAS and BoLAS_NEXT experiments, the research efforts have been focused on the study of the properties and performances of ^{10}B layers deposited by laser ablation [300] when coupled to different charge particle detectors (semiconductors and scintillators). ^{10}B conversion layers have been deposited by pulsed laser deposition obtaining a good uniformity and thickness control ($\simeq$10%) on relatively large areas ($\simeq 5 \times 5\,\text{cm}^2$). The deposited films are free of contaminants and exhibit a density comparable to that of the bulk material. In particular, these conversion layers have been tested in combination with conventional silicon detectors [301] or a promising perovskite-based scintillating material ($CsPbBr_3$). In the first case, a sandwich of two ^{10}B-enriched conversion layers (1.5 μm-thick deposited on carbon fiber) has been coupled with a double-sided silicon detector. This configuration enhances the detection efficiency, while the outer silicon is exploited to measure the background, consisting mostly of gamma ray, allowing an effective subtraction. In the second case, the ^{10}B layer has been coupled to a 1 μm-thick film of $CsPbBr_3$ perovskite [302], deposited as well by pulsed laser deposition, whose scintillating properties revealed to be very interesting when irradiated with alpha particles. In fact, all inorganic perovskite materials are recently attracting a lot of interest as indirect radiation detectors because of their outstanding photophysical properties and high stopping power.

4.3 Innovative neutron detectors

New scintillation materials and detector concepts are being studied by several groups with the aim of going beyond the state of the art. In the next subsections, new kind of scintillators for fast and high-energy neutron are presented, together with some novel ideas to track fast neutrons.

4.3.1 CLYC scintillators

The quest for new materials for neutron detection is also developing with the aim of not only revealing a neutron, discriminating it from gamma rays or other particles, but also measuring its energy without resorting to time-of-flight techniques. One of such new developments is represented by the CLYC scintillators [303–307]. Most importantly, using the anode signal of a highly ^{7}Li enriched CLYC scintillator it is possible to detect and discriminate between γ-ray radiation and neutrons in a wide energy range. Different pulse shape analysis techniques were developed in these last decades to easily perform this distinction (see, for example, Refs. [303–306] and references therein). In addition, the CLYC scintillator has an energy resolution which is better than that of NaI but slightly worse than that of LaB3:Ce [303]. The relatively high probability of fast neutrons undergoing ^{35}Cl(n,p)^{35}S or ^{35}Cl(n, α)^{32}P reactions makes CLYC an attractive option for neutron detection. Ref. [307] had shown that the energy of the proton or of the alpha particle released in these reactions varies linearly with the energy of the incoming neutron. The cross section for ^{35}Cl(n,p)^{35}S reaction increases to approximately 200 mb at a neutron energy of approximately 3 MeV and then decreases to about 50 mb. For neutron energies above 3 MeV, the ^{35}Cl(n, α)^{32}P reaction has a cross section of the order of 50 mb, but at around 4-5 MeV this process has a probability similar to that of ^{35}Cl(n,p)^{35}S.

In addition to the discrimination between neutron and gamma radiation, it is also possible, in some cases, to measure the incoming neutron kinetic energy without the use of the time-of-flight technique. In the case of a monochromatic fast neutron beam, using CLYC, one can obtain (with a precision of the order of 10%) the neutrons kinetic energy. In the case of a continuum energy spectrum of the fast neutrons (like, for example, the one from an AmBe source), the measurement of the neutron kinetic energy is only possible for a i) neutron energy below 4-5 MeV and with ii) the identification of the nuclear reaction that the fast neutron performs in CLYC. Practically, this last condition is fulfilled in the case one is able to distinguish proton-induced signals from the alpha ones. The distinction between alpha particles and protons simply using the CLYC anode signal is at the moment effective only starting from 3 MeV [305, 306]. In fact, for lower neutron energies the anode signals, produced in both the reactions, are too similar because of the unavoidable statistical fluctuations [305].

The existing neutron detector arrays which can provide the measurement of neutron energy (e.g., MONSTER [308], VANDLE [309]) use the time-of-flight technique and suffer from low efficiency for neutron detection mainly because of the large distance of the detectors from the target (typically, more than one meter) and because of the detector thickness. An array (not necessarily composed of a large number of detectors) based on CLYC scintillators would make possible the measurement, in the same detector, of both the energy of the neutron and that of the coincident gamma ray/rays. Therefore, it could be used in all the physics cases where it is needed to both measure over the whole solid angle and, at the same time, identify the neutrons events.

This array could be used, for example, coupled with the ISOL SPES facility at INFN-LNL providing radioactive neutron-rich beams. These neutron-rich radioactive nuclei, combined with the CLYC scintillator array, will open the practically unexplored field of neutron spectroscopy especially for weak neutron transitions. Using such an array, it will be also possible: i) to study in detail the neutron delayed emission in the beta decay; of neutron-rich nuclei with large Q–values (several MeV); ii) to populate particular Pygmy Dipole Resonance states [310, 311] and then measure their subsequent gamma decay to the ground state or to excited states; iii) the measurement of the gamma decay of the hot Giant Dipole Resonance; and iv) to detect neutrons from direct reactions such as (^{3}He,n), (d,n) with stable and radioactive beams.

Currently, it is not possible to measure the fast neutron energy over a wide range (e.g., 0.5-10 MeV) using CLYC scintillators with PSA techniques. This limitation arises from the need to analyze the CLYC anode pulse for identifying the nuclear reaction mechanism and the requirement to avoid potential nuclear excitation of Sulfur or Phosphorus nuclei. As a result, the available energy window for neutron measurement is restricted to a narrow range between 3 and approximately 4.5-5 MeV.

The extension of this window at low and high neutron energy is one of the main objectives of the CLYC related research studies. It is important to remember that there are other "Elpasolite" crystals which have been discovered in these last years with properties similar to those of CLYC (for example, the CLLB, the CLLC, the CLLBC, the TLYC [312–315]) but all are expected to suffer from the previous limitation.

The midterm plan for the development of this line of study foresees more accurate PSA algorithms or PSA via fast Fourier transformation, as already done in Refs. [305, 306], to reduce the threshold for the identification of the proton/alpha induced pulses. The availability of large-volume CLYC crystals, instead, could make possible the identification of "hybrid" pulses associated with the interaction (in the same crystal) of both a neutron and a ^{32}P or ^{35}S gamma ray. These solutions could, in principle, increase the energy windows for the measurement of neutron energy without using TOF techniques, namely using CLYC scintillators.

4.3.2 Siloxane-based scintillators

Aiming at the production of efficient, flexible and radiation-resistant detectors for ionizing radiation and neutrons, the Materials Physics Lab at INFN-LNL has pursued for over one decade the synthesis of polysiloxane-based hybrid and composite scintillators. The in-depth study of chemical structure-optical properties has led to produce ions, γ-rays and neutrons sensors with optimal light output, thermal resistance, radiation hardness and n-γ discrimination capability [316–318]. Recently, the entrapment of ^{6}Li compounds in the form of nanoparticles into polysiloxane loaded with inorganic scintillating powder (EJ-600) resulted in the production of fully flexible thermal neutron detectors. They successfully proved to lead to efficient triple pulse shape discrimination between γ-rays, thermal and fast neutrons [319]. The use of bendable, large-area, radiation-resistant fast and thermal neutrons scintillators might be of great advantage in case of mixed radiation fields investigation, such as radiation monitoring at borders (homeland security), workers safety in nuclear power, medical physics plants or high-energy physics facilities. Exciting achievements in the field of bendable thermal neutrons detectors are close at hand with the progress of the project BEYOND [320], where the technology of Physical Vapor Deposition of thin layers of ^{10}B is exploited to match the performance of flexible devices based on perovskite and polymers.

4.3.3 Upgrade of the FOOT BGO calorimeter

As already mention above (see Sect. 3.7), FOOT is a fixed target experiment [209] designed and developed to measure the fragmentation cross sections induced by the interaction of light ions (^{1}H, ^{4}He, ^{12}C and ^{16}O) in the energy range of 100-800 MeV/u with light nuclei targets [321, 322], of interest in the fields of particle therapy and radiation protection in space [209, 323–325]. While the FOOT detector has been optimized for charged fragments identification, some minor upgrades of the actual setup would provide the possibility to measure also the neutron production cross section in the fragmentation process for the same beam/target combinations [326, 327]. An improvement of the comprehension of neutron production in the mentioned nuclear reactions, through the measurement of the double differential cross sections in neutron emission angle and kinetic energy, is fundamental for both particle therapy and radiation protection in space [323, 324, 328, 329]. In this section, some ideas, which can be accomplished and further developed in the midterm future, for an optimization of the FOOT setup for neutron detection, will be discussed.

The FOOT setup implementing the magnetic spectrometer (see Fig. 3 of Ref. [209]) can be optimized to the case of neutrons using the pre-target detectors for beam monitoring and for the TOF measurement [330, 331], followed by the target, the magnetic system and a tracking station (three layers of silicon microstrip detectors [332]) for charged particle rejection. Finally, the BGO calorimeter can provide the neutrons kinetic energy through the TOF measurement [209]. The FOOT calorimeter is composed of 320 BGO crystals with a truncated pyramid shape with a front (back) face of about $2 \times 2\,\mathrm{cm}^2$ ($3 \times 3\,\mathrm{cm}^2$) and a length of 24 cm. SiPM tiles coupled to the back face are used for the light readout. While the neutron angular measurement is ensured by the calorimeter granularity, the kinetic energy measurement depends on the relative TOF and path length L uncertainties through:

$$\Delta E_{kin}/E_{kin} = \gamma \cdot (\gamma + 1) \cdot \sqrt{((\Delta L/L)^2) + (\Delta ToF/ToF)^2)}$$

Preliminary measurements have shown that a TOF resolution between 600and 800 ps can be reached. The uncertainty on the path length ΔL is dominated by the inelastic interaction length of a neutron in BGO which is in the interval 15-25 cm for the energy range of interest. Clearly, the FOOT calorimeter has been developed to measure the kinetic energy of charged fragments; therefore, the readout is inefficient for neutron detection and not suited for the TOF measurements necessary to determine their energy. An upgrade of the calorimeter able at the same time to:

1. further reject the noise coming from charged fragments impinging on the BGO crystals and
2. reduce the uncertainty ΔL on the path length, providing a more precise neutron energy measurement

can be reached by:

1. coupling to each BGO crystal front face a thin, fast, plastic scintillator layer in “Phoswich” mode [333],
2. providing a double readout in the front/back BGO faces and adding a SiPM tile in the front face of the crystal, directly coupled to the Phoswich plastic scintillator.

The readout at the entrance of the crystal (the Phoswich side) will allow tagging and identification of the residual charged particles, thanks to the prompt signal, in combination with the output of the silicon microstrips. This result is possible thanks to the fact that the signal time shape can be accurately reconstructed and the prompt component of the plastic scintillator can be easily disentangled from the slow BGO light component. Preliminary measurements with such setup have shown that a precision of $\Delta \mathrm{L} \sim 1-2\,\mathrm{cm}$ can be reached looking at the front/back asymmetry of the light read by the SiPM tiles. The expected improvements with this upgrade in terms of kinetic energy resolution ranges between factors of 1.5 and 2, depending on the neutron energy, assuming a distance between target and calorimeter of 3 m. The energy resolution improves from 7% (single SiPM tile) to 4% (double SiPM tile) for 50 MeV neutrons and from 10% (single SiPM tile) to 5%(double SiPM tile) for 200 MeV neutrons.

Depending on the experimental room available space, the BGO calorimeter could be moved to angles of 20°-30° with respect to the beam axis, in order to measure the double differential cross sections for neutrons. The production of neutrons at larger angles can be measured with an optimized version of the FOOT emulsion spectrometer (see Fig. 10 of [209]). In this case, the setup would consist of pre-target detectors for beam monitoring followed by the target and finally by the Emulsion Cloud Chambers (ECC) [215, 334]. In order to optimize the emulsion spectrometer setup to neutrons detection, the ECC sensitive layers can be interleaved by passive layers of hydrogen-rich materials in order to maximize the probability of neutron–proton elastic process. The further possibility to interleave the target and the emulsion detector with a magnetized volume to swap out charged particles needs to be studied. The ECC design foresees a non-uniform structure, composed by three sections (see Fig.10 of Ref. [209]), each one made of nuclear emulsion films interleaved with passive layers with increasing density (polystyrene, lexan and carbon). To this purpose, the upstream part of the ECC (Section 1, see Fig.10 of Ref. [209]) will act as a neutron target and will be made of a sequence of about 200 nuclear emulsion films, 0.35 mm thick, alternated with polystyrene layers, 0.21 mm thick. Each film is made of two active layers, 0.07 mm thick, deposited on both sides of a polystyrene support, 0.21 mm thick. The polystyrene supports and layers, with an 8% hydrogen content, will act as the neutron target. Neutron candidates will be identified by vertices with one outgoing track (a proton elastically scattered) and without any charged parent particle. The incoming angle of the neutron will be determined by connecting its interaction point to the target region. The kinetic energy of the incoming neutron will be estimated by measuring the range of the emerged proton and its emission angle. To fully measure the proton range, the neutron-target section (Section 1) will be followed by a sequence (Section 2, see Fig.10 of Ref. [209]) of about 30 nuclear emulsion films interleaved with lexan layers, 1 mm thick, and a sequence (Section 3, see Fig. 10 of Ref. [209]) of about 150 nuclear emulsion films interleaved with carbon layers, 1 mm thick. The longitudinal size of these sections will account for the range of the produced particles, ensuring full containment. The expected resolution for the reconstructed neutron kinetic energy has been evaluated through a Monte Carlo simulation with neutrons at several energies: for 20 MeV neutrons, a resolution of about 5% can be achieved.

4.3.4 BGOOD/MAMBO

The BGO calorimeter of the BGOOD experiment [335] is segmented into 480 crystals of 24 cm depth arranged in order to cover the range $\theta = 25^\circ \div 155^\circ$ in polar angle and the full azimuthal range. Each crystal is coupled to a PMT and signals are processed in WIENER Sampling ADCs, (AVM16) which provide both energy (the signal integral I) and time information (the signal start time t_0). The preliminary discrimination between charged and neutral particles is provided by means of the geometrical coincidence between the BGO and a cylinder of plastic scintillator bars. In the following, a "cluster" represents the group of contiguous crystals associated with the interaction of the same particle with the detector and its "multiplicity" is the number of crystals composing the cluster. It is not possible at the moment to identify unambiguously a neutral signal as a neutron or a photon, but it has been possible to perform a discrimination by means of multiple selections which are based on the different physics processes underlying the detection of neutrons and photons. Those are indeed responsible of the different features of the clusters (multiplicity, released energy/crystal, energy distribution) produced by these two kinds of particles. These PID criteria have been derived from a clean experimental sample of photons and neutrons in the BGO[4]. The time information provided by the sampling ADCs allows to discriminate in TOF the neutrons from the background due to low-energy photons and out-of-time events. A description of these PID criteria is provided in Ref. [7]. The investigation of more refined discrimination neutron–photon methods is in progress: For instance, it is possible to increase the resolution in TOF difference between neutron and photon taking into account the small modulation of the reference time in the azimuthal angle (of the order of 0.5 ns) observed in the data. One of the features of the AVM16 module is to record the whole sampling of the signal in each ADC channel (with a frequency of 160 MHz), so that, for test purposes, it is possible to reconstruct and compare the pulse shape of the signal produced by a neutron or a photon. Based on the results of this comparison, it will be possible to explore how to utilize additional information that has not yet been incorporated into standard analysis but is present in the raw data collected so far. For instance, this includes the maximum height of the signal and its corresponding time value.

4.3.5 RIPTIDE

Neutron tracking can be accomplished by using kinematical properties of two-particle reactions. The neutron–proton elastic scattering is the simplest, promising interaction, and its cross section is well known [336–339]. State-of-the-art approaches for neutron tracking by using neutron–proton single and double elastic scattering—referred to as Recoil Proton Track Imaging (RPTI)—have been proposed [340–344]. Their limits are related to detection efficiency, complexity, cost and implementation. For instance, Ref. [340] reports the feasibility study of a RPTI detector to be used for neutron spectrometry measurements, combining a gas scintillator (CF_4) with a real-time imaging device. The experimental setup was adjusted in a fixed angle scattering geometry by using a CH_2 foil, thus exhibiting a poor detection efficiency (∼ 10-6%). Moreover, the scintillation yield is weak, and several amplification stages are in place to enable a reliable proton track reconstruction on the image-intensified CCD camera. Fine tracks of the recoil protons were obtained leading to a good energy resolution by proton range measurement in CF_4 (2.33% at $E_n = 14\,\text{MeV}$). On the other hand, a different and more complex approach has been proposed either by the SONTRAC [345, 346] and the MONDO [341, 342, 347]

---

[4] The simulation software packages currently in use cannot describe perfectly the behavior of neutrons in the BGO for the energy range of interest, $E_n = 10 \div 500\,\text{MeV}$. In particular, they cannot reproduce the cluster features at the base of this identification.

trackers (see Ref. [348] for an overview of the technique). Both systems are based on sequential neutron–proton elastic scatterings: SONTRAC being developed for Solar MeV-neutron detection in spacecraft and MONDO (see next section) for tracking fast neutrons produced in particle therapy treatments. In both cases the recoiling protons are detected using a matrix of plastic scintillating fibers and the produced light is amplified by CMOS single-photon avalanche diode arrays (SPAD) in MONDO or readout by silicon photomultipliers in SONTRAC.

Nuclear physics and particle therapy seem to be the most demanding applications. Astrophysics in the space environment requires low-power consumption (< 100 W), and radiation hardness and space electronics certification must be assessed by a proper R&D program. In all cases, gamma and charged particle background must be rejected. It must be stressed that background suppression is a prerequisite that can be achieved event by event by dE/dx track characterization.

RIPTIDE [349–351] (RecoIl Proton Track Imaging DEtector) was conceived for full neutron momentum reconstruction, using the two-body kinematics of neutron–proton elastic scattering: The neutron energy E_n is related to the proton recoil angle and energy (θ_p,E_p) by the formula $E_n = E_p/cos^2(\theta_p)$. From the geometrical point of view, the neutron momentum can be reconstructed in the 3D active volume of RIPTIDE in two cases:

1. single neutron–proton elastic scattering, by knowing the primary vertex of neutron trajectory (e.g., point-like target in nuclear physics experiments);
2. double or multiple neutron–proton elastic scattering in the detector active volume.

RIPTIDE is conceived for both cases depending on the application. A detector sketch, describing the RIPTIDE working principle, is shown in Fig. 18 (left). The 3D single- or multiple-proton recoil track reconstruction is obtained by 2D projections on orthogonal planes. The central plastic scintillator (active volume) is surrounded by three optical systems coupled to CMOS or Micro Channels Plates (MCP) imaging devices together with Timepix4 (or similar) pixel detectors. It is important to mention that a "proof-of-principle" experiment for 3D tracking of charged particles by scintillation light successfully demonstrated its feasibility (see ref. [352] for details).

For the preliminary design of a RIPTIDE demonstrator, a cubic active volume is used with the dimension resulting from a compromise between detection efficiency ($\epsilon_n > 10\%$ at $E_n = 10$ MeV) and the geometrical constraints given by the wide-angle optics. In this first configuration, proton track lengths in the range $0.2 < R_p < 30$ mm ($4 < E_p < 50$ MeV) are expected to be studied. In addition, absolute detection efficiency of approximately 15% for monoenergetic neutrons at $E_n = 10$ MeV has been determined by performing Geant4 [353] simulations [354]. Among the concurring neutron scattering interactions in scintillator material (BC-408) the ^{12}C(n,n') is the most prominent. Neutron elastic scattering ($E_n = 20 - 200$ MeV) from C nuclei (and some inelastic scattering channels as well) produces light below typical PMT detection, anyhow, these kinds of events can occur with high rates in the active volume: For instance, a 90 MeV neutron in the detector volume is three times more likely to elastically scatter from C compared to scattering from H.

The optical system is the most challenging part of RIPTIDE. It must be coupled to the plastic scintillator in order to minimize light losses and achieve the best compromise between depth of field, aperture and aberrations. In order to fit with a specific application two complementary readout systems for imaging will be investigated:

1. Back illuminated, high-efficiency low-noise CMOS devices (diagonal size from 1/3" to full-frame);
2. High conversion efficiency photocathode coupled to MCP (single and chevron setup) with pixel sensors such as Timepix [355] or MIMOSIS [356].

Resolution (HxV) and pixel size will be matching the optics in order to obtain a 50-100 μm resolution in proton track reconstruction, and a reasonably small detection threshold for photons produced along the track. An external fast trigger implemented by SiPM will provide a time reference for starting track-image selection (CMOS or MCP-Timepix 2D-frame acquisition) and time-of-flight measurement. Fully embedded readout electronics makes them suitable for advanced and on-the-field neutron dosimetry (nuclear waste and nuclear reactors monitoring) and in space environment applications.

Concerning the complementary readout option, it is well known that MCPs provide suitable spatial resolution (about 10-100 μm) and a large detection surface. Timing is a key feature of such a device, reaching time resolution of 100-200 ps. MCP anodic plane will be coupled to Timepix or similar devices as reported by Tremsin and Vallerga [357]. A detector based on a vacuum tube, with transmission photocathode, MCP and the Timepix4 ASIC as active anode is being developed by Fiorini et al. [358], targeting a timing resolution of tens of picoseconds together with a position resolution of 5-10 microns.

4.3.6 MONDO

Secondary neutrons produced during particle therapy treatments can deposit an absolute non-negligible energy in and out of field even far away from the target volume (voxel) as they are weakly interacting with the patient body [359, 360]. To properly take into account for their contribution with the highest possible precision when performing the treatment plans optimization and evaluating the dose absorbed by the organs at risk, a high-precision experimental characterization of their production energy, flux and angular distributions is eagerly needed.

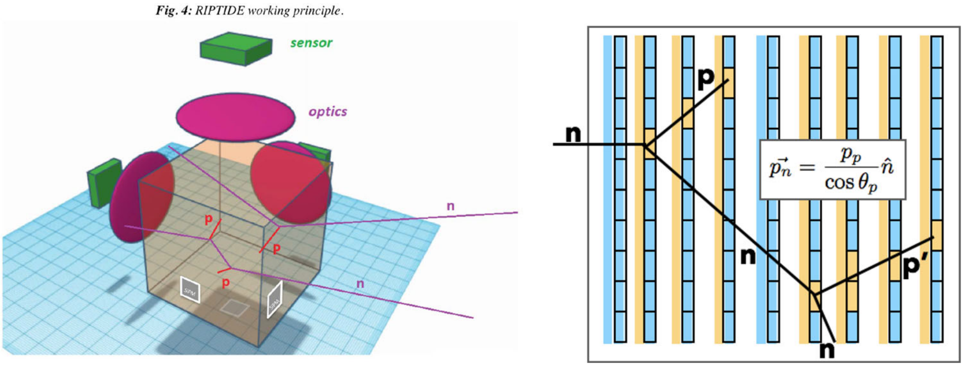

Fig. 18 Schematic representation of a neutron double elastic scattering interaction in the RIPTIDE detector (left) and in MONDO (right). By reconstructing the proton tracks, and measuring their kinetic energies and angles, it is possible to reconstruct the neutron four momentum

The MONDO experiment [347, 361] addresses the technical challenge of secondary ultra-fast neutron detection and tracking with a detector that exploits single and double elastic scattering interactions allowing for a complete neutron four momentum reconstruction. To back-track neutrons, it is indeed crucial to maximize the double elastic scattering probability on hydrogen: The detector is based on a compact matrix of scintillating fibers (squared, 250 μm side, polystyrene-based for the core) readout by an integrated and pixelized electronic system.

The detection efficiency benefits by the highly hydrogenated active material and by the very high granularity of the readout system that has been designed in CMOS-based SPAD array technology. The readout sensors, with pixels of $125 \times 250\ \mu\text{m}^2$ size, are organized in tiles covering the full detector surface, implementing an auto-trigger strategy to identify the events of interest. The tracker layout has been optimized to ensure a detection efficiency of the order of 10^{-1} and 10^{-3} for single and double elastic scattering, respectively. The details on the fiber choice (squared fibers with 250 μm side), the implemented layout and the related readout performed using the SPAD technology have been already presented elsewhere [362]. The readout sensor will be able to cover the full detector area providing the necessary spatial resolution (matching the fiber granularity) and detection efficiency. An auto-trigger algorithm will be implemented using a two level strategy (at pixel and chip level) allowing a significant combinatorial background reduction while keeping a very high efficiency for signal events [363].

A FLUKA simulation has been implemented using an accurate description of the detector geometry and accounted also for the trigger strategy. The simulation has been used as the basis for the background rejection algorithms development and to evaluate the performance of the fragments energy measurement strategies (both for partially and fully contained tracks).

The potential of the MONDO tracker in characterizing the neutrons produced in a particle therapy treatment with carbon ions has been explored using neutrons from a point-like source placed 20 cm from the detector face, according to the energy spectrum of neutrons produced in particle therapy conditions (from FLUKA simulation). Results have been obtained and presented in Ref. [364] for monoenergetic beams and for neutrons generated with the energy spectrum expected in particle therapy applications. An energy resolution of $\sim 3-6\%$ has been evaluated for double elastic scattering events, while the expected back-pointing resolution is below 3.5 mm (for a neutron source placed 20 cm from the detector surface).

The promising outcomes and positive results achieved with various MONDO prototypes provide optimism for the imminent finalization of the SPAD design readout chip and the realization of the complete tracker.

5 Detectors for gamma/X radiation

Many physics processes are followed by or include the emission or one or more photons, with a very wide range of energies depending on the phenomena under investigation. Among these photons, X- and gamma rays are very interesting in many fields of science, from nuclear and high-energy physics to astrophysics, medical physics, imaging, elemental mapping, security, agrifood and many others. Even if a worldwide established convention is still not existing, photons are considered as X-rays when their energy is in the range 0-120 keV, where all the characteristic fluorescence lines of the various materials in the periodic table can be found; beyond this range, photons are gamma rays. Depending on the physics processes involved and on the photons' properties under investigation (energy, position, polarization, etc.), several different types of detectors can be used for their detection; in this chapter, an extensive overview on the recent developments in the detectors' technologies for both X- and gamma rays will be given.

5.1 X-ray radiation detector

Since their discovery in 1895, the detection of X-rays had a strong impact and various applications in several fields of science and human life like nuclear physics, astrophysics, quantum physics, X-ray fluorescence (XRF), X-ray emission spectroscopy (XES), extended X-ray absorption fine structure (EXAFS), particle-induced X-ray emission (PIXE), plasma emission spectroscopy, monochromators, synchrotron radiation, radioprotection, telescopes and space engineering, medical applications, food and beverage

Fig. 19 Schematic representation of a GPD

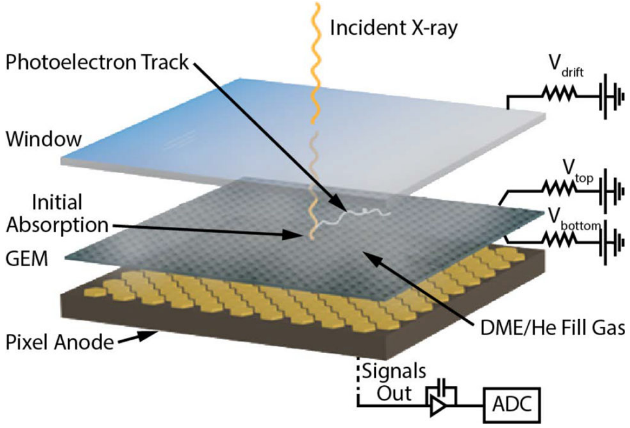

quality control and elemental mapping. Impressive efforts have been done to develop new type of detectors and new techniques, aiming to obtain higher precisions both in terms of energy and position. Depending on the applications, solid-state detectors, microcalorimeters and various types of spectrometers provide nowadays the best performances as spectroscopic and imaging detectors. The now reachable few microns and MeV precisions open the door toward ground breaking applications in fundamental physics, medical science, astrophysics, cultural heritage and several other fields. In this review, the most recent advances in the X-ray detection technology are given, focusing on the following devices: Gas Pixel Detectors (GPDs), pinhole coupled CCD, CdZnTe detectors, high-purity germanium (HPGe) microstrips, hybrid detectors, Transition Edge Sensors (TES) microcalorimeters and large source Bragg spectrometers.

5.1.1 Gas pixel detector

A Gas Pixel Detector [8] (GPD) is a device able to measure the linear polarization of X-rays by exploiting a well-known property of the photoelectric effect: Photoelectrons extracted from an atomic K-shell, which is by far the dominant process when the required energy threshold is met, are emitted preferentially in the direction of oscillation of the photon electric field. Indeed:

$$\frac{d\sigma^K}{d\Omega} \propto \cos^2\phi$$

where ϕ is the azimuthal angle between the direction of the photoelectron and that of the photon polarization vector. By sampling the distribution of azimuthal angles for a given set of photoelectrons, one can statistically recover the linear polarization state (polarization degree and direction) of the parent photon population.

A GPD works as follows (Fig. 19): X-rays enter a gas cell from the top through a window of a transparent material (like beryllium) where they are absorbed by the gas molecules, producing photoelectrons. The negative component of the ionization charge generated by each photoelectron is drifted by an electric field toward the bottom of the gas cell, where it is amplified by a suitable charge multiplication stadium, like a Gas Electron Multiplier [365]. Finally, the charge is collected on a 2D segmented anode, so that an image of the track, projected onto the azimuthal plane, is produced. Typical tracks of $E < 10\,\text{keV}$ have a length of a few hundreds of microns in a gaseous medium: Thus, a spatial resolution $\lesssim 100\mu\text{m}$ is required to properly sample the track development.

Individual track images can be analyzed to extract the initial direction of emission of the photoelectron, either analytically [366] or through machine learning techniques [367]. The energy and the impact point of the X-ray on the detector can also be inferred, allowing for simultaneous imaging and spectroscopy.

Currently, GPDs are employed by the Imaging X-ray Polarimetry Explorer Mission (IXPE), using a custom ASIC with a pixel size of 50 μm as readout anode [368, 369]. The polarimetric capability of the GPDs realized for IXPE is showcased in Fig. 20.

Building on that successful design, a new generation of GPDs is currently being developed. Thanks to an updated readout chip, an order of magnitude smaller dead time per event can be achieved [370], with no measurable degradation of the capability of the detector. At the same time, alternative multiplication stages are being explored, in an attempt to mitigate some of the limitation of the GEMs described in [368].

The new detectors will provide a good match for the next generation of X-ray missions, such as the proposed multi-instrument mission e-XTP, which is designed to host 4 GPDs in its Polarimetric Focusing Array. e-XTP will contribute to our understanding of the nature of strong interactions by studying the equation of state of neutron stars, where “exotic” states and phases of matters such as nuclear superfluids, hyperons and deconfined quarks are most likely formed.

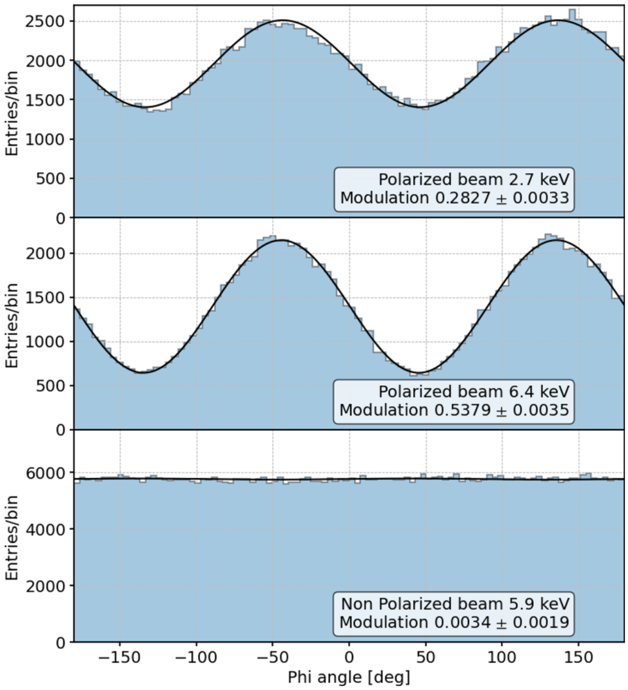

Fig. 20 Distribution of the reconstructed azimuthal photoelectron angle for 100% polarized X-rays of 2.7 keV (*top*), 100% polarized X-rays of 6.4 keV (*middle*), unpolarized X-rays of 5.9 keV (*bottom*) collected during IXPE ground calibrations. ,[368]

5.1.2 Pinhole CCD system for X-ray imaging and spectroscopy

An innovative multi-diagnostic system with advanced analytical methods has been designed and implemented in the recent past at the LNS, in collaboration with the ATOMKI laboratories in Hungary, [9, 371]. It is based on several detectors and techniques: optical emission spectroscopy, RF systems, interferometry, polarimetry, X-ray detector; in the following we will focus on high-resolution spatially resolved X-ray spectroscopy, performed by means of a X-ray pinhole camera setup operating in the 0.5–20 keV energy domain. This technique is particularly utilized to improve the diagnostics tools available for the PANDORA setup [372, 373]. PANDORA (Plasma for Astrophysics, Nuclear Decay Observation and Radiation for Archaeometry) is a project supported by INFN, which aims to measure β-decays of nuclear astrophysical interest for the first time in laboratory plasmas emulating some stellar-like conditions [10]. The aim of the X-ray imaging and space-resolved spectroscopy within the PANDORA project is to support the measurement of β decays in magnetized plasmas, providing the plasma volume, density and temperatures at which the decay lifetime is expected to decrease by several orders of magnitude. The achieved spatial and energy resolutions are currently 0.5 mm and 300 eV at 8 keV, respectively. Innovative analysis algorithms were properly developed for obtaining single-photon-counted (SPhC) images providing the local plasma emitted spectrum in a high dynamic range (HDR) mode [9]. The developed post-processing analysis is also able to remove the readout noise that is often observable at very low exposure times (msec). Figure 21(a) and (b) shows the overall system, including the multi-collimation designed to suppress X-ray scattering, and a perspective front view of the plasma chamber, respectively. The figure also highlights the materials composing the plasma chamber walls: This special design allowed to distinguish between the X fluorescence photons emitted by the Ar plasma from those ones produced by electrons escaping the confinement and impinging on the plasma chamber walls, thus producing fluorescence from the walls materials (Ti, for the chamber endplate), as shown in the post-processed X-ray spectrally resolved image (Fig. 21(c)). SPhC analysis allows quantitative and absolute evaluation of local emission emissivities. Models development to extrapolate space-resolved plasma parameters (density and temperature) from the acquired data is ongoing [374]. A fast X-ray shutters and trigger systems will be implemented in the setup in order to allow simultaneously space and time-resolved plasma spectroscopy during transients, stable and turbulent regimes, with ms timescale.

The development of diffractometric X-ray spectroscopy measurements with high-energy resolution is also foreseen. This technique, based on the use of “gratings,” will allow to reach resolutions of the order of $\Delta\lambda/\lambda = 10^{-3}$ at 565 eV, opening the possibility to carry out XRF peak broadening measurements, so giving access to the indirect measurement of the ion temperature in the plasma.

Advanced plasma diagnostics, especially in the range of soft X-rays, can thus play a crucial role in the new scientific scenario where laboratory ECR plasmas can become new environments for fundamental nuclear physics investigations. They also allow to characterize the mechanisms of plasma instability that are scientifically relevant by itself, since there is the opportunity to reproduce and to study phenomena of astrophysics interest (such as the Cyclotron Maser Instability [376], which is a typical kinetic turbulence occurring in astrophysical objects). PANDORA is expected to start its operations in 2024. Meanwhile, a dedicated test bench, named FPT (Flexible Plasma Trap) [11], will be used at LNS for R&D on diagnostics and detectors.

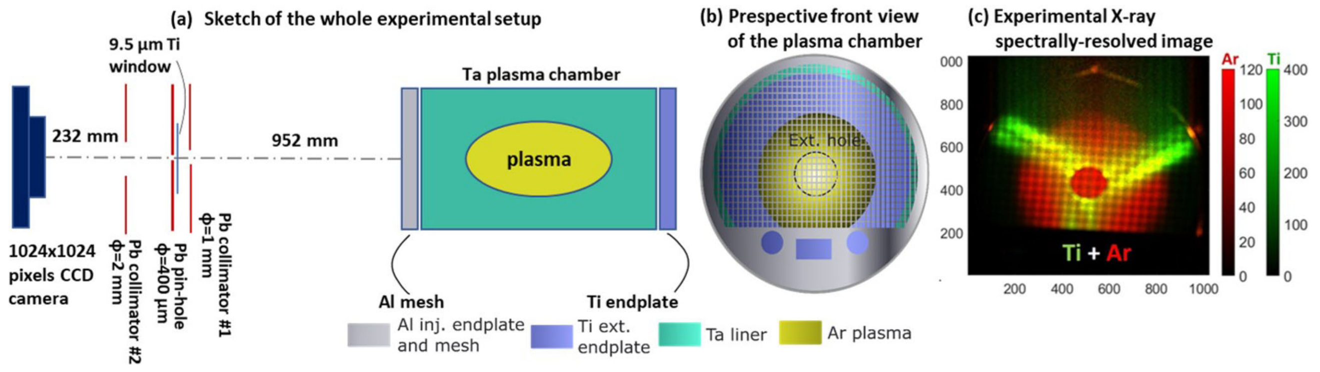

Fig. 21 **a** Overall X-ray imaging pinhole camera setup including anti-scattering collimators and the plasma chamber; **b** front view of the plasma chamber showing the Al mesh allowing for a direct inspection of the plasma chamber inner volume;**c** typical energy-filtered X-ray image including fluorescence coming from the Ar-plasma and the Ti endplate of the plasma chamber [9, 375]

5.1.3 CdZnTe detectors for precision X-ray spectroscopy

The development of semiconductor nuclear radiation detectors has rapidly progressed in recent years. The imaging capabilities, superior energy resolution and the opportunity to create compact systems [377] make these detectors a highly desirable option compared to other types of devices, such as gas detectors and scintillators. Among semiconductor compounds, cadmium-zinc-telluride (CdZnTe or CZT) has become increasingly popular in the field of X- and gamma-ray detection, thanks to its high atomic number, high density and wide bandgap. State-of-the-art digital detection systems based on CZT detectors ensure excellent room temperature energy resolution (2 keV @122 keV[12], 5.1 keV @660 keV[13]), large detection efficiency ($>$ 98% @60 keV with 1-mm-thick detector) and high time resolution ($\sim$ 50 ns) [14].

The applications of X- and gamma-ray detectors span several fields from specific research topics (e.g., astrophysics, fundamental physics) to more practical sectors related to the everyday life (inspection of industrial products, security controls). The characteristics of CZT detectors allow them to be employed in a number of different application fields, including:

- *Hadron physics*. The recent advancements in dynamic range and energy resolution of CZT detectors enable their implementation in experimental apparatuses. An example is that of the SIDDHARTA-2 experiment at LNF (Laboratori Nazionali di Frascati), searching for X-ray transitions emitted from kaonic atoms. CZT detectors will allow, in the near future, to perform extremely important measurements in the low energy strangeness sector using targets of aluminum, lead, sulfur or carbon, having relevant transitions in the 40-300 keV range [15].
- *Astrophysics*. The capability of detecting high-energy photons has a crucial role in the observation of celestial bodies and cosmic radiation. CZT detectors [378–382] allow to investigate the energy band from few keV to MeV, essential to covers the whole electromagnetic spectrum.
- *Medical imaging*. The use of solid-state technology is crucial in the development of innovative medical equipment. Techniques as SPECT (single-photon emission computed tomography) [383–385] and CT (computed tomography)[386] are becoming more and more common in the preventative medicine or surgical applications and the use of such devices have been a great help in the cure[387, 388] and detection of diseases.
- *Environmental monitoring*. Techniques to detect Radiological and Nuclear (RN) agents are strongly requested in the field of homeland security and environmental monitoring, for the rapid scanning of sensitive areas that are possible targets for terrorist threats like dirty bombs or silent sources. In these fields, the development of smart radiation detector systems [389–392] able to detect, measure, identify and analyze gamma-ray emitting radioactive sources is a primary need.
- *Imaging*. International research facilities are investigating high-Z materials [393–395] to replace the current detection systems based on silicon which are limited by a low efficiency above 20 keV. The properties of CZT crystals allow to realize large-area devices ($>$ 1 cm^2) with a fine spatial resolution (down to 55μm) and high stopping power ($>$ 98% @60 keV with 1 mm detector).

The scientific community is working intensively on CZT detectors in each one of discussed applications. For example, next improvements will be: i) enhancement of maximum operative flux, contact quality and spatial resolution in imaging and synchrotron applications; ii) evaluation of radioisotope identification system in operative scenario for environmental monitoring; iii) evaluation of radiation damage and flight planning in gamma-ray telescope development; and iv) realization of a large-area detector with improved time resolution in the study of kaonic atom spectroscopy.

5.1.4 The XH cryogenic detector system

The XH cryogenic detector system [16, 17] provides the unique combination of charge-integrating front-end electronics coupled to one high-purity germanium (HPGe) microstrip sensor made of 1024 strips with 50 μm pitch. The system aims at providing a

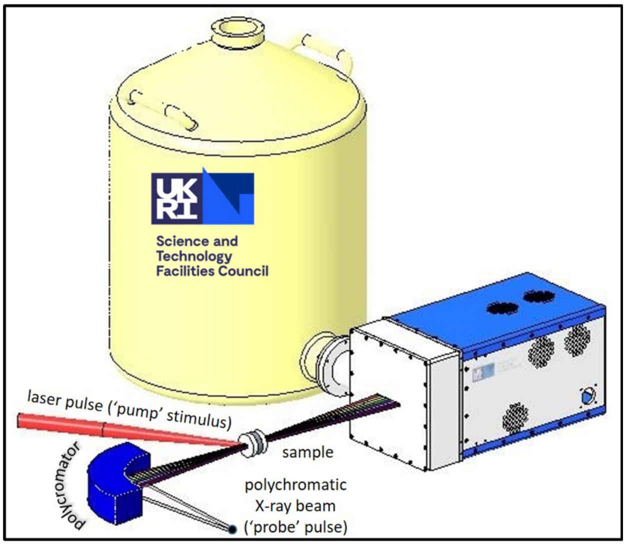

Fig. 22 The sketch of the XH cryogenic detector system taking data in time-resolved energy-dispersive absorption spectroscopy

technical solution suitable for the direct detection of a transmitted beam of hard X-rays over a large area with a uniform and fast response, and with a high spatial resolution. The XH system was developed by UKRI-STFC Daresbury Laboratory in Daresbury (UK). It is now commercially available and it was recently upgraded with commercially supplied HPGe sensors to operate at 4th generation synchrotron facilities. Specifically, this is the case of the high power laser facility (HPLF) [396] at beam line ID24 at the European Synchrotron Radiation Facility (ESRF) in Grenoble (FR). The HPLF is designed to perform energy-dispersive X-ray absorption spectroscopy in time-resolved mode [397] with X-ray beams of energy from 5 keV to 27 keV. The HPLF makes use of dynamic compression techniques to study extreme conditions of pressure and temperature in matter [398]. The facility couples a 100 J ns-pulse laser to an X-ray energy-dispersive spectrometer to perform experiments with the pump-and-probe technique. Figure 22 shows a sketch of the operation principle. The polychromatic X-ray beam from the 4th generation synchrotron is angularly dispersed as a function of the spectral energy by the beam line optics. The beam is focused on the sample and transmitted to the HPGe microstrip sensor. The position of each microstrip is correlated with a particular spectral component of the transmitted beam. The intensity of the signal in each strip is proportional to the intensity of a transmitted spectral component. Note that this concept enables the fast collection (e.g., single shot) of an energy spectrum via the simultaneous acquisition of the different spectral components. The spectrum measures the absorption coefficient of a material over an energy range of $\sim$1 keV centered around the material's absorption edge. The energy resolution of the spectrum is units of electron volts (e.g., 1-2 eV).

HPGe sensors provided the best properties to meet the experimental requirements of a fast response with a high spatial resolution over a large and uniform area. Radiation hardness to total ionizing dose (TID) is also a requirement since the sensor is exposed to a transmitted flux of $\geq 10^9$ photons s^{-1} mm^{-2}. Germanium is an elemental semiconductor with a face-centered diamond-cubic crystal structure that is grown into a highly regular and uniform bulk material. It has a high-Z (32), a high density ($\sim$ 5.3 g cm^{-3}) and a low electron–hole pair-creation energy ($\sim$ 2.96 eV). This results in a high quantum efficiency for hard X-rays. Both charge carriers contribute to a fast signal formation due to their fast mobility, respectively $\sim$ 3900 cm^2 V^{-1} s^{-1} for electrons and $\sim$ 1900 cm^2 V^{-1} s^{-1} for holes. Commercial foundries are capable of high yield fabrication processes by using wafers with a standard diameter of 90 mm, and by segmenting features as small as a few tens of μm. The HPGe sensor deployed at the HPLF is made of 1024 strips with 50 μm pitch. The strip length is 5 mm, and the sensor thickness is 1.5 mm. The strips are patterned on the front-side of the wafer by using a proprietary semiconductor process technology. These strips act as the junction contacts and they are connected to the readout electronics. The back-side is a p-type implant, which is directly exposed to the impinging X-rays. The above design leads to a back-illuminated sensor with a large uniform area and a fine pitch. The large area determines the range of energy detectable with a single sensor. The fine pitch improves spectral/spatial resolution. The back illumination protects the readout contacts from the accumulation of TID. A total of 8 X3CHIPs are installed in the cryostat and wire-bonded to the sensor strips. The X3CHIP is a charge-integrating ASIC designed in AMS 350 nm technology. Each of its 128 front-end channels is made of a preamplifier followed by a sample-and-hold circuit. The X3CHIP is capable of integrating a maximum charge of 50 pC per front-end channel. The minimum integration time is nominally 180 ns, and the maximum is 1 s. The dead time is 1.2 μs.

The XH cryogenic detector system has synergies with applications in nuclear physics. For instance, the XH system required the development of a liquid-nitrogen cryostat that is capable of operating the sensor at a temperature $< -170^{\circ}$ C, while having an internal power consumption of $\sim$11 W. This cryostat is currently being used as a test bed for the development of a Compton camera deploying HPGe double-sided strip sensors [399]. Here, the XH cryostat needs to accommodate the installation and cooling of multiple sensors (i.e., the scatter and the absorber in Compton configuration) with related readout electronics. Furthermore, the XH system would benefit from R&D on new techniques to process radiation hard contacts with a small pitch on HPGe sensors. This requirement could potentially benefit from the pulsed laser diffusion of thin hole-barrier contacts researched by the INFN Nuclear Physics community [400] for gamma-ray detectors.

5.1.5 Hybrid pixel detectors at PSI

In hybrid pixel detectors, the sensor i.e., the layer where the photon interaction happens, is separated from the readout electronics, where the signal is digitized. Each pixel in the sensor is electrically connected to a channel in the readout chip using solder bumps of the order of a few microns. The feasibility of the bump-bonding technique together with the space limitations required by the complexity of the CMOS readout electronics poses a limitation to the achievable pixel size to a few ten microns (25 μm).

The Photon Science detector group at the Paul Scherrer Institut (PSI) has a long history of development of hybrid pixel detectors for X-rays detection at synchrotrons, free electron lasers and laboratories: Detectors have a square pixel pitch ranging from 75 μm of EIGER and JUNGFRAU down to 25 μm of MÖNCH. The development aims to optimize both the sensor, to extend the use of the hybrid detector technology to a wider energy range, and the fast highly parallelized readout chip, which will have to sustain fluxes of order of 10^{10} photons/s/mm^2 at the new generation synchrotron and free electron laser facilities. Sensors and readout electronics can be combined depending on the application.

The choice of the sensor mainly depends on the X-ray energy range. Standard planar silicon sensors with thickness of $\approx$ 300 μm reach their maximum quantum efficiency in the range 4 keV–12 keV, while thicknesses up to 1 mm allows to reach a fair sensitivity up to 20 keV photons. High Z sensor materials, like GaAs and CdTe or CdZnTe, are being studied [401, 402] to reach high absorption efficiency up to 120 keV, although the technology still suffers from poor crystal quality and limited availability. Soft X-rays ($<$ 1 keV) penetrate less than a micron in the silicon sensor, posing strict limitations on the thickness of the metallization and passivation layers at the entrance window of the detector, thus requiring a high-charge collection efficiency even close to the silicon surface. PSI in collaboration with FBK is developing a thin entrance window technology, which has shown a quantum efficiency $>$ 60% down to 250 eV [403]. This technology has been combined with Inverse Low Gain Avalanche Detectors (iLGAD). The charge generated by the absorbed X-rays is multiplied in a high electric filed gain layer, increasing the SNR of low energy photons. Already in the first iLGAD generation optimized for X-ray detection, 452 eV could be detected with a SNR $\approx$ 23, compared to an SNR $\approx$ 2 using standard silicon sensors [404].

Single-photon counting readout chips [405, 406] are used to measure the intensity of photons. If the signal is above one or more programmable thresholds, the pixel itself increments an on-pixel counter that keeps track of how many photons impinged on the pixel. The detector has the advantage of being noise free after the threshold is properly set and long acquisitions can be performed as the intensity information remains on the pixel till the readout. To overcome pileup limitations at high photon fluxes charge-integrating detectors with dynamic gain switching [407, 408], i.e., adapting the dynamic range of each pixel individually depending on the detected intensity, can be used for fluxes > 10 Mcounts/pixel/s, as well as for a pulsed source. As a disadvantage, the conversion to the number of photons needs to be computed off-line from the deposited charge and a fast readout is mandatory both to compensate for the limited dynamic range for a single acquisition and the effect of the increasing leakage current for long acquisitions.

The detector [409], with its 25 μm pixel pitch, allows imaging with high spatial resolution that, at low occupancy ($\approx$ 1%), can be improved beyond the pixel pitch using interpolation techniques, as shown in Fig. 23, combined with a moderate energy resolution ($\approx$ 700 eV FWHM) [410].

At PSI, there is an ongoing work on the characterization of high-Z sensors in order to select the best candidate material for large-area pixels detectors, investigating in particular the time response for time-resolved studies. Moreover, after the first encouraging results, further optimization of the iLGAD technology is ongoing in order to achieve single-photon detection down to 250 eV in the next few years. A new generation of single-photon counting detectors with multiple independent counters and comparators (MATTERHORN) aims at increasing the count rate capability of at least an order of magnitude (up to 20 MHz/pixel) by faster shaping of the analogue signal and by counting "piled up" photons, while charge-integrating detectors readout at 10 kHz frame rate will further improve the detection up to 200 MHz photon flux. We are also designing a large-area version of MÖNCH (single chip $\sim 2 \times 3\,\mathrm{cm}^2$, modules $\sim 4 \times 3\,\mathrm{cm}^2$) with optimized noise, which will be used for energy resolved high-resolution imaging as well as for X-ray spectrometers exploiting interpolation, both for hard X-rays using planar silicon and soft X-rays if combined with LGAD sensors.

5.1.6 Transition edge sensors for ultra-high-resolution X- and gamma-ray spectroscopy

Transition Edge Sensors (TES) are highly sensitive cryogenics thermometers that exploit the temperature dependence of a superconductor's resistance to measure incident power [411]. By operating at their superconducting transition temperature ($T_c \sim 100 - 400\,\mathrm{mK}$), TES can detect even small variations in temperature with high accuracy. First realized by Andrews [412], TESs are now the most sensitive detectors to radiation from the gamma-ray through the millimeter wave [413]. When coupled to a suitable absorber, TESs become radiation detectors with outstanding spectroscopic capabilities. In the case of X-rays and gamma rays, the energy of single photons can be measured with resolving powers $E/\Delta E > 10^3$ [18].

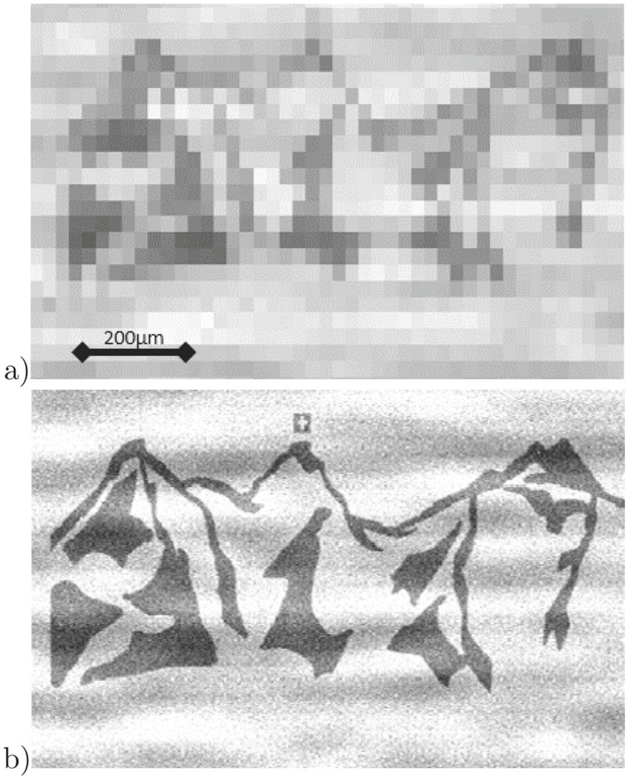

Fig. 23 Image of a gold-on-silicon sample representing the Eiger, MÖNCH and Jungfrau mountains acquired using the MÖNCH detector. a) Shows the image using the 25 μm physical pixels size, while b) after applying the interpolation methods described in [410] using 2.5 μm bins. The width of the cross in the 25 μm Swiss flag is only 7 μm, i.e., well beyond the pixel pitch

When a particle with energy E is absorbed by the TES (Fig. 24, left), the temperature of the detector increases by an amount $\Delta T = E/C$, where C is heat capacity of the absorber. This causes a corresponding increase in the resistance of the superconductor, which diverts current through the shunt resistor, varying the current flowing through the SQUID input coil (Fig. 24, right). The device then returns to its steady-state temperature with an exponential decay time constant $\tau = C/G$ (Fig. 24, center), where G represents the thermal conductance to the bath. In a typical SQUID readout system, the TES operates in series with the input coil L, which is inductively coupled to a SQUID that acts as an ammeter (Fig. 24, left). Any variation in the TES current results in a modification of the input flux to the SQUID, and its output can amplified and read by electronics at room temperature.

The initial research on TES-based microcalorimeters was driven by the need to investigate astronomical entities. In ground-based astrophysics observatories, arrays of TESs are utilized for studies in the energy spectrum of X-rays and gamma rays [414]. Over the past decade, as TES spectrometers have grown in size and resolving power, applications outside astronomy have proliferated are now commonly employed at a variety of light sources, accelerator facilities and laboratory-scale experiments. The HOLMES collaboration, led by INFN, will assess the neutrino mass by study the electron capture of the 163-holmium by implanting this radioactive isotope into gold absorbers coupled to TESs [19, 20]. The interaction between kaons and nucleons has been studied using TES by measuring the X-rays emitted during the decay of a kaonic atom. These studies have provided important insights into the nature of the strong force [415, 416]. TES detector has also promising applications for improving branching ratios in nuclear decays [417], for the characterization of trace radionuclides [418], for the study of transuranium elements [419] and for tracing nuclear material in soil for analysis at contaminated test sites [420].

5.1.7 High-precision nuclear physics measurements with HAPG mosaic crystals: the VOXES spectrometer

Atomic and nuclear physics experiments do quite often rely on precise measurements of X-rays emitted from various type of transitions, requiring a continuous technological boost toward cutting-edge radiation detectors. Bragg spectroscopy is among the most consolidated techniques to perform high-energy resolution X-ray measurements, being, however, strongly limited to detect photons produced from almost point-like (few tens of microns) or well-collimated sources. This limitation prevented the employment of such a technique for all those experiments in which targets with millimetric or even centimetric dimensions are to be used, like in the case of gaseous kaonic atoms where the sub-eV precision measurements of their characteristic radiative transitions are highly craved from the strangeness nuclear physics community [421]. The VOXES (high-resolution VOn hamos X-ray spectrometer using HAPG for Extended Sources) collaboration at the INFN Laboratories of Frascati (LNF) exploited the unique properties of Highly Annealed Pyrolytic Graphite (HAPG) mosaic crystals to develop a high-resolution X-ray spectrometer, a schematic view of which is presented in Fig. 25 [21], able to reach few eV resolution and sub-eV precision measurements of photons emitted from millimetric targets.

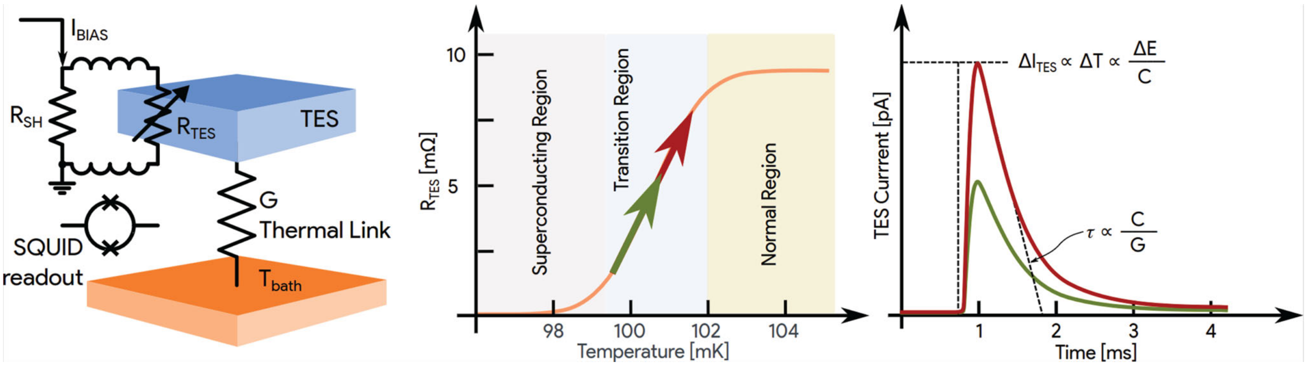

Fig. 24 (left) Basic architecture of a TES detector. The SQUID amplifier is employed as an ammeter that measures changes in TES current due to absorption of energetic particles. (center) TES transition curve with polarization within its transition region. (right) TES current pulse events as function on time generated by two different photons with different energies

Fig. 25 Schematic view of the VOXES spectrometer [422]

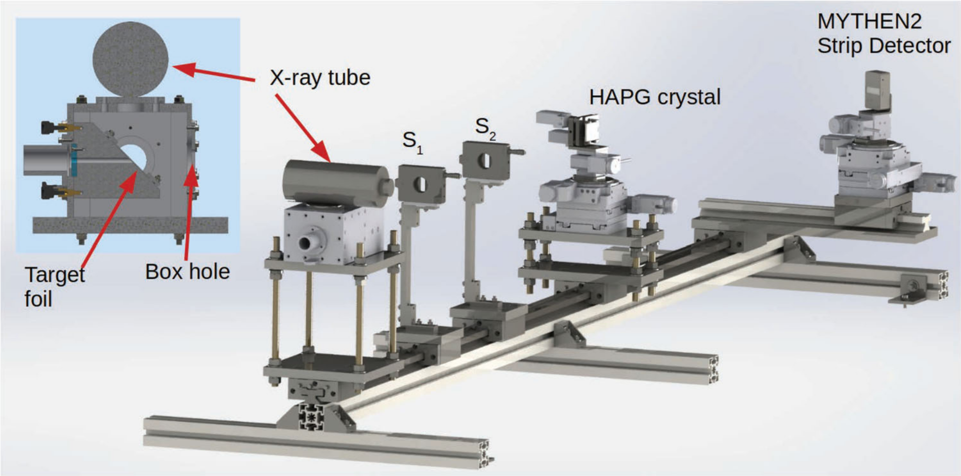

Highly Annealed Pyrolytic Graphite (HAPG) are mosaic crystals consisting in a large number of nearly perfect small crystallites, slightly misoriented with respect to the main crystal's nominal axis; the angular deviation from this direction follows either a Gaussian or a Lorentzian distribution, the FWHM of which is called mosaicity. This particular arrangement makes it possible that even a photon with energy and direction not perfectly matching the $n\lambda = 2d\sin\theta$ Bragg relation, where n is an integer number, d the crystal lattice constant, λ the photon wavelength and θ its impinging angle on the crystal surface, may still find a properly oriented crystallite and be reflected, thus enhancing the reflection efficiency [21, 422] Thanks to a lattice spacing constant d = 3.514 Å, HAPG crystals are highly efficient in the 2-20 keV energy range; furthermore, their growth procedure makes them suitable to be used in the VOn hamos configuration combining the standard dispersion of a flat crystal with the focusing properties of cylindrically bent ones. The VOXES collaboration performed, starting in 2016, a detailed investigation on the influence of the main parameters of HAPG crystals, like mosaicity, thickness and curvature radius, on the energy resolution as well as a deep study of their calibration function and reflection efficiency, crosschecking all these results with ad-hoc ray-tracing Monte Carlo simulations [422–424]. The very promising results achieved with VOXES could be used to perform extreme (sub-eV) precision measurements of kaonic atoms transitions allowing for fundamental measurements like the charged kaon mass, still representing a pending open puzzle also impacting the D-meson sector [425, 426]. A more accurate kaon mass determination may also become appealing for first-principle calculations on the lattice and, finally, measurements of very narrow kaonic atoms lines (few eV or below eV FWHM) could provide crucial information on the highly debated nature of the $\Lambda(1405)$ resonance [427]. The VOXES spectrometer has been included in a proposal for future kaonic atoms measurements at the DAΦNE collider of the INFN Laboratories of Frascati [428]. Beyond high-precision kaonic atoms' measurements, the VOXES spectrometer has possible applications in several fields, ranging from fundamental physics, synchrotron radiation and X-FEL applications, to the agrifood sector. This latter one has been already explored by the VOXES collaboration within the TASTE and MITIQO follow-up projects at LNF, where the possibility to exploit the good performances of the HAPG-based spectrometer also with liquid samples is being investigated. The aim of these two projects is that of providing information about the quality of edible liquids through the detection of the shift of the typical fluorescence lines of metals induced by oxidation mechanisms like, for example, that of the iron in wines (browning). For these and further future applications and fundamental measurements, the VOXES spectrometer has been recently equipped with a full set of motorized carriers, for a more

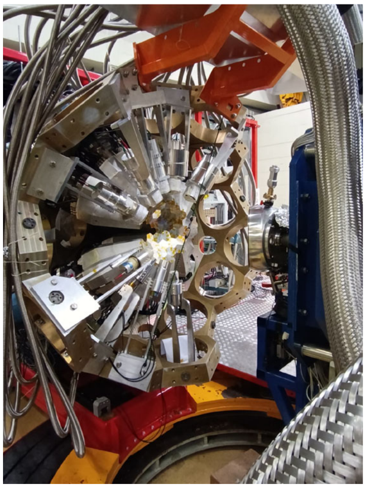

Fig. 26 AGATA system at LNL-INFN with 13 ATCs installed

efficient and precise alignment, as well as with a 13 micron pixel size CCD; this latter, when used as position detector in place of the currently used 50 micron pitch MYTHEN2 strip detector, will allow for an improvement both in the fitting sensitivity and in the background rejection, exploiting the possibility to detect eventual focal aberration and to measure the curved profile of the Bragg-reflected photons typically induced by cylindrical crystals [429].

5.2 Gamma-ray radiation detectors

Gamma radiation, discovered in the early twentieth century through the decay of an excited nucleus of radium, possesses remarkable penetrating power through dense materials. This unique characteristic renders gamma radiation exceptionally versatile and indispensable across numerous practical applications. Among these there are radiotherapy, medical imaging, mechanical component testing and security measures. Moreover, in research laboratories, gamma radiation plays a pivotal role in exploring atomic structure, nuclear reactions and various physical and chemical properties of materials.

In recent years, significant advancements have been made in gamma-ray detection technologies within the realm of nuclear spectroscopy. Notably, the portable spectrometer AGATA represents a monumental leap forward in this field. AGATA facilitates precise and intricate tracking of gamma rays, empowering scientists to glean more precise insights into the nuclear properties of the elements and compounds under scrutiny. Presently, efforts are underway to implement new contact methodologies utilizing pulsed laser melting (PLM) techniques for hyperpure germanium detectors, akin to those employed in the AGATA project. This research aims to enhance the performance of future detectors, enabling heightened sensitivity and superior resolution by amalgamating the development of ASIC-type electronics with dynamic energy ranges and an innovative fast-reset circuit. When operating under neutron beam conditions, hyperpure germanium detectors may incur damage necessitating recuperative annealing processes. Subsequently, to identify and assess potential structural damage, AGATA detectors undergo characterization utilizing a three-dimensional scanning table outfitted with highly collimated and intense gamma sources. GALILEO HPGe detectors [430] are slated for use in β decay experiments like PANDORA, facilitating the detection of gamma rays emitted by decaying nuclei within confined plasma. For such experiments, these detectors must guarantee a high counting rate within a gamma range spanning from 100KeV to 2MeV. Gamma detectors, such as $LaBr_3 : Cr : Sr$ crystal scintillators coupled with 3-inch silicon photomultipliers (SiPMs), are currently in development alongside digital acquisition electronics featuring automatic gain control (AGC) across an expansive energy spectrum. Within the OREO project, inorganic scintillators have been refined to obtain beam-oriented crystals for its integration into electromagnetic calorimeters. These innovations find applications in high-energy physics, astroparticle physics and forthcoming high-performance detectors for nuclear/hadronic and medical physics realms.

5.2.1 AGATA array installation at LNL and detectors characterization

The European gamma array system consists of 30 triple clusters (ATCs) n-HPGe detectors presenting 36 segments + 1 core. The mechanical structure at LNL is a 2π configuration which allows to install up to 27 triple clusters [22]. Indeed, the AGATA system is coupled with the PRISMA spectrometer at Tandem-Alpi-Piave accelerator facility, forming a unique experimental tool for nuclear physics. The AGATA-PRISMA system can rotate between 20° and 110° in the present configuration; a future AGATA installation phase is planned to perform 0° measurements. The AGATA array can be moved back and forward with respect to the reaction chamber, changing the solid angle of the system and allowing the installation of other detectors in between (Fig. 26).

The capsules replacement is one of the most important upgrades that is being done: All the detector capsules will be progressively replaced by new ones, presenting an improved vacuum system. The welded capsules (old design) [431–433] may suffer leakage current (about one out of three) after the annealing process (2 days at 102°C). The new capsule design includes a particular gasket allowing several openings and easier repairs [23, 433, 434]. Moreover, a more reliable annealing process is now implemented, the capsules being pumped during the annealing. During the AGATA array installation at Legnaro Laboratories several other mechanical upgrades were implemented. A new ATC mounting system was developed, allowing to insert each cluster horizontally. To guarantee a precise mounting, new pins are installed in the bearing structure, and with a new laser tracker tool was installed on the ATC end-cup. Thanks to these improvements, the detector alignment precision leads to a spacing of 0.4mm between ATCs [149, 431].

Thanks to a collaboration with IPHC in Strasbourg (FRA), a HPGe detector characterization is possible, making use of an automatic scanning table based on the PSCS technique [435] and of an intense collimated ^{137}Cs source [24]. HPGe detector is scanned in vertical (x) and horizontal (y) positions and an energy spectrum and pulse shapes are acquired for each x,y position. After a complete scan, data are analyzed and a spatial volume reconstruction is performed. Information such as crystal lattice orientation, local detection efficiency, energy resolution, pulse rise time and peak shift may be extracted. In one specific case (an AGATA symmetric n-type detector), a crystal lattice anomaly is evidenced leading to an enhanced electron trapping effect, which defect area can be reconstructed. Studies on the trapping half-life, trap energy-depth and collection efficiency are ongoing. Moreover, thanks to the collaboration with LNL groups, other analyses on new HPGe detectors are planned, such as scanning of different passivation techniques and of junctions created with the pulsed laser melting (PLM) technique (see section 5.2.2).

5.2.2 N3G project

The *Next Generation Germanium Gamma Detectors* (N3G) project is an ongoing R&D activity, currently funded by INFN-CSNV. This project aims to develop a new type of high-purity germanium coaxial segmented detectors based on a novel type of doping procedure, the pulsed laser melting technique [436]. This project is based on a strong collaboration between different groups present at LNL, Ferrara and Milano INFN sections and the University of Padova (UNIPD).

Nowadays, commercial detectors for gamma spectroscopy trackers are segmented n-type HPGe crystal with a segmented boron implanted junction on the external surface (p contact) and an evaporated lithium doped layer on the central hole (n contact). The space sensitivity of these detectors is based on the collection of holes at the segmented junctions, but it is known that during the detector life, the exposure to neutrons damages the detector by creating hole traps in the bulk [437], thus degrading the resolution: For this reason, electron collecting devices should be preferred. On the other hand, lithium that is used for n^+ electron collecting contact presents a high diffusivity on Ge, which forms a 0.5–1-mm-thick junctions, preventing a stable and thin segmentation. For these reasons, today the segmentation must be performed on boron p contact and a lack of thin and stable under damage recovering annealing is a strong technological limitation.

The pulsed laser melting (PLM) process [27] is an out-of-equilibrium technique able to create thin doped layers on semiconductor materials, and also on HPGe, preserving the purity of the crystal bulk [29]. In particular, the process consists of the use of a UV pulsed laser that locally heats the surface at a temperature above the Ge melting point, generating a liquid Ge phase. After the laser pulse, the heating diffusion and dissipation govern the process: At first, the liquid region expands toward the bulk due to the heat diffusion (from some nm to some hundreds nm, depending on the laser parameters), but after some tens of nanoseconds, the temperature of system drop below the melting temperature and the liquid layer starts to epitaxially regrow from the liquid–solid interface toward the surface. This regrow is characterized by a very high speed, reconstructing the crystal structure and embedding in the lattice any other impurities that may be present in the melted phase. Indeed, the PLM induced surface doping is based on a thin layer of impurities added on the surface of Ge before the PLM process, to diffuse them into the melted Ge phase during the PLM. This technique allows to produce both n^+ and p^+ type doping on HPGe, maintaining the HPGe bulk uncontaminated thanks to the high thermal gradient near the solid–liquid interface, combined with the speed of the process. In particular, the bulk remains essentially at the room temperature during the PLM process and the time between the laser pulse and the complete re-solidification is in the order of a few hundred of nanoseconds [438]. Thanks to this dopant diffusion and activation process, 150-200 nm junctions can be easily created [26], allowing an easy thin segmentation (possible on both n and p contacts) and increasing the detector active volume with respect to the Li doped HPGe.

The process to fabricate one of these innovative detectors has already been successfully studied on thin planar geometry [25, 27, 439]: A Sb-doped n^+ contact made by using PLM technique and segmented via photolithography was revealed to be effective. Low leakage currents and good spectroscopy data with different gamma-ray sources were obtained, proving also a very good detector stability to standard damage annealing processing. The upgraded fabrication process for coaxial geometries consists of major renew in sputtering, PLM and photolithographic systems to allow them to be compatible with coaxial geometry crystals. Both n and p contacts may be formed using PLM technology, but posing some technological challenges.

The fabrication process will consist in a grinding and polishing step with wet etching (3:1 HNO_3: HF acid solution), a dopant sputtering deposition inside a chamber with one rotational axis to deposit on the full lateral surface of the coaxial crystal, two perpendicular linear axes to move the crystal in the chamber and a 90° joint to allow deposition on the frontal tip of the crystal. Then PLM doping process is performed moving and rotating the sample under the laser beam with six motorized degrees of freedom and three manual ones for tilting compensation. Then gold plating of the sample external surface is performed in the same sputtering chamber as before and a photolithographic process is performed using a six-joints industrial robotic arm with a UV laser diode

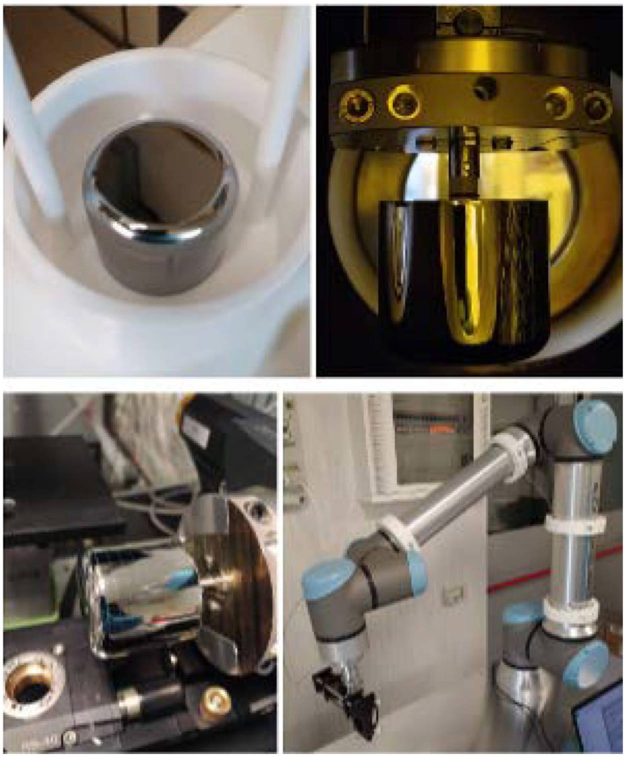

Fig. 27 From top left to bottom right: coaxial sample in a PTFE becker before etching, mounted in the sputtering chamber and under the UV laser beamline. Finally, the robotic arm, ready to expose the photoresist for the segmentation of a detector

mounted on. Several dummy samples are being used to singularly test every step described above (Fig 27). The final detector will be mounted on a prototyped cryostat to perform I-V measurements and gamma spectroscopy to perform acceptance tests on every external n^+ segment and the p^+ central core.

In the last years, the LNL and UNIPD research groups focused the attention to Ge surfaces, developing surface treatments for dopant precursor deposition and for electrical passivation [440–442]. The study of new dopant methodology was addressed with the aim of producing conformal deposition of dopants potentially useful to produce complex detector geometry on a large scale, but also for electronic devices on a nanometric scale. More in detail, monolayer doping (MLD) technique uses adsorbed molecular precursors as surface source of dopant: After a self-limited chemical deposition of molecular precursor on Ge, the formed layer is thermally processed and the molecular source releases a dopant species from the surface into the bulk.

Different studies demonstrate that some phosphorus-based molecular precursors treated with pulsed laser melting are effective [28, 443], forming an n^+ junction in Ge. Moreover, also a Sb monolayer can be formed by a self-limiting gas phase deposition [444, 445], but due to the high deposition temperature, this procedure is not compatible with HPGe. The research is now focused on the scalability of this process to obtain a homogeneous and continuous layer able to cover an entire HPGe coaxial detector; moreover, the handling of a monolayer functionalized detector during different processing steps is a source of issues that must be addressed [446].

N3G electronics The N3G project is also devoted to developing front-end electronics components for new segmented coaxial HPGe detectors.

The HPGe crystal is connected to the readout electronic chain by means of a custom contact system developed by the INFN group of Milano (Italy). This is made of two parts: The first is a flexible PCB realized on a thin polyimide substrate that envelops the detector completely. It holds four sets of gold-coated pads to be folded and leant against the detector electrodes. This system of pads guarantees the electrical contact of the electrodes without scratching or damaging their brittle surfaces. The second part is a rigid PCB. It provides a system of electric connectors that brings the current signals from the flexible PCB to the Charge Sensitive Preamplifiers (CSPs), housed outside the vacuum chamber containing the crystal.

With respect to the state-of-the-art HPGe readout chain, the collaboration is developing ASIC (Applied Specific Integrated Circuits) CSPs. Compared to those made with discrete components, integrated devices occupy a smaller area and volume and are much less power-consuming. As a matter of fact, the first ASIC CSP developed in the framework of the N3G project is characterized by 6 mW power consumption and 8 MeV dynamic range, which can be extended up to 40 MeV thanks to an innovative fast-reset circuit [196, 447]. The described device has been tested at room temperature on a dedicated test bench. Below its saturation threshold, set by the power supply voltages, the preamplifier removes the charge collected from the detector by its feedback resistor, which can be discrete [448] or integrated [200]. The CSP shows an excellent linear behavior and a leading-edge fall-time in the order of 20 ns. Its energy resolution, reported in Fig 28, has been tested filtering its output signal by a 4^{th} order quasi-Gaussian shaping amplifier and using a 15 pF capacitance to simulate the detector’s one. An equivalent noise charge (ENC) of 154 electrons (rms) and

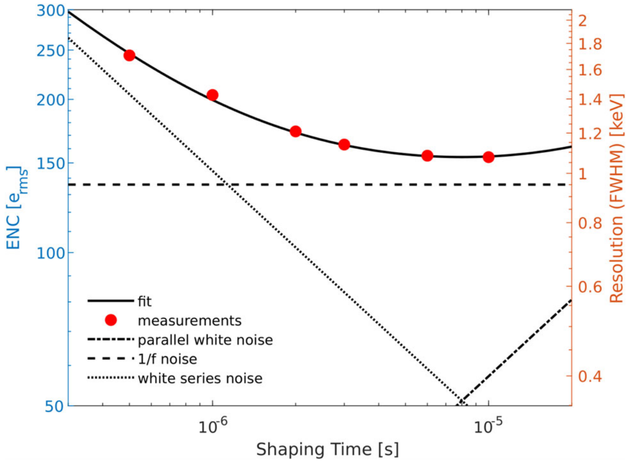

Fig. 28 Equivalent Noise Charge and Energy Resolution Measurements with an Ortec 572 Shaping Amplifiers

an energy resolution (expressed as FWHM) of 1.08 keV have been obtained with 10 μs shaping time, simulating 1 MeV interactions inside the detector. Above the saturation threshold, the energy of the interactions can be retrieved thanks to the previously introduced fast-reset mechanism, which discharges the CSP input node. The time-duration of the saturated signal is proportional to the charge accumulated and, as a consequence, to the energy released inside the detector itself [190, 197]. For events of energy greater than 15 MeV, the measured resolution, expressed as FWHM, is better than 0.1%.

Further improvements in resolution performances are expected in the next few years. Specifically, the collaboration plans to develop cryogenic ASIC preamplifiers housed in the cold-part of the cryostat, to work in close proximity to the detector. This solution would guarantee the possibility to reduce the thermal noise of the devices and the parasitic capacitances due to the long cables and electric connections otherwise needed. Developing cryogenic ASICs is particularly challenging because of the lack of simulation-models describing the transistors working behaviors at liquid-nitrogen or liquid-argon temperatures. Specifically, the quantities that mostly determine the behavioral differences between room and cryogenic temperature are the threshold voltage and the carrier mobility that in turn influence the transconductance [449, 450]. The collaboration would approach this problem realizing an integrated circuit housing a set of p-Mos and n-Mos transistors characterized by different parameters. By studying the devices behavior at cryogenic temperatures, it would be possible to retrieve the information necessary to correctly model them in simulation tools. Once achieved this goal, the collaboration would be able to simulate more complex circuits, as the CSPs themselves, and keep on their production.

5.2.3 PANDORA project

In the last decades, many theoretical and experimental efforts were dedicated to improve our knowledge of the weak interactions in environments similar to those where nucleosynthesis proceeds. Despite the attempts, the present lack of accurate experimental data calls for a new approach able to elucidate the effects of stellar plasma on the different β decay processes. Lifetimes of radioactive nuclei are known to be affected by the degree of ionization and the level configurations of their respective atomic shells [451, 452]. Beta decay in stellar plasmas can result in lifetimes shortened down to few orders of magnitude if compared to those measured, for the same nuclei, in terrestrial environment, even nuclei which are stable in terrestrial conditions may become radioactive once heavily ionized in the plasma [452].

To get a deeper knowledge on these phenomena, a new experiment, named PANDORA, has been proposed [31]. It is based on the use of a plasma trap to emulate some specific stellar-like conditions and to study the evolution of the β-decay main features of selected radioisotopes as a function of plasma parameters. The plasma trap will be used to confine the hot plasma in which a known concentration of the isotope is injected and to keep it in dynamical equilibrium using the magnetic field generated by three superconducting axial coils and an hexapole. Once the β-decay will occur, the daughter nuclei, still confined in the plasma, will emit γ-rays, which will be detected by an array of HPGe detectors allowing for the identification of the decaying nuclei. The measurement of the decay rate as a function of time will be correlated with the plasma temperature and density, both measured through a wide set of noninvasive diagnostic tools allowing for a mapping of the evolution of the β decay rate as a function of main plasma parameters [31, 453].

While the HPGe detector array and the multi-diagnostic system play a fundamental role in the experiment, in the following we will concentrate only on the HPGe detector array which is made of 14 large-volume HPGe detectors (with about 70% relative efficiency) [31, 454]. Twelve detectors will be installed around the magnetic trap, in correspondence to a set of radial lines of sight, conically shaped, created between the warm bore radius and the external iron joke through the cryostat and the inner cold mass at a radial distance of a few centimeters from the yoke using a dedicated mechanics. At such a distance, the estimated stray field will be of the order of 100 G, and therefore, no effects on the charge collection efficiency leading to a deterioration of the energy resolution

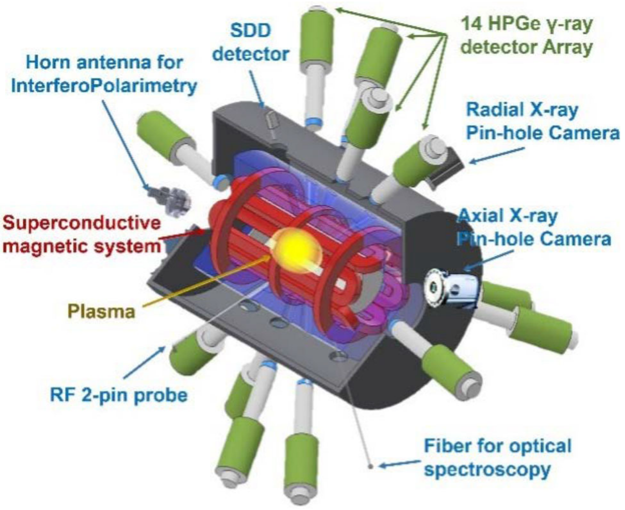

Fig. 29 Rendering of the PANDORA setup with the systems used to measure in-plasma activity (14 HPGe detector array) and to monitor plasma properties (multi-diagnostics system)

due to the magnetic field are expected. Two further detectors will be placed axially [31, 454]. A rendering of the PANDORA setup with the whole diagnostic and detection system is shown in Fig 29.

The design of the array represents a compromise between the best detection efficiency achievable and the mechanical constraints imposed by the feasibility of creating a large number of apertures in the cryostat and the yoke without altering the magnetic field shape. The chosen configuration is optimized to rule out the regions of the magnetic trap where an intense background noise is present due to the in-plasma electron bremsstrahlung and fluorescence by deconfined electron impinging on plasma chamber walls, leading to strong X-rays emission.

GEANT4 simulations were performed to evaluate the total detection efficiency of the array [454]. An ellipsoidal isotropic source placed in the center of the plasma trap with a size of 79 mm, 79 mm and 56 mm (x, y, z) was used to describe the plasma emission volume. The HPGe array was modeled using GALILEO HPGe detectors features as they will be used during the first PANDORA experimental campaign thanks to a collaboration agreement signed between GAMMA and PANDORA collaborations. The detection of gamma rays in the range from 100 keV to 2 MeV was investigated. The results of the simulations indicate that the total photopeak detection efficiency reaches a maximum of 1.6 10^{-3} at E_{γ} around 200 keV and then smoothly decreases with increasing energy reaching a value of about 8×10^{-4} at 2 MeV. Such a value, while being apparently small compared to the typical values of the photopeak efficiency of the arrays used nowadays, is compensated by the high number of decaying ions in plasma, allowing for the measurement of the predicted variations of beta-decay half-life of different interesting physics cases using experimental run durations up to three months [453, 454].

Plasma X-ray self-emission creates harsh experimental conditions for HPGe detectors which will be subjected to up 50 kHz counting rate over a large period. Dedicated preamplifier based on the successful discrete-type model used to perform the readout of the GALILEO array were developed by the colleagues of LNL to cope with such a high counting rate [32]. Tests performed on the new devices using a multi-source setup, able to simulate different low energy background counting rates, clearly indicate that the detector energy resolution measured on the 1332 keV transition as a function of the total counting rate remains around 3 keV at about 60 kHz [32]. At the same time, tests of the stability of the preamplifier and readout electronics did not show any significant deviation in the peak position over 60 h test runs [32]. The detector support system is under development. It includes several hardware components as detector preamplifier and digitizer LV power supply, automatic HPGe cooling system as well as an integrated slow-control software to manage and supervise the detector operations. All these components are needed to guarantee the proper operation of the 14 HPGe detectors placed around the plasma trap.

5.2.4 *Gamma-ray detector based on* $LaBr_3$*:Cr:Sr scintillators with SiPMs and ASICs readout*

An R&D activity concerning $LaBr_3$ codoped scintillators detectors R&D and the developing of the associated ASICs are under development at Milano INFN section (Italy).

A cylindrical large-volume codoped $LaBr_3$:Cr:Sr crystal (3x3") was coupled to a square 3" silicon photomultipliers (SiPMs) matrix composed by 144 units. Each SiPM unit is a square of 6 mm and consists of approximately 40000 single-photon avalanche diode (SPAD). Each SPAD has a side of approximately 30 μm [455, 456]. The SiPM was the NUV-HD type produced by FBK in Trento (Italy).

The detector was tested with calibration gamma sources (e.g., ^{60}Co, ^{137}Cs, *AmBeNi*), and no differences were observed in the measured energy spectra when compared with those acquired using photomultipliers (PMT) from Hamamatsu (Model R6233-100), a custom Voltage Divider [457] and an analogue electronics chain. The maximum count rate at which the resolution of the SiPM

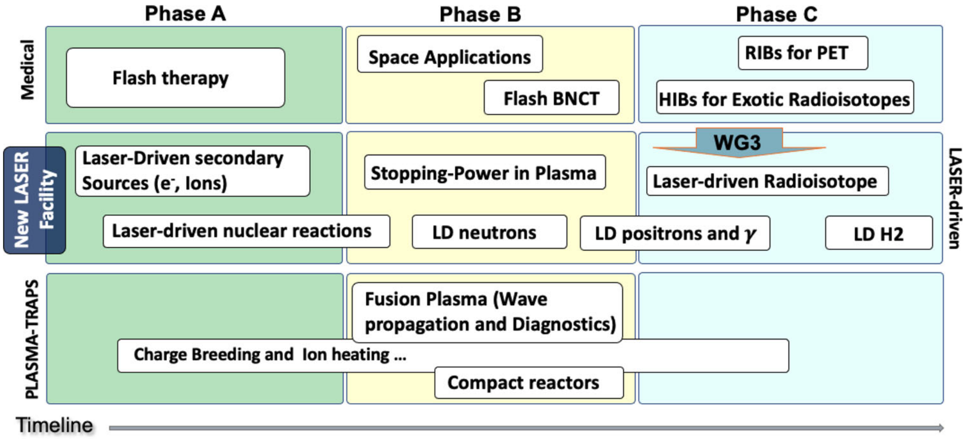

Fig. 30 Time-line organization of the future activities in the field of Nuclear Applications at LNS

read crystal is not degraded is of the order of 40 KHz. The detector was also used in the measurement of monochromatic gamma rays of 15.1 MeV emitted in the reaction $^{11}B(D, n)^{12}C$ [458]. As for the case of low energy gamma rays, no differences in the energy spectra (if compared with some previous measurements with photomultipliers) were noticed.

The $LaBr_3$:Cr:Sr crystal nonlinearity measured by SiPM shows a similar value to the PMT case. The detector nonlinearity was tested in the range of 90 keV to 15.1 MeV.

The detector digital electronics is made by nine custom-designed ASICs [30] and it operates in a stand-alone mode using an USB connection interface for the DAQ and also for the SiPM power supply. The electronics can provide an analogue energy signal, a NIM time signal and a signal related to the interaction position of the gamma-ray that will be developed in the future. Moreover, the system has an event-by-event gain value, named automatic gain control (AGC), which has a very large dynamic range, namely from 50 keV to 25 MeV. A possible application of this detector technology could be the measurement of the fine structure of dipole transitions in unstable exotic neutron-rich nuclei that may exist in astrophysical environments. This fine structure will help to better understand the properties of the Pygmy Dipole Resonance (PDR) located at the low energy tail of the Giant Dipole Resonance.

5.2.5 *OREO project*

The CSN5 OREO project aims to fully exploit the potential of inorganic scintillator crystals, in which the radiation length, and consequently the shower length, can be strongly reduced when a crystal axis is aligned with the beam direction [459], to develop highly compact electromagnetic calorimeters with a significant reduction of the amount of material, volume and weight with respect to state-of-the art detectors in high-energy and astroparticle physics [35].

Indeed, even for hundred-MeV photons the conversion in pairs is strongly enhanced in case of oriented crystals, leading to a faster signal formation and therefore to the possibility to use more compact detectors also in this energy range. In addition, from preliminary studies, the formation of the scintillation light seems to be dependent on the crystallographic quality of the material (and orientation) independently on the primary particle energy. This effect will be further investigated by the OREO project.

In summary, the outcome of the OREO project could be very interesting in the future development of high-performance and faster gamma detectors for nuclear/hadronic physics, but also for industrial and medical applications (Fig. 30).

6 Detectors for medical applications

Radiation detection plays a fundamental role in the biomedical field, enabling the measurement, monitoring and characterization of radiation exposure, both for diagnostic and therapeutic purposes. This section discusses several notable initiatives in the development and study of detectors for medical applications. We identified three main categories based on the types of radiation, detector requirements and specifications across different applications:

- Treatment monitoring and optimization: these detectors are aimed at tracking the delivery of radiation during therapies, provide online range verification and assess target fragmentation;
- Dosimetry, quality assurance and radiotherapy: this category covers detectors used to measure radiation doses accurately, ensuring patient safety and treatment effectiveness;
- X-ray and nuclear medicine imaging: these detectors capture detailed images of internal structures and biological functions using various types of radiation, aiding in diagnosis and guiding treatment decisions.

The discussion of each category is reported in the following.

6.1 Treatment monitoring and optimization

Particle Therapy (PT) treats cancer by using charged particles such as protons or ions, up to $450 AMeV$, to destroy cancer cells. Compared to conventional radiation therapy, PT delivers a highly targeted dose of radiation to the tumor while minimizing damage to surrounding healthy tissue, by exploiting the specific energy deposition pattern of charged particles, characterized by the Bragg peak at the end of range. PT achieves a very high precision by controlling the direction of the particles and their energy, which is correlated with the depth of the Bragg peak. Particle therapy is effective in treating a variety of cancers, including those difficult to treat with conventional radiation therapy. In particular, PT is becoming an increasingly popular option for treating head and neck, and pelvic cancer; also, its minimal dose release to healthy tissues makes it particularly suitable for treating pediatric cancer. As of the end of 2022 [460], more than 100 PT facilities operate in over 30 countries: The majority of them are located in Japan, the USA and Europe, with some centers in South Korea, China and Australia. The global diffusion of particle therapy continues to expand as more countries invest in this advanced form of cancer treatment, although there are still several challenges that need to be addressed: PT facilities are expensive to build and operate, and their accessibility is therefore limited.

PT treatment planning involves several steps. After an imaging-based protocol, usually based on computed tomography (CT), provides high-quality images of the tumor and surrounding tissues, the target tumor volume is defined, as well as volumes to be spared, corresponding to organs at risk. A specialized software will then compute the treatment plan, determining the optimal beam incoming angles and, for each position in the transverse plane, the set of energies and corresponding intensities of the particle beam. The treatment plan also provides the dose of radiation that will be delivered to the tumor and surrounding tissues. The treatment delivery typically involves a series of daily sessions of about $2\,Gy$ each, for up to 6 weeks: Throughout this process, the patient's response to therapy must be closely monitored to ensure that the treatment is compliant, effective and to manage potential side effects. Although PT is conceptually very precise, some issues still hinder the exploitation of its full potential:

- Range uncertainty: arising from a variety of factors, such as patient positioning precision, anatomical changes over the course of the treatment and inaccuracies in treatment planning and beam delivery, it can cause the particle beam to deposit its maximum dose at a location different from the intended target, resulting in underdosing or overdosing of the tumor and healthy tissue, respectively. Since the dose profile is very steep, even a slight discrepancy between the expected and actual range can cause a significant mismatch between the planned and delivered dose. Currently, robust treatment plans take into account range uncertainties by enlarging the target volume of about $2.5-3\% + 1-3\,mm$. However, a better treatment control would allow a significant reduction of this margin, with a corresponding sparing of healthy tissues or, eventually, the possibility to improve treatment for tumors closer to organs at risk than the current safety margin.
- Dose rate: it can affect the biological response of the tumor and normal tissue to radiation. PT current dose rates range between $1-10\,Gy/min$ and $0.5-5\,Gy/min$ for proton and ion treatments, respectively. High dose rates improve the efficacy of radiation-induced cell killing by increasing the probability of cell death and reducing the likelihood of cell repair; also, they decrease the time for which healthy tissues are exposed to radiation, reducing the risk of radiation-induced damage. The FLASH effect, observed in preclinical studies of radiation therapy in which radiation is delivered at an extremely high dose rate (larger than $40\,Gy/s$) over a very short period of time ($< 200\,ms$), has a significant impact on the biological response to radiation, including reduced normal tissue toxicity and improved tumor control, compared to standard radiation therapy delivered at conventional dose rates. The exact mechanisms underlying the FLASH effect are still being studied, but some hypotheses suggest it to be related to the ability of high-dose rate radiation to activate certain cellular signaling pathways that promote DNA repair and cell survival, while suppressing pathways that lead to cell death and tissue damage. Despite the promising results observed in preclinical studies, the implementation of FLASH radiotherapy in clinical practice is still in the early stages of development. Research is currently focusing on methods for delivering high-dose rate radiation, such as using electron beams or ultra-short proton pulses, and evaluating the safety and efficacy of these approaches in human clinical trials.
- Projectile and target fragmentation. Although most of the beam charged particles lose energy by electromagnetic interactions, generating the typical Bragg curve for the energy loss as a function of the depth, a not-negligible fraction undergoes nuclear interactions, either inducing tissue fragmentation or, in the case of carbon ions, beam fragmentation. Target fragments deposit all their energies within tens of microns of their production point, while beam fragments travel further in tissue than the primary particles and deposit their energy at locations different from the intended target: Both effects lead to dose deposition outside the tumor volume and cause unintended damage to healthy tissue. The magnitude and extent of projectile and target fragmentation depend on a variety of factors, including the type and energy of the particle beam, the thickness and composition of the tissue being irradiated and the geometry of the treatment field. Measuring fragmentation cross sections would provide invaluable input for the development of new treatment planning algorithms that account for the effects of fragmentation on the dose distribution.

Alongside new protocols for PT-based treatment, research is focusing on Boron Neutron Capture Therapy (BNCT), a type of radiation therapy based on the delivery of a boron compound into cancer cells, followed by irradiation with thermal neutrons. When the boron atoms are exposed to thermal neutrons, they undergo a nuclear reaction that produces high-energy α particles and ^{7}Li ions: Their short range and high ionization density allows them to selectively destroy cancer cells while sparing normal tissue. The implementation of BNCT is currently limited by several technical challenges, such as the need for a high neutron flux and a selective delivery of boron to cancer cells. Researchers are currently working on developing more efficient and effective methods

Fig. 31 Beam projection on the axis perpendicular to silicon strips for 115 MeV protons (green-filled distribution) and 398 $AMeV$ carbon ions (magenta-filled distribution)

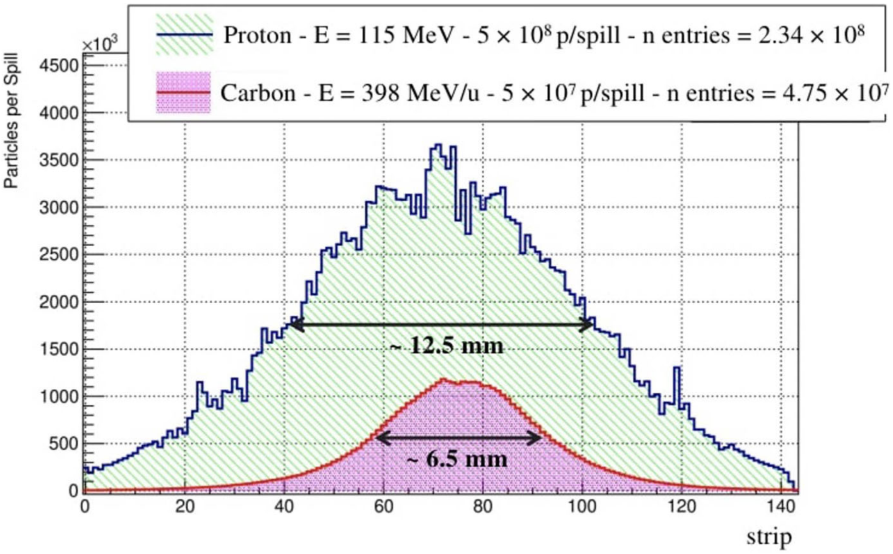

for delivering boron compounds to cancer cells, new neutron sources that can generate the required neutron flux for BNCT, as well as treatment monitoring and verification systems.

The above-discussed topics are being addressed in several R&D projects, around the world. The present contribution summarizes the recent and ongoing INFN projects, focusing on the issue of treatment monitoring and optimization, both for the standard delivery with charged particles, and for other approaches such as Flash Radio-Therapy (FRT) and BNCT.

6.1.1 Dose delivery systems

Currently, ionization chambers (ICs) are the standard device for the monitoring of therapeutic beams (i.e., the verification of their position and their intensity) in PT facilities. The introduction of fast beam delivery techniques in particle therapy, such as fast re-scanning modalities, promises to improve the accuracy, to shorten the treatments and to increase the patient throughput. On the other hand, advanced approaches are crucial to guarantee and verify the dose delivery precision. However, in order to implement these features, *ICs* limitations (sensibility threshold of about 10^4 $particles/s$, collection time up to 100 μs, recombination effects) must be overcome [461]. INFN, in collaboration with other institutions, is developing several prototypes of thin silicon sensors with the capability of counting single protons and carbon ions in the clinical energy range [462], so as to directly measure their energy with time-of-flight techniques [463] and provide single primary particle time tags that can be correlated with the emission time of secondary signals (e.g., prompt photons), providing an integrated beam monitoring and range verification system [464]. Thin silicon sensors are sensitive to single particles and their very short charge collection time (1 ns) allows them to reach large counting rates. A 60 μm thick diode sensor and a 50 μm thick Low Gain Avalanche Diode (*LGAD*) sensor are used for the counter detector of protons and carbon ions, respectively. The sensitive area of both sensors (2.6×2.6 cm^2), sufficient to cover the cross section of a pencil beam, is segmented in 146 strips with 180 μm pitch [462]. The readout is based on 6 custom $24 - channel$ front-end ASICs able to discriminate particle signals in a wide charge range ($4 - 150$ fC) with a maximum dead time of about 10 ns. The digital pulses produced by the discriminator are sent to 3 Kintex7 FPGA boards implementing counters for each channel, while a LabVIEW program reads and saves the data for off-line analysis.

The measurements performed with protons and carbon ions in CNAO (Pavia) result in beam projections (Fig. 31) with a FWHM comparable with measurements performed with gafchromic films. The proton counting efficiency, which depends on the beam energy, geometrical acceptance, inefficiencies caused by low-gain in some parts of the detector as well as pileup effects (Fig. 32), is in the $35 - 51$ % range, depending on the beam intensity. For carbon ions, the efficiency reaches 90 %, with losses only related to the geometrical acceptance, since at lower intensities the pileup is negligible and the carbon signal, which is larger, is detected also in low-gain areas; also, its energy dependence is smoother. Further research is presently focusing on addressing the issues related to the design and construction of a detector suitable for clinical conditions: in particular, achieving a size compatible with beam delivery windows ($20 \times 20 cm^2$) and optimizing the radiation resistance of silicon devices, since they will be installing on the beam path.

6.1.2 Online range verification

Online range verification is crucial in particle therapy for several reasons:

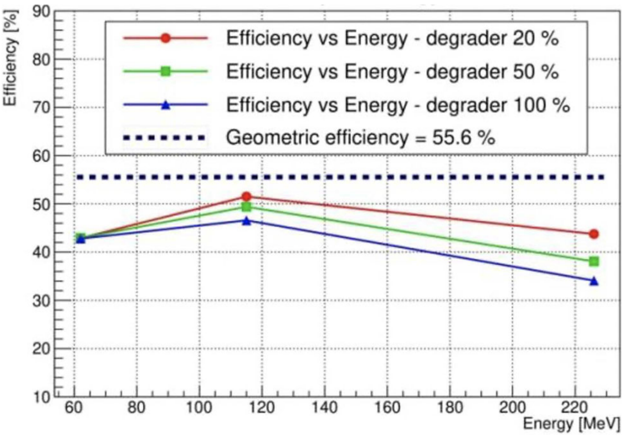

Fig. 32 Proton counting efficiency as a function of the energy for different beam intensities

- Accuracy of treatment delivery. As PT relies on the precise delivery of particles to the tumor site while minimizing damage to surrounding healthy tissues, and the maximum dose release is at the end of range, an increase in range with respect to the nominal value would cause an unwanted dose in healthy tissues beyond the tumor volume, while a decrease would cause a reduced dose release in the tumor volume. Both effects are harmful. Accurate range verification must ensure that the particles stop at the intended location within the patient's body, precisely targeting the tumor and sparing healthy tissue.
- Patient safety. Verifying the range of particles online helps to ensure that the prescribed dose is being delivered correctly and reduces the likelihood of errors. By continuously monitoring the particle range, any deviation or unexpected behavior can be detected in real time, allowing for immediate corrective actions to be taken to safeguard the patient.
- Adaptive treatment planning. Online range verification can in principle enable adaptive treatment planning that is the ability to modify the treatment plan based on the patient's current condition. During the course of treatment, morphological changes can occur, such as tumor shrinkage or organ motion, which may affect the particle range. By verifying the range online, clinicians can make necessary adjustments to the treatment plan, to compensate for these changes and ensure optimal treatment outcomes.

As primary beam particles do not exit the patient, range verification measurements must rely on secondary signals, induced by the beam. Indeed, while the majority of primary particles lose energy through electromagnetic processes, a not-negligible fraction also undergoes nuclear interactions with the tissues nuclei. Most frequently, these interactions cause an excitation of target nuclei that on a very short timescale emit γ rays, with energies in the $1 - 10\,MeV$ range: By detecting them, their emission profile along the beam direction can be reconstructed.

Beam target nuclear interactions, however, could also cause the emission of neutrons from target nuclei that, being mostly ^{12}C and ^{16}O, induces the production of ^{11}C and ^{15}O: Both these isotopes are β^+ emitters, with half-life of about 20 and 2 minutes, respectively. The emitted positrons, by annihilating with electrons, generate the typical signature of Positron Emission Tomography (PET): a pair of back-to-back $511\,keV\,\gamma$ rays. By installing PET detectors around the patient, it is possible to reconstruct the 3D activity distribution.

In case of ion beams, also primary particles can fragment, by emitting both neutrons (thereby leading, via the formation of β^+ emitting isotopes, to PET signals) and protons that can escape the patient and be detected: Their trajectory can be backtracked and its intersection with the beam trajectory provides the emission point.

The γ rays emission profile, the 3D activity distribution and the proton emission profile are all correlated with the range of the primary beam: By means of properly tuned simulations, it is then possible to provide a range measurement.

INFN staff and associates are involved, with leading/major roles, in several research projects focused on both defining range verification clinical protocols (INSIDE, INSIDE2) and developing innovative approaches (I3-PET, PAPRICA), with the ultimate goal of proving the feasibility of in- vivo direct measurement of the stopping power, i.e., the Bragg curve (MERLINO). In parallel, the design of a hybrid system for beam and range verification, to be installed as part of the future ion gantry at CNAO, is being addressed within the SIG-PNR project.

INSIDE, INSIDE2 INFN has contributed to the design and construction of the INnovative Solution for In-beam Dosimetry in hadronthErapy (INSIDE) hybrid online range verification system [465], which combines a PET detector and a charged particle tracker, so as to be able to monitor both proton and ion treatments. The PET unit [465], which exploits the detection of annihilation photons produced by beam-induced β^+ emitters, is composed of two planar heads placed at $30\,cm$ from the treatment room isocenter. Each head $(10 \times 25cm^2)$ consists in a matrix of lutetium fine silicate (LFS) scintillating crystals read out by silicon photomultipliers (SiPMs), which yields a 3D activity image that is indirectly correlated with the delivered dose. The image reconstruction is performed on the fly with an iterative multicore maximum likelihood expectation maximization (MLEM) algorithm, and its results are provided online during the treatment.

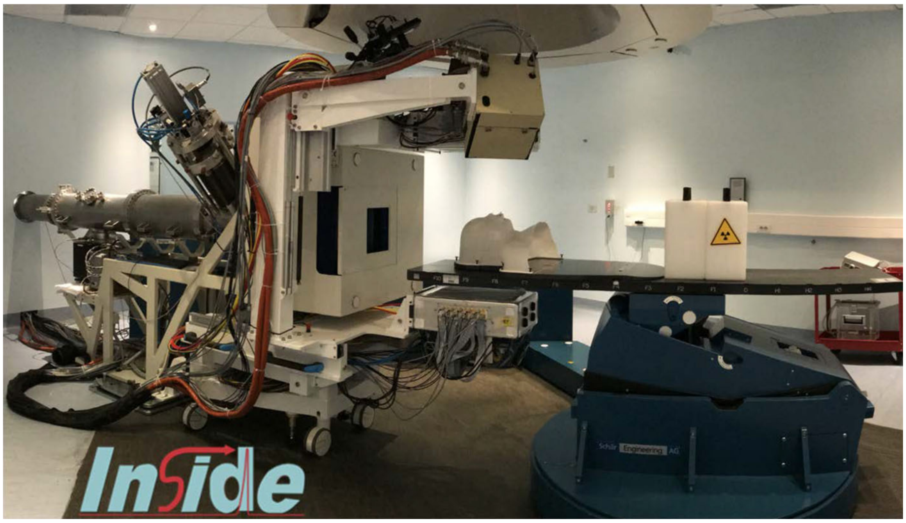

Fig. 33 The INSIDE hybrid range verification system, installed in the CNAO treatment room

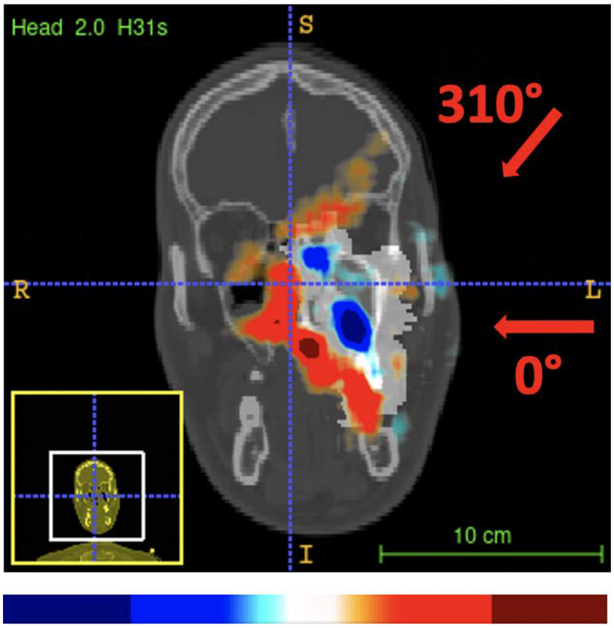

Fig. 34 2D projection of the activity difference between two clinical carbon ion treatment sessions, corresponding to the planning and control CT

The PET detector provided, in 2016, the first ever online reconstruction of the beam-induced activity during a clinical treatment [466]. The project was initially supported by MIUR, then by CNAO. It also developed a method that allows the reconstruction of the activity induced by subsequent treatment fields, corresponding to different patient positions during the same delivery session [467].

The Dose Profiler [468], designed to detect the charged secondary fragments escaping from the patient, is made of 8 plastic scintillating fibers planes ($20x20\,cm^2$), read out by SiPM to detect and measure the trajectory of the fragments. The production points of the fragments are hence obtained as Points of Closest Approach (PCA) of the reconstructed track with the nominal incoming beam direction, provided by the Dose Delivery System. The 3D maps of emitted charged fragments are strictly correlated with the density of tissues crossed by the primary beam. The devices are installed on a movable cart which is locked in proximity of the beam nozzle as shown in Fig. 33.

Both devices can be used to spot inter-fractional morphology variations by comparing the measured 3D maps of β^+ activity or secondary fragment emission with respect to a reference distribution.

Currently, the INSIDE system is undergoing a clinical trial at CNAO (ClinicalTrials.gov ID: NCT03662373): The first phase was completed in 2020, having enrolled 20 patients treated with protons and carbon ions [469–471] and obtained promising clinical results (Figs. 34, 35) that provide invaluable information for the design of future systems, such as the one to be installed in the CNAO ion gantry presently under development within the SIG-PNR project.

INSIDE has indeed shown its capability to detect small morphological changes that take place over the course of the treatment (several weeks), with both the PET and the tracker systems, thus prompting a re-calculation of the treatment plan.

Fig. 35 Profile of the detected protons emitted during a clinical carbon ion treatment: comparison between three measurements corresponding to different sessions

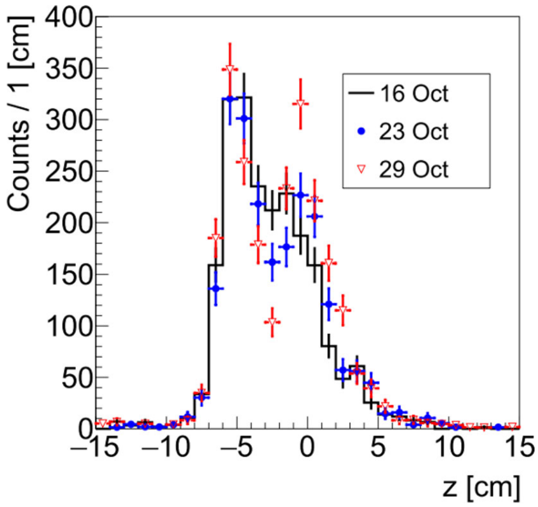

Within INSIDE, a novel approach for PET image reconstruction has been developed to mitigate the statistical limitations in case of in vivo range verification in carbon ion treatments, exploiting the multiple field activity along the whole treatment, mainly related to projectile fragmentation into ^{11}C (half-life of about 20 min) and therefore close to the Bragg peak, to improve PET image quality and capability of detecting inter-fractional morphological changes during the treatment. Since most of the annihilation signals is located within the Clinical Target Volume (CTV) that is monitored for all the irradiation angles, it is possible to reconstruct, through a MLEM approach and a patient-tailored response model, one image from the ^{11}C signals of all the irradiated fields. A quantitative analysis to spot inter-fractional morphological changes by means of Voxel-Based Morphometry (VBM) has been performed on patients enrolled into the INSIDE clinical trial. Simulations from both the planning and control CT have shown the possibility to detect anatomic differences, such as the emptying of an air cavity and the growth of the tumor mass. Although unique, INSIDE suffers from some limitations. Some of them are intrinsic, such as the fact that it is not possible to install a full PET ring around the patient, as it would limit the range of beam incoming angles. Therefore, INSIDE only provides a partial coverage, with 2 heads, above and below the patient. Such configuration provides an excellent measurement of the coordinate along the beam and transverse to it, but the vertical position is not well defined. Similarly, the angular acceptance of the charged particle tracker is limited by clinical constraints.

Also, in the case of PET, the input to the reconstruction stage is only collected during the so-called *inter-spill* stage that is in the dead time between the delivery of beam spills by the CNAO synchrotron. Such a condition provides a clean signal, with no background, but limits the statistics and completely misses the contribution of short-lived (half-life $< 1\,s$) isotopes, whose production is strongly correlated with the beam position and range. During the spill, however, the background caused by the emission of prompt photons is very large, and it is difficult to disentangle it from the signal itself without any further information.

I3-PET The experience gained by operating the INSIDE PET detector, as well as the goal of gathering more information during the spill delivery, triggered the idea proposed by the I3-PET project that developed a hybrid system for joint PET and prompt photon detection. Besides detecting annihilations, the PET modules are used to identify time coincidences between primary beam particles, detected by an LGAD sensor placed on the beam trajectory, and secondary prompt photons, detected by the PET modules themselves (although with lower efficiency with respect to annihilation photons). The time of flight is then used, according to the Prompt Gamma Timing (PGT) technique [472], to reconstruct the beam range.

The experimental feasibility of detecting such coincidences was demonstrated during a beam test at CNAO (Fig. 36), by triggering on the scintillator signals and analyzing the corresponding time buffer of the silicon detector strips. In principle, within the acquisition time frame (200 ns), more than one primary is present (depending on the beam intensity), so each secondary generates more than one entry in the time-of-flight distribution: In case of multiple coincidences, one of them must be selected. After the reconstruction stage, the correlation between the average time of flight and the corresponding average emission coordinate along the beam direction is obtained: The farthest emission point corresponds to the beam range. The PGT approach provides two major advantages compared to standard prompt gamma detection: It does not require a collimator. Therefore, it is much simpler to accommodate the layout in the treatment room; besides, the collected statistics is much larger. Clearly, the performance critically depends on the achieved time resolution, which is dominated by the scintillator signal ($150 - 200\,ps$), since the silicon detector achieves $30 - 50\,ps$.

PAPRICA Similarly, the operation of the INSIDE tracker prompted the development of the PAir PRoduction Imaging ChAmber (PAPRICA) prototype [473, 474], which proposes a novel detection strategy to image prompt photons, based on the pair production mechanism, that would also discriminate photons from uncorrelated neutrons. The detector prototype design, shown in Fig. 37,

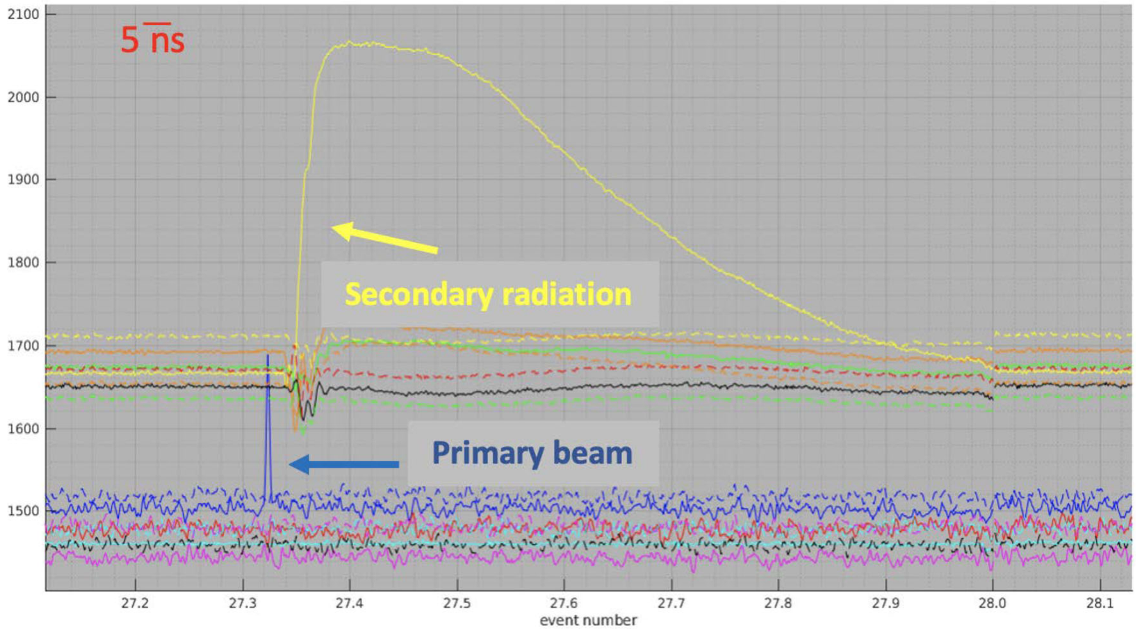

Fig. 36 Example of a coincidence between the signals corresponding to a primary beam proton crossing the silicon beam monitor (blue) and a prompt photon detected by an I3-PET LFS scintillator module (yellow)

Fig. 37 Sketch of the PAPRICA prototype

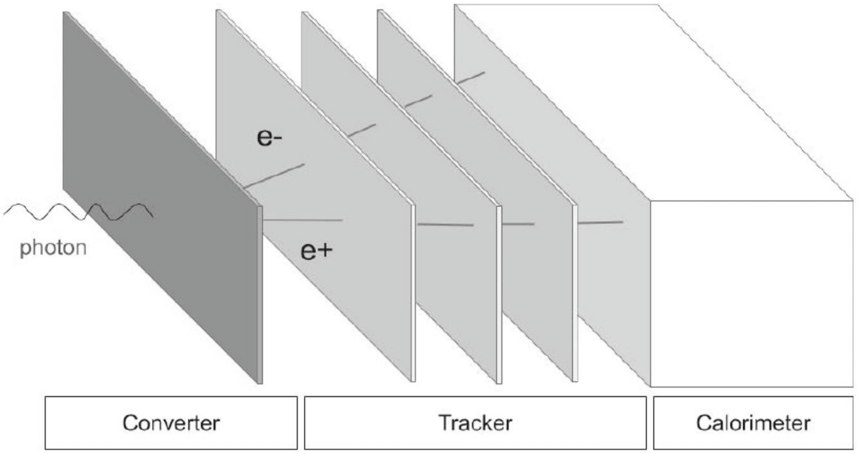

consists of a converter made by a layer of LYSO fibers, in which the prompt photons conversion occurs, a tracking station based on the ALPIDE pixel sensors [475, 476] for the e^+e^- momentum reconstruction, and a plastic scintillator calorimeter which measures the residual e^+e^- kinetic energy.

As the photon production depends on the density of the tissues crossed by the beam, the 3D photon emission maps carry information about potential morphological variations, which may be detected by comparing the reconstructed maps obtained in different treatment fractions, using the gamma test [477].

MERLINO The implementation of the PGT technique with the I3-PET detector proved its feasibility; however, the system was not optimized for prompt photon detection. A system prototype comprising 2 LaBr3:Ce- detectors and an LGAD was developed within the Measurement of the EneRgy Loss for IN vivo Optimization in particle therapy (MERLINO) project: It operates with much higher efficiency and allowed the validation of the technique in conditions compatible with clinical operations. The measured time of flight is a sum of 3 contributions: the primary particle time from the silicon detector to the target, which can be calculated, the time corresponding to the primary particle propagation in the target and the flight time of the emitted photon, from the emission point to the detector. Although single contributions cannot be disentangled, not being known the actual emission point, the shape of the measured TOF distribution depends on the detector position. By continuing the work started with I3-PET, in collaboration with a team from the University of Lubeck, a custom reconstruction algorithm, based on MLEM methods, was developed and validated, providing the first experimental results of the spatiotemporal emission reconstruction for treatment verification in proton therapy [478]. The space-time distribution of the emitted prompt photons is correlated with both the primary particle range and, even more importantly, its motion inside the target. Experimental measurements with a $227\,MeV$ proton beam impinging on a homogeneous phantom were taken at CNAO [479, 480]. First comparisons between data and simulation show excellent agreement, with a 98% average correlation of the prompt gamma timing distributions. A preliminary reconstruction of the prompt photons spatiotemporal emission was achieved for the first time with experimental data. The corresponding simulation was carried out with the FLUKA Monte Carlo tool. The results shown here represent the first step toward the experimental validation of the technique, which, as a final result, provides a measurement of the Bragg curve, compatible with in vivo acquisitions.

SIG-PNR The SIG-PNR project aims at studying and developing the key elements of a novel generation gantry for multi-ion particle therapy, from helium to oxygen. A superconducting dipole magnet demonstrator for a rotating gantry, capable of reaching $4-5\,T$ with a small curvature radius of $1.3-1.7\,m$ and a magnetic aperture of $70-90\,mm$, and a high-field scanning magnet system are being designed and built. In parallel, a novel single-particle tracking approach, based on silicon detector, and a new concept range verification system, based on the detection of PET and prompt photon signals, are being designed, so as to integrate them in the gantry and provide required information for particle therapy. New thin silicon sensors for a single-ion counter at clinical rates are being developed, starting from existing sensors developed for the INFN MoVeIT project. The final aim is to develop a beam monitoring device able to directly measure the crossing time and position of each particle. Parameters are defined in order to match the sensors with the existing counting readout electronics, optimize the tagging capability, reduce pileup effects and improve the radiation resistance. The front-end readout with timing capabilities is under development based on the CERN picoTDC coupled to ABACUS ASICs. The optimal solution for range verification in ions treatments is being investigated, by considering both annihilation photons from fast decaying positron emitters (e.g., ^{12}N, ^{8}B) and prompt photons, exploiting the PGT technique [472]. Currently, the I3-PET hybrid detectors are under test in order to assess their performance with carbon ion beams and new detectors based on $LaBr_3$ monolithic crystals are going to be built to further investigate the prompt photon production during ion clinical treatments and obtain useful information to propose an optimized design fitting the SIG rotating gantry geometry. The integration between the beam and range monitoring system is crucial to provide online feedback during treatment, paving the way for adaptive therapy and real-time motion mitigation strategies. In order to make the monitoring information available in the shortest possible time, new tools based on GPU for data analysis and integration between beam and range monitoring systems are under study.

6.1.3 Boron neutron capture therapy

Boron Neutron Capture Therapy (BNCT) is a neutron-based technique that allows selective cancer treatment at the tumor cellular level, especially suitable for the treatment of brain, head, neck and skin cancers. Similarly to standard PT, it delivers a highly targeted radiation dose to cancer cells while minimizing damage to the surrounding healthy tissue. However, it is still considered an experimental therapy and is only available at a limited number of specialized medical centers worldwide. BNCT is based on the high affinity of ^{10}B for absorbing thermal neutrons: The neutron capture leads to the formation of ^{11}B, which then breaks into an α particle and a ^{7}Li nucleus. Both particles are highly ionizing, and their range is in the order of a few cell diameters: Therefore, they are highly effective in inducing cell apoptosis. To administer BNCT, a ^{10}B compound is injected into the patient, either intravenously or directly into the tumor site. After a waiting period, the patient is exposed to a beam of neutrons that triggers the above-described process, selectively damaging the cancer cells. BNCT is undergoing a major resurgence of interest around the world as recent progress in accelerator technology allows the procedure to be undertaken in clinics.

INFN designed and constructed an RFQ proton accelerator delivering a 5 MeV, 30 mA proton beam in continuous wave (CW) mode [481]. Via the $^{9}Be(p,n)^{9}B$ reaction on a beryllium target, a high intensity ($30\,mA$) proton beam, provided by a radiofrequency quadrupole, generates neutrons with a rate of $10^{14}s^{-1}$, with an energy spectrum centered at 1.2 MeV; a proper moderator made of heavy water, PTFE and graphite will then reduce the energy to the thermal-epithermal range [482]. The final neutron spectrum is designed to be suitable for Boron Neutron Capture Therapy (BNCT). The INFN-ENTER-BNCT studied the target performances and the optimization of their design.

In order to fully exploit the BNCT cell-level selectivity, BNCT, a real-time, in vivo dose verification system, must be developed, in particular for the assessment of the dominant dose component, i.e., the therapeutic dose due to ^{10}B cellular accumulation. A possible approach, being explored at INFN-Pavia since 2017, is the development of preclinical prototypes of BNCT-SPECT and Compton camera systems based on room-temperature semiconductor photon detector CdZnTe (CZT) that would detect the 478 keV γ ray signal coming from the ^{10}B capture reactions. The implementation of such a system must address some relevant issues:

- the mechanical collimator must be effective in the range of the emitted photon energy ($478\,keV$);
- operations must be compatible with the intense n and γ background, in particular the 2.2 MeV γ ray from ^{1}H captures;
- compactness and portability are required: As the neutron beam is fixed, the layout must be adapted to different patient positions.

The INFN-3Cats project is designing and implementing a *single stage* Compton camera exploiting 3D positioning sensing CdZnTe (CZT) detectors.

Moreover, the natural occurrence of ^{113}Cd, with its large cross section for thermal neutron capture, in the CZT alloy, suggests that the very same technology could be used as a real-time thermal neutron flux monitor, a key factor in improving the accuracy in the dose estimation of the non-selective dose components (in particular coming from ^{14}N capture reactions).

6.1.4 Target fragmentation

As already discussed, proton or ^{12}C beams used to treat deep-seated solid tumors exploit the characteristics of charged particles energy deposition in matter, with the maximum dose deposition at the end of the beam range, in the Bragg peak (BP) region, where the tumor is located. The increase in the radiation linear energy transfer (LET) in the BP region enhances its Relative Biological Effectiveness (RBE) in cell killing when comparing with conventional radiotherapy using photons. Even though the track structure also plays a role, as a general approximation, high LET corresponds to high RBE, so the effect is particularly important for ions like ^{12}C or ^{16}O, where the LET increases significantly near the BP region. The RBE increase as a function of LET stops around $100 - 200 keV/\mu m$, where the RBE peaks and then drops down for further LET increases [483, 484].

However, beam-induced nuclear interactions with the patient tissues can cause the fragmentation of projectiles and/or target nuclei, an effect that should be carefully taken into account when planning the treatment. In proton treatments, the target fragmentation produces low-energy, short-range fragments along all the beam path that deposit a non-negligible dose especially in the first crossed tissues. On the other hand, in ion treatments, performed using ^{12}C, or other ions (e.g., ^{4}He or ^{16}O), the main concern is related to the production of long range fragments that release a non-negligible dose in the healthy tissues beyond the BP. Understanding nuclear fragmentation processes is of interest also for radiation protection in human space flight applications, in view of deep space missions. In particular ^{4}He and high-energy charged particles, mainly ^{12}C, ^{16}O, ^{28}Si and ^{56}Fe, are the main source of absorbed dose in astronauts outside the atmosphere. In order to optimize the shielding against the space radiation, the nuclear fragmentation properties of the materials used to build the spacecraft must be known with high accuracy. The knowledge of the impact of fragmentation processes, which is of interest both for PT and space radioprotection applications, presently suffers from the limited experimental precision achieved on the measurement of relevant nuclear cross sections, which compromises the reliability of the available computational models.

FOOT The INFN-funded FOOT (FragmentatiOn Of Target) collaboration [485] that also involves researchers from France, Germany and Japan is completing the construction of an experiment to study nuclear fragmentation processes and measure their cross sections.

Measuring target fragmentation in the proton-Nucleus ($p - N$) collisions field is an exceptionally challenging task, because of the very short range of the produced fragments that results in a very low probability of escaping the target. Their range is limited to tens of microns and even a very thin solid target would stop them or badly spoil their energy measurement. FOOT will therefore address the issue by using an inverse kinematic approach, swapping projectile and target, with the goal of measuring differential cross sections with respect to the kinetic energy ($d\sigma/dE_{kin}$) for the target fragmentation process with an accuracy better than 10% and double differential cross sections ($d^2\sigma/d\Omega dE_{kin}$) for the projectile fragmentation process with an accuracy better than 5% on the determination of the fragment yields in angle and in kinetic energy. To achieve these performances, the charge and isotopic identification precision of the fragments should reach the level of $2 - 3\%$ and 5%, respectively, so as to obtain a clear separation of all the isotopes under study.

The FOOT experiment (Fig. 38) implements an *upstream region* composed by the pre-target detectors that will be used to monitor the impinging beam, and a region, including the target, for the tracking and the identification of the fragments that consists in two alternative and complementary setups:

- a setup that implements a magnetic spectrometer, coupled with detectors for tracking, optimized for the identification of fragments heavier than ^{4}He. It covers an angular acceptance up to a polar angle of about 10 deg with respect to the beam axis;
- a setup based on an emulsion spectrometer, optimized for the identification of low Z fragments emitted at large polar angles that will extend the angular acceptance of FOOT up to about 70 deg.

The construction of the FOOT detector started in 2019 and was completed by the end of 2023.

The Upstream Region The upstream region is composed of pre-target detectors that will be used to monitor the beam, providing its direction and the interaction point on the target, and to count the number of impinging ions. The overall material budget, crossed by the beam, must be minimized, so as to reduce the out-of-target fragmentation, as well as the beam multiple scattering. The selected configuration includes two detectors: the Start Counter (SC), a thin plastic scintillator read out by SiPMs, and the Beam Monitor (BM), a drift chamber, placed upstream of the target. The SC provides the Minimum Bias trigger of the experiment, measures the incoming ion flux (with an efficiency $\epsilon > 99\%$), provides the reference time for all the other detectors and the *start* signal to the TOF system, which is then combined with that of the *Tof-Wall* (TW), made of 2 layers of thin plastic scintillator bars placed about $2\,m$ downstream. The BM detector, placed between the SC and the target, is used to measure the direction and impinging point of the beam ions on the target, a crucial information needed to correct for pileup effects in the tracking devices downstream the target and to discard events in which the beam fragmentation took place in the SC.

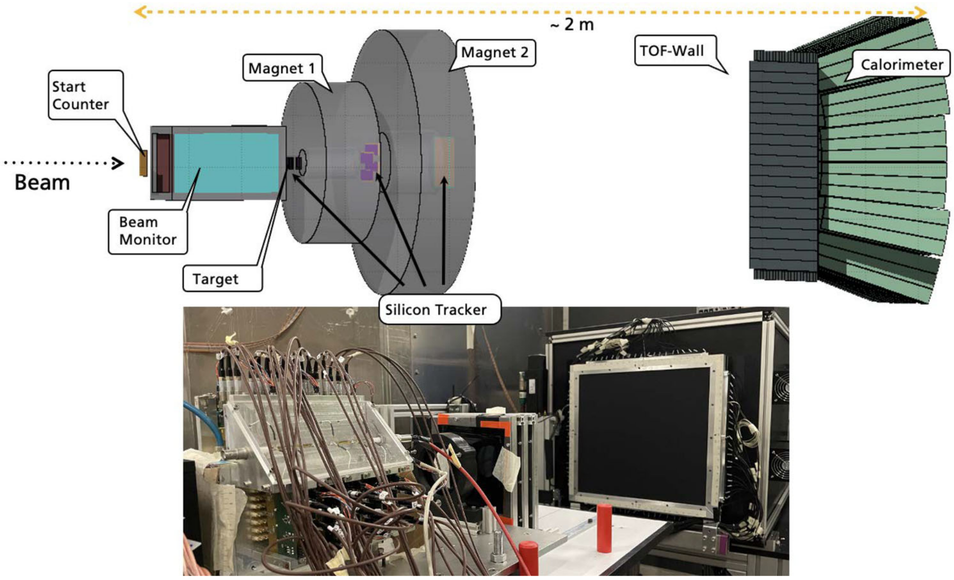

Fig. 38 Sketch of the full FOOT electronic layout and picture of the available configuration as of November 2022

The magnetic spectrometer The driving criterion of the FOOT detector design is the need for an accurate charge and isotopic identification of the produced fragments. To achieve the experimental goals a redundancy in measuring the different kinematic variables is needed, exploiting different particle identification (PID) techniques. For this reason, the FOOT setup includes a *TOF* system and a calorimeter for the fragments energy measurement, combined with the measurement of the energy released in thin detectors and with the information provided by the magnetic spectrometer, allows the isotope mass identification. The charge (Z) of fragments reaching the *TW* can be identified from the energy loss Δ_E and the *TOF* information, making use of the Bethe–Bloch formula. The tracking in the magnetic field volume provides the fragment rigidity (p/Z) and its path L that coupled with the measurement of *TOF* and Z yields the momentum p and the velocity β. Finally, the fragment mass identification can be achieved by momentum p, velocity β and kinetic energy E_{kin} measurements, making use of the following relationships: $p = mc\beta\gamma$, $E_{kin} = mc^2(\gamma - 1)$, $E_{kin} = \sqrt{p^2c^2 + m^2c^4} - mc^2$, where γ is the Lorentz factor. In order to achieve the precision requirements on the final cross-section measurements, it is necessary to obtain the following experimental resolutions: $\sigma_p/p \sim 4 - 5\%$, $\sigma_{TOF} \sim 100\,ps$, $\sigma_{(E_{kin})}/E_{kin} \sim 1 - 2\%$, $\sigma_{\Delta E}/\Delta E \sim 5\%$.

The detector must also minimize the fragmentation induced by the detector material as well as keep the full apparatus sufficiently compact to be transported and installed in different facilities. The overall FOOT detector size is about $2 - 3\,m$, depending on the distance between the momentum spectrometer and the TOF/Calorimeter.

The Emulsion Spectrometer The Emulsion Spectrometer (ES) has been designed to characterize the production of low Z fragments, which are emitted at large angles, beyond the acceptance of the magnetic spectrometer. The SC and BM, placed upstream the ES, are only used to perform an online control of the beam flux on the active ES surface, and their DAQ System is completely decoupled from the ES that acts as a complete, stand-alone, layout. Among all tracking devices used in particle physics, nuclear emulsion detectors achieve the highest spatial resolution (sub-micrometric) for tracking ionizing particles. Emulsion chambers integrate target and detector in a very compact setup and provide a very accurate reconstruction of the interactions occurring inside the target.

Measurements The FOOT measurements campaign with the complete layout, which will start in 2024, foresees an extensive program focused on the nuclear fragmentation of ^4He, ^{12}C and ^{16}O beams impinging on thin C and H rich targets, like polyethylene C_2H_4, in the $100 - 800 AMeV$ energy range of interest for PT and radioprotection in space applications.

6.2 Dosimetry, quality assurance and radiotherapy

The advent of FLASH therapy, driven by the demonstrated tissue sparing effect (FLASH effect) in ultra-high dose-rate (*UHDR*) electrons and proton irradiation, is focusing the research effort on the development of detectors able to overcome the nonlinearity of conventional ion chambers caused by saturation effects in *UHDR* regimes. FLASH Radiotherapy (*FRT*) delivers the therapeutic beam at ultra-high dose rates ($> 40\,Gy/s$) in a short treatment time ($< 200\,ms$) through narrow (order of μs) pulses each carrying a high dose ($> 1\,Gy/pulse$), triggering, for pulsed LINAC beams or laser-driven beams, an enhanced radio-resistance on healthy tissues while keeping an anti-tumor efficacy comparable to conventional *RT*. A detector capable of providing an accurate characterization and real-time verification of the beam intensity and spatial distribution in FLASH regime is now eagerly needed to make a substantial step toward the clinical implementation of FRT.

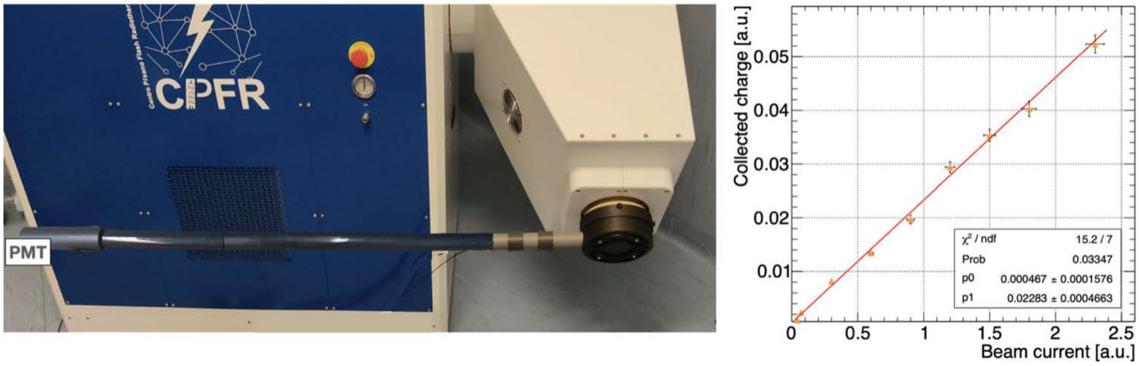

Fig. 39 Prototype of the fluorescence-based beam monitor (left) and correlation between the signal collected by the PMT and the beam intensity (right)

6.2.1 The FRIDA project

INFN activities on the topic of FLASH Radiotherapy are developed within the FRIDA project. The FRIDA (Flash Radiotherapy with hIgh Dose-rate particle beAms) project addresses several challenges posed by this potential revolution. A crucial task is represented by the mechanistic understanding and modeling of the effect. A dedicated work-package addresses the challenge of producing a model capable of describing the relation between the obtained sparing and the beam delivery conditions and will coordinate the efforts toward an evaluation of the effect using known cellular lines and performing in vivo experiments. Experiments will be carried out at FLASH beam facilities that are (or will be in the near future) available, complementing the multiscale FLASH mechanism modeling efforts.

Another key ingredient is the necessary research and development phase in the acceleration and beam delivery fields to provide the required dose rates with a clinically acceptable precision. The efforts will be mainly focused on developing a C-band accelerating section capable of bringing the energy of IOeRT FLASH electrons (like the ones already available at the Centro Pisano for Flash Radiotherapy, CPFR, in Pisa) up to the 100–150 MeV energy needed to treat deep-seated tumors. At the same time, the laser-plasma acceleration of both e- and p will be explored in the context of possible FLASH therapy applications.

Within FRIDA, several different approaches will be pursued, ranging from scintillators, gas detectors exploiting the air luminescence, silicon detectors, SiC, alanine pellets, ICT systems. All these techniques showed the potential of overcoming the main limitation of current clinical implementations: the saturation of the detector response at ultra-high dose rates.

Silicon sensor pads, 45 μm thick and with an active area of $2\,mm^2$, are being tested at the Centro Pisano for Flash Radio Therapy (CPFR) where the SIT ElectronFlash Linac is installed [463]. The readout is performed using the TERA08 ASIC, a 64-channel current-to-pulse-frequency converter [486]. With a $9\,MeV$ electron beam and a pulse duration of $4\,\mu s$, the results show excellent linearity up to the maximum achievable dose per pulse of $20\,Gy/pulse$, which corresponds to a charge of $600\,nC/pulse$ collected on the silicon pad. The Flash Detector beam Counter (*FlashDC*) prototype will instead measure the yield of optical photons produced from excited states of nitrogen molecules. Early measurements for the case of electron beams provided an almost constant value of $4\,photons/min$ per interacting electron in a wide range of kinetic energies of the primary beam $(1-1000\,MeV)$. Thus, a device exploiting air fluorescence would require a beam of very high instantaneous flux across the sensitive volume to detect a useful number of photons, such as in the emerging field of FRT.

Fluorescence-based beam monitor is expected to provide a linear response as a function of the instantaneous dose rate, with the possibility of application in a wide range of dose rates and energies without saturation and/or nonlinear dependencies. Besides, the device would be simple and economical, with minimal impact on the treatment delivery. To test the feasibility of this technique and perform proof-of-principle studies, several prototypes have been developed at the Basic and Applied Sciences for Engineering Department of Sapienza University of Rome, with geometry optimization performed by means of a FLUKA Monte Carlo simulation. Each prototype consists of a volume of air, contained inside a box with black walls to shield from external background; the light produced by the electron beam is then collected by a commercial PMT (H10580), giving information on the beam intensity and position. The latest prototype is represented in Fig. 39 (left), with the PMT placed at $125\,cm$ from the beam line. The data collected from test beam campaigns with electrons delivered at FLASH intensities by research LINACs at S.I.T. Sordina IOeRT Technologies SpA (Aprilia, Italy) and by the ElectronFlash LINAC at the CPFR in Pisa demonstrated that the background evaluation is a crucial requirement for the detector design, due to the relevant number of particles escaping from the beam line and inducing a PMT spurious signal. The response has been studied as a function of the beam current (thus changing the dose within a micro-pulse) within a range of values between 3 and 100 *mA*, corresponding to dose-per-pulse values from 0.3 to 20 *Gy/pulse*.

The results (Fig. 39, right) show a linear correlation between the signal collected by the PMT and the beam intensity over the explored range of intensities, providing a first reliable indication that fluorescence can be used to perform beam monitoring for studies on FRT. The final goal of the *FlashDC* project is to develop a detector capable of reconstructing a 2*D* map of the beam position delivered during the treatment and measuring the dose rate.

Finally, software tools for FLASH treatments planning are needed to evaluate the technique potential and enable clinical applications. Within FRIDA, the tools needed to plan FLASH therapy treatments will be developed and the resulting plans will be compared with state-of-the-art results from IMRT, VMAT and proton therapy treatments.

The authors acknowledge partial funding from the FRIDA INFN-CSN5 project and from the regional Public Notice *Gruppi di ricerca 2020*—POR FESR Lazio 2014-2020 (project number A0375-2020-36748), and the Fondazione Pisa for the use of the EF (grant n. 0104712/2021).

6.2.2 Unbalanced core detector (UCD)

FLASH radiotherapy electron beams typically exhibit pulsed structure with 2-30 Gy/pulse, pulse duration in the microsecond range and repetition rate up to 200 Hz. The response of an active clinical dosimeter should be ideally independent of dose rate, energy and direction distribution of the field.

In 2020 Di Martino and coworkers [487] tested the performance of commercially available radiotherapy dosimeters based on scintillators, semiconductors and ionization chambers, finding severe saturation effects. This findings motivated research groups to develop innovative dosimeters.

To date, the following devices, among others, exhibit promising characteristics: (1) diamond Schottky diode detectors [488], (2) ultra-thin parallel plate ionization chambers [489] and (3) the unbalanced core detector (UCD) from INFN-LNF [490] (patent pending).

UCD is based on a spherical sensitive core whose diameter can be chosen from 4 to 10 mm and thus is intrinsically isotropic. It is waterproof, linear up to about 25 Gy/pulse, and its radiation-induced fading is as low as $< 1\%$ / 100 kGy. The front-end electronics was designed to provide a time description of the radiation pulses with resolution in the order of hundreds of ns. The percentage depth-dose (PDD) curves and lateral profile distributions were measured with ElectronFlash machines using 7 and 9 MeV electron beams with 10 cm diameter in water phantom. The results satisfactorily compare to the reference curves obtained with Radiochromic or FLASH diamond dosimeters, qualifying the UCD as a very promising dosimeter for this novel radiation modality.

6.2.3 Microdosimetry

Microdosimetry is becoming an essential instrument for assessing the microscopic patterns of energy deposition by radiation, which, ultimately, governs the effects of ionizing radiation on living cells.

The reference physical quantity adopted in order to estimate the biological effects induced by the radiation to the tissues is the absorbed dose, defined as the absorbed energy per unit mass. However, for heavy ions, the only absorbed dose value is not sufficient to fully describe the biological effectiveness of the radiation. To this purpose, it is necessary to introduce the concept of radiation quality that depends on the particle type and energy spectrum. A more detailed description of the radiation effectiveness can be achieved by the measurement of microscopic dosimetric quantities, allowing to determine the local radiation quality. To this purpose, microdosimetric detectors were developed to provide the spectrum of the lineal energy in a micrometric volume. The spectra of the lineal energy together with the value of the absorbed dose at the same point can be thus used to predict the response of the irradiated cells.

Tissue-equivalent proportional counters (TEPCs) are the main instruments employed for estimating beam quality. TEPCs are characterized by full tissue equivalence (both the walls and the filling gas of the detector are tissue-equivalent). Currently solid-state detectors (i.e., diamond, silicon and silicon carbide) are also adopted to acquire microdosimetric spectra. These devices are not tissue-equivalent or radiation-hard detectors but have an increased resolution and a user-friendly operating mode.

Diamond detector Synthetic single-crystal diamond is an ideal material to produce high-spatial resolution and high radiation hardness devices for microdosimetric applications thanks to its excellent properties such as the wide bandgap, near tissue equivalence, a near-constant ratio of stopping power with water for proton and carbon ions, low dielectric constant and high radiation hardness.

Diamond-based microdosimeters (DBMs) were proposed in a boron-doped diamond/intrinsic diamond/metal Schottky diode configuration, featured by different sensitive volume (SV) and shape, at laboratories of Industrial Engineering Department of Rome “Tor Vergata” combining microwave plasma-enhanced chemical vapor deposition and photolithography techniques. The thickness and the cross-section area of diamond SV vary in the range $0.5\,\mu$m - $10\,\mu$m and $10 \times 10\,\mu\text{m}^2$ - $300 \times 300\mu\text{m}^2$, respectively. Details of the DBMs design and fabrication are reported elsewhere [491]. Spectroscopic characterizations including IBIC test of diamond microdosimeters using different ion beams and energies were performed showing a well-defined confinement of the CCE within the SV with a good homogeneity as well as a linear response as a function of the LET of the incident particle in the range 100-3000 keV/μm.

The microdosimetric performance of the developed DBMs have also been successfully investigated with high-energy scanned carbon beams and therapeutic proton beams at different ion-beam therapy centers such as CNAO [492], CATANA [493] and MedAustron [494].

Recently, the DIODE (Diamond Integrated devices fOr haDronthErapy) project, financed by INFN-CSN 5, address the development and test of a novel compact detection system based on synthetic single-crystal diamond able to simultaneously perform dosimetric and microdosimetric characterization of clinical ion beams. The proposed device allows a fast and exhaustive beam characterization and radiation quality in ion-beam therapy centers and can partially overcome some drawbacks of the diamond microdosimeter regarding low sensitivity to low LET radiation and detector position evaluation.

Gas detectors Tissue-equivalent proportional counters (TEPCs), the reference devices in microdosimetry, are gas detectors filled with tissue-equivalent (TE) gas and built with TE materials. They operate in pulse mode to collect a signal pulse for each ionization event occurring in the sensitive volume (SV). They are spherical or cylindrical detectors. The presence of the electronic avalanche amplifies the signal of primary electrons making these detectors highly sensitive.

The gas is usually propane, and its density is scaled in the SV to simulate site sizes of less than 2 μm in tissue. It is important to use these detectors sealed because for safety reasons it is not possible to introduce propane in clinical facilities.

Due to the high intensity of clinical beams, miniaturized TEPCs have been developed at INFN-LNL [495, 496]. They are cylindrical TEPCs with a cylindrical SV of 1 mm of diameter and height. Engineered detectors have been designed to meet the standards of reproducibility required in the clinical environment. Five engineered mini-TEPCs have been successfully tested, and their response function is highly reproducible.

TEPCs with boron-doped walls for applications in BNCT have also been developed at the INFN-LNL. Measurements were performed at the MUNES thermal column at the CN accelerator at INFN-LNL suggesting the ability of detect the boron neutron capture reaction when coupled measurements with and without boron are performed [497].

Standard TEPCs have sizes between 0.5 μm and 2 μm. To measure at smaller site sizes, avalanche confinement TEPCs have been developed that have successfully measured down to 20 nm [498]. The importance of investigating small site sizes is related to the stronger correlation with biological damage.

The future step is to develop an innovative multi-site TEPC with three electrodes capable of measuring two site sizes in a ratio of 1:10 without changing the gas pressure but only the electric field between grid and cathode. The multi-site information will allow us to validate more complex models that consider the clustering of damages at different sites.

6.2.4 New devices for dosimetric purposes

Dosimetry detectors are essential tools used in the field of radiation dosimetry to measure and quantify the amount of ionizing radiation to which an object or individual has been exposed. These detectors play a crucial role in various applications, including medical radiation therapy, industrial radiation monitoring and radiation protection. There are several types of dosimetry detectors, each with its own advantages and limitations. A widely used detector is the ionization chamber. Solid-state dosimeters are also used for relative dosimetry. These devices use semiconductor materials, such as silicon, diamond or silicon carbide to detect and measure ionizing radiation. Solid-state detectors offer real-time dose monitoring and can provide immediate feedback to the user.

Silicon carbide Silicon Carbide (SiC) technology represents one of the most reliable solutions in order to develop new dosimetric systems. Recent studies have encouraged the use of SiC detectors for both photon and charged particle dosimetry [90, 499]. In this context, the PRAGUE (Proton RAnGe measure Using silicon carbidE) project takes place. It aims to realize a system able to measure, in real-time and with a high longitudinal spatial resolution (150 μm water equivalent), the PDD distribution of a 30-150 MeV proton beam. It consists of 60 SiC devices (10 μm active layer, $15 \times 15\,\mathrm{mm}^2$ sensible area) placed in a stack configuration. The electronic chain will work properly with high (10^{10} pps) and low (10^5 pps) intensity beams and involves the use of the TERA08 chip. To avoid loss of efficiency in charge collection with high-intensity beams, a customized interface board between the detectors and the TERA08 is being developed. The 60 SiC detectors were electrically characterized by performing the I-V (current vs. voltage) and C-V (capacitance vs. voltage) measurements. The stability, reproducibility and linearity of the devices were also analyzed, by irradiating the detectors with an X-Ray Tube (2.5-15 mA, 10-25 kV at Roma Tor Vergata University). A prototype of the final detector, composed of 4 SiC devices, was realized and tested by acquiring the PDD distribution of a 70 MeV proton beam (delivered at Proton Therapy Centre, Trento, Italy) and a 30 MeV proton beam (delivered at ÚJV Řež Centre, Czech Republic). In both cases, the PDD distribution of the proton beam was also acquired with a full EBT3 stack. Results highlight that the PRAGUE prototype is able to reconstruct a PDD distribution with a peak/plateau ratio better than that obtained with the EBT3. Future steps comprehend detector assembling and tests with clinical and high-dose rate proton beams. SiC technology is being analyzed also in the field of Microdosimetry. This is the aim of the DoT-SiC project. The detectors have an active layer of 10 μm and a sensible area of $4 \times 4\,\mathrm{mm}^2$, in turn divided into four independent sub-areas. Future steps include tests with 12C and 4He beam and the optimization of the electronic readout.

Hydrogenated Amorphous Silicon Amorphous silicon was used mainly for photovoltaic panels and flat panels for X-ray imaging; however, it was also used to characterize proton beams at CNAO [500]. The HASPIDE INFN project (Hydrogenated Amorphous Silicon PIxel Devices) aims to develop further the a-Si:H technology to produce ionizing radiation detectors for clinical dosimetry. The material is very radiation-resistant and can be deposited as a thin layer ($\sim$ 10μm) on various substrates such as kapton, hence allowing the construction of devices well suited for clinical dosimetry and transmission detectors. Different detector configurations have been produced at EPFL-Neuchatel and studied both in the absence and the presence of radiation sources. The tested configurations include sensors differing in thickness, area, contact type and deposition substrate. Results obtained so far (laboratory X-ray tube) include noise at the level of a few pA, capability to work at 0 V bias, sensitivity ranging from ∼ 1 nC/cGy at 0 V bias to 10-20 nC/cGy at 30 V bias, linearity of response ∼ 1% up to 24 mGy/s [249]. Test under clinical LINAC and Synchrotron beams have been carried out confirming the results obtained with X-ray beams, namely an excellent linearity ($R^2 > 0.999$), a close superposition with standard dosimeters for PDD measurements (better than 8%), a precise definition of the sensitive volume with a signal variation of 100% in less than 200 μm when exiting from the region covered by the contact [501]. To test the radiation resistance, the devices were irradiated with photons up to 700 kGy at the Australian Synchrotron and the leakage current increased from less than 1 pA to 1.5 pA, while the signal remained quite stable from 100 to 700 kGy after a reduction of 25-30% in the first 100 kGy irradiation. Further study to check for annealing effect has been done after a neutrons irradiation of other devices with fluence up to 5×10^{16} n_{eq}/cm^2 at Josef Stefan Institute facility (Ljubljana). The linearity of the response to X-rays flux was confirmed after the irradiation and, after 12 h annealing at 100 °C, the leakage current and the noise fully recovered to the values before irradiation, while the sensitivity only partially recovered maintaining, however, the linearity of the response [502].

3D diamond devices Use of diamond as a sensitive material in medical dosimetry was dictated by its closeness to tissue equivalence ($Z_{carbon} = 6$ vs $Z_{tissue} = 7.14$), its low dark current and high breakdown voltage. Diamond dosimeters are generally parallelepiped detectors in two main configurations: with electrodes both on front and back sides (called planar configuration) or, the present state-of-the-art, interdigitated electrodes inside the diamond substrate (3D configuration) [503]. For conventional planar detectors, the separation of the electrodes is directly coupled to and limited by the thickness of the substrate, as they are typically fabricated on the top and backplane of the diamond. A 3D device has columnar electrodes inscribed within the bulk of the sensitive material, decoupling the inter-electrode distance from the substrate thickness. Synthetic production allows for devices classified as single crystal (scCVD) or polycrystalline (pCVD). Dosimeters made with scCVD diamond films have a stable, fast and reproducible response, but cannot be easily used for a large-scale application in radiotherapy dosimetry due to the maximum achievable wafer size (1 cm diameter) and their higher cost compared with pCVD. On the other hand, it has been demonstrated that pCVD 3D devices are precise enough and with a sufficient fast response to meet the requirements of radiotherapy dosimetry [504]. One development that could optimize these devices is to produce graphite pads on the diamond surfaces using the laser beams to produce a graphite layer where perform the microbonding to connect the device with the bias and the DAQ, obtaining an all-carbon device. A first prototype, tested on clinical beams, shows a better behavior with respect to the normal metallic pads [505]. A study of the performance dependence on the device's pixel size shows that a size smaller than 1 mm is necessary to avoid volume averaging effects when beam size is smaller than 1 cm [506]. One of the main goals is to produce a pixelated device with pixel size below 1 mm with an area big enough ($30 \times 30\,mm^2$) to measure at the same time the whole shape of a clinical small beam, including the penumbra region.

6.3 X-ray and nuclear medicine imaging

The development of advanced detectors plays a crucial role in pushing the boundaries of biomedical imaging. This section delves into the research and development efforts focused on two main areas: radiological imaging and nuclear imaging. Radiological imaging typically deals with X-rays in the 10-150 keV energy range, while nuclear imaging utilizes gamma rays with energies in the hundreds of keV range.

The challenges typical of X-ray imaging are related to the requirements of high spatial resolution (10-10^2 μm) and high rate of events (up to 10^9 counts $mm^{-2}\,s^{-1}$), as well as high interaction efficiency and low electronic noise. In this field, the two major innovations reported concern the development of perovskite X-ray imaging detectors, and hybrid detectors with photon-counting and spectral capabilities. Perovskite-based detector is a promising candidate for high-efficiency, large-area and cost-effective solution for X-ray imaging. Photon counting detectors allow for electronic noise suppression with proper signal thresholding and spectroscopic capabilities may enable the implementation of spectral techniques which are the next breakthrough in diagnostic.

In the field of nuclear medicine imaging the development of gamma detectors for the measurement of the internal activity distribution in patients undergoing targeted radionuclide therapy is presented. Also, the radiation generated by nuclear decays as charged particles can be used for diagnostic tasks: β detectors were developed for radio-guided surgery with β-emitting radiotracers and for microscopy imaging by contact.

6.3.1 Hybrid pixel detectors: Timepix4 and Medipix4

Hybrid pixel detectors are based on the separation of the sensor element and the readout electronics into layers which are manufactured independently and then coupled through the bump-bonding interconnection technique. Such detectors allow to separately optimize sensor and electronics to obtain the best overall performance. The Medipix4 Collaboration at CERN, launched in 2016, is aimed at designing two readout chips: Timepix4, which provides particle detection with excellent spatial and timing precision at high rates, and Medipix4, which will target spectroscopic X-ray imaging at rates compatible with medical CT scans [507, 508]. INFN became an official member of the Medipix4 Collaboration in November 2020 with the aim of studying and testing the possible applications of this technology in a wide range of fields, from X-ray spectral imaging to nuclear medicine and dosimetry. In addition, an ERC funded project hosted by INFN is developing a single-photon detector based on a vacuum tube with transmission photocathode, a

Table 4 Timepix4 technical specifications

Timepix4		
Technology	65 nm–10 metal	
Pixel size	55 µm × 55 µm	
Pixel arrangement	512 × 512, 4-side buttable	
Sensitive area	6.94 cm^2	
Operation mode	Data driven (tracking)	Frame-based (imaging)
Mode	Time over threshold (ToT) and Time of arrival (ToA)	Continuous read write (CRW): Photon counting (PC) (8 or 16 bit)
Time resolution	~200 ps	–
Energy resolution	< 1 keV	–
Max rate (hits/mm^2/s)	3.58×10^6	$\sim 5 \times 10^9$
Readout bandwidth	< 1 163.84 Gbps (16 × 10.24 Gbps)	

Table 5 Medipix4 specifications

Medipix4		
Technology	130 nm–9 metal	
Operation mode	Fine pitch (FPM)	Spectroscopic (SM)
Pixel size	75 µm × 75 µm	150 µm × 150 µm
Pixel arrangement	320 × 320, 4-side buttable	160 × 160, 4-side buttable
Sensitive area	5.76 cm^2	
Energy thresholds	2	8
Max Count Rate (hits/mm^2/s)	$\sim 5 \times 10^6$	

micro-channel plate for electron multiplication and the Timepix4 as active anode [358], for applications in high-energy physics, life sciences and quantum optics. A summary of the technical specifications for the Timepix4 and Medipix4 chips is reported in Tables 4 and 5, respectively.

6.3.2 SYRMA, KEST and PEPI

In addition to participating in collaborations developing new radiation detectors, INFN is active in the application of the developed technologies. One example is the use of hybrid detectors for X-ray imaging, where photon-counting and spectral capabilities bring major advantages in terms of image noise and radiation dose reduction, and material-specific quantification. In this framework, the Syrma-CT/3D projects carried out the development of an imaging setup dedicated to the first X-ray phase-contrast breast CT clinical study, in collaboration with the Elettra synchrotron radiation facility [509]. The setup makes use of a large-area photon-counting detector, Pixirad8, developed by Pixirad srl (an INFN's spin-off). The device features a 650 µm thick CdTe sensor, ensuring high detection efficiency (~100% up to 50 keV), a dead-time-free readout and a small pixel pitch of 60 µm, resulting in high resolution. Owing to the combined use of Pixirad and phase-contrast, the developed system has been shown to outperform commercial scanners, yielding up to a threefold increase in SNR and a fivefold improvement in spatial resolution [510], as shown in Fig. 40. Along with the drive toward clinical imaging applications, INFN has been funding research on systems for preclinical or non-clinical imaging. In this context, KEST [511] and PEPI [512] projects developed a micro-CT spectral scanner including a Pixirad detector equipped with the latest readout chip, PixieIII. This chip, similarly to other state-of-the-art ASICs such as Medipix3, features a charge-sharing compensation mode that allows assigning to a single pixel the signal, and hence the energy that is spread across multiple pixels due to charge sharing. This feature is key for spectral imaging, where a high-fidelity spectral response reduces cross-talk among energy bins, ultimately improving image quality. Following a complete energy characterization, Pixirad has been included in the imaging system, yielding high sensitivity (few mg/ml) for the quantification of several contrast media commonly used in biomedical imaging, at a spatial resolution better than 50 µm [513]. Owing to the sharpness of their spatial response, hybrid detectors are also suited for phase-contrast imaging techniques making use of X-ray beam modulators (e.g., edge-illumination, speckle imaging), thus paving the way for the combined use of spectral and phase-contrast imaging [512].

6.3.3 PEROV

Along with the development of new readout chip architectures and their imaging applications, INFN is also actively promoting research in the field of innovative sensor materials for hybrid detectors. X-ray imaging detectors available on the market include

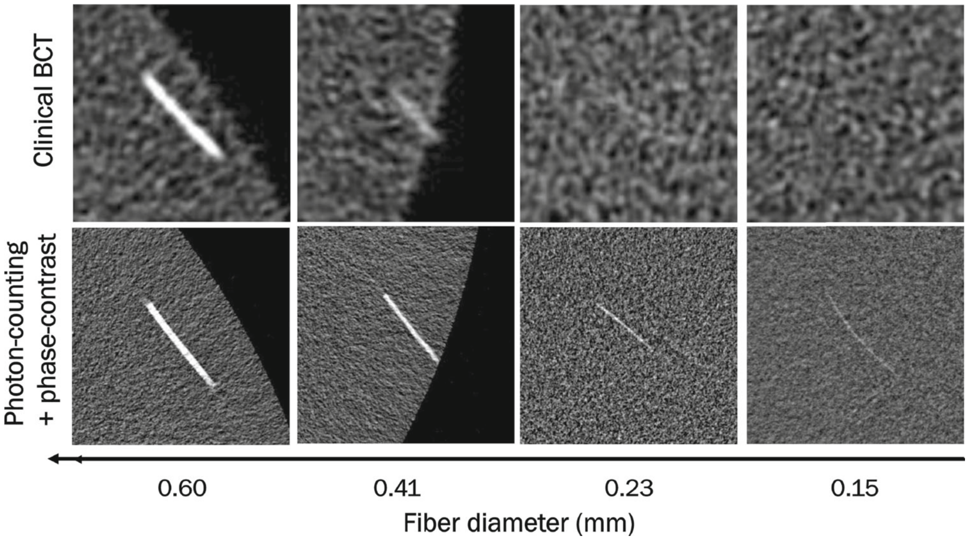

Fig. 40 Comparison between conventional (top row) and phase-contrast (bottom) row CT visibility of soft tissue-equivalent fibers as a function of their diameter. Figure adapted from [510]

both direct and indirect systems with differences in cost, size, efficiency and spatial resolution. The indirect detection of X-rays is usually performed with scintillators, which provide a lower signal/noise ratio (SNR) if compared to direct detection. The most common materials used for the direct detection of X-rays from a few keV to 100 keV are silicon, amorphous selenium (a-Se) and CdTe/CZT [514]. Each of these materials has some limitations: Si has a low stopping power for high-energy X-rays, a-Se detectors are typically operated in charge integration mode, offering a low SNR if compared to photon-counting detectors, and CdTe/CZT detectors are expensive and complex to manufacture when large areas are required. In the last few years, halide lead perovskites are emerging as very attractive candidates for X-ray detection due to their strong stopping power, defect tolerance, large mobility lifetime product, tunable bandgap and simple single-crystal growth from low-cost solution processes [515]. In this framework, the goal of the follow-up of the INFN-funded Perov project for the coming years is the development of a device suitable also for X-ray detection, combining a perovskite absorption layer and a CMOS silicon active layer, for X-ray energies in the tens of keV range. The high-Z perovskite absorption layer can provide a high detection efficiency for X-rays in this range with a fraction of the thickness used for silicon direct detectors, thus allowing the collection of charges by drift without spoiling the spatial resolution. Available CMOS substrates with aluminum pads will be used to investigate the possibility of directly growing a perovskite detector, from a precursor solution [516], on the surface of a CMOS chip. This first phase is crucial to verify the compatibility of materials and deposition techniques required for the growth of hybrid detectors. In the longer term, the perovskite layer will be deposited on a silicon Readout Integrated Circuit (ROIC) to realize radiation detectors with integrated electronics that will enable the production of multi-channel detectors for X-ray imaging applications [517].

6.3.4 WIDMApp

A systematic measurement of the internal activity distribution in patients undergoing Targeted Radionuclide Therapy (TRT) would enable treatment improvements and individualization of the activity to be administered. This is essential to increase therapeutic effectiveness, optimize treatment planning and establish dose-effect relationships for tumor and normal tissues. Accurate internal radiation dosimetry (IRD) is not an easy task, since the dose absorbed by tissues depends on several interconnected key factors largely fluctuating from patient to patient. A new approach for individual radioagent biokinetics determination is proposed with the Wearable Individual Dose Monitoring Apparatus (WIDMApp) [518]. The WIDMApp system is conceived as a wearable, noninvasive multi-channel detector system for in vivo real-time radiation detection and a data analysis tool that provides a continuous mapping of the radioactive agent transit and accumulation in TRT patients. The goal of the WIDMApp approach is the deconvolution of the cumulative detected signal to distinguish the contribution of each emitting volume/organ, the reconstruction of the activity map at the organ level and its evolution over time. Hence, WIDMApp will enable precise reconstruction of the biological time-activity trend in lesions and in healthy tissues over a large temporal interval, characterizing both the accumulation and uptake behavior and the long tail retention with an uncertainty below those originating from activity quantification in conventional nuclear medicine imaging.

6.3.5 CHIRONE

The technique of radio-guided surgery (RGS), a nuclear medicine approach that aids in achieving complete tumor resection during surgery, relies on the detection of radiation emitted by a radiopharmaceutical that selectively binds to tumor cells. As traditional RGS based on γ emission is limited by the high penetration of γ-rays, an approach using $\beta-$ emitting radiotracers has been developed within the CHIRONE project, funded by the INFN-CSN5. Specifically, A dedicated particle detector with high efficiency for $\beta-$ particles and transparency to photons has been created, and its performance with $\beta+$ emitting sources commonly used in nuclear medicine has been explored. A notable innovation in the development of a β-RGS proof was represented by the introduction of novel high Light Output (LY) organic scintillating materials, such as the p-terphenyl that, thanks to its high beta sensitivity and intrinsic gamma transparency, can be effective both with PET radiopharmaceuticals and pure beta-emitting tracers [519, 520]. At the moment, in vivo experimentation of this probe is ongoing, both on prostate cancer with 68Ga-PSMA and on neuroendocrine tumors with 68Ga-DOTATOC, with very promising, albeit still unpublished, results.

6.3.6 Beta imaging with MAPS

Electron imaging has been widespread for a long time in the electron microscopy field, where technology moved recently from traditional chemical films to solid-state pixel sensors. In this application, the typical electron energy ranges from a few tens of keV to a few hundred keV, which is enough to produce a strong signal from a single impacting electron in silicon, the most common material used for pixel sensor production. In fact, many beta-emitting radioactive materials of interest for medicine and biology fall within a similar range (as the case of Ag-111, the novel radioisotope under study in the ISOLPHARM project [521] at LNL, with 360 keV average β energy). Electrons of such energies have a large cross section in silicon, making it possible to detect them with full efficiency using just a few tens of microns of high-purity, depleted silicon, contrary to X and γ rays, which requires higher Z materials (like Ge or CdTe) and/or much thicker sensitive layers. Silicon is the material used to build 99.9% of modern microelectronic devices; the fact that it shows excellent detection efficiency for electrons in the aforementioned energy range has the important consequence that it is possible to integrate the sensing layer and the electronics into a single monolithic device, building an integrated sensor that can be entirely produced by the existing facilities of the microelectronics industry. This combination makes it possible to realize very large areas (many tens of cm^2 or even square meters), and high-performance pixel sensors at a very competitive cost. By combining the large area with the small pixel pitch ($10 \div 40\,\mu\mathrm{m}$) which characterizes these monolithic pixel sensors (MAPS) is possible to achieve microscopy imaging by contact, where a large sample (or a multitude of samples) is recorded with micrometric precision over an area of many cm^2, compared to the few $\mu\mathrm{m}^2$ of traditional optical and electron microscopy. While the spatial resolution cannot be comparable to classic microscopy methods (roughly $10\,\mu\mathrm{m}$ vs 100 nm), the huge advantage in the area makes it possible to parallelize operations, operate on batches, devise completely new techniques based on patterning and/or comparison of multiple samples imaged at the same time.

7 Target development for nuclear physics

Targets represent extremely important components in nuclear physics experiments with accelerators, either for experimental activities in fundamental science or for applications such as the production of radioisotopes or neutrons. In case of nuclear physics experiments, targets are usually composed of either thin films of specific isotopic species deposited on substrates, self-sustaining foils or gases. Targets for the production of radioisotopes or neutrons are usually exposed to high power deposition from the primary beam. Their design must therefore be accurate so as to satisfy strict requirements in terms of power dissipation, mechanical properties or material microstructures, to maximize production without incurring in failure. In the following, recent advancements on innovative target design, production and characterization at INFN is reported, divided in two sections: targets for nuclear physics experiments and targets for new production facilities.

7.1 Innovative targets for nuclear physics experiments

In any nuclear physics experimental study with accelerated beams, the choice of a proper target is a crucial issue, as important as the choice of the impinging beam and of the detection systems. Thus a careful production and characterization procedure of the target foils for nuclear physics experiments is a main objective in the preparation of an experiment.

At INFN, the main target laboratories are located at LNS and LNL and have decades-long experience in the production of targets for nuclear physics experiments. In the present section, an overview of the activities related to the target manufacturing and characterization at INFN is given.

7.1.1 The target laboratory at Laboratori Nazionali del Sud

The target laboratory (laboratory of physical-chemical techniques) at LNS produces targets for nuclear physics experiments performed by local researchers and international collaborators. It typically makes foils of metal and non-metal materials, salt compounds, organic compounds for a wide variety of stable isotopes, as listed in Ref. [522]. Moreover, the laboratory deals with the preparation of the stripper foils for the accelerator machines (Tandem Van de Graff and K800 Superconducting Cyclotron) and the cathodes for the sputtering negative ion sources and develops and carries out chemical treatments and special chemical cleaning. It also takes care of the deposition of specific BaF2 viewers for beam diagnostic.

Three main machines for target preparation are presently available:

- a Leybold L300 evaporator with two thermic sources;
- a Leybold-Heraeus L560 with a thermic and an electron beam sources;
- a rolling mill

Both the evaporators are equipped with a quartz crystal microbalance which monitors the thickness of the deposited material during the evaporation process. It is possible to set the distance between the source and the substrate by using cylindrical glasses of several heights. Moreover, the L560 evaporator has a halogen heating element to set the temperature of the substrate, if needed. The physical vapor deposition technique is typically used to produce thin foils (thickness less than 1 μm) by thermal evaporation or using an electron beam source depending on the fusion temperature of the material. The depositions are done on thin backing foils (made of C, Al, Au, etc.) or self-supporting. Cold lamination (rolling) techniques are used in the case of metal targets with thicknesses larger than 1 μm. Solvent casting techniques are also used to prepare polyethylene or deuterated polyethylene films.

The targets manufactured at LNS are typically characterized in terms of thickness and uniformity. When high precision in the thickness determination of the produced thin foil is needed, it is analyzed by using a dedicated machine, based on alpha-particle energy loss measurements. The machine consists of a high-vacuum chamber with four movable plates which hold the foils to be characterized. The measuring system is made of an arm containing a collimated ^{241}Am alpha source located in front of a surface barrier silicon detector. The target to be characterized is located in between the source and the detector. The arm has been designed to scan the whole target size. A software has been developed for the control of the machine which automatically performs the measurement of a sequence of targets. This system also provides the uniformity of the targets, determining the thickness on different points of the surface of the same target which differ of less than 1 mm. When the thickness of the film is larger than about 1 μm and can be easily handled, its weight can be determined also by an analytical balance and the thickness deduced accordingly.

Other pieces of equipment available at the LNS target laboratory are:

- an optical microscope;
- an analytical balance with precision 10^{-5} g;
- a technical balance with precision 10^{-2} g;
- a chemical hood;
- an oven to heating up till 200°

In the coming years, the laboratory will be equipped with a new evaporator with two thermal sources, one electron beam source, a heating/cooling system to set the substrate temperature and a system to change the distance between the source and the target substrate. The possibility to produce thin targets, high performing in terms of thickness uniformity, together with an accurate measurement of thickness, is an important challenge in present and forthcoming years at LNS. This task is crucial especially when the targets are used for nuclear physics experiments where absolute reaction cross sections need to be measured with high precision. This request is even more stringent for experiments with relatively low energy beams or medium to heavy beams (such as the ones available at LNS), where the energy and angular straggling of the beam in the target foil plays a crucial role.

The production of thin and uniform targets of quite large area (10 cm^2 or more) for their application with large spot size beams, such as radioactive beams, has also required and will require some effort at LNS.

In addition, in view of the high beam intensities expected after the LNS upgrade, which is presently ongoing, the development of targets which are tolerant to high beam rate conditions is becoming a crucial task. As an example, the study of deposition procedures on specific substrates of graphene-based foils is ongoing.

The minimization of the amount of material used for the preparation of the targets is another challenge in view of the limited availability and of the increasing cost of many compounds or isotopic materials. Improvements of the parameters of the already used vapor deposition techniques or further development of chemical deposition techniques can help in specific cases.

The use of noble-gas targets is a request of different nuclear physics experiments. Ion-implantation techniques based on the use of ion implanters, such as the one present at the physics and astronomy department of the University of Catania, are being explored at LNS. In addition, the possibility to exploit the already available technology of Electron Cyclotron Resonance (ECR) source for ion-implantation purposes is also an interesting opportunity.

7.1.2 The target laboratory at Laboratori Nazionali di Legnaro

The main activities of the Targets Laboratory for Nuclear Physics (NP) studies are the study and preparation of targets for nuclear physics experiments to be conducted at LNL or in foreign laboratories. In most cases, thin films of isotopically enriched elements are obtained using different techniques. Different types of targets can be obtained:

- Self-supporting;
- With backing;

- Strip-targets;
- Sandwich-targets;
- Plunger-targets;
- Cryogenic ^{3,4}He targets at 9 °K are also being developed to achieve thicknesses of 3-5 10^{20} at/cm^2 to carry out inverse kinematic nuclear reactions studies.

The instrumentation to carry out these activities includes many devices, including a fume hood designed to work with powders, equipped with a high-precision scale, a roller working under inert atmosphere (with a glove box used also to manage reactive substances), three high-vacuum evaporators including a cryogenic one, and a tube furnace capable of working in inert or reactive gas or vacuum that can operate at temperatures up to 1500 °C. About the cryogenic target, a Gifford McMahon device is used as cryogenic source. It is conceived to be a portable device. At the time being, the following target preparation techniques for thin films and foils are available:

- Thermal evaporation from crucibles and boats;
- Thermal resistance heating of high-purity carbon;
- DC ion-beam sputtering;
- Electron beam evaporation;
- Rolling mills;
- Rolling mills under inert gas atmosphere.

Thickness as well as characterization of produced target are controlled by:

- Quartz Crystal Monitor (QCM) during vacuum evaporation;
- Weighing the obtained film after determining the exact area with a proper software;
- Alpha source and proton/alpha beams from the CN accelerator for the cryogenic target.

For the coming years, it is planned the development of multi-isotope standard and plunger targets and the upgrade of ion-beam sputtering devices to develop new type of targets.

Another activity started a few years ago is the development of innovative techniques to produce targets for beam irradiation at cyclotrons aimed at nuclear cross-section measurements and medically relevant radionuclides production in the framework of the new SPES LARAMED facility (see Sect. 7.2.3).

The laboratory is also equipped with a cryogenic mill for grinding at a few micrometric sizes inhomogeneous, sponge-like, isotope-enriched powders delivered by manufactures.

This laboratory is being used in different experiments and collaborations regarding solid targets production and characterization. The laboratory is equipped with different physical vapor deposition (PVD) magnetron sputtering apparatuses, dedicated to the synthesis of novel materials for NP experiments. The target thickness achievable by using the existing setups are in the range from a few nanometers to several micrometers.

The characterization of developed targets includes morphological and compositional analysis with standard techniques (Laboratory of Material for NP) and ion-beam analysis (IBA) nuclear techniques (using the Van de Graaff CN and AN2000 accelerator facilities present at LNL). The main characterization techniques are:

- Optical microscopy (OA);
- Scanning electron microscopy (SEM);
- Energy-dispersive X-ray spectroscopy (EDX);
- Atomic force microscopy (AFM).

Nuclear IBA techniques are:

- Elastic backscattering spectrometry (EBS);
- Nuclear reaction analysis (NRA (d,p), (p,α), (d,α));
- Elastic recoil detection;
- Proton-induced X-ray emission (PIXE and micro-PIXE)
- Proton-induced gamma-ray emission (PIGE)

7.1.3 LUNA solid target development by PVD magnetron sputtering technology

Cross-section measurements in astrophysics research play a crucial role in studying various fields, such as elementary nucleosynthesis, energy generation and neutrino flux generation. The precise knowledge of cross sections is essential for defining stellar models accurately [523]. Given the very small cross sections of nuclear reactions involving light elements in the stellar energy range, these measurements require maximizing the signal-to-noise ratio while minimizing background interference. To address this, the LUNA (Laboratory for Underground Nuclear Astrophysics) collaboration focuses its main activities at the Gran Sasso underground laboratories. The substantial rock overburden of about 1400 m drastically reduces natural background sources, including cosmic muon components, neutrons and gamma rays [524]. Currently, cross-section measurements are performed using a 400 keV accelerator, while a new MV accelerator will be soon available. The accelerators are located in the underground LNGS laboratories. However, one of the background sources is the beam-induced background (BIB), resulting from the interaction of the beam with target contaminations like fluorine, oxygen, carbon and deuterium. The presence of these elements could compromise the quality of cross-section measurements, making their reduction mandatory. To produce nuclear targets for LUNA experiments, various techniques are employed, such as thermal or electron beam evaporation for pure elements, anodization for oxides and magnetron sputtering techniques (MS) for composites like nitrides [525]. The National Laboratories of Legnaro (LNL) have been involved in the production of targets, focusing on reducing contaminants in both target materials (nitrides and oxides) and backing materials (Tantalum). All produced targets undergo characterization using ion-beam analysis techniques, such as elastic backscattering spectrometry and nuclear reaction analysis, available at AN2000 and CN facilities of LNL [526]. Regarding the Tantalum backing treatment, a specific cleaning procedure has been developed to minimize surface contaminations, particularly fluorine and organic compounds. The procedure involves three sequential steps: chemical etching using an acid bath to remove organic and fluorine contamination from surface, physical cleaning using a CO_2 snow jet cleaner gun for removing environmental dust and, finally, in situ plasma etching to remove natural metal passivation. This combined approach reduces the BIB up to ten times, then previous cleaning procedure. For nuclear target experiments, the interested materials are deposited using MS and reactive magnetron sputtering techniques after plasma cleaning in the same chamber without vacuum breaking, preventing further contamination induced by exposure to air. The sputtering chamber used for nuclear target production is a custom apparatus available at LNL Nuclear Physics Materials Laboratory. It has been adapted with custom devices, including a rotating polarizable sample holder, an active gettering system, Helmholtz coils, etc. These components are designed to improve coating quality and prevent contaminant presence. The coatings are made using commercial sputtering sources in close field configuration coupled with various power supplies (DC, Pulsed-DC, RF and HiPIMS), depending on the material in use and the desired coating properties. Composite materials like oxides, nitrides and hydrides are synthesized using reactive magnetron techniques driven by an optical emission monitor system, ensuring the desired stoichiometry of the composites.

The selection of materials used for target production for LUNA experiments requires high-purity metals (at least 99.95%) and high-purity gases (at least 99.9% for isotopically enriched gases).

The targets produced at LNL in recent years include oxides and nitrides (TiN, ZrN, TaN, Ta_2O_5), used as calibration standards or targets for cross-section measurements. LNL is currently involved in preparing a tantalum nitride target using isotopically enriched ^{14}N gas. This target will be used in the first experimental campaign ^{14}N(p, γ)^{15}O at the new Bellotti Facility at LNGS, utilizing the 3.5 MV accelerator. Additionally, LNL is participating in other planned LUNA experiments, such as ^{12}C +^{12} C and ^{23}Na(p, α)^{20}Ne.

7.1.4 Electron screening study with supersonic gas jet targets

In nuclear reactions performed in laboratories, the interacting projectiles and targets are usually in the form of ions and atoms (or molecule), respectively. Due to the electronic cloud surrounding the latter, the impinging particles undergoes a reduced Coulomb field compared to a bare target nucleus, which shifts the actual nuclear reaction energy enhancing the resulting cross section. Also projectile ions, if heavier than protons, can retain one or more electron, further lowering the Coulomb interaction [527]. Electron screening is mostly negligible at the higher energies but becomes relevant at the lower ones (around 100 keV up to few MeV depending on the nuclear charge), as in the case of nuclear astrophysics studies [528]. In addition, often stellar energies cannot be directly investigated causing stellar models to rely on extrapolations; for this, even a small offset due to an incorrect inclusion of the electron screening effect may lead to significant errors.

The enhance factor caused by electron screening is usually related to the variation on the penetrability factor caused by the energy shift. This latter is usually deduced by atomic physics as difference on the binding energy of the outermost electron in the compound nucleus and the sum of binding energies of both projectile and target outermost electron binding energies [528, 529]. This approach meets theoretical estimates [530] and was experimentally verified for heavier ion collisions in backward angles [531]. For the approximations used in theoretical evaluations and for the possibility that for light ions other effects may alter the results (e.g., shell effects), new direct measurements of the electron screening effect on light nuclei are still desirable. As an example, ^{3}He +^{3} He reaction, already studied in LUNA [532], could be a very interesting case study. Indeed, the reaction could be investigated down to 20 keV, energy at which the screening effect is believed to enhance the cross section by a factor 1.2. The reaction could be studied in the very same low background environment of LNGS and at the same energies with LUNA400 employing a ionized gas target to directly measure the electron screening enhancement factor, from which the screening potential can be derived.

A supersonic gas jet target (SGJT) [533] is a candidate target to perform such a study. Being gas molecules of SGJT faster than sound speed, the recombination of excited ions is unlikely in the scale length of the target itself ($\sim$ 10 mm). Target gas may then be ionized before its injection in the accelerating nozzle, and even if a partial recombination could still happen before the gas reaches supersonic velocities, one can obtain a partially ionized SGJT to be employed in electron screening investigations. This is also the functioning principle of Plasma Wind Tunnels [534]). SGJT can also be dense ($\sim 10^{18}$ atoms/cm^2) and short ($3-5$ mm) [533, 535], making it a desirable target for the expected low rate at the energy of interest for electron screening effects study. A preliminary evaluation on a ionized SGJT [536] shows that with commercially available arch torches, a ionization of 20% can be obtained for the gas in the beam interaction region. The S/N $\sim$ 6 at $E_{cm} = 20$ keV for the LUNA measurements of ^{3}He(^{3}He, 2p)^{4}He is promising

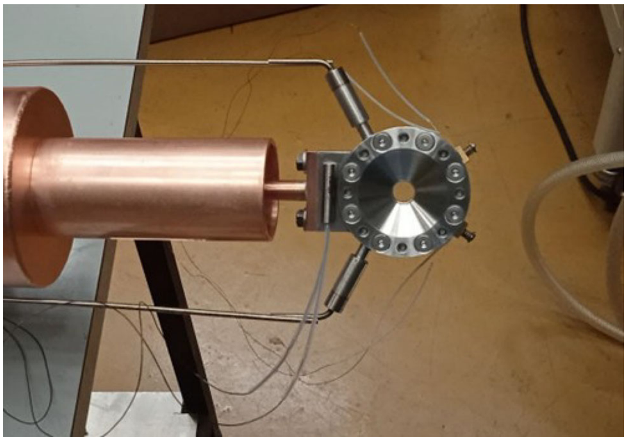

Fig. 41 CTADIR without Havar windows assembled for cryogenic test under vacuum

for this study, since the SGJT can also be easily made thicker (regulating injection pressure). Considering similar conditions as in Ref. [532], with a SGJT and the same running time as in Ref. [532] one can measure statistically relevant differences in the reaction yield already with an injected pressure of ∼4 bar at the energy of $E_\alpha = 50\,\mathrm{keV}$, easily achievable with LUNA400.

7.1.5 A new cryogenic target at LNL: the CTADIR project

Direct reactions of exotic beams with cryogenic targets are powerful tools for studying the single-particle structure of atomic nuclei using direct reactions in inverse kinematics.

Reactions like (^{4}He,^{3}He) of (^{3}He,d), where one neutron or proton is added to a heavier nucleus, are fundamental to explore the evolution of single-particle structure in neutron-rich nuclei.

The study of nuclei far from stability increasingly relies on measurements performed at exotic beam facilities, like upcoming SPES at LNL. These reaction Q-values are well matched with typical beam energies of the ALPI accelerator at LNL (10-15 MeV/u), which implies cross sections of several mbarns for neutron-rich ion beams. However, the low intensity of exotic beams requires thick light targets to achieve the necessary luminosity.

Feasible measurements can be performed with beams down to an intensity of 100 pps, if the target has a thickness at least 10^{20} at/cm^2. In this context, the CTADIR [537, 538] project has been developed, aiming at coupling a Helium cryogenic target with the AGATA [149] gamma-ray detector array and GRIT [539] silicon detector for light charged particles. With the CTADIR cryogenic target, where helium is kept at temperatures $< 10\,\mathrm{K}$, the desired target density can be obtained within only 4 mm along the beam direction. The body of the cryogenic target [537] is made out of aluminum (Al), and its assembly is shown in Fig. 41. Two special laser-welded transitions Al/Stainless steel (SS) were designed to be able to connect the SS capillary pipes for the gas supply to the gas cell of the target. The helium gas is confined within two $3.8\,\mu$m thick Havar windows with a diameter of 10 mm. The tightness between the helium gas and the vacuum is achieved by pressing each Havar window onto the indium seal housed in the “V” shaped groove. The target is anchored to a copper cold finger attached to the second stage of a cryocooler. A copper thermal shield (see Fig. 41), attached to the first stage of the cryocooler, is present in order to reduce the radiation heat load from the surrounding “hot” objects. The target casing was designed to allow for the detection of the reaction products in the total angle of 140 degrees on both sides of the target. The temperature of the target is regulated by a cryogenic temperature controller with temperature sensors and a programmable heater for closed-loop temperature control in proportional–integral–derivative mode.

7.1.6 Cryotargets for high-intensity heavy-ion beams for NUMEN

The NUMEN (NUclear Matrix Elements for Neutrinoless double beta decay) project proposes an innovative technique to access experimental information on Nuclear Matrix Elements (NME) involved in neutrinoless double β decay ($0\nu\beta\beta$), by measuring the cross section of heavy-ion induced double charge exchange (DCE) reactions, thus establishing an alternative experimental driven approach for the determination of the $0\nu\beta\beta$ NMEs [80, 540].

An experimental campaign has already started at LNS by using targets made with $0\nu\beta\beta$ candidate isotopes such as ^{48}Ti, ^{76}Ge, ^{76}Se, ^{116}Cd, ^{116}Sn, ^{130}Te using ^{18}O and ^{20}Ne beams at incident energies of 15-22 MeV/u [541–543], and first data have been measured at the MAGNEX magnetic spectrometer [128, 544]. The full list of isotopes of interest as target for the future NUMEN experiments is presented in Ref. [80]. The very low DCE cross sections (few nb) and the importance of this physics case have triggered the upgrade of the LNS superconducting cyclotron and of the related infrastructures, which is presently ongoing, to increase the intensity of the delivered beams to 10^{13} pps at the MAGNEX target point. Consequently, an upgrade of the whole MAGNEX detection apparatus is also ongoing [127, 545, 546] to withstand these intense beams (see also Sect. 8.2.1. In particular, a new target system, capable of dissipating the power released by these beams, is under study [547].

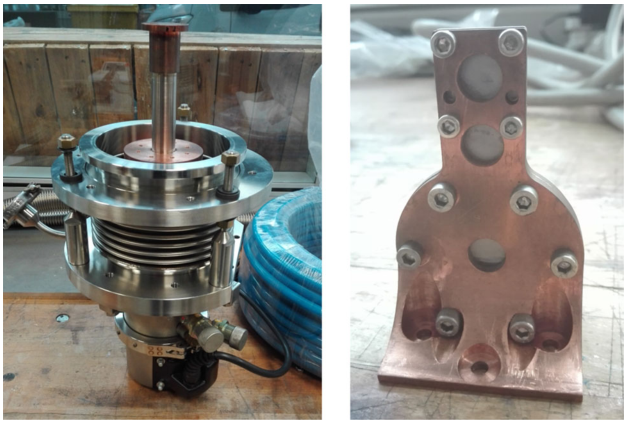

Fig. 42 (left) The NUMEN target cryocooler. The sample stage is the topmost copper object and can be cooled down to 10 K. (right) Graphite target enclosed in the copper sample holder, to be mounted on the cryocooler sample stage

The main constraints in the design of the NUMEN target system are related to:

- the heat deposited by the beam in the target (the power dissipated in typical NUMEN conditions is about 1 W);
- the resolution on the energy measurement of the DCE reaction products (typical required energy resolution of 400-500 keV);
- the required compactness of the whole target/cooling system.

The heat dissipation can be enhanced by depositing the target material on highly thermally conductive substrate, e.g., thin (2μm) graphite foils. These can be of different types, e.g., high oriented pyrolytic graphite (HOPG), characterized by a thermal conductivity ranging between 1700-2200 $\mathrm{Wm^{-1}K^{-1}}$, or can be graphite foils produced by accumulation or rGO or pyrolysis of polymeric foils with high thermal conductivities ranging from 1500 to 1800 $\mathrm{Wm^{-1}K^{-1}}$. It has been estimated that a 450 μg/cm^2-thick HOPG is able to dissipate up to 10 W [548]. Moreover, a dedicated cooling system has been designed to help the heat dissipation: The target will be encased in a copper holder, mounted on top of a cryocooler and kept at 40 K, see Fig. 42.

Concerning the second point, the kinematics of the DCE reactions will be reconstructed from the energy and angle of the reaction products measured by the MAGNEX spectrometer. The reconstructed inclusive energy spectra typically show several peaks and structures due to the population of the ground state and of the excited states of ejectiles and residual nuclei of the nuclear reaction. In order to distinguish transitions to the ground state and to the first excited state of the residual nucleus, the measured energy resolution should be better than the energy difference between these two states, which is usually about 500 keV. To achieve such a resolution, the targets (both the substrate and the evaporated isotopic material) must be thin (few hundreds of nm) and uniform. The presence of non-uniformities in the graphite and/or in the deposited film can indeed contribute to worsening the energy resolution. For this reason, a detailed analysis of the non-uniformity for each produced target is performed. This is typically done characterizing the target by field emission scanning electron microscope (FESEM), Rutherford backscattering spectrometry (RBS) and alpha-particle transmission (APT). In particular, APT measurements are performed at LNS using the CACTUS (Chamber for Alpha-particle Characterization of target Thickness and Uniformity by Scanning) setup, recently installed at the target laboratory [549]. This technique allows to obtain information on the average target thickness by the energy loss measurement of the α particles crossing the target. Moreover, it allows to estimate the "local" uniformity, i.e., the uniformity of the target inside the alpha-beam spot, and the "global" uniformity, in different regions of the target foil. The target non-uniformity can be then deduced by comparing the full width at half maximum (FWHM) of the experimental spectrum with the FWHM of a simulated one, in which an ideally uniform target is considered [550]. In Fig. 43, a typical FESEM view and a corresponding APT spectrum are shown for a 320 μg/cm^2 thick ^{nat}Te target evaporated on a 450 μg/cm^2 HOPG substrate. In the FESEM image (Fig. 43(left)), some Te grains of nm size are visible. Such structures do not impact much on the uniformity, as demonstrated in Fig. 43(right), where the measured energy loss distribution (black) is compared with the simulated one (red). The simulated spectrum includes the previously measured HOPG non-uniformity, and thus, the difference in the simulated and experimental spectra is attributed to the Te non-uniformity, which is estimated to be about 10%.

Finally, the NUMEN target system must be as compact as possible, in order to guarantee both sufficient room for the gamma-ray calorimeter placed around the scattering chamber and a large solid-angle aperture toward the detectors and instruments inside the scattering chamber.

Another aspect under study within the NUMEN collaboration is the damage to the target, and therefore to the graphite foils backing, produced by the high-intensity beams. Such eventual damages could modify the HOPG properties, possibly compromising its main functionality, which is the dissipation of thermal energy during the experiments. Simulations using SRIM/TRIM (TRansport of Ions in Matter) [551] allowed to determine the effect of the density of defects in the crystal lattice of HOPG on the loss of heat sink capacity.

In addition, a characterization of graphite foils and evaporated composite targets is necessary before and after being subjected to the effects of ionizing radiation. In particular, the exposure to neutrons of about $9 \times 10^9/\mathrm{cm}^2$ fluence at 14 MeV energy has been explored at the Deuteron-Tritium (D-T) Neutron Generator of the Instituto de Estudos Avançados (IEAv) in São José dos

Fig. 43 FESEM image (left) and APT spectrum (right) measured for a 320 μg/cm^2 thick ^{nat}Te target evaporated on a 450 μg/cm^2 HOPG substrate

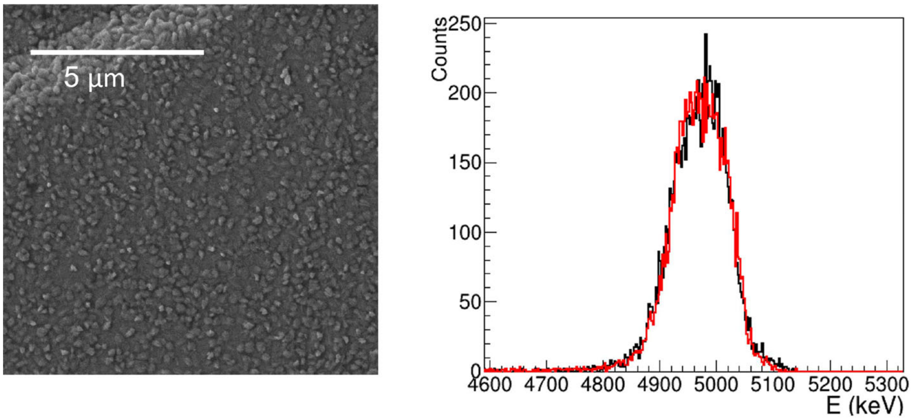

Fig. 44 The SPES target disks

Campos (Brazil). High-intensity heavy-ion beams delivered by the Pelletron facility at the University of Sao Paulo (Brazil), which would produce the same damage as that obtained in the NUMEN experiments, affecting both the crystallinity of the HOPG and the stacking orientation between graphene foils, will be also used. The samples are typically characterized by X-ray diffractometer transmission mode (XRD), confocal microscope Raman, atomic force microscopy (AFM) and scanning electron microscopy (SEM). Such analyses can indicate the effects of radiations, such as the weakening of the bond between graphene sheets, the disorder increase and the alterations in the lattice parameters.

7.2 Innovative targets for new production facilities

The development of innovative targets is a key aspect for any new production facility. Regardless of the specific species of interest to produce (radioactive ion beams, radioisotopes for medicine, neutrons, etc.) the availability of efficient, high power targets are fundamental to fulfill the needs of experimental users. An extensive research and development program is currently being carried out at INFN regarding this topic. In the following, an overview of these activities is given.

7.2.1 Production target for the SPES ISOL facility at LNL

The target represents the heart of the SPES ISOL facility in which the proton beam, coming from the cyclotron, is converted in a radioactive ion beam by means of nuclear reactions. Once produced, the isotopes are extracted by keeping the target at high temperature and then ionized and accelerated to form a radioactive ion beam. This beam is then sent to experimental users for nuclear physics studies or medical isotopes research (e.g., ISOLPHARM project) [552].

The SPES target is made of seven separate thin disks of ceramic material, inserted in a graphite box, as shown in Fig. 44. In order to efficiently release the produced isotopes, and at the same time to work in extreme conditions of high temperature and high vacuum, the SPES high power target has to possess two important set of properties: It has to be porous, with open interconnected porosity, and it must have high thermal properties to dissipate heat. This combination of properties is difficult to achieve, and only a limited set of materials, such as carbides, can be used for this application [553]. Uranium carbide in particular is the most used target in ISOL facilities, due to its capability of producing a large set of neutron-rich isotopes by means of fission.

The standard SPES target production techniques, based on the carbothermal reduction of oxides in high vacuum at high temperature, have been developed in the last fifteen years [554]. They are useful to produce porous materials with high reproducibility but, usually, the porosity is not optimized. Indeed, to be efficient in releasing isotopes, a target must have porosity at the nanoscale and therefore high specific surface areas.

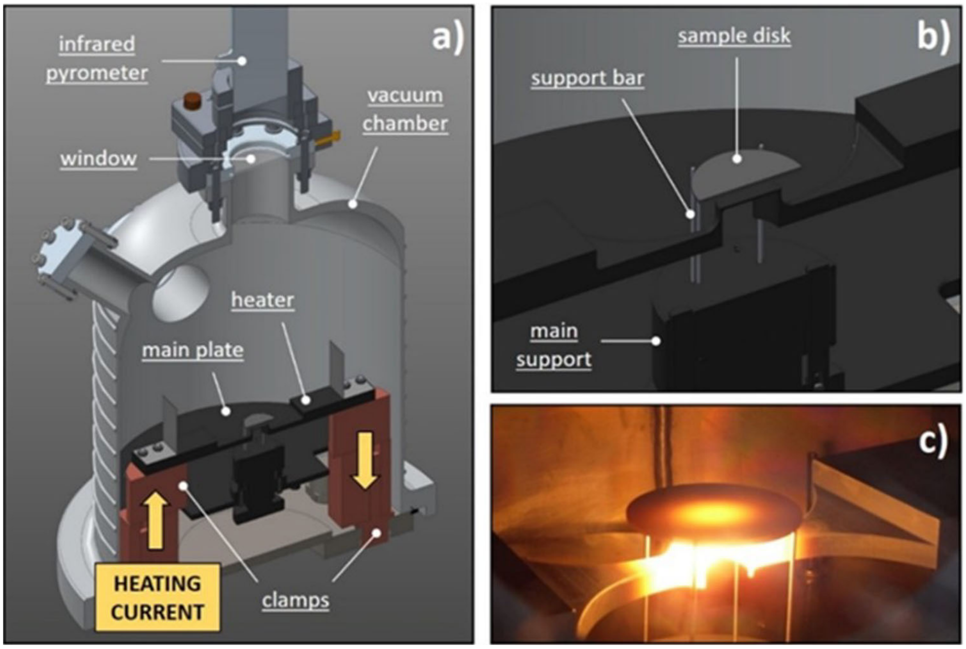

Fig. 45 The apparatus for thermal characterization at INFN-LNL

In order to improve the control of properties in the SPES targets, other innovative production techniques have been used in recent years, such as sol–gel [555] and the use of new, more efficient carbon sources for the carbothermal reduction [553]. The sol–gel method, based on the development of an interconnected metal–oxygen–carbon network which is converted to a carbide, can be used to obtain porous carbides with micro and mesoporosity ($d < 50\,\text{nm}$) and high specific surface area as recently demonstrated for titanium carbide [556]. The use of nanostructured carbon sources such as nanotubes or graphene is a useful way to improve thermal properties, as demonstrated for uranium carbide [557].

Several characterization techniques can be used to study porosity. Helium pycnometry is important to discern open from closed porosity because the latter is detrimental for isotopes release. Gas permeability was found to be a useful tool to verify the presence of permeable pores, very effective in releasing isotopes because they directly connect two sides of a target disk. Electron microscopy, either scanning or transmission, gives information on the micro and nanostructure of the material. Gas physisorption is extremely useful in characterizing nanopores amount and size distribution and to calculate specific surface area. An experimental setup built at LNL can be used to measure the thermal and structural properties of SPES target disks [558]. It is based on the creation of a strong thermal gradient on the surface of a disk and the measurement of temperature and emissivity in the center and the edge (Fig. 45). By combining experimental measurements with numerical simulations, it is possible to calculate thermal conductivity. Moreover, pushing the gradient to high values it is possible to induce mechanical failure in the samples and to measure critical stresses, which must not be exceeded during target operation. In this way, it is possible to estimate the survival probability of a target given a thermal load during operation.

Among the new developments for the SPES targets, additive manufacturing and the use of fibers stand out as the most promising. The use of carbon fibers has very recently demonstrated in a pilot study to be a promising way of improving thermal and mechanical properties of porous materials [559]. For example, porous silicon carbide/carbon fibers composites have proven to have higher thermal properties than porous SiC and at the same time do not undergo fragile failure typical of fully dense SiC under thermal stress. A research team at CNR-ISSMC developed a new process to realize short or continuous fiber-reinforced ceramic matrix composites by slurry impregnation followed sintering [559]. This method is not a conventional approach to realize ceramic matrix composites, which are typically realized by chemical vapor infiltration or polymer impregnation and pyrolysis. The method was designed to realize dense ultra-high temperature ceramic matrix composites for aerospace field but thanks to this collaboration, the method was also found effective to produce porous ceramic matrix composites. The homogeneity of material and the strong fiber/matrix interface obtainable by sintering are the hallmark of these materials. The process is sustainable and time saving if compared to above cited manufacturing technologies. Another item of interest is the use of additive manufacturing to tailor the porosity of the target material, in the framework of AM4INFN and HISOL experiments. The fabrication of titanium carbide targets is under investigation starting from the commercial powders and by using direct ink writing technique. However, this optimization of the geometrical porosity might be unable to overcome the shortcoming related to the textural properties of the material, resulting in a very low value of specific surface area, thus limiting the release of radioisotopes from the target. Hence, future works will be focused on combining additive manufacturing with the sol–gel chemistry, in order to provide a powerful tool to finely tune the textural properties of our material.

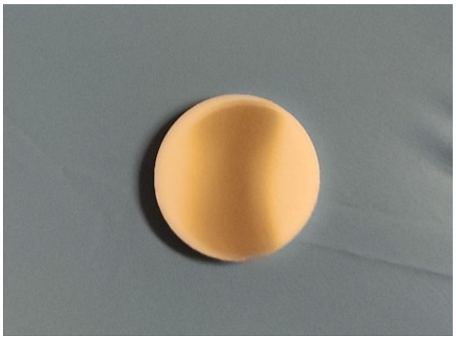

Fig. 46 Implantation substrate irradiated with stable Ag ions

7.2.2 Secondary targets for the ISOLPHARM project at LNL

At LNL, the radioactive ion beams (RIBs) produced in the future ISOL (Isotope Separation On Line) SPES (Selective Production of Exotic Species) facility will be exploited as an innovative and visionary production method for radiopharmaceuticals within the multidisciplinary ISOLPHARM project (ISOL technique for radioPHARMaceuticals) [552].

The ISOLPHARM project aims primarily to produce, purify and deliver extremely pure radionuclides for medical purposes. The production with the ISOL technique and the processing of the radioactive material toward the radiopharmaceutical preparation are closely connected by a crucial step: collecting the radionuclides on appropriate materials, i.e., secondary targets or implantation substrates. Radioactive beams have been successfully implanted on substrates in solid-state physics applications of ISOL beams [560], but this technology cannot be directly applied for medical purposes without further adjustments. Several metal-based substrates are currently employed in existing ISOL facilities: At CERN, several terbium radioisotopes were collected on gold foils coated with zinc [561–563]; aluminum-based targets were used at TRIUMF for the recovery of francium beams or actinium-225 [564, 565]. However, metal-based collection targets may intrinsically carry disadvantages, as they may release metallic contaminants [565], which may act as competitors of the radionuclide of interest during the labeling of the radiopharmaceutical. In order to mitigate this issue, several approaches can be tested, from salt-coating of the surfaces [566], to the investigation of alternative target materials. At LNL, self-sustaining targets are currently being produced with a broad panel of materials different from aluminum or zinc. Soluble and insoluble targets are currently under evaluation as potential alternative collection substrates for radioisotope harvesting in ISOL-type facilities. The first deposition experiments were performed with stable metal ion beams of copper and silver onto saline disks (Fig. 46), which provided full recovery of the metal by complete dissolution in an aqueous environment [567, 568]. While advantageous for metal recovery, these targets showed signs of brittleness and fragility during handling processes. This limitation could be detrimental when the targets are moved by an automatized target handling system, which requires targets resistant to impacts and friction. Thus, a systematic analysis of the mechanical properties was performed, and the salt-based disks were compared with targets made of organic materials, particularly pharmaceutical excipients for tablets.

The targets were produced with a 13 mm dye in a manual press by application of 10 t of pressure. Several materials were considered to achieve an efficient recovery, starting from sodium chloride (NaCl) and sodium nitrate ($NaNO_3$), toward water-soluble (dextrates) and insoluble cellulose-based powder mixtures (silicified microcrystalline cellulose or rapidly disaggregating microcrystalline cellulose) in different weights. All the developed materials underwent the same testing procedures to evaluate their vacuum compatibility, mechanical resistance and compatibility with the deposition of some elements of interest. Whereas all materials proved to be suitable for their use in a high-vacuum environment, mechanical strength testing highlighted the higher fragility of the salt-based disks.

The preliminary ionization and deposition tests were performed with stable ions, and the recovery of the metals was quantified by atomic absorption spectroscopy. In particular, stable silver ion beams were deposited, being the radioisotope ^{111}Ag one of the radionuclides under investigation in the context of ISOLPHARM. Both soluble and insoluble disks allowed good recovery of the deposited Ag. In fact, it was demonstrated that the deposition of silver, as well as different metals, occurs within less than 0.5 mm from the target surface. Thus, this study confirmed the possibility of using low-porosity materials for metal depositions without completely dissolving the implantation substrate to recover the deposited atoms [569].

An automated system for the deposition targets handling is currently under development and validation at LNL to insert and extract the substrates without the operators' radiation exposure. Such device, called IRIS (Isolpharm Radionuclide Implantation Station), will be able to handle simultaneously up to three deposition targets and will be equipped with a system of detectors for the performance of spectroscopic analysis to identify the possible presence of contaminants within the collected radionuclides, prior of delivering them to the radiochemistry laboratories.

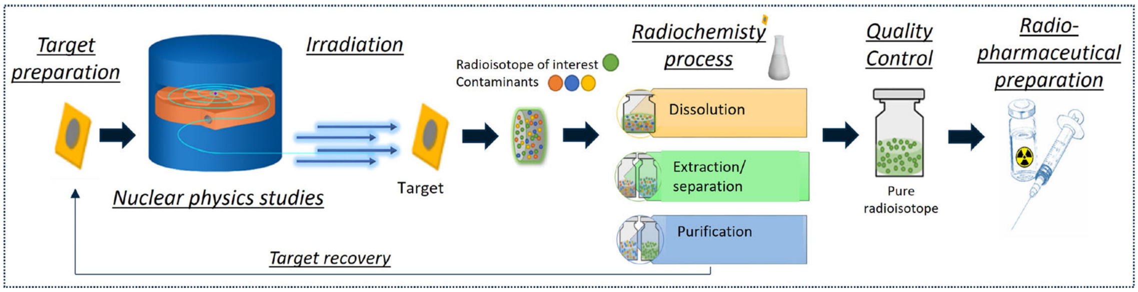

Fig. 47 Multidisciplinary research approach of the LARAMED project to produce radiopharmaceuticals

Fig. 48 Examples of cyclotron targets manufactured by High Energy Vibrational Powder Plating (left), spark plasma sintering (center) and magnetron sputtering (right)

7.2.3 LARAMED targets for direct production of medial radioisotopes at LNL

The goal of LARAMED (LAboratory of RAdionuclide for MEDicine) project is to establish a research infrastructure at LNL aimed at the development as well as production of innovative medical radioisotopes [570]. Besides the irradiation bunkers, located at the underground level of the SPES building [571], dedicated laboratories are under completion on the second floor. The multidisciplinary approach of the LARAMED project, shown in Fig. 47, allows to reach the final goal, the preparation of a radiopharmaceutical, starting from the irradiation of a specific target [572]. The target preparation is thus the first fundamental step because it influences the quality of the final product. Indeed, besides the radiochemistry and gamma-spectrometry laboratories, the target manufacturing laboratory is foreseen to conduct research on innovative technologies to expand the availability of suitable targets for emerging medical radionuclides. It is worth noting that radiopharmaceuticals labeled with some emerging radionuclides have shown great potentialities in nuclear medicine [573], albeit the technology needed for their routine supply has yet to be established. The main technological challenge is the target manufacturing to allow a consistent radionuclide supply for clinical trials.

The target main requirements for this application are essentially driven by the nuclear physics: The thickness is chosen to exploit the energy range based on the nuclear cross-section data [573]; the choice of the starting material, which is usually isotopically enriched and thus very expensive, supplied in powder form, is defined on the basis of the nuclear reaction route to produce the radionuclide of interest. Moreover, the thermomechanical properties should ensure an efficient heat transfer process during the irradiation stage as well as the integrity of the target until the dissolution process. The particular backing material should moreover take into account the activation under the beam and the subsequent radiochemistry approach adopted (i.e., acid or basic solution, sometimes at high temperature). Finally, the target should be easy to handle in the hot-cell with telemanipulators. To meet all such requirements, tailored manufacturing techniques and characterization are of crucial importance. In the framework of LARAMED project, innovative target manufacturing techniques have been developed to overcome the limits of the standard one. A brief description of the techniques and the state of the art is reported and shown in Fig. 48 [574].

The High Energy Vibrational Powder Plating is a valid solution for the realization of thin metallic targets starting from enriched isotopic material powder. The process is highly efficient ensuring negligible waste of the material during the deposition. ^{48,49,50}Ti targets have been prepared by using an apparatus developed at LNL within a CSN5 young researcher grant, named E-PLATE [575]. Targets have been used for the nuclear cross-section measurements for the production of ^{47}Sc, a promising theranostic radionuclide [576–578], within PASTA and REMIX projects (INFN-CSN5). Up to now, the irradiation runs are planned at GIP ARRONAX facility (France) [579]; however, within 2024 these kinds of targets are planned to be irradiated at LNL exploiting the SPES cyclotron.

The spark plasma sintering technique is a special technique that allows to sinter metals or oxide materials in a short time and to bond different materials to each other [580]. In the framework of INFN TT_Sinter project, a dedicated machine was jointly developed by INFN-Pavia and Pavia University with the aim to acquire the specific know-how in this field and potentially enlarge the use of this versatile technique to other applications at INFN. The evidence of the potentials of application of SPS technique for cyclotron targets has been shown with several target configurations realized and tested in medical cyclotrons. Some examples are: ^{100}Mo, ^{52}Cr, Y targets for the production of ^{99m}Tc, ^{52}Mn and ^{89}Zr [574, 581].

Magnetron sputtering technique is well known for many applications and its versatility allows to deposit thin or thick films onto any substrates. An INFN international patent WO/2019/053570 describes a method to obtain target for radiopharmaceutical

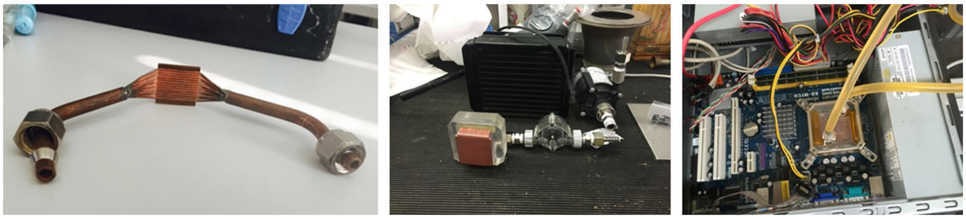

Fig. 49 Micro-channel tested prototype (left) and its application as a heat sink of a computer CPU (center and right)

production by using such a technique, coupled to the brazing of an inert ceramic material onto a metallic substrate. In addition, this target configuration was designed for a new dissolution reactor developed by INFN [582], object of an INFN R4I project called STarDiS (Solid Target Dissolution System), funded in 2023. Mo and Y sputtered targets have already been successfully tested under the proton beam of medical cyclotron [583, 584]. However, the main disadvantage of the magnetron sputtering technique is its efficiency in terms of deposition material usage. For this reason, a material saving approach and a method to increase the efficiency of this technique to avoid the losses of the material have been started to be implemented [585] and within a dedicated project, INTEFF_TOTEM (funded by MISE in 2021-2022), first targets have been manufactured with a new inverted magnetron configuration and they have been tested under a medical cyclotron beam.

In future, the production of other emerging medical radionuclides is foreseen, such as ^{67}Cu and ^{155}Tb through the proton irradiation of ^{70}ZnO and ^{155}Gd$_2$O$_3$ targets, studied in the framework of CUPRUM-TTD (INFN-CSN5, 2023-2025) and REMIX (INFN-CSN5, 2021-2023) projects, respectively.

With the aim to reuse the enriched material to produce recycled target, the development of a tailored recovery procedure is encouraged. This process should consider the target manufacturing process and the radiochemical process the target went through to achieve suitable physical and chemical characteristic of the material. This is also object of study within the LARAMED project, as already shown for the case of Mo recovery for direct ^{99m}Tc production [586].

Once identified the manufacturing technique and performed the target characterization, the development of high power targetry to increase the production yield of some radionuclide, will involve also the thermomechanical and fluid dynamic simulations and the design of new heat sink configurations [587].

Such R&D on target manufacturing technologies is the first step toward the future targets production for the LARAMED facility at LNL, foreseen in 2025. In addition, the targets may be easily adapted to the requirements of different solid target stations available on the national and international network of medical cyclotrons.

7.2.4 Targets for neutrons at LNL

Micro-channels for cooling In many technological fields, it is necessary to dissipate high specific powers. By using cooling micro-channels, heat generated can be transferred to the cooling fluid by forced convection with a high cooling mass-flow rate: This is achieved by means of a decrease in the thickness of the thermal boundary layer due to the microscopic dimension of the channels and to the consequent decrease in the convective resistance to heat transfer. Moreover, the specificity of microfluids dynamic (which is not the same of ordinary fluid applied to micro tubes) has been proved to be the best way to achieve high specific power removal since the 60's. The main limitation of this technique comes from the practical implementation of micro-channels. Because of the small cross section of the capillary, it is possible to operate such heat sinks with high pressures of the cooling fluid while maintaining the extremely reduced thicknesses of the tubes, in favor also of the conductive coefficient. This invention was conceived for cooling targets at accelerators irradiation facilities, such as for BNCT and radio pharmaceutical production. It is also suitable for other applications such as for CPU heat sinks. The producing method has been patented by INFN (patent n. PCT/IB2014/067156). Figure 49 (left) shows the prototype; the experimental results have shown that a maximum specific power dissipation of 3.5 kW/cm^2 will keep the maximum surface temperature below 150 °C for applications using lithium. (The safe working temperature to keep the lithium in a solid state is 150 °C.) Using different material layers (like beryllium, for instance), where much higher temperatures is allowed, the specific power increases almost linearly. The patented method allows the construction of large heat sink, in different shapes and materials (e.g., diamond). Figure 49 shows the application to a heat sink of a computer CPU.

Rotating and composite targets For the irradiation facilities, the rotating targets are a way of distributing the power delivered by a beam over a large effective area. This approach is used at LNL for two projects, LENOS, an experiment for astrophysics, and NEPIR, a neutron irradiation facility at SPES to study single event effects in microelectronics.

The LENOS target is a rotation graphite disk (Fig. 50 left) designed to shape an intense beam of 5 MeV protons from a 50 mA accelerator. The target has been designed to work as proton energy shaper for the LENOS project which, between the graphite disk and the micro-channel target, has to dissipate 250 kW from the beam [588].

The NEPIR [589] project uses the ANEM (Atmospheric Neutron Emulator) target to use 70 MeV proton beam from SPES to produce neutrons with an atmospheric-like distribution in the 1-70 MeV energy range. ANEM (Fig. 50 center) is a composite target: A W disk and a Be circular sector rotate on a common water-cooled hub and alternatively intercept the proton beam; an effective

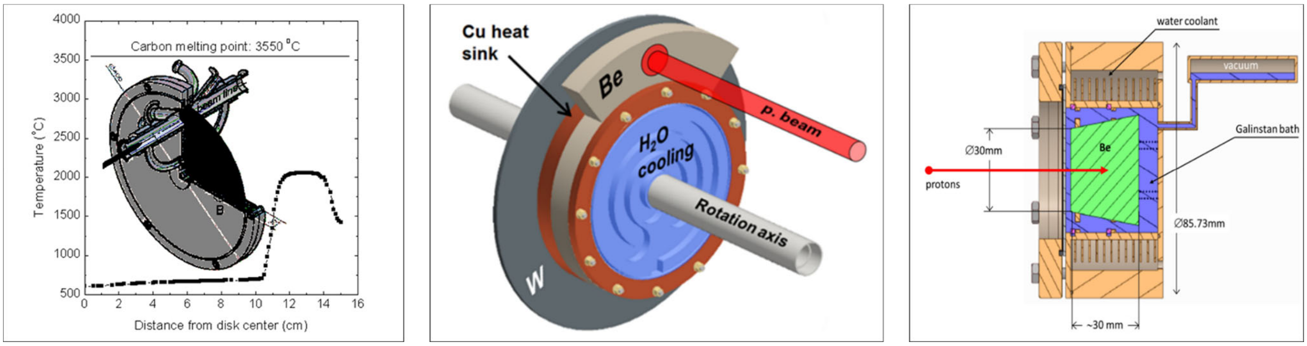

Fig. 50 Micro-channel tested prototype (left) and its application as a heat sink of a computer CPU (center and right)

atmospheric-like neutron spectrum is composed directly, without the use of moderators. The ANEM target is designed to handle a 30µA proton beam current (2 kW) [590].

The NEPIR facility will be built in phases. A phase-0 facility will be limited to 1 μA 70 MeV proton current (70 W). For this purpose, a novel liquid Galinstan cooled target, CoolGAL, has been developed (Fig. 50) [591]: A neutron-producing 30-mm-thick Be cylinder is immersed in a bath of Galinstan (metal liquid eutectic alloy of GaInSn), contained by an outer copper cladding. The liquid metal ensures always a good thermal contact with the external area of the cladding, where the water-cooling circuit is used. A thin Havar membrane (robust enough to withstand a pressure difference up to 1 atm) separates the liquid metal from the beamline vacuum. The containment cladding is made of Cu with a gold layer deposited inside to prevent corrosion and erosion effects from the liquid metal. The machined copper includes a closed-circuit water-cooling system and cooling fins. Preliminary ANSYS calculations indicate that this target can easily handle 700 W. Such a target can withstand much higher power and it has been especially designed for safety, crucial in the NEPIR application, since the target is mounted very close to the exit of the accelerator. Indeed, in case of rupture, no debris must reach the accelerator. In case of breaking of the Havar window (even if it is cooled by the liquid metal), radioactive wastes are trapped in the liquid metal that, since no pressure difference is present (only the hydrostatic one due to the liquid metal), does not explode.

7.2.5 Target for FRAISE facility at LNS

The Laboratori Nazionali del Sud of INFN are undergoing an upgrade of the research infrastructures (POTLNS project) in these years (see Fig. 51). Core of the program is the upgrade of the K800 superconductive cyclotron (CS) [592]: the implementation of a new extraction channel, based on the stripping technique, will allow producing light and medium mass beam ($A <\approx 40$) up to a power of $\approx$ 10 kW, to be compared to the 100 W maximum power available in the past. In order to exploit the high-power beams delivered by the upgraded CS, the POTLNS program has included the construction of a new facility to produce radioactive ion beams (RIBs), named FRAISE (Fragment In-flight Separator) [97, 593–598]. FRAISE will make use of the so-called in-flight technique [599], and it will be able to operate with primary beams of power up to 2-3 kW. The fragment separator will be constituted by a new production station, where exploiting fragmentation reaction of the primary beam into the production target, among the others, unstable isotopes will be produced. Then, a series of magnetic elements [97, 594] will select the specific unstable isotopes of interest, removing the primary beam and other produced ions. This facility will allow to greatly enlarge the beam opportunities for the LNS users. Light and medium mass RIBs, with typical intensities from 10^7 pps, for ions near to the stability valley, to 10^3 pps, for the ones far, and with energies in the range of 20-60 AMeV will be produced [593–598]. As in the FRIBS facility [600], operating at the INFN-LNS in the last decades, material used in the target will be preferably beryllium. In fact, the use of light elements, as Be, in the production target has the advantage of forward focusing the reaction products, allowing to get a high yield of secondary products within the limited acceptance. Thickness from 1500 to 250 μm, respectively, for lighter and heavier primary beams, will be employed. In some case, also the use of C target will be considered, given the low cost and the easier manageability. However, the target must face the problems related to high-energy deposition of the primary beam into it, with subsequent heating and degradation of the target material. In order to face these issues, the adopted solution will be a copy of the CLIM target system [601], already operating at the LISE fragment separator of the GANIL laboratories [602], in conditions very similar to the ones foreseen in FRAISE. The target system will operate under vacuum inside a dedicated chamber. In order to distribute the energy deposition into a wide area, the target is a rotating disk of 150 mm radius, with a typical rotation velocity of 2000 rpm. The system allows also to change the impact point of the beam on target from 130 to 147 mm, and to choose the angle of incidence of the beam on the target (from 90 to 50 deg), in order to change the effective thickness of the target. The power dissipated into the target will be $\approx$ 500 W, with a maximum sustainable primary beam power of $\approx$ 3 kW. After the test of a new beam control system considering the operation dead time of experiments, the possibility to increment this maximum power will be verified. The whole target disk, except for the small portion of the area where interaction with the primary beams take place, is hosted into a Cu water-cooled screen

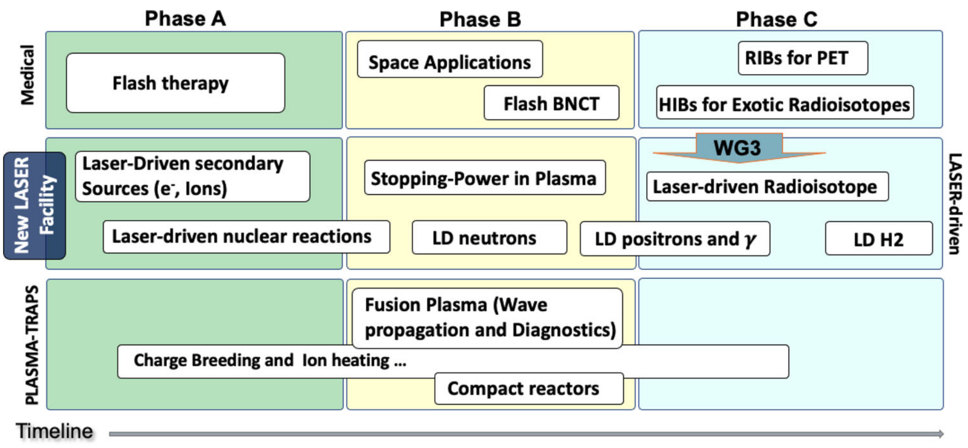

Fig. 51 Time-line organization of the future activities in the field of Nuclear Applications at LNS

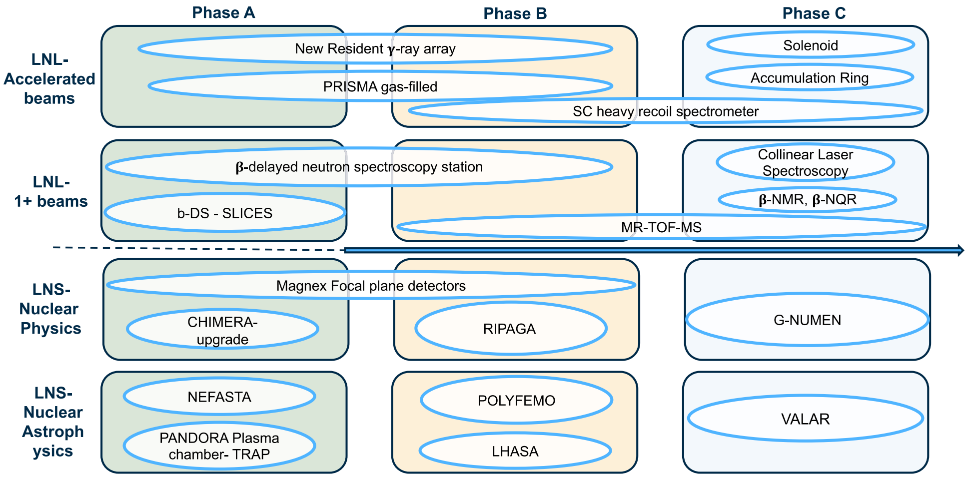

Fig. 52 Summary of the new experimental facilities for LNL and LNS

support, including also the motor for rotation. In general, temperatures up to ≈ 1000 °C will be reached around the impact points region, going down to ≈ 600 °C in the jaws holding the disk target and to ≈ 100 °C in the surrounding material. The system includes a pneumatic-based extraction system. Also, an automatic system for target change and storage, in a dedicate shielded cabinet, has been designed by the LNS staff and is under construction.

8 Future facilities at LNL and LNS

The LNL (Laboratori Nazionali di Legnaro) and LNS (Laboratori Nazionali del Sud) National Laboratories are both undergoing a renovation phase which will make intense stable and exotic beams available in the coming years. At LNL, the SPES (Selective Production of Exotic Species) facility will provide post-accelerated unstable beams produced by the ISOL technique, while LNS will host an upgraded facility able to deliver intense high-energy stable beams to experiments as well as to the in-flight fragmentation facility FRAISE to produce light-to-medium-mass radioactive nuclei. In addition, at LNS two new facilities will be constructed: PANDORA, a plasma-based facility conceived for multidisciplinary studies in nuclear physics and nuclear astrophysics, and the laser facility I-LUCE. The complementarity of these approaches will put the Italian community at the forefront of nuclear physics research in the worldwide scenario.

These developments have spurred a wide effort toward the conception, designing and building of new experimental facilities to thoroughly exploit the opportunities provided by the new beams. This working group has convened national and international experts on the experimental setups associated with high-intense stable and exotic beams, to outline a midterm plan for the two national laboratories. Figure 52 and Table 6 present a summary of the foreseen midterm developments, with a tentative timescale, where phases A, B and C indicate the near, medium and further future, respectively. Details on the new facilities are then reported in Sect. 8.1 for LNL, and in Sect. 8.2 for LNS.

Table 6 Detailed phasing of the new experimental facilities for LNL and LNS

Tag	Facility	Description	Phase
LNL-NF-GR	GALILEO-III	New resident γ-ray array	A, B
LNL-NF-PMS	PRISMA mass spectrometer	Gas-filled mode	A, B
LNL-NF-SCH	Zero-degree spectrometer	Superconducting heavy recoil spectrometer	B, C
LNL-NF-ACR	Accumulation ring	Superconducting heavy-ion ring	C
LNL-NF-SOL	Solenoid	Superconducting solenoid for light ejectiles	C
LNL-NF-b-DS	β-decay station	e^- and γ-ray β-delayed neutron spectroscopy	A
LNL-NF-bN	TOF neutron detector	β-delayed neutron spectroscopy	A, B
LNL-NF-MRT	MR-TOF-MS spectrometer	multi-reflection TOF mass spectrometer	B, C
LNL-NF-COL	Collinear laser system	Collinear laser spectroscopy	C
LNL-NF-NMR	β-NMR, β-NQR	Nuclear magnetic resonance for β decay	C
LNL-NF-RIM	Low-energy mass separator	Off-line separator for medical isotope production	C
LNS-NF-MG	MAGNEX focal plane detector	Gas tracker+PID system	A, B
LNS-NF-MG-GA	G-NUMEN	γ-ray array coupled to MAGNEX spectrometer	C
LNS-NF-CH	CHIMERA upgrade	SiPM to improve γ-ray detection + n-detector wall	A
LNS-NF-RP	RIPAGA	Array for charged particles and hard γ-rays	B
LNS-NA-NE	NEFASTA	Si-strip-telescope array	A
LNS-NA-PO	POLYFEMO	neutron calorimeter for β-delayed neutron emission studies	B
LNS-NA-LH	LHASA	High-resolution Si array for nuclear astrophysics studies	B
LNS-NA-PA	PANDORA	Plasma magnetic trap	A
LNS-NA-VA	VALAR	Array for laser-induced nuclear astrophysics research	C

8.1 New facilities at LNL

In this section, we describe some ideas on opportunities to widen the experimental reach at LNL, either improving or complementing existing setups or implementing new approaches. As it is reported in the previous issue dedicated to the Physics Opportunities [1], LNL has a longstanding and worldwide recognized expertise in nuclear structure and reaction studies based on γ-ray spectroscopy techniques combined to several reaction mechanisms, ranging from Coulomb excitation to deeply inelastic processes, passing through fusion-evaporation and multi-nucleon-transfer reactions. Quantities such as excited level energies and lifetimes, inclusive and exclusive cross sections and charged and neutral particle angular distributions are essential tools to a deeper understanding of the evolution of the nuclear structure toward more exotic systems, contributing also to the description of the astrophysical processes involved in stellar nucleosynthesis. The operation of the SPES ISOL facility in the coming years will enlarge the experimental reach and offer the opportunities—and necessity—of conceiving new approaches. SPES will provide exotic—mainly neutron-rich—beams which can be studied directly after extraction from the ISOL source, the so-called *non-accelerated*. We divide this contribution into two sections ideally served by non- and post-accelerated ISOL beams. The opportunities provided by improved separation tools are described in the beginning as common items.

8.1.1 Separation tools

SPES ISOL facility is based on reactions induced by a proton beam impinging on thick targets which can be made of several materials [603]. The extraction from the source is based on the hot-cavity concept through two main mechanisms: surface ionization (SIS) or plasma induced (PIS). In order to increase the selectivity, laser-ionization schemes have been developed (LIS). In addition to achieve isotopically pure beams, laser ionization also opens up the possibility to perform collinear laser spectroscopy using β-NMR or β-NQR techniques, as described in the next section.

The resolving power expected to be achieved using the HRMS (high-resolution mass spectrometer) is one of the highest (1/20000), and its best exploitation would see the parallel use of a Multi-Reflection Time-of-Flight Spectrometer, MR-TOF, mass separator, to be coupled to a radiofrequency quadrupole, RFQ, cooler/buncher.

At the most powerful and prominent ISOL facilities, RFQ-based coolers and bunchers [604, 605] have been the key devices to enable high-precision and high sensitivity experiments with pulsed beams (mass, laser and decay spectroscopy) [606]. They are the central technology for all ion-trapping experiments and applications. The ability to generate cooled and bunched beams without losing ions is, of course, the main advantage. It can be used in numerous applications: (i) to improve the signal-to-noise ratio by orders of magnitude for collinear laser spectroscopy [607], (ii) to adjust the kinetic energy of the ions with a pulsed drift tube afterward, (iii) for experiments searching beyond standard model physics in the beta decay [608] and fundamental research with radioactive molecules [609], (iv) producing highly charged ions [610], (v) half-life measurements [611] and (vi) mass spectrometry. Moreover, the RFQ cooler can also be used for additional mass separation [612], cleaning [613] and ion manipulation [614].

The same state-of-the-art ISOL facilities that installed 20 to 25 years ago RFQ cooler and buncher systems to boost their sensitivity upgraded their instrumentation ten years ago with multiple-reflection time-of-flight mass spectrometers (MR-TOF-MS) [615, 616]. These systems allow, with their unique combination of high mass resolving power, dynamic range, sensitivity and non-scanning measurements, unprecedented capabilities to identify and tune ISOL beams [617].

The inclusion of a MR-TOF-MS system along the 1^+ low-energy line of SPES, to be used in conjunction with the HRMS, will provide a sensitivity higher than the usual yield stations, making it possible to measure the yields of the most exotic species. The high sensitivity of a MR-TOF-MS system would allow mass measurements at the limits of nuclear stability, typically extending the experimental reach to nuclei with one or two neutrons more than those measurable with other methods, such as Penning traps [618]. It is worth noting the possible use as isobar [619] or even isomer separator[620], to provide clean beams to other experiments [621]. The separation and detection method is universal and independent of chemical or decay properties: Even stable molecular backgrounds in the beam can be identified and separated.

8.1.2 New facilities for post-accelerated beams: new tools

After charge breeding using the newly installed ADIGE system [622], the exotic beams produced by the SPES ISOL target will be accelerated in the LNL ALPI LINAC, to be then delivered to the three experimental halls and serve several experimental setups. Performing experiments using radioactive species poses a series of challenges, since they exploit low-intensity beams, which, in addition, are short-living and emit secondary particles after decay. The possible contamination coming from long-living species, produced in the decay process toward stability, is a source of background to be also taken into account.

Several new ideas for upgraded or newly designed equipment have already been included in the current issue and the previous one dedicated to the Physics Opportunities [1], while here we indicate new experimental facilities that have not been yet presented.

Upgraded GALILEO, resident γ-ray detection array In view of the foreseen departure of AGATA (Advanced GAmma Tracking Array) to GANIL around mid-2028, the GAMMA group has envisaged a plan for an upgrade of the resident GALILEO γ-ray array at LNL [430]. This array will be developed with the flexibility necessary to exploit both the high-intensity stable beams from the Tandem-PIAVE/ADIGE-ALPI accelerator complex and the radioactive ion beams from the SPES facility. The upgrade will be designed considering the following parameters: peak-to-total, detection efficiency, Doppler correction capabilities and modularity to adapt to the different ancillaries and setups at LNL.

Given the experience gained in recent years in developing and maintaining the AGATA array, the collaboration envisages to base the upgrade of GALILEO on segmented triple clusters of the same type of AGATA, which represents the state-of-the-art detector for γ-ray spectroscopy. A further advantage of this choice is that these proprietary detectors can be combined to the ones owned by the AGATA collaboration when they are not in use in the other laboratories (mainly GANIL and GSI), or in case other AGATA campaigns will take place at LNL in the future.

This new resident array is envisaged to be used in two different configurations. A first implementation is a compact configuration able to work together with the PRISMA spectrometer [141], while a second one envisages the detectors to work stand-alone coupled to the existing GALILEO triple clusters [430] in a new configuration and/or in conjunction with other ancillary arrays such as NEDA [261] and PARIS [623].

The coupling to PRISMA will allow one to perform γ-ray spectroscopy of exotic nuclei produced in multi-nucleon-transfer reactions with both stable and exotic beams. The key observables will be level energies, γ-ray angular distributions and polarization for spin-parity assignment, and the lifetime of excited states. Conversely, when the new detectors will be coupled, for example, to NEDA, an ancillary array for fast neutron detection, GALILEO will be used to investigate nuclear structure and isospin symmetry in neutron-deficient nuclei using fusion-evaporation reactions with stable and exotic beams. The γ-ray spectroscopy of the high-spin states populated by such reactions will also help to understand phenomena like collective rotation at high spins in moderately neutron-rich nuclei. The selectivity of the fusion-evaporation reaction channels will be crucially improved by ancillary silicon detector arrays to detect the light particles evaporated. In this configuration, GALILEO can also be coupled to large-volume scintillator arrays, such as PARIS, to study Giant and Pygmy resonances in stable and exotic systems.

Table 7 Schematic view of possible upgrades of the PRISMA spectrometer and new developments with associated selected physics cases, with an increasing degree of complexity (from top to bottom) going from upgrades which can be achieved in a short time range (2–3 years) to new projects tailored for a mid-long time range (3–5 years)

ITEM	PHYSICS CASES	TO BE DEVELOPED
Sub-barrier transfer using PRISMA with SPES beams for reactions near 0° and intensities $< 10^5$ p/s	Nucleon correlations, density dependent forces, neutron skins	Improvement of tracking, third x, y position of the Ionization chamber via drift time and segmented anode
A,Z determination for heavy neutron-rich nuclei with stable and SPES beam with Intensities $> 10^5$ p/s	Evaporation effects, direct determination of production cross sections for the heavy partner, nuclear spectroscopy	Direct detection of the heavy fragment: improvement of the tracking system of PRISMA
Fission fragments for neutron-rich nuclei produced via transfer-induced fission mechanism	Determination of fission barriers and gamma spectroscopy of neutron-rich nuclei	Silicon strip detector with high resolution for Z up to 20 for ions detected in kinematic coincidence with PRISMA
Separation and reuse of transfer and deep inelastic products, also at very forward angles	Transfer mechanism and nuclear spectroscopy of exotic nuclei produced with very low cross sections	Development of a 2-stage spectrometer: a separator (gas-filled magnet, solenoid or a radiofrequency device) followed by a PRISMA-like high-resolution spectrometer

The versatility of this upgraded GALILEO-III array will make it possible to also study direct nucleon-transfer reactions in inverse kinematics, measuring γ rays in coincidence with the light ejectiles. These particles will be detected by segmented silicon arrays, such as GRIT or TRACE, placed at the center of the array around the target point. These reactions will provide a direct access to observables related to the single-particle structure of neutron-rich nuclei, probing shell evolution far from stability.

This upgraded GALILEO-III array will benefit from the development in electronics and readout started by the AGATA collaboration, allowing the handling of high data flux and improved Doppler reconstruction capabilities.

Upgrades and new developments of a PRISMA-like spectrometer Reactions exploiting radioactive beams are often performed in inverse kinematic, and therefore, one has to face the issue of the rejection of the primary beam for heavy recoil forward detectors. Several solutions can be put in place to overcome these difficulties while keeping a large detection efficiency and resolution in both nuclear charge and Q-value.

The large solid-angle magnetic spectrometer PRISMA has been successfully employed over the last twenty years for studies of the mechanism of multi-nucleon-transfer reactions [141, 624] and nuclear spectroscopy of neutron-rich nuclei, in a stand-alone configuration or in conjunction with large γ-detection arrays.

In the next years, developments aim at improving the performances of the spectrometer and at configuring completely new devices, having in mind as reference the detection and manipulation of transfer reaction products at very forward angles. A schematic view of the possible upgrades of the PRISMA spectrometer, several of them that were already presented in Sect. 3.4.1, is outlined in Table 7, together with a description of selected physics cases associated with them.

At the most general level, one may think of a “first stage device” which should act a as pre-separator for a standard mass spectrometer. It should be able to work in stand-alone configuration but designed in such a way to collect and focus ions of the wanted specie for precise mass and atomic number identification, following injection into a high-resolution PRISMA-like spectrometer or stopping the products into some detector array for the study of their decays or for further manipulation.

A solenoid could serve as this first stage device, whose main advantage would be the very high geometrical acceptance since, placed along the beam optical axis at specific distances from the target, it could integrate the transfer yield, corresponding to the selected part of the angular distribution, over the whole 2π azimuthal range. One could also study the feasibility of placing a radiofrequency device acting as velocity filter for rejecting the primary beam in front of a spectrometer. The idea behind this is to tune the frequency and phase of the device in time, correlating with the bunches of a pulsed beam to properly separate the wanted reaction products on the basis of their different velocity with respect to the primary beam. Such an idea was developed for fusion-evaporation studies in Munich [625] and could be further investigated also for transfer reactions.

Another possible device may be a properly designed magnetic system acting as separator when used in a gas-filled mode operation, a method that is based on the behavior and focusing effects of ions in gas as function of nuclear charge which allows to achieve a certain degree of spatial separation at the focal plane. Concrete studies of magnetic spectrometers used in a gas-filled mode have been already carried out in direct kinematic heavy-ion reactions with a Split Pole Spectrograph [626] and with the magnetic spectrometer VAMOS [627]. The recently constructed separator AGFA [628] will be possibly employed for the separation of deep inelastic products and a similar concept may be considered for building such kind of devices, also as injector into a PRISMA-like spectrometer.

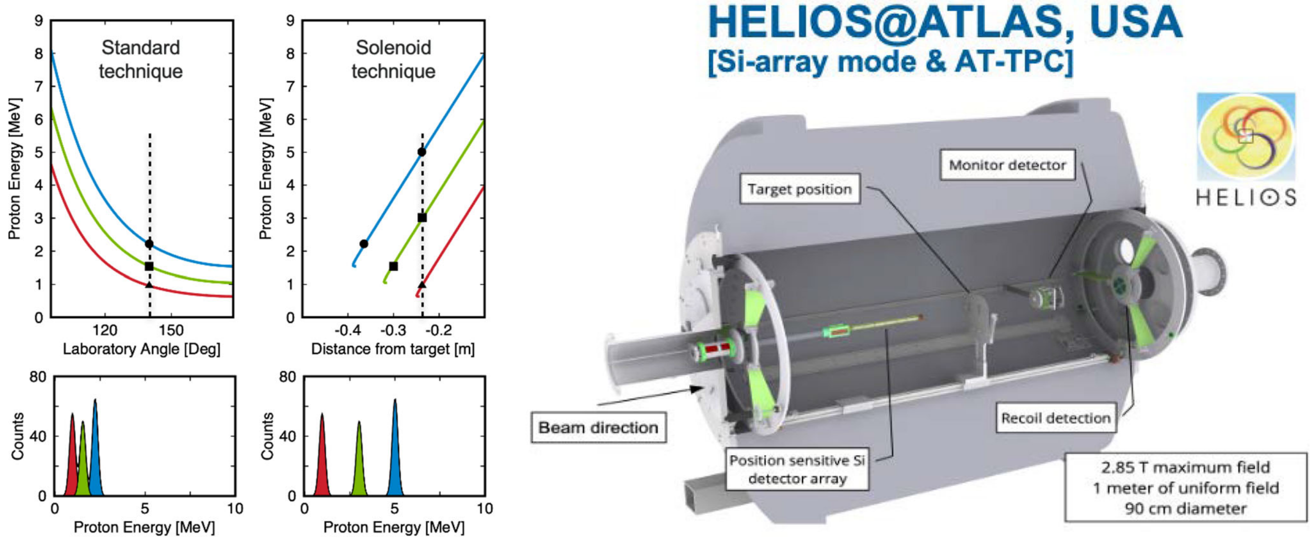

Fig. 53 (left) A comparison between a standard technique to measure light particles in direct reactions in standard kinematics whereby the outgoing protons from a typical (d,p) reaction are measured at a fixed angle for three different final states (red, green and blue), and the solenoid technique by which the protons are instead measured at a fixed distance from the reaction target after completing a single cyclotron orbit within the solenoid field. The dashed vertical lines correspond to fixed detector positions either in angle or position. (right) A schematic view of an experimental setup within the HELIOS spectrometer for a typical single-neutron adding (d,p) reaction

Solenoid The scientific achievements of solenoid spectrometers are proved by the ongoing research programs conducted with the HELIOS device at the ATLAS User Facility at Argonne Nat. Lab. [629] (Fig. 53), the Isolde Solenoid Spectrometer (ISS) device positioned at HIE-ISOLDE [630] and, most recently, both the active target mode with the AT-TPC [631] and the vacuum-mode results from the SOLARIS spectrometer located at FRIB. Many types of direct and indirect reactions over a range of energies have been studied by these devices, including single-nucleon pick-up [632–634], single-nucleon removal [635], multi-particle reactions [636], scattering reactions [637] and many others.

This midterm plan project proposes the implementation of a dedicated high-resolution multi-mode solenoidal spectrometer at LNL to leverage the high-quality beams ranging from $\sim$ 1 to $>$ 10 MeV/nucleon with intensities of 10^2-10^8 particles per second. Such a project will allow for the study of properties of specific exotic nuclei with the dual aim of investigating i) the nuclear structure in regions far from stability and ii) how the properties of short-lived exotic isotopes influence the formation of the chemical elements. Specifically, a solenoidal spectrometer will allow the measurement of transfer reactions in inverse kinematics, providing insight on the ordering and properties of single-particle states. Moreover, it will probe the inelastic scattering of the exotic post-accelerated beam, to determine the collective response of nuclei, shape changes and co-existence. A variety of light-ion induced reactions can also be studied, to determine reaction rates and nuclear structure effects relevant to astrophysics. The physics opportunities opened by these studies have been largely covered in the Ref. [1].

There are two principal operating modes for the proposed spectrometer: the first as a vacuum-mode helical-orbit spectrometer based on a Si array and the second as an active target. Both make use of a large-bore superconducting solenoid, of 2–4 T of field strength that is the core of the instrument. In the spectrometer mode, the emitted light charged particles follow helical orbits in vacuum, returning to the axis of the magnet, where their position, time of flight and energy are measured by a position-sensitive Si array. The resulting excitation energy spectra are free from certain classes of kinematic effects that affect other techniques, yielding excellent Q-value resolution as shown in Fig. 53. The time of flight also provides a natural way to identify the light particles through the cyclotron period. In the active target mode, instead, the beam enters a gas volume that acts both as target and detector, giving the benefit of a thick target in which ions are tracked, free from degradation of resolution by target energy loss effects, which can be measured and corrected. The thickness of the target allows beams as low as 100 particles per second to be employed—giving access to the most exotic systems. The key advantage of this device, in either modes, is the superior excitation energy resolution which can be achieved.

Another critical aspect for the development and success of solenoidal spectrometers has been the coupling to various ancillary devices, including fast-counting ionization and high-granularity detectors for recoil selectivity, the use of a $\sim 2\pi$ CsI/LaBr$_3$(Ce) scintillator array for γ-ray detection at the target position and within the uniform magnetic field, proportional counting detectors for fission fragments and electron–positron detection. Further progress to incorporate other systems, such as the use of HPGe detectors for γ-ray detection, is ongoing. In addition, various target flavors have been used successfully, such as solid foils (10 μg/cm^2 - $\sim$ 1 mg/cm^2), cryo-cooled circulating gas targets, tritiated titanium targets and planned developments with gas jet targets.

Coupled with the anticipated rates and beam energies provided by re-accelerated SPES beams, there are a number of regions throughout the nuclear chart which may be impacted by new and more precise reaction data. In particular, the evolution of the

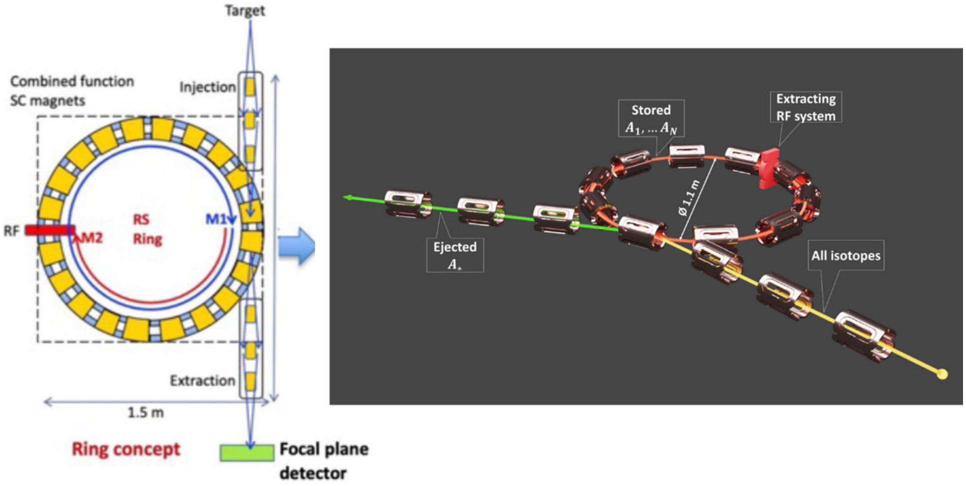

Fig. 54 Conceptual FFAG ring layout for a compact recoil separator

proton single-particle energies (SPEs) outside of $Z = 50$ will be able to be tracked beyond the last stable isotope of ^{124}Sn to ^{132}Sn via the proton-adding reaction (α,t). Similarly, the neutron SPEs outside of the $N = 82$ closed shell can be explored above ^{144}Sm by invoking the complementary (d,p) and (α,^{3}He) single-neutron adding reactions. Such reactions will allow for the exploration of SPEs through a shell-gap crossing. Furthermore, the use of two-neutron adding and removing reactions, (t,p) and (p,t), sensitive to coherent pairing correlations, and the use of inelastic scattering reactions, provide essential probes of evolving shapes in the $Z \approx 40$ region. Moreover, the inelastic scattering reaction measurements will provide new or complementary information on octupole and other forms of static deformations. Finally, there are numerous high-impact regions around the nuclear chart for which surrogate-type reactions can extract and map out (n, γ) reaction rates, for example, via the (d,p) surrogate reaction.

Superconducting recoil separator and storage ring In the study of reactions induced by radioactive beams, either transfer reactions, Coulomb excitation, deep inelastic or fusion reactions, a significant experimental challenge is the identification of the medium to large mass reaction fragments produced. This calls for a specifically designed high-resolution recoil separator, able to reject the primary beam and identify the reaction products.

A possible, innovative solution is represented by a versatile recoil separator for radioisotopes based on a compact superconducting (SC) Fixed-Field Alternating-Gradient (FFAG) ring. The design is based on a mini-ring of approximately 3.5 m circumference formed by superconducting magnets with both bending and focusing capabilities. The spectrometer will be able to operate with light and heavy radioisotopes and separate the reaction fragments from the main beam. It also presents the advantage of significantly reducing the size with respect to standard non-SC recoil separator configurations. A first design for such a spectrometer is given in Ref. [638, 639].

The recoil separator is designed to be used with radioactive beams, with intensities of the order of $\sim 10^5$ particles per second (pps) at target position. The reaction products of interest typically account for less than 1% of the primary unscattered beam. The main purpose is to separate the heavy fragments above mass $A \sim 100$ produced in nuclear reactions. Limitations on target thicknesses, less than 1 mg/cm^2, and difference in mass between reaction products and unscattered beam, $< 5\%$, define the properties of the separator. The beam must be pulsed. After impinging on a target, the main beam and its reaction products are injected into a compact FFAG ring, where they circulate for a typical time of the order of $\tau \sim$ 1-10 μs. The orbit of the reaction fragments is differentiated by their cyclotron frequency. One of the main advantages of this proposed recoil separator is its compactness and the easy mobility of the equipment.

A possible layout for such a ring recoil separator is presented in Fig. 54. Recent developments in superconducting magnet technology, namely the CCT solenoid FUSILLO [639], have opened the path for a multi-harmonic systems for which the possibility of a double function can be explored: on the one hand, the heavy recoil separator described above and on the other hand an accumulation ring for radioactive beams. This second operation mode would provide the LNL with a state-of-the-art compact accumulation ring to perform experiments with weak radioactive beams that are recirculated many times in the ring impinging on a thin target for reaction studies at each revolution, thereby increasing the overall luminosity by orders of magnitude. Possible implementations of such a combined new facility are foreseen in a 2030 timescale.

8.1.3 New facilities for low-energy beams: decay studies and ground-state properties

Right after their production in the target of SPES, the beams are extracted from the ISOL source at low energy (40 keV) and transported through a periodic line thanks to electrostatic elements serving two areas: the so-called A13 area, where devices devoted

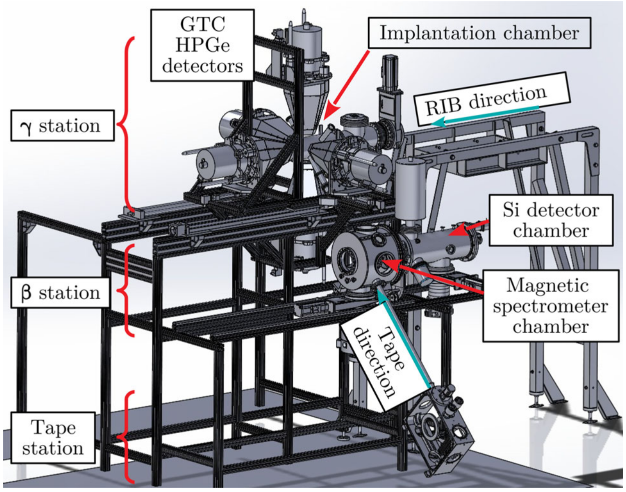

Fig. 55 The SPES β-decay station (b-DS) array at LNL

to decay studies and research for new radiopharmaceutical species are installed, and the post-acceleration area, starting from the charge breeding elements.

In this section, a description of the equipment foreseen for low-energy studies is described, together with possible future developments.

Facilities for β-decay studies The direct access to most exotic species provided by low-energy beams of SPES offers the opportunity of studying the properties of the decay of nuclei both in terms of gross properties, such as decay half-lives and decay branches, as well as providing an insight to nuclear structure evolution, by measuring transition energies and specific levels' lifetimes.

Given the low energy of the incoming beam, the optimal way to measuring the decay is to implant the species onto a passive medium, surrounded by an efficient particles' detector setup: This is the core of the SPES β-decay station (b-DS) depicted in Fig. 55, where one sees, on the bottom of the structure, the tape-delivering cassette, and two decay chambers, the upper one dedicated to decay studies and the second one, named "magnetic spectrometer chamber," hosting the setup devised for the measurement of conversion electrons and E0 transitions, SLICES. A description of the array is given in Ref. [1].

The decay scheme of exotic species becomes more complex owing to the opening up of new decay channels (β-delayed particle emission or fission) and to the rapid increase in the Q-value window, giving access to new states and new de-excitation schemes. In order to study these complex decays and to allow to probe a larger portion of the β-strength function, a standard high-energy array of HPGe detectors needs to be supplemented by large-volume scintillator detectors ($LaBr_3$ or $CeBr_3$). They increase the efficiency of the measurement of high-energy γ-rays up to, and possibly even above, the particle emission threshold. The setup would also crucially benefit from the addition of detectors for neutron spectroscopy, such as the last-generation CLYC scintillators [640–642].

SPES aims at producing neutron-rich nuclei using proton-induced fission of ^{238}U. As one goes further from stability on the neutron-rich side, Q_β-windows tend to get larger, whereas neutron separation thresholds get smaller. Therefore, the β-delayed neutron emission probability becomes significant. The current plan for decay spectroscopy at SPES does not include setups dedicated to neutron detection.

In order to have access to the full β-strength distribution, neutron spectroscopy has to be performed or at least the fraction of β-strength converted into neutron has to be measured. There are currently two main technologies to do so. On the one hand, neutron counting using a ^{3}He-based neutron counter takes advantage of the high cross section of thermal neutron capture of ^{3}He, in order to measure the β-delayed neutron emission probability; this technique requires to lose the energy information as the neutron has to be thermalized in a moderator in order to have a high efficiency, see, for example, TETRA at ALTO [643] or BRIKEN at RIKEN [270]. On the other hand, the energy information can be measured using time-of-flight spectrometer such as MONSTER developed by CIEMAT for FAIR [644] or VANDLE [645] or the innovative Neutron dEtector with Xn Tracking (NEXT) [646], but the efficiency of detection is quite low and the γ-sensitivity requires pulse shape analysis in order to discriminate between neutron and γ-ray events.

Complementing the picture, experiments employing the TAS (Total Absorption Spectrometer) scheme, therefore able to measure, through a calorimetric approach, the decay strength function, are expected to be installed at the low-energy facility of SPES.

Ultra-purified beam and decay spectroscopy In order to make SPES a unique facility in Europe, it is proposed to add a setup dedicated to improve beam purity (isobar purity or even better isomer purity) upstream of the decay setup. Several options can be considered, starting from double Penning trap, MR-TOF-MS and/or laser-based resonant ionization system. The choice of a MR-TOF-MS system, for example, would allow to achieve isomeric separation, being able, in parallel, to handle the high beam intensities of SPES. Only the IGISOL facility at the University of Jyväskylä is running a similar program [647], but the beam intensity achieved there is two orders of magnitude lower than the one foreseen for SPES.

The purity of the beam is essential for low-energy ISOL-type experiment. Indeed, a good knowledge of the initial state (spin-parity, excitation energy, etc.) is often the key in order to extract physical information from data that are relevant for nuclear structure.

Collinear laser spectroscopy Establishing a laser spectroscopy setup at SPES is an interesting opportunity that has been pursued in parallel to the development of the LIS system.

Collinear laser spectroscopic studies exploit a laser beam superimposed to the beam of atoms or ions, returning fundamental properties of exotic nuclei, such as nuclear ground-state spins, electromagnetic moments and charge radii. These quantities are obtained from high-resolution measurements of atomic spectral lines which exhibit hyperfine structure and isotope shift caused by the interaction of the shell electrons with the nucleus.

Thanks to a scanning of laser wavelengths specific atomic transition can be excited, followed by isotropic photon emission that is detected by detectors located perpendicular to the beam line.

Optical pumping and polarization of the laser light can allow β-NMR e β-NQR measurements providing access to dipole magnetic and quadrupole electric moments.

Given the large competition worldwide and the need of having a laser system on site, one may consider the different options for laser spectroscopy inside the SPES ion source. Exploiting new techniques such as the laser ion source trap (LIST), developed at the University of Mainz, in a specific geometry, high-resolution laser spectroscopy becomes feasible for some cases while maintaining the high sensitivity of in-source resonant ionization laser spectroscopy. If the laser systems from the Laser Ion Source can be used, this would require moderate changes to the setup and would allow first steps into this field of science.

High-resolution mass spectrometers Mass measurements and laser spectroscopy experiments give access to observables such as binding energies, mean-square charge radii and nuclear moments that allow us to track the nuclear structure evolution in exotic nuclei. When pushing far from stability, yields are dropping rapidly and beam purity often becomes a limiting factor, specifically at ISOL systems. This can be mitigated to some extent by laser ionization. However, a mass separator with a resolving power sufficient for isobar separation is often required. In addition to the magnetic separator foreseen at SPES, a multi-reflection time-of-flight mass spectrometer (MR-ToF-MS) could help performing mass measurements. Such a versatile device can serve as a diagnostic tool to determine the beam composition (broadband mode), as an isobar separator in combination with a nuclear spectroscopy setup (trap-assisted nuclear spectroscopy), and as high-precision mass spectrometer (mass measurements).

Perspectives Looking at the worldwide competition in laser spectroscopy and mass spectrometry at facilities like ISOLDE, Jyväskylä, TRIUMF, GSI/FAIR and FRIB, as well as upcoming facilities like S3 at GANIL, it will be challenging to establish a competitive program at SPES in the next five years. Thus, one should identify a niche where SPES could be more unique. In this respect, one should investigate specific applications for studies of fundamental symmetries/interactions, also with atom traps, and make a push toward heavier beams addressing, e.g., nuclei featuring octupole deformation. Also, the studies of isomers in conjunction with the MR-TOF-MS may be of interest.

The combination of high rate, high-resolution MR-TOF-MS separator and an advance decay spectroscopy setup will make the SPES facility unique in the world.

Off-line mass separator for pure medical radionuclides production Direct methods and ISOL techniques for medical radionuclides production are being developed at the INFN-LNL. The LARAMED [648, 649] and ISOLPHARM [521, 650] projects, part of the PRISMAP consortium [651], are facilities with a huge potential impact in medical radionuclides supply for the research community. In this framework, the need of a dedicated off-line mass separator at the INFN-LNL devoted to the separation of isotopes produced by direct activation has been highlighted by the community. The direct activation method, followed by an optimized chemical separation process to extract the desired radionuclide from the irradiated bulk material, can provide a final product with some isotopic contaminants that cannot be chemically removed. In terms of radiation dose, it is paramount to expose the patient to the minimal and most effective one. Therefore, a dedicated off-line mass separation system to purify the radionuclides of interest and to obtain high purity could prove crucial for medical applications. However, the use of this indirect technique must be taken into consideration only when the advantages clearly overcome the loss of efficiency due to this additional step in the overall production chain. A demonstrator facility equipped with an ion source capable of producing some mA ion current coupled to a well optimized magnetic separator can reach a production rate of milligrams per days of pure isotopes, satisfying a first complete test production chain. A case which can be tested with such facility is the production of medical Sc radionuclides starting from ^{nat}Ti target irradiated by the SPES proton cyclotron. The chemical separation can isolate the Sc atoms from other species but with the magnetic separator it is possible to have pure ^{43}Sc or ^{44g}Sc or ^{47}Sc for medical applications. Likewise, another interesting example is given by the proton irradiation of ^{nat}Gd target: It is possible to obtain several species, among them the Tb-isotopes that can be chemically extracted from the bulk target and then further selected with the magnetic mass separator to obtain pure ^{149}Tb, ^{152}Tb, ^{155}Tb or ^{161}Tb radionuclides.

8.2 New facilities at LNS

In this section, we describe the upgrades currently undergoing at LNS and the proposals of new experimental facilities that will allow one to broaden the opportunity of research in nuclear physics and nuclear astrophysics. In particular, concerning nuclear physics studies, important upgrades of the MAGNEX spectrometer and of the CHIMERA detector are foreseen and/or undergoing. Moreover, a new installation is proposed, RIPAGA, a facility for the detection of charged particles and gamma rays. The nuclear astrophysics studies will be based on two pillars: nuclear reactions using indirect methods and decays and nuclear reactions studies in plasma medium. Different facilities are proposed to carry out these investigations.

8.2.1 The upgrade of the MAGNEX magnetic spectrometer

MAGNEX is a large acceptance magnetic spectrometer made up of a large aperture vertically focusing quadrupole and a horizontally bending dipole magnets [128]. It allows for the identification of heavy ions with very good resolution in mass ($\Delta A/A \approx 1/300$), angle ($\Delta\Theta \approx 0.2°$) and energy ($\Delta E/E \approx 1/1000$), within a large solid angle ($\Omega \approx 50$ msr) and momentum range ($-14\% < \Delta p/p < +10\%$). High-resolution measurements for quasi-elastic processes, characterized by differential cross sections as low as tens of nb/sr, were already performed by this setup [652, 653]. A crucial feature was the implementation of a trajectory reconstruction technique, based on differential algebra, which allows one to solve the equation of motion of each detected particle to the 10^{th} order [654]. Together with the superconducting cyclotron installed at INFN-LNS, MAGNEX is the fundamental instrument to perform the experimental activity of the NUMEN project [127], aiming at the measurement of double charge-exchange (DCE) reaction cross sections relevant for $0\nu\beta\beta$ decay. These processes are characterized by very low cross sections (few nb), and high-resolution measurements are required to isolate the transitions of interest. Thus, beam intensities much higher than those manageable with the present-day facility, keeping the background of the order of 1 nb, are required, as those foreseen in the POTLNS project. Consequently, an upgraded MAGNEX setup, able to work with a two or three orders of magnitude higher current than the present, is necessary. A first upgrade will consist in the enhancement of the maximum accepted magnetic rigidity corresponding to a power supply upgrade to obtain $2.1-2.2$ Tm. Moreover, the MAGNEX experimental hall will be equipped with a beam dump to stop the high-power beams. Other significant upgrades regard the technologies of the detectors that are described in the following.

The G-NUMEN gamma array The objectives of NUMEN require separate measurement of the cross section of each exit channel state of the DCE reaction (in particular, the ground state and first excited state of each fragment). When higher beam energies are used (such as 20 AMeV or above) and/or when the reaction target-like fragment nucleus is strongly deformed, the MAGNEX energy resolution is insufficient for this purpose. For such cases, the measurement of the low lying gamma-ray transitions in temporal coincidence/anti-coincidence with the projectile-like fragments of the DCE reaction detected at the focal plane of MAGNEX is foreseen. The proposed design of the gamma array, denominated G-NUMEN [127], consists of more than 100 $LaBr_3$(Ce) crystal scintillator detectors distributed in 7 rings around the beam axis, directed toward the target at about 24 cm distance. The size of each crystal (38 mm diameter and 50 mm length) is a compromise of increasing the photopeak efficiency while keeping the count rate per detector limited, in order to avoid excessive pileup. The total photopeak efficiency of the array is about 4% at 1 MeV. A good timing resolution, well below 10 ns, is expected for this type of scintillator, therefore adequate for bunch discrimination at typical cyclotron beam frequencies. The beam intensity of such experiments, however, has to be limited due to the increasing random-coincidence gamma background of the high gamma multiplicity nuclear reactions competing with the DCE signal within the time width of each beam bunch (1-2 ns). Extensive GEANT4 simulations corroborate the design of the system, achieving, in principle, an observational limit of about 1 nb in typical conditions of month-long experiments with beam intensities of 10^{12} particles per second. A view of the G-NUMEN array surrounding the scattering chamber is shown in Fig. 56a.

The MAGNEX Focal Plane Detector: Gas tracker A new 3D gas tracker for the MAGNEX focal plane detector (FPD), designed to work with the upgraded facility, is under development [127, 545, 655, 656]. It will cover an active volume of $1200 \times 150 \times 107$ mm^3. The new FPD tracker must satisfy two main demands: It must provide a high resolution of the phase space parameters at the focal plane (X_{foc}, Y_{foc}, θ_{foc}, ϕ_{foc}), and it must be very fast since it should be able to bear a rate of the order of 40 kHz/cm expected after the accelerator upgrade. The structure of the new tracker consists of three main stages: i) a drift region that is the active volume of the detector, crossed by the ejectiles of interest; ii) an electron multiplication stage, based on Micro-Pattern Gas Detectors (MPGDs); and iii) a segmented readout electrode.

When an incident charged particle exiting the MAGNEX dipole crosses a thin Mylar window (separating the high-vacuum region from the gas-filled one), it leaves a track of ionized atoms and primary electrons in the low-pressure gas (typically Isobutane from 10 to 100 mbar) between the cathode and the electron multiplication element. The electrons drift with constant velocity under a uniform electric field that depends on the voltage and gas pressure. By measuring the drift time of electrons, the vertical positions and angles are determined. After reaching the multiplication stage, electrons are accelerated in the strong electric field in correspondence of the MPGD multiplication elements. The resulting electron jets are then directed toward the segmented readout electrode, where the horizontal positions and angles are measured. From this information, the 3D track of the ion can be fully reconstructed.

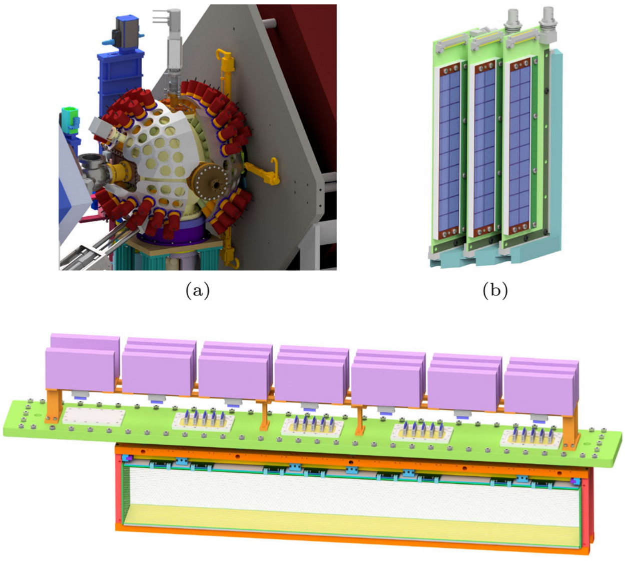
(a) (b)

(c)

Fig. 56 **a** The G-NUMEN gamma array detector. **b** A group of three towers of the PID wall.**c** The gas tracker

For the multiplication stage, Thick Gaseous Electron Multiplier (THGEM) has been chosen due to its intrinsic rate capability higher than 10^6 Hz/mm^2 (much higher than the expected rate for NUMEN), a very high spatial resolution (submillimeter accuracy) and timing in the 10 ns range [657]. A tracker prototype based on multiple THGEM (M-THGEM) has been developed and tested; details can be found in Ref. [658]. The readout electrode is segmented in 1240 pads $5 \times 10\,\mathrm{mm}^2$ large, arranged in 5 rows. A view of the full gas tracker is shown in Fig. 56c. 64-channel charge sensitive preamplifiers (CAENMOD. 1429) and CAEN VX2745 multichannel digitizers will be used for the readout [656].

The MAGNEX Focal Plane Detector: PID system The NUMEN experiments require the precise identification of the reaction ejectiles over a range of atomic ($4 < \mathrm{Z} < 12$) and mass numbers ($10 < \mathrm{A} < 25$). The new particle identification (PID) system should comply with the requirements for the new era of experiments at the MAGNEX facility with high-intensity beams and, in particular, should present high radiation tolerance (of the order of 10^{11} ions/(cm^2 yr)), good energy resolution (ΔE/E better than 2%), good time resolution (2-3 ns), high degree of segmentation to avoid double-hit events and good geometrical efficiency (similar to the one reported in Ref. [659]). Moreover, it should be able to work in the low-pressure gas environment of the tracker.

The different ions crossing the gas tracker will be discriminated based on their atomic number by means of the conventional ΔE-E technique. Subsequently, their $\sqrt{m}/q$ ratio, where m, q are the ion mass and charge, respectively, will be identified using a technique based on the correlation between the ions' kinetic energy and their measured horizontal position at the focal plane of the spectrometer [660]. The ΔE-E technique will be performed using the information provided by a wall of telescope detectors (PID wall) placed downstream to the tracker. Each telescope will cover an area of $1.5 \times 1.5\,\mathrm{cm}^2$ leaving a 0.04 cm dead interleave between them. It will be composed of a large-area thin silicon carbide (SiC) detector, served as ΔE, followed by a thallium-doped caesium iodide (CsI(Tl)) inorganic scintillator for measuring the ions' residual energy [127]. The SiC detectors [82] are square modules with an area of $1.54 \times 1.54\,\mathrm{cm}^2$ and a thickness of $100\,\mu$m. First prototypes have been recently produced and several characterization are ongoing (see Sect. 3.2.7). The CsI(Tl) scintillators have an active area of $1.5 \times 1.5\,\mathrm{cm}^2$ with a thickness of $5000\,\mu$m, and they are coupled to $1 \times 1\,\mathrm{cm}^2$ Hamamatsu photodiodes enabling the light collection. The telescopes will be arranged in towers (10 rows and 2 columns each). The full length of the focal plane detector will be covered by 36 PID towers placed downstream to the gas tracker, for a total of 720 ΔE-E telescopes. A partial view of a group of three towers is illustrated in Fig. 56b. The signal readout will be performed with the same preamplifiers and digitizers of the gas tracker.

8.2.2 The upgrade of the CHIMERA multi-detector

CHIMERA (Charged Heavy-Ion Mass and Energy Resolving Array) is a multi-detector operating at LNS with stable and unstable beams since 2000 in its complete 4π configuration [661]. Originally, it was built to study the complex phenomena in the intermediate energy regime ($E_{beam} =$ 10-100 MeV/A, known also as Fermi energy range), being able to detect and identify in charge, mass and energy of particles emitted in nuclear reactions, by using various particle identification techniques [7]. The device consists of 1192 telescopes, each one made of a two-pad silicon detector, followed by a caesium iodide thallium-activated scintillation detector, coupled to a photodiode. The telescopes are arranged in a cylindrical geometry around the beam axis direction, covering the polar angle between 1° and 176° and the total azimuthal angle. The whole array covers the 94% of the total solid angle.

In the first operational stage, CHIMERA used the identification methods ΔE-E, time of flight, pulse shape discrimination in CsI (Tl) for a complete detection of the charged particles emitted in nuclear collisions. Furthermore, the CsI(Tl) crystals can be used to detect and identify neutrons and gamma rays. In the second operational stage (starting in 2008), the Pulse Shape technique on the silicon detectors was implemented, allowing also the charge identification of the fragments stopped in them, and extending the possibility to use CHIMERA also for studying low energy reactions and phenomena [662, 663].

Recently (2015-2020), a new ancillary detector was realized, FARCOS (Femtoscope ARray for COrrelations and Spectroscopy) [664], devoted to high angular and energy resolution particle-particle correlation studies. It consists of 20 modules, each one made up of two stages of double-sided silicon strip detectors (DSSSD) with thickness of 300 and 1500 μm, respectively, and a third stage with a CsI(Tl) crystal+Si photodiode for a total of 132 detection channels, with a new custom dedicated front-end electronics and digitized acquisition. FARCOS allows also to perform correlation measurements between intermediate mass fragments (IMF) in heavy-ion collisions, and coupled with CHIMERA, to study exotic nuclear states. Taking advantage of a stop period of the accelerator machines at LNS (mainly due to relevant upgrade of the Cyclotron and installation of the new fragment separator FRAISE), CHIMERA is going to be upgraded and renewed to be ready for the experimental activity that will be performed with the new high-intensity stable and radioactive beams.

Development of CHIMERA specialized tagging system In view to use the exotic beams delivered by the in-flight methods at LNS, the development of a new tagging system, to be used in the CHIMERA line is needed [98, 593]. The idea is to use a system of SiC detectors that can be used with high-intensity beams for their capability in radiation resistance (see Sect. 3.2). The array will allow for ion identification by ΔE-ToF, with a time resolution of 100-200 ps. A dedicated electronic system will be developed in collaboration with Politecnico di Milano.

Development of an ancillary hodoscope for neutron, γ and charged particle detection The new detector will be based on stacks of plastic scintillators, featuring both good energy and angular resolution. It will be sensitive to neutrons and charged particles within the same detection cell in the kinetic energy of our interest (1-100 MeV for neutrons and up to 100 AMeV for charged particles). The detector is based on elementary cells having the dimension of $3 \times 3 \times 3\,\text{cm}^3$. The foreseen material is the plastic scintillator EJ-276 G (the green-shifted version). Each elementary cell will be independently read by a matrix of SiPMs and the signal acquired through digital electronics. Geometrical configuration will be implemented to achieve a good compromise among granularity, angular resolution and neutron detection efficiency.

8.2.3 RIPAGA (RIvelatore per PArticelle e GAmma): a new array for charged products and hard gamma rays

Various physics cases related to a deeper knowledge of nuclei far from stability are still open. Some of them are related to: i) role of cluster configurations and of collectivity in nuclear systems and correlations in nuclei at high excitation energies; ii) cross section for different reaction channels with radioactive beams (i.e., branching ratios); and iii) details of the excitation and decay modes of reaction products with increasing exoticity. Examples of recent studies on the first subject are in Refs. [665–668] and pertain mostly to low energies although not strictly [669–672]. We would like to extend these studies to medium-light systems using exotic FRAISE beams, focusing on some relevant channel clearly manifesting specific structure/shape properties, exploiting both charged products and electromagnetic probes. As for cross-section measurements, data at Fermi energies and beyond [673, 674] are still necessary even for stable beams and represent a step forward in the description of the various reaction processes, again revealing details on the possible cluster structure or on unusual shapes for exotic systems. Finally, the study of the excited fragments created with exotic beams of FRAISE is very appealing for the isospin transport and nuclear EoS investigation [69, 72, 73, 133].

We propose a composite detector, fully digital, to measure charged particles and hard gamma rays, being inspired by the INDRA-FAZIA (GANIL) and GARFIELD-RCo (LNL) setups for the detection of charged products and by the MEDEA detector (LNS) for hard gammas; the reuse of the high-performance BaF_2 crystals of the latter device might represent an additional advantage; moreover, the new installation can benefit of the long-term activity at LNS on collective modes toward the limit of multifragmentation [675]. A preliminary design is shown in Fig. 57a. Very forward angles can be covered with typical geometrical configurations of FAZIA telescopes. Also, zero-degree setup can be considered when using low-intensity FRAISE beams (below 10^4 pps). The FAZIA-like telescopes [132, 676] represent a good option for the detection of charged species as they achieve isotopic separation up to $Z = 25$ at Fermi energies, with low thresholds; they are therefore suitable for the detection of quasi-projectiles (QP) and fusion-like remnants. Light charged particles can be measured by the FAZIA telescopes and, at larger angles, with an array of conventional CsI scintillators, mounted to cover wide angular regions around the target. The granularity and the detailed features of this array will be a compromise between electronics density, total cost and needs imposed by the physics subjects. Finally, by coupling charged particle and gamma detectors, we would like to measure some features of the Giant Resonances, in particular through the use of BaF_2 crystals such as those of MEDEA.

Technical developments for this new array could be planned. For the very forward sensors, the use of SiC-based layers instead of conventional Si-diodes will be considered. For large inorganic scintillators, a technical development could be obtained by substituting the well-performing phototubes (rather large and difficult to operate under vacuum) with more compact readout avalanche Si sensors. (Test is needed to validate this option.) In the case of forward telescopes (not including zero degree), the cross-section absolute

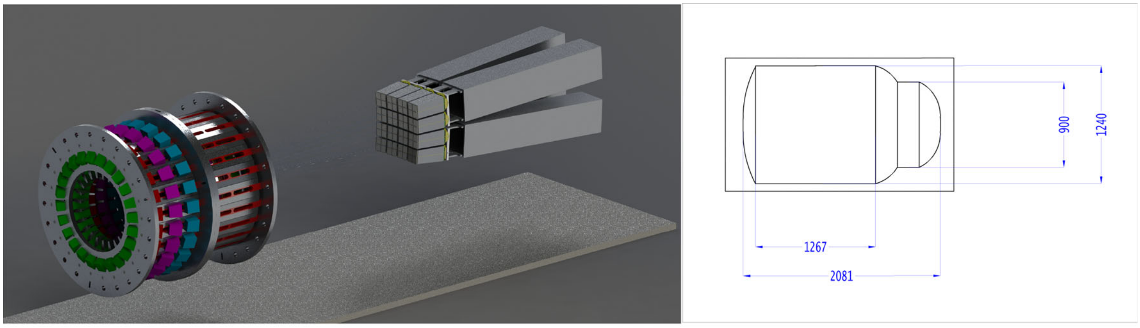

(a) (b)

Fig. 57 a): Render of the possible setup. The forward telescope wall based on current FAZIA blocks is complemented by multi-detectors at larger angles; the target position, not visible, is located in the middle of the cylindrical structure on the left side of the render. The forward hemisphere is covered with an array of scintillators for particles, while at angles beyond 90^o rings of BaF_2 crystals are foreseen (painted in magenta and cyan colors). b): Scheme of the present general purpose scattering chamber GIRA

measurement will be guaranteed by an azimuthally symmetric array of small detectors at very forward angles for the Rutherford scattering normalization. It is evident that whatever the setup architecture will be used, a large and well equipped scattering chamber will be mandatory for these experiments. The minimum length for such a chamber, assumed hosting a multi-detector of the type reported in the figure, should be about 250 cm in length and 100 cm wide. The already available GIRA chamber, whose scheme is illustrated in Fig. 57b, seems to be too small for this purpose. While it could be a good starting point, a larger chamber should be planned to host the proposed setup that should also feature a remotely controlled target system and an efficient beam diagnostics equipment.

8.2.4 Detector arrays for nuclear astrophysics

In the forthcoming years, a new range of astrophysical reactions will be investigated: (i) reactions induced by stable nuclei from the LNS tandem accelerator, including noble gases; (ii) long-lived radioactive ion beams (such as ^{10}Be [677], ^{26}Al or ^{60}Fe) produced in batch mode from the LNS tandem; and (iii) high-intensity radioactive ion beams from FRAISE. The peculiar needs of nuclear astrophysics studies have triggered an R&D activity to develop a devoted multipurpose detector array. Among these, we underscore: the need of low detection thresholds, since many key reactions such as the ^{22}Ne(α, n)^{25}Mg are endoenergetic; the possibility to stand high-intensity beams (to access micro/nano-barn-scale cross sections at sub-Coulomb energies); and a high signal-to-noise ratio.

The NEFASTA detector array The knowledge of cross sections around the so-called Gamow peak, induced by reactions with stable and radioactive nuclei, is of fundamental importance for nuclear astrophysics [278]. The typical low-energy range required leads to the need of extrapolation procedures, in order to access the Gamow region [678]. The Trojan Horse method (THM), developed in a close collaboration between INFN-LNS and University of Catania in the last decades, is an indirect technique that allows to perform such studies without the need of extrapolation procedures [679, 680]. Briefly, the THM allows one to measure a two-body reaction of astrophysical interest from a suitable three-body one. In order to perform these kind of experiments, it is mandatory to detect at least two out of the three emerging particles. The NEFASTA detector array (NEar FAr Silicon Telescope Array) is under development for its peculiar application to THM experiments. It is composed of 8 telescopes arranged into two groups. One group can be placed close to the target and will be made of two pairs of telescopes, set in the vertical and in the horizontal planes. Each telescope will be composed of one double-sided silicon strip detector 1000-μm thick (32x32 strips, 51.2×51.2 mm^2 active area) and one silicon pad detector 1500-μm thick, to stop high-energy light particles. A second group of 4 telescopes (each made up of a 16-strip single-sided silicon strip detector, 20-μm thick, plus a 16x16-strip double-sided silicon strip detector, 1000-μm thick) can be placed far from the target position in order to span small laboratory angles and measure forward-focused heavier ejectiles. A first measurement with a reduced version of NEFASTA was performed at LNS to study the ^{27}Al(p, α)^{24}Mg reaction at astrophysical energies via the ^{27}Al(d, α^{24}Mg)n three-body reaction, profitably testing the feasibility of THM experiments with this kind of detector array [681, 682].

LHASA-2: a new Large High-resolution Array of Silicon for Astrophysics Based on the expertise gained through the development of LHASA [683], NEFASTA [684] and ELISSA [685], we are presently developing a barrel shaped array, LHASA-2, with the aim of implementing the different requirements posed by nuclear astrophysics studies [680]. Low thresholds and efficient background suppression will be ensured by the use of pulse shape discrimination and kinematic identification of the reaction products at those energies where pulse shape analysis fails to discriminate among different emitted particles. Kinematic identification calls for high energy and angular resolutions to discriminate close kinematic loci (due to, for instance, the population of close excitation energies in the recoil nuclei). As in NEFASTA, this might be achieved using the newly developed W6 DSSSDs [686] for the cylindrical barrel section. Kinematic identification has proven very successful in ELISSA and LHASA, while high angular resolution will be a key aspect for the application to indirect methods, which needs high angular resolution to increase the energy resolution in the indirectly measured excitation functions. Endcap detectors will follow the QQQ3 design [686], i.e., double-sided multi-element active area of sectors and annular strips with central hole, and the use of SiC in the place of standard silicon detectors is foreseen at forward angles to stand the expected high count rate. As in ELISSA, the barrel shape and the compact design will make it possible to couple the array with ancillary detectors, such as neutron counter, for exclusive measurement of neutron-emitting reactions.

The POLYFEMO-2 neutron counter The GW170817 gravitational wave signal, linked to the merger of two neutron stars, marks a new era in nuclear astrophysics. Observations of GW170817 and the astronomical transient in galaxy NGC 4993, across various telescopes from radio to X-ray wavelengths, revealed a plausible site for the r-process, responsible for creating over half of the elements heavier than iron. These observations confirmed the production of neutron-rich material, akin to the debris resulting from a neutron-star merger [687]. During the r-process, a large number of n-rich nuclei are formed, up to the neutron drip line, later β-decaying back to the valley of stability. If the daughter-nucleus excitation energy is higher than the neutron emission threshold, neutrons are emitted, resulting in less neutron-rich nuclei. This enriches the expanding debris of neutrons after neutron freeze-out and leads to more neutron-rich nuclei through neutron capture reactions. This interplay is crucial for understanding the r-process [688]. The installation of FRAISE at LNS will make it available a broad range of radioactive ion beams, complementary to most facilities using U fission for the production of unstable nuclei. Therefore, it will be possible to explore a region of the nuclear chart seldom addressed and, therefore, showing large uncertainties in the β-delayed neutron emission probabilities. For this reason, the POLYFEMO (POLYcube detector array For Experimental Multimessenger astrOnomy) decay station has been designed and implemented at LNS [689], starting from the POLYCUBE neutron counter [690].

However, POLYFEMO shows many limitations, restricting the discovery potential of the decay station, such as the use of ^{3}He tubes as neutron detectors, which are both very expensive and with no position sensitivity; the impossibility to establish a correlation between neutron energy and the capture position in the detector, which may open the possibility of better background rejection (and sensibility increase) of future detectors.

For these reasons, POLYFEMO-2 is presently under design stage. The driving idea is to reach high efficiencies and sensitivities replacing ^{3}He tubes with ^{10}B lined RPCs (resistive plate chamber) detectors [691], having millimeter resolution for thermal neutrons and intrinsic detection efficiencies of the order of 50% for stacks of detectors. In these detectors, the cathode is lined with a 2-μm thick $^{10}B_4C$ neutron converter enriched in ^{10}B, making it possible to instrument large volumes with reduced costs. Simulations are presently being carried out to optimize the RPCs positions within a high-density polyethylene matrix.

8.2.5 Experiments with magnetically confined and laser-induced plasmas at LNS

In stars, the temperatures are so high that the atoms are nearly completely ionized, i.e., they form a plasma. An important breakthrough in nuclear astrophysics would be to perform studies, like nuclear decay or nuclear reaction measurements, with matter in a plasma state. To this aim, various experimental facilities are being developed at LNS which will allow this important breakthrough.

PANDORA: a new facility at LNS PANDORA (Plasma for Astrophysics, Nuclear Decay Observation and Radiation for Archaeometry) [692] is a plasma-based facility conceived for multidisciplinary studies especially in the nuclear physics and nuclear astrophysics framework. Laboratory plasmas can emulate, in terms of electron density n_e, temperature T_e and charge state distribution (CSD), certain conditions of astrophysical plasmas. Furthermore, they provide several applications in accelerators technology, material analysis and other fields. In a midterm perspective, PANDORA could add relevant research capabilities, opening new possibilities to study:

- for the first time, β-decay measurements in plasmas, with huge impact on nuclear physics and stellar nucleosynthesis [693];
- plasma opacity measurements in kilonovae ejecta-like conditions, studying heavy elements production in n-star merging.

It also represents an unprecedented setup for applications. In fact, it will be the biggest B-minimum magnetic trap with potentiality as ion source, as test bench for magnetic fusion studies and as a radiation source for Archaeometry.

PANDORA consists of the following three subsystems (details can be found in the Technical Design Report [694], and Fig. 58 summarizes them):

1. an innovative superconducting magnetic plasma trap [695], able to produce and confine plasmas with electron-ion density up to 10^{13} cm^{-3}, electron temperature of $T_e \sim 0.1$-30 keV and ion temperature of $T_i \sim 1$ eV;
2. an advanced plasma multi-diagnostic system [696], consisting in a set of noninvasive diagnostic tools operating simultaneously for monitoring the plasma thermodynamic properties and measuring the plasma parameters;
3. an array of 14 HPGe (high-purity germanium) detectors [697, 698] for γ-ray spectroscopy, surrounding the plasma trap.

PANDORA core is an innovative magnetic trap providing a magnetic field able to confine the plasma at densities and temperatures suitable to reach ionization states comparable with the astrophysical ones. The magnetic system is composed of 3 superconducting

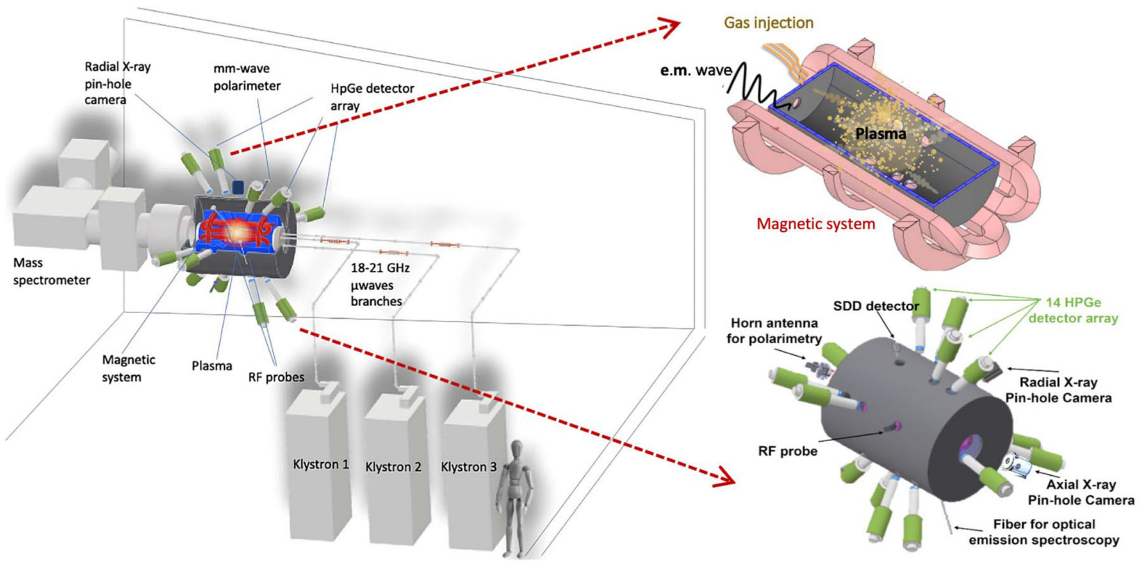

Fig. 58 3D render of the PANDORA facility under design and construction at INFN-LNS, including the superconducting magnetic system (red), the experimental setup for measuring the in-plasma activity (14 HPGe detector array) and on-line monitoring thermodynamic plasma parameters (i.e., two X-ray CCD cameras, optical spectrometer, interfero-polarimetry, two-pin RF probe, SDD)

coils (NbTi) and a hexapole (NbTi) for axial and radial confinement, respectively. It is the largest magnetic trap ever designed in a “B-min scheme,” supporting a plasma chamber of 70 cm length and 28 cm inner diameter. The maximum fields of 3 T along the chamber axis and 1.5 T along the chamber inner surface will allow stable plasma generation through an RF field at the frequencies of 18 and 21 GHz via Electron Cyclotron Resonance (ECR). The magnet cryostat houses the complete superconducting magnet system and provides magnetic shielding of the stray field produced by the superconducting magnet system. ECR plasmas emit radiation from microwave to hard X-rays which can be used to investigate plasma parameters (T_e, n_e, CSD) in different regimes. The developed advanced multi-diagnostic [696] and detection system consists of:

- a SDD (Silicon Drift Detector) for volumetric spectroscopy in soft X-ray domain;
- two CCD cameras with pinhole systems and multi-disks collimators for imaging and space-resolved spectroscopy in the soft X-ray domain. A CCD camera will be radially installed, the other one axially;
- an optical spectrometer for the plasma-emitted visible light characterization;
- multi-pins RF probes installed inside the plasma chamber and connected to a spectrum analyzer or to a scope for time-resolved RF and soft/hard X-ray spectroscopy, allowing timely characterization of turbulent plasma regimes;
- mm-wave polarimetric system for Faraday rotation detection for the line-integrated total electron density measurement;
- Thomson scattering system for the absolute electron density and the global electron drift velocity measurement;
- an analyzing magnet with a Faraday cup to measure the CSD and to analyze the extracted beam;
- a 14 HPGe detector array surrounding the plasma trap for γ-rays spectroscopy (to tag β-decays by detecting the γ-rays emitted by daughter nuclei) and for diagnostic purpose in the hard X-rays domain, with conical collimators to intercept the plasma core only.

All diagnostics tools will operate simultaneously. The most relevant characteristics—in terms of sensitive range and resolution—and the experimental measurements that can be done with the typical uncertainties are described in Refs. [692, 694, 696–698]. In the following, we will focus only on few selected tools, describing possible future developments and the plasma parameters that can be monitored.

The polarimetric measurement is based on the evaluation of the Faraday rotation angle of the polarization plane of a probing wave crossing the plasma, which is proportional to the square of the wavelength λ, to n_e (measured by fitting) and to the (known) magnetic field B. The developed microwave polarimetric system consists in two highly directive horn antennas connected to orthomode transducers (OMTs) and allows the total line-integrated density n_e measurement in a compact trap with an uncertainty of about 30% [699]. Further improvements are expected in the next future by a new approach under development, based on superheterodyne scheme to detect the Lissajous figure of the probing RF signals crossing the plasma [700], by using a mm-wave polarimetric system. Preliminary benchmark measurements have been recently performed in a compact plasma trap used as a down-sized test bench of PANDORA. Moreover, an approach that allows the reconstruction of the density profile is being developed by means of the microwave imaging profilometry through the solution of a one-dimensional inverse scattering problem [701] and the preliminary simulations are encouraging [702].

The innovative pinhole CCD camera technique [703], operating in single-photon-counted (SPhC) mode using a proper algorithm, was developed at INFN-LNS in collaboration with the ATOMKI laboratories [704]. It allows spectrally resolved imaging in the soft X-ray domain and, therefore, a deeper investigation of the parameters of the warm component of the electron energy spectrum. A typical post-processed SPhC soft X-ray image allows to distinguish the X-rays coming from plasma due to ionized K_α Argon lines and X-rays coming from plasma chamber wall materials, due to their characteristic fluorescence lines allowing for the investigation of the plasma spatial structure [705] and confinement dynamics (plasma vs. losses by X-ray emission, also distinguishing radial losses vs. axial ones) [706]. A model to link the experimental information to local plasma parameters is under development [707, 708].

In PANDORA, two CCD pinhole cameras will be used simultaneously to estimate the plasma volume and thermodynamic conditions by a multi-pinhole tomography approach [709].

Plasma stability can be monitored by means of a multi-pins RF probe connected to a spectrum analyzer, able to perform spectral analysis in the radiofrequency domain [710]. Since plasma kinetic instabilities are characterized by RF and X-ray bursts (respectively, with timescales of ns and ms), plasma radio-emission can be used as a signature of turbulences. A new parameter was semi-empirically defined to estimate, for the first time in a quantitative way, the plasma instability strength. In order to improve the resolution (both in time and in frequency), the RF probe can be also connected with a diode and a scope (80 Gs/s) for studying very fast phenomena (timescales below ns). In that way, it is possible to obtain high-resolution time-resolved (but totally integrated in frequency) power emitted from the plasma, using this value as trigger signal for hard/soft X-ray detectors in order to perform volumetric X-ray spectroscopy [710]. This tool allows spectrally and time-resolved characterization of turbulent plasma regimes, with a twofold outcome: i) provide a new “knob” for mastering plasma instabilities and maintaining the plasma stable for weeks; ii) deliver an experimental scenario to reproduce and study phenomena of astrophysics interest (kinetic turbulence occurring in astrophysical objects, i.e., Cyclotron Maser Instability [711]) in laboratory plasmas, measuring several properties even in the transient regimes.

In the next future, space and time-resolved spectroscopy will be performed simultaneously by triggering the pinhole system at the onset of plasma turbulences: This will allow to reach unprecedented capability of analysis of plasma dynamics, studying how the plasma shape and morphologies change during the time in a turbulence regime, also locally determining plasma parameters.

VALAR: a roaming device for nuclear astrophysics in-plasma measurements The study of nuclear reactions in laboratory has always been hindered by the very low cross-section values at energies of astrophysical interest ($1 \div 100$keV). This leads nuclear astrophysicists either to build underground laboratories where to perform long experiments with low and controlled background (LUNA [712], JUNA [713]), or to exploit indirect methods usually involving nuclear structure models such as the Trojan Horse method (THM) or asymptotic normalization coefficient (ANC) [680, 714]. Both approaches have proven to be successful to a great extent; nevertheless, plasma in stellar objects is a very different state from the solid, liquid or gas targets commonly used in standard nuclear physics experiments involving conventional accelerators. It is well known that the plasma state affects in a non-negligible way many nuclear processes, such as the electron screening (ES) in fusion reactions [715]. By measuring the cross sections of selected nuclear fusion reactions in a laboratory plasma, it is possible to infer the ES potential provided that the bare nucleus cross section (i.e., without the electron contribution to the Coulomb barrier) is known. In order to do so, a dedicated system able to induce such a laboratory plasma, detect the fusion products (charged particles, neutrons and γ-rays) and measure the plasma ion energy spectra (possibly with particle identification capabilities) is needed. Such a setup is being implemented at LNS by the AsFiN group in collaboration with various colleagues from INFN and international laboratories. VALAR (Versatile Array for Laser-induced Astrophysics Research) comprises:

- a cryogenic supersonic nozzle;
- an array of charged particle detectors;
- an array of neutron detectors;
- a compact ion spectrometer.

Our current knowledge on laser–matter interaction, nurtured by the recent developments in laser pulse amplification, provides a scenario where the interplay between the laser intensity (in the regime above 10^{16} W/cm^2) and the target composition (thickness and structure) holds a key role in determining the paradigm of the ion acceleration and its scale [716]. The interaction of a material prepared in a thermodynamic state close to the critical point (i.e., the temperature at which a gas mixture cannot liquefy regardless of its pressure) with lasers has many interesting features. First, it is more intense than an interaction with conventional materials such as a gas or a solid target and results in super-hot matter and higher laser absorption. For example, cluster targets irradiated by ultra-fast laser pulses show peculiar optical properties [717]. Ditmire et al. [718] demonstrated the formation of plasmas with multi-keV temperature alongside a strong electromagnetic pulse (EMP) and X-ray emission. The temperatures measured in these plasmas overlap with the ones which are typical of stellar cores where thermonuclear reactions occur, thus making this paradigm a perfect scenario for this kind of research. The interaction of ultra-short laser pulses with an expanding gas mixture at controlled temperature and pressure inside a vacuum chamber has long been investigated [275–277, 281, 719, 720]. The formation of molecular clusters maximizes the laser absorption, causing the full ionization of the molecules/atoms of the gas. The sudden onset of a positive space charge triggers the Coulomb dissociation of the clusters resulting in multi-keV ion acceleration with a nearly isotropic emission (Coulomb explosion, CE). The accelerated ions interact in the surrounding plasma and nuclear reactions take place.

By measuring the ion energy distribution and detecting the products of the nuclear reactions, one can infer important information on the cross section of the reaction process. Despite the non-thermal nature of this process, the plasma ion energy distribution is usually well described by a Maxwell–Boltzmann function (and thus by a temperature).

In order to maximize the laser absorption by the clusters and CE to occur, the mixture must be prepared close to the critical point for the liquid phase transition. This leads to an enhancement of the laser absorption efficiency which in turn translates into an increment in the number of accelerated ions and eventually in an increase in the fusion reaction rate [721], while controlling the temperature of the plasma by tuning the energy released by the laser and the average size of the clusters inside the nozzle (of the order of 10 nm).

To detect the fusion products and to measure the laser-accelerated ion distribution, the ToF technique is widely used. Due to the hard electromagnetic background (γ-flash and EMP [722]), fast detectors with high radiation hardness must be used; Faraday cups have been widely used to successfully measure the accelerated ion spectra for the low energy part; and silicon carbides (SiC) [723] and diamond detectors [491] have a recent positive history of use for detecting both the higher energy part of the spectra and the charged particles produced in fusion reactions.

Diamond detectors with a specific layout might represent a perfect choice for VALAR for measuring both the accelerated particle spectra and the $1-20$ MeV light ions coming from fusing nuclei, owing to a thin "dead layer" in the detection direction, the wide dynamic range of their response and their well-known excellent radiation hardness. Also concerning the detection of the neutrons coming from the fusion reactions, the ToF technique is the most efficiently used. The use of very fast detector is strongly suggested, as described in subsection 4.1.4 of this document.

In a nuclear reaction, gamma radiation, along with charged particles and neutrons, is expected to be produced both directly (radiative capture) and through the production of an isotope in an intermediate (excited) state whose decay leads to a monochromatic gamma (or more, depending on the accessible levels) in the exit channel. Measuring these reactions in a plasma is very important for astrophysical reasons and equally challenging for technical issues. In fact, even though one can count on the narrow energy spread of the gamma in the exit channel, the ToF technique is not applicable because of the nearly simultaneous generation of laser-induced hard x-rays and gammas.

So far, all the efforts in trying to use germanium detectors in this kind of environment did not pay off because of the aforementioned hard electromagnetic background. This is mainly due to the hard X/gamma peak and the strong EMP following the sudden ionization of the target (and the generation of a plasma). While the former can be disentangled from a massive particle by moving far away the detectors, provided one has sufficient solid-angle coverage, the latter is preventing the use of any standard electronics (such as spectroscopic amplifiers, complex integrated devices) sometimes even behind concrete walls.

A small calorimeter with stacked thin plastic scintillators read by robust and simple electronics is currently built and will be tested soon. However, the signal must be properly reconstructed from the different layers and the procedure may add significant uncertainties possibly resulting in poor energy resolution.

Another approach is to use a converter (aluminum, beryllium, etc.) to produce electrons which are then propagated through a gas and generate Čerenkov radiation which can be detected by optical sensors or micro-channel-plate, MCP, Gas Cherenkov Detectors (GCDs). The development of these detectors had been fueled by the high-energy physics demands for CERN, JLAB and inertial confinement fusion research at laser facilities such as NIF, and there is a window of opportunity of using the acquired know-how and apply it to the physics of VALAR: A feasibility study is in fact ongoing.

Contrary to the most studied mechanism of ion acceleration with lasers known as Target Normal Sheath Acceleration (TNSA [724]), where the impurities of the target may also play a significant role in the accelerating mechanism (e.g., protons from TNSA on Al targets), in laser-cluster experiments there is little to no on-target contaminants since only one single species (or compound with a known stoichiometric ratio) in introduced from a gas tank. This usually leads to clean ToF spectra of the accelerated ions.

In the simple case study of deuterium fusion, two deuterium ions fuse and produce (with the same branching ratio) either a ^{3}He ion and a neutron with nearly 2.45 MeV or a ^{3}H and a proton of around 3 MeV energies. In this case, when measuring the deuterium energy distribution with ToF detectors, it is also possible to detect 3 MeV protons coming at times between the X-ray photopeak and the keV-peaked deuterium accelerated ions, provided that the detector used has low gamma-sensitivity and ns-scale response (or better). The measured proton yield is thus directly related to the neutron one.

When studying other reactions of astrophysical interest involving heavier nuclei (such as ^{11}B, ^{12}C and above) the species of light charged particles in the exit channels may be different and their respective ToF signals in the detectors easily overlap one another and possibly with the high-energy tail of the accelerated species. In this case, a more complex deconvolution of the ToF signal is required, and an additional information on the spectra of the accelerated particles can be inferred by using a Thomson Parabola (TP) spectrometer. The TP is a simple spectrometer that uses transverse E and B fields to separate particles according to their e/m ratio and send them toward a position-sensitive detector, which can be active or passive.

Due to the different fields involved in such a complex scenario, it is clear that specific skills are required and a team from various institutions and laboratories has been formed to overcome all the technical difficulties that this challenging research project requires.

9 Conclusions

The wide plethora of particle detection techniques described in the previous chapters proved how dynamic and expanding is the field of radiation detection and identification. It is based on the comprehension of the underlying mechanisms governing the interaction between matter and radiation that can be exploited in many different ways to identify different particles and to reconstruct their energy and momentum. Developing the technology at the basis of nuclear physics experiments also implies a dedicated activity of R&D devoted to the targets, a crucial part of the experimental stations. Such a development can also serve as the starting point for applying the same tools for medical application, as the many examples discussed in Chapter 6 showed. The field is evolving, and many new strategies can be developed for identifying particles in wider and wider energy ranges: In this perspective, a combined research program as the ones foreseen at the Italian National Laboratories of INFN—simultaneously devoted to the understanding, through dedicated experiments, of the fundamental mechanisms underlying the formation and the structure of nuclear and hadronic matters, and to the necessary and complementary development of proper detection techniques—represents the perfect approach to take on the challenge.

Funding Open access funding provided by Alma Mater Studiorum - Università di Bologna within the CRUI-CARE Agreement.

Data availability No data associated with the paper.

References

1. M. Ballan et al., Nuclear physics midterm plan at Legnaro National Laboratories (LNL). Eur. Phys. J. Plus **138**(8), 709 (2023). https://doi.org/10.1140/epjp/s13360-023-04249-x
2. C. Agodi et al., Nuclear physics midterm plan at LNS. Eur. Phys. J. Plus **138**, 1038 (2023)
3. R. Buompane et al., Nuclear physics midterm plan at LNGS. Eur. Phys. J. Plus **139**, 224 (2024)
4. "Nuclear Physics Midterm Plan in Italy - Physics at INFN National Laboratories in Frascati", accepted in EPJ Plus.
5. G. Benzoni et al., Nuclear physics midterm plan in Italy: introduction to the series. Eur. Phys. J. Plus **138**, 1–3 (2023)
6. C. Broggini et al., Experimental nuclear astrophysics in Italy. Nuovo Cimento Rivista Serie **42**, 103 (2019). https://doi.org/10.1393/ncr/i2019-10157-1. arXiv:1902.05262 [nucl-ex]
7. A. Badalà, M. La Cognata, R. Nania, M. Osipenko, S. Piantelli, R. Turrisi et al., Trends in particle and nuclei identification techniques in nuclear physics experiments. La Rivista del Nuovo Cimento **45**(3), 189–276 (2022). https://doi.org/10.1007/s40766-021-00028-5
8. E. Costa et al., An efficient photoelectric x-ray polarimeter for the study of black holes and neutron stars. Nature **411**(6838), 662–665 (2001). https://doi.org/10.1038/35079508
9. E. Naselli et al., Innovative analytical method for X-ray imaging and space-resolved spectroscopy of ECR plasmas. Cond. Matter. (2022). https://doi.org/10.3390/condmat7010005
10. S. Palmerini et al., Presolar grain isotopic ratios as constraints to nuclear and stellar parameters of asymptotic giant branch star nucleosynthesis. APJ (2021). https://doi.org/10.3847/1538-4357/ac1786
11. S. Gammino et al., The Flexible Plasma Trap (FPT) for the production of overdense plasmas. J. Instrum. **12**, P07027 (2017). https://doi.org/10.1088/1748-0221/12/07/P07027
12. A. Buttacavoli et al., Incomplete charge collection at inter-pixel gap in low-and high-flux cadmium zinc telluride pixel detectors. Sensors **22**(4), 1441 (2022)
13. U. Roy et al., Impact of selenium addition to the cadmium-zinc-telluride matrix for producing high energy resolution x-and gamma-ray detectors. Sci. Rep. **11**(1), 10338 (2021)
14. N. Auricchio et al., A czt 3d imaging spectrometer prototype with digital readout for high energy astronomy. Nuclear Instrum. Methods Phys. Res. Sect. A Accel. Spectr. Detect. Assoc. Equip. **1047**, 167869 (2023)
15. L. Abbene et al., New opportunities for kaonic atoms measurements from CdZnTe detectors. Eur. Phys. J. Special Top. **232**, 1487 (2023)
16. M. Borri et al., Characterisation of Ge micro-strip sensors with a micro-focused X-ray beam. Nuclear Instrum. Methods Phys. Res. Sect. A Accel. Spectr Detect. Assoc. Equip. **988**, 164932 (2021). https://doi.org/10.1016/j.nima.2020.164932
17. M. Borri et al., Prototyping experience with Ge micro-strip sensors for EDXAS experiments. Nuclear Instrum. Methods Phys. Res. Sect. A Accel. Spectrom. Detect. Assoc. Equip. **1017**, 165800 (2021). https://doi.org/10.1016/j.nima.2021.165800
18. J.N. Ullom, D.A. Bennett, Review of superconducting transition-edge sensors for x-ray and gamma-ray spectroscopy. Supercond. Sci. Technol. **28**(8), 084003 (2015). https://doi.org/10.1088/0953-2048/28/8/084003
19. B. Alpert et al., HOLMES—the electron capture decay of ^{163}Ho to measure the electron neutrino mass with sub-eV sensitivity. Eur. Phys. J. C **75**(3), 112 (2015). https://doi.org/10.1140/epjc/s10052-015-3329-5. arXiv:1412.5060 [physics.ins-det]
20. B. Alpert et al., High-resolution high-speed microwave-multiplexed low temperature microcalorimeters for the HOLMES experiment. Eur. Phys. J. C **79**(4), 304 (2019). https://doi.org/10.1140/epjc/s10052-019-6814-4
21. A. Scordo et al., High resolution multielement XRF spectroscopy of extended and diffused sources with a graphite mosaic crystal based Von Hamos spectrometer. J. Anal. At. Spectrom. **35**, 155–168 (2020). https://doi.org/10.1039/C9JA00269C
22. J.J. Valiente-Dobón et al., Conceptual design of the AGATA 2π array at LNL. Nuclear Instrum. Methods Phys. Res. Sect. A Accel. Spectrom. Detect. Assoc. Equip. (2023). https://doi.org/10.1016/j.nima.2023.168040

23. P. Reiter, J. Eberth, H. Herbert, S. Thiel et al., Receiving Container for a Detector Which Operates in an Ultrahigh Vacuum or in a Protective Gas Atmosphere Consisting of High-purity Gas. US10107923B2, (November 2015)
24. M. Ginsz, G. Duchene, B. Pirard, F. Didierjean, M. Filliger, M.-H. Sigward, A new gamma-ray detector, 3-dimension, fast scanning table for pulse-shape analysis. In: 2015 4th International Conference on Advancements in Nuclear Instrumentation Measurement Methods and Their Applications (ANIMMA), pp. 1–4 (IEEE, 2015). https://doi.org/10.1109/ANIMMA.2015.7465546
25. S. Bertoldo, G. Maggioni, W. Raniero, C. Carraro, S. Riccetto, F. Sgarbossa, D. Scarpa, A. Andrighetto, A. Mazzolari, A. Gadea et al., New method for the production of thin and stable, segmented n+ contacts in HPGE detectors. Eur. Phys. J. A **57**(6), 177 (2021). https://doi.org/10.1140/epja/s10050-021-00487-8
26. C. Carraro, R. Milazzo, F. Sgarbossa, D. Fontana, G. Maggioni et al., N-type heavy doping with ultralow resistivity in GE by SB deposition and pulsed laser melting. Appl. Surface Sci. **509**, 145229 (2020)
27. G. Maggioni, S. Carturan, W. Raniero, S. Riccetto, F. Sgarbossa, V. Boldrini, R. Milazzo, D. Napoli, D. Scarpa, A. Andrighetto et al., Pulsed laser diffusion of thin hole-barrier contacts in high purity germanium for gamma radiation detectors. Eur. Phys. J. A **54**, 1–6 (2018). https://doi.org/10.1140/epja/i2018-12471-0
28. F. Sgarbossa, S.M. Carturan, D. De Salvador et al., Monolayer doping of germanium by phosphorus-containing molecules. Nanotechnology **29**(46), 465702 (2018). https://doi.org/10.1088/1361-6528/aade30
29. V. Boldrini, G. Maggioni, S. Carturan, W. Raniero, F. Sgarbossa, R. Milazzo, D.R. Napoli, E. Napolitani, R. Camattari, D. De Salvador, Characterization and modeling of thermally-induced doping contaminants in high-purity germanium. J. Phys. D Appl. Phys. **52**(3), 035104 (2018). https://doi.org/10.1088/1361-6463/aae9c0
30. L. Buonanno, D. Di Vita, M. Carminati, C. Fiorini, Gamma: a 16-channel spectroscopic asic for sipms readout with 84-db dynamic range. Trans. Nuclear Sci. **68**(10), 2559–2572 (2021). https://doi.org/10.1109/TNS.2021.3107333
31. D. Mascali, D. Santonocito, S. Amaducci, L. Andò, V. Antonuccio et al., A novel approach to β-decay: Pandora, a new experimental setup for future in-plasma measurements. Universe **8**(2), 80 (2022). https://doi.org/10.3390/universe8020080
32. A. Goasduff, D. Santonocito, R. Menegazzo, S. Capra, A. Pullia, W. Raniero et al., A high resolution γ-ray array for the Pandora plasma trap. Front. Phys. (2022). https://doi.org/10.3389/fphy.2022.936081
33. F. Alemanno, Q. An, P. Azzarello, F. Barbato, P. Bernardini, X. Bi, M. Cai, E. Catanzani, J. Chang, D. Chen et al., Measurement of the cosmic ray helium energy spectrum from 70 GeV to 80 TeV with the DAMPE space mission. Phys. Rev. Lett. **126**(20), 201102 (2021). https://doi.org/10.1103/PhysRevLett.126.201102
34. W. Atwood, R. Bagagli, L. Baldini, R. Bellazzini, G. Barbiellini, F. Belli, T. Borden, A. Brez, M. Brigida, G. Caliandro et al., Design and initial tests of the tracker-converter of the gamma-ray large area space telescope. Astropart. Phys. **28**(4–5), 422–434 (2007). https://doi.org/10.1016/j.astropartphys.2007.08.010
35. L. Bandiera, V. Haurylavets, V. Tikhomirov, Compact electromagnetic calorimeters based on oriented scintillator crystals. Nuclear Instrum. Methods Phys. Res. Sect. A Accel. Spectrom. Detect. Assoc. Equip. **936**, 124–126 (2019). https://doi.org/10.1016/j.nima.2018.07.085
36. B. Mauss et al., Commissioning of the ACtive TARget and time projection chamber (ACTAR TPC). Nucl. Instr. Methods A **940**, 498–504 (2019). https://doi.org/10.1016/j.nima.2019.06.067
37. E. Koshchiy et al., Texas active target (TexAT) detector for experiments with rare isotope beams. Nucl. Instr. and Methods A **957**, 163398 (2020). https://doi.org/10.1016/j.nima.2020.163398
38. S. Ota et al., CNS active target (CAT) for missing mass spectroscopy with intense beams. J Radioanal. Nucl. Chem. (2015). https://doi.org/10.1007/s10967-015-4130-5
39. J. Bradt et al., Commissioning of the active-target time projection chamber. Nucl. Instr. Methods A **875**, 65–79 (2017). https://doi.org/10.1016/j.nima.2017.09.013
40. O. Poleshchuk et al., The SpecMAT active target. Nucl. Instr. Methods A **1015**, 165765 (2021). https://doi.org/10.1016/j.nima.2021.165765
41. D. Bazin et al., Low energy nuclear physics with active targets and time projection chambers. Prog. Particle Nuclear Phys. **114**, 103790 (2020). https://doi.org/10.1016/j.ppnp.2020.103790
42. S. Beceiro-Novo et al., Active targets for the study of nuclei far from stability. Prog. Particle Nuclear Phys. **84**, 124–165 (2015). https://doi.org/10.1016/j.ppnp.2015.06.003
43. Y. Ayyad et al., Physics and technology of time projection chambers as active targets. Eur. Phys. J. A (2018). https://doi.org/10.1140/epja/i2018-12557-7
44. O. Sorlin, M.-G. Porquet, Nuclear magic numbers: new features far from stability. Prog. Particle Nuclear Phys. **61**(2), 602–673 (2008). https://doi.org/10.1016/j.ppnp.2008.05.001
45. T. Otsuka et al., Evolution of shell structure in exotic nuclei. Rev. Mod. Phys. **92**, 015002 (2020). https://doi.org/10.1103/RevModPhys.92.015002
46. C.E. Demonchy et al., Maya, a gaseous active target. Nucl. Instr. Methods A **573**(1), 145–148 (2007). https://doi.org/10.1016/j.nima.2006.11.025
47. I. Tanihata et al., Measurement of the two-halo neutron transfer reaction ^{1}H(^{11}Li, ^{9}Li)^{3}H at 3 AMeV. Phys. Rev. Lett. **100**, 192502 (2008). https://doi.org/10.1103/PhysRevLett.100.192502
48. R. Broglia et al., *Fifty Years of Nuclear BCS: Pairing in Finite Systems* (World Scientific, Singapore, 2013)
49. T. Furuno et al., Neutron quadrupole transition strength in ^{10}C deduced from the ^{10}C(α, α') measurement with the MAIKo active target. Phys. Rev. C **100**, 054322 (2019). https://doi.org/10.1103/PhysRevC.100.054322
50. M. Vandebrouck et al., Measurement of the isoscalar monopole response in the neutron-rich nucleus ^{68}Ni. Phys. Rev. Lett. **113**, 032504 (2014). https://doi.org/10.1103/PhysRevLett.113.032504
51. S. Ceruti et al., Study of giant resonances in exotic Ni isotopes at LISE (Proposal accepted by the GANIL 2018 PAC)
52. J. Giovinazzo et al., 4D-imaging of drip-line radioactivity by detecting proton emission from ^{54m}Ni pictured with ACTAR TPC. Nat. Commun. **12**, 4805 (2021)
53. J. Giovinazzo et al., First direct observation of two protons in the decay of ^{45}Fe with a time-projection chamber. Phys. Rev. Lett. **99**, 102501 (2007). https://doi.org/10.1103/PhysRevLett.99.102501
54. M.L. Avila et al., Experimental study of the astrophysically important ^{23}Na(α, p)^{26}Mg and ^{23}Na(α, n)^{26}Al reactions. Phys. Rev. C **94**, 065804 (2016). https://doi.org/10.1103/PhysRevC.94.065804
55. P.F.F. Carnelli et al., Measurements of fusion reactions of low-intensity radioactive carbon beams on ^{12}C and their implications for the understanding of X-ray bursts. Phys. Rev. Lett. **112**, 192701 (2014). https://doi.org/10.1103/PhysRevLett.112.192701
56. G. Charpak et al., Micromegas, a multipurpose gaseous detector. Nuclear Instr. Methods A **478**(1), 26–36 (2002). https://doi.org/10.1016/S0168-9002(01)01713-2
57. GARFIELD++ reference page: https://garfieldpp.web.cern.ch/garfieldpp/

58. M. Cortesi et al., Studies of THGEM-based detector at low-pressure Hydrogen/Deuterium, for AT-TPC applications. J. Instrum. **10**(09), 09020–09020 (2015). https://doi.org/10.1088/1748-0221/2015/09/p09020
59. M. Cortesi et al., Multi-layer thick gas electron multiplier (M-THGEM): a new MPGD structure for high-gain operation at low-pressure. Rev. Sci. Instrum. **88**(1), 013303 (2017). https://doi.org/10.1063/1.4974333
60. Y. Ayyad et al., CO_2 operation of an active target detector readout based on THGEM. J. Instrum. **12**(06), 06003–06003 (2017). https://doi.org/10.1088/1748-0221/12/06/p06003
61. R. de Olivera, M. Cortesi, First performance evaluation of a multi-layer thick gaseous electron multiplier with in-built electrode meshes-MM-THGEM. J. Instrum. **13**(06), 06019–06019 (2018). https://doi.org/10.1088/1748-0221/13/06/p06019
62. Y. Ayyad et al., Next-generation experiments with the active target time projection chamber (AT-TPC). Nuclear Instr. Methods A **954**, 161341 (2020). https://doi.org/10.1016/j.nima.2018.10.019. (**Symposium on Radiation Measurements and Applications XVII**)
63. J.S. Randhawa et al., Beam-induced space-charge effects in time projection chambers in low-energy nuclear physics experiments. Nuclear Instr. Methods A **948**, 162830 (2019). https://doi.org/10.1016/j.nima.2019.162830
64. J. Pancin et al., Electrostatic mask for active targets. J. Instrum. **7**(01), 01006–01006 (2012). https://doi.org/10.1088/1748-0221/7/01/p01006
65. C. Rodríguez-Tajes et al., A mask for high-intensity heavy-ion beams in the MAYA active target. Nuclear Instr. Methods A **768**, 179–185 (2014). https://doi.org/10.1016/j.nima.2014.08.046
66. S. Fracassetti, Study of the ISGMR in Kr Isotopes with CAT-M Active Target. PhD Thesis, KU Leuven (2024). https://lirias.kuleuven.be/4203953
67. S. Piantelli et al., Isospin diffusion in binary collisions of ^{32}S $+^{40,48}$Ca and ^{32}S $+^{48}$Ti at 17.7 mev/nucleon. Phys. Rev. C **96**, 034622 (2017). https://doi.org/10.1103/PhysRevC.96.034622
68. L. Morelli et al., Full disassembly of excited ^{24}Mg into six α particles. Phys. Rev. C **99**, 054610 (2019). https://doi.org/10.1103/PhysRevC.99.054610
69. S. Piantelli et al., Dynamical fission of the quasiprojectile and isospin equilibration for the system ^{80}Kr $+^{48}$Ca at 35 AMeV. Phys. Rev. C **101**, 034613 (2020). https://doi.org/10.1103/PhysRevC.101.034613
70. A. Camaiani et al., Influence of fast emissions and statistical de-excitation on the isospin transport ratio. Phys. Rev. C **102**, 044607 (2020). https://doi.org/10.1103/PhysRevC.102.044607
71. I. Lombardo et al., Study of the ^{33}Cl spectroscopic factors via the ^{32}S (^{3}He , d)^{33}Cl one-proton transfer reaction. J. Phys. G Nuclear Particle Phys. **48**(6), 065101 (2021). https://doi.org/10.1088/1361-6471/abdee4
72. A. Camaiani et al., Isospin diffusion measurement from the direct detection of a quasiprojectile remnant. Phys. Rev. C **103**, 014605 (2021). https://doi.org/10.1103/PhysRevC.103.014605
73. S. Piantelli et al., Isospin transport phenomena for the systems ^{80}Kr $+^{40,48}$Ca at 35 MeV/nucleon. Phys. Rev. C **103**, 014603 (2021). https://doi.org/10.1103/PhysRevC.103.014603
74. T. Roger et al., Demonstrator detection system for the active target and time projection chamber (ACTAR TPC) project. Nuclear Instrum. Methods Phys. Res. Sect. A Accel. Spectrom. Detect. Assoc. Equip. **895**, 126–134 (2018). https://doi.org/10.1016/j.nima.2018.04.003
75. L. Domenichetti, Advanced tracking techniques for active target time projection chamber detectors in nuclear physics experiments. Master's thesis, Università degli Studi di Padova (2022). https://thesis.unipd.it/bitstream/20.500.12608/35841/1/Domenichetti_Lorenzo_v2.pdf
76. F. Nava et al., Radiation tolerance of epitaxial silicon carbide detectors for electrons, protons and gamma-rays. Nuclear Instrum. Methods Phys. Res. Sect. A Accel. Spectrom. Detect. Assoc. Equip. **505**(3), 645–655 (2003). https://doi.org/10.1016/S0168-9002(02)01558-9
77. M. Bruzzi et al., Characterisation of epitaxial sic Schottky barriers as particle detectors. Diam. Relat. Mater. **12**(3), 1205–1208 (2003). https://doi.org/10.1016/S0925-9635(02)00350-3. (**13th European Conference on Diamond, Diamond-Like Materials, Carbon Nanotubes, Nitrides and Silicon Carbide**)
78. G. Izzo et al., Electrical properties of high energy ion irradiated 4h-sic Schottky diodes. J. Appl. Phys. **104**(9), 093711 (2008). https://doi.org/10.1063/1.3018456
79. G. Raciti et al., Detection properties and radiation damage effects in sic diodes irradiated with light ions. Nuclear Phys. A **834**(1), 784–787 (2010). https://doi.org/10.1016/j.nuclphysa.2010.01.146. (**The 10th International Conference on Nucleus-Nucleus Collisions (NN2009)**)
80. F. Cappuzzello et al., The NUMEN project: nuclear matrix elements for neutrinoless double beta decay. Eur. Phys. J. A **54**, 72 (2018). https://doi.org/10.1140/epja/i2018-12509-3
81. C. Ciampi et al., Nuclear fragment identification with ΔE-E telescopes exploiting silicon carbide detectors. Nuclear Instrum. Methods Phys. Res. Sect. A Accel. Spectrom. Detect. Assoc. Equip. **925**, 60–69 (2019). https://doi.org/10.1016/j.nima.2019.01.085
82. S. Tudisco et al., SiCILIA-silicon carbide detectors for intense luminosity investigations and applications. Sensors (2018). https://doi.org/10.3390/s18072289
83. R. Betti, O.A. Hurricane, Inertial-confinement fusion with lasers. Nat. Phys. (2016). https://doi.org/10.1038/nphys3736
84. S. Almaraz-Calderon et al., Study of the ^{26}Al$^{m}(d,\ p)^{27}$Al reaction and the influence of the ^{26}Al 0^{+} isomer on the destruction of ^{26}Al in the galaxy. Phys. Rev. Lett. **119**, 072701 (2017). https://doi.org/10.1103/PhysRevLett.119.072701
85. F. Cappuzzello et al., The role of nuclear reactions in the problem of $0\nu\beta\beta$ decay and the NUMEN project at INFN-LNS. J. Phys. Conf. Ser. **630**(1), 012018 (2015). https://doi.org/10.1088/1742-6596/630/1/012018
86. S. Gales et al., New frontiers in nuclear physics with high-power lasers and brilliant monochromatic gamma beams. Physica Scripta **91**(9), 093004 (2016). https://doi.org/10.1088/0031-8949/91/9/093004
87. F. Schillaci et al., Elimed, medical and multidisciplinary applications at ELI-beamlines. J. Phys. Conf. Ser. **508**(1), 012010 (2014). https://doi.org/10.1088/1742-6596/508/1/012010
88. S. Tudisco, Silicon carbide detectors: a concrete perspective for nuclear-astrophysics experiments. EPJ Web Conf. **227**, 01017 (2020). https://doi.org/10.1051/epjconf/202022701017
89. M.H. Kushoro et al., Silicon carbide characterization at the n_TOF spallation source with quasi-monoenergetic fast neutrons. Nuclear Instrum. Methods Phys. Res. Sect. A Accel. Spectrom. Detect. Assoc. Equip. **983**, 164578 (2020). https://doi.org/10.1016/j.nima.2020.164578
90. G. Petringa et al., First characterization of a new silicon carbide detector for dosimetric applications. J. Instrum. **15**(05), 05023 (2020). https://doi.org/10.1088/1748-0221/15/05/C05023
91. S. Tudisco et al., Silicon carbide for future intense luminosity nuclear physics investigations. Nuovo Cimento C (2019). https://doi.org/10.1393/ncc/i2019-19074-1
92. C. Altana et al., Radiation damage by heavy ions in silicon and silicon carbide detectors. Sensors **23**, 14 (2023). https://doi.org/10.3390/s23146522
93. M. Rebai et al., New thick silicon carbide detectors: response to 14 MeV neutrons and comparison with single-crystal diamonds. Nuclear Instrum. Methods Phys. Res. Sect. A Accel. Spectrom. Detect. Assoc. Equip. **946**, 162637 (2019). https://doi.org/10.1016/j.nima.2019.162637
94. S. Nida et al., Silicon carbide x-ray beam position monitors for synchrotron applications. J. Synchrotron Radiat. **26**(1), 28–35 (2019). https://doi.org/10.1107/S1600577518014248

95. Y. Blumenfeld et al., Facilities and methods for radioactive ion beam production. Physica Scripta **2013**(T152), 014023 (2013). https://doi.org/10.1088/0031-8949/2013/T152/014023
96. O.B. Tarasov, D. Bazin, LISE++: radioactive beam production with in-flight separators. Nuclear Instrum. Methods Phys. Res. Sect. B Beam Interact. Mater. Atoms **266**(19), 4657–4664 (2008). https://doi.org/10.1016/j.nimb.2008.05.110. (**Proceedings of the XVth International Conference on Electromagnetic Isotope Separators and Techniques Related to their Applications**)
97. A.D. Russo et al., Preliminary design of the new FRAgment In-flight SEparator (FRAISE). Nuclear Instrum. Methods Phys. Res. Sect. B Beam Interact. Mater. Atoms **463**, 418–420 (2020). https://doi.org/10.1016/j.nimb.2019.04.037
98. N.S. Martorana, Status of the fraise facility and diagnostics system. IL Nuovo Cimento (2022). https://doi.org/10.1393/ncc/i2021-21001-2
99. I. Lombardo et al., Use of large surface MicroChannel plates for the tagging of intermediate energy exotic beams. Nuclear Phys. B Proc. Suppl. **215**(1), 272–274 (2011). https://doi.org/10.1016/j.nuclphysbps.2011.04.028. (**Proceedings of the 12th Topical Seminar on Innovative Particle and Radiation Detectors (IPRD10)**)
100. S. Ottini-Hustache et al., CATS, a low pressure multiwire proportionnal chamber for secondary beam tracking at GANIL. Nuclear Instrum. Methods Phys. Res. Sect. A Accel. Spectrom. Detect. Assoc. Equip. **431**(3), 476–484 (1999). https://doi.org/10.1016/S0168-9002(99)00380-0
101. L. Lavergne-Gosselin et al., On the use of thin ion implanted Si detectors in heavy ion experiments. Nuclear Instrum. Methods Phys. Res. Sect. A Accel. Spectrom. Detect. Assoc. Equip. **276**(1), 210–215 (1989). https://doi.org/10.1016/0168-9002(89)90634-7
102. V.V. Avdeichikov, Ultra-thin strip silicon detectors. Nuclear Instrum. Methods Phys. Res. Sect. A Accel. Spectrom. Detect. Assoc. Equip. **313**(3), 561–562 (1992). https://doi.org/10.1016/0168-9002(92)90837-T
103. G. Cardella et al., A monolithic silicon detector telescope. Nuclear Instrum. Methods Phys. Res. Sect. A Accel. Spectrom. Detect. Assoc. Equip. **378**(1), 262–266 (1996). https://doi.org/10.1016/0168-9002(96)00164-7
104. S. Tudisco et al., A new large area monolithic silicon telescope. Nuclear Instrum. Methods Phys. Res. Sect. A Accel. Spectrom. Detect. Assoc. Equip. **426**(2), 436–445 (1999). https://doi.org/10.1016/S0168-9002(98)01235-2
105. C.A.J. Ammerlaan, R.F. Rumphorst, L.A.C. Koerts, Particle identification by pulse shape discrimination in the p-i-n type semiconductor detector. Nuclear Instrum. Methods **22**, 189–200 (1963). https://doi.org/10.1016/0029-554X(63)90248-9
106. J.B.A. England, G.M. Field, T.R. Ophel, Z-identification of charged particles by signal risetime in silicon surface barrier detectors. Nuclear Instr. Methods A **280**(2), 291–298 (1989). https://doi.org/10.1016/0168-9002(89)90920-0
107. G. Pausch et al., Particle identification in solid-state detectors by exploiting pulse shape information. Nuclear Instr. Methods A **322**(1), 43–52 (1992). https://doi.org/10.1016/0168-9002(92)90356-9
108. S. Barlini et al., New digital techniques applied to A and Z identification using pulse shape discrimination of silicon detector current signals. Nuclear Instrum. Methods Phys. Res. Sect. A Accel. Spectrom. Detect. Assoc. Equip. **600**(3), 644–650 (2009). https://doi.org/10.1016/j.nima.2008.12.200
109. G. Pasquali et al., Energy measurement and fragment identification using digital signals from partially depleted Si detectors. Eur. Phys. J. A **50**(5), 86 (2014). https://doi.org/10.1140/epja/i2014-14086-9
110. N. Le Neindre et al., Comparison of charged particle identification using pulse shape discrimination and ΔE-E methods between front and rear side injection in silicon detectors. Nuclear Instr. Methods A **701**, 145–152 (2013). https://doi.org/10.1016/j.nima.2012.11.005
111. S. Barlini et al., Effects of irradiation of energetic heavy ions on digital pulse shape analysis with silicon detectors. Nuclear Instrum. Methods Phys. Res. Sect. A Accel. Spectrom. Detect. Assoc. Equip. **707**, 89–98 (2013). https://doi.org/10.1016/j.nima.2012.12.104
112. n_TOF Collaboration web page: https://ntof-exp.web.cern.ch/
113. ISIS neutron source: https://www.isis.stfc.ac.uk/
114. F.H. Ruddy et al., Silicon carbide neutron detectors for harsh nuclear environments: a review of the state of the art. IEEE Trans. Nuclear Sci. **69**(4), 792–803 (2022). https://doi.org/10.1109/TNS.2022.3144125
115. F.H. Ruddy et al., Nuclear reactor power monitoring using silicon carbide semiconductor radiation detectors. Nuclear Technol. **140**(2), 198–208 (2002). https://doi.org/10.13182/NT02-A3333
116. L. Bertalot et al., Present status of ITER neutron diagnostics development. J. Fusion Energy **38**, 283–290 (2019). https://doi.org/10.1007/s10894-019-00220-w
117. D.S. McGregor et al., Design considerations for thin film coated semiconductor thermal neutron detectors-I: basics regarding alpha particle emitting neutron reactive films. Nuclear Instrum. Methods Phys. Res. Sect. A Accel. Spectrom. Detect. Assoc. Equip. **500**(1), 272–308 (2003). https://doi.org/10.1016/S0168-9002(02)02078-8. (**NIMA Vol 500**)
118. B.F. Phlips et al., Neutron detection using large area silicon detectors. Nuclear Instrum. Methods Phys. Res. Sect. A Accel. Spectrom. Detect. Assoc. Equip. **579**(1), 173–176 (2007). https://doi.org/10.1016/j.nima.2007.04.033. (**Proceedings of the 11th Symposium on Radiation Measurements and Applications**)
119. L. Cosentino et al., Silicon detectors for monitoring neutron beams in n-TOF beamlines. Rev. Sci. Instrum. **86**(7), 073509 (2015). https://doi.org/10.1063/1.4927073
120. L. Cosentino et al., Silif neutron counters to monitor nuclear materials in the Micado project. Sensors (2021). https://doi.org/10.3390/s21082630
121. Y. Jiang et al., A neutron beam monitor based on silicon carbide semiconductor coated with ^{6} LiF converter. Nuclear Instrum. Methods Phys. Res. Sect. A Accel. Spectrom. Detect. Assoc. Equip. **921**, 14–17 (2019). https://doi.org/10.1016/j.nima.2018.12.014
122. P. Kavrigin et al., Pulse-shape analysis for gamma background rejection in thermal neutron radiation using CVD diamond detectors. Nuclear Instrum. Methods Phys. Res. Sect. A Accel. Spectrom. Detect. Assoc. Equip. **795**, 88–91 (2015). https://doi.org/10.1016/j.nima.2015.05.040
123. C. Weiss et al., Selective data analysis for diamond detectors in neutron fields. EPJ Web Conf. **146**, 03004 (2017). https://doi.org/10.1051/epjconf/201714603004
124. M. Grodzicka- Kobylka et al., Comparison of detectors with pulse shape discrimination capability for simultaneous detection of gamma-rays, slow and fast neutrons. Nuclear Instrum. Methods Phys. Res. Sect. A Accel. Spectrom. Detect. Assoc. Equip. **1019**, 165858 (2021). https://doi.org/10.1016/j.nima.2021.165858
125. F. Negoita et al., Laser driven nuclear physics at ELINP. arXiv preprint arXiv:2201.01068 (2022)
126. M. Assié et al., Characterization of light particles (Z≤ 2) discrimination performances by pulse shape analysis techniques with high-granularity silicon detector. Eur. Phys. J. A **51**(1), 1–11 (2015)
127. F. Cappuzzello et al., The NUMEN technical design report. Int. J. Mod. Phys. A **36**(30), 2130018 (2021). https://doi.org/10.1142/S0217751X21300180
128. F. Cappuzzello, and others, The MAGNEX spectrometer: results and perspectives. Eur. Phys. J. **A52**(6), 167 (2016). https://doi.org/10.1140/epja/i2016-16167-1arXiv:1606.06731 [physics.ins-det]
129. D. Carbone et al., Characterization of newly developed large area sic sensors for the numen experiment. Nuclear Instrum. Methods Phys. Res. Sect. A Accel. Spectrom. Detect. Assoc. Equip. **1069**, 169960 (2024). https://doi.org/10.1016/j.nima.2024.169960
130. M.B.H. Breese et al., A review of ion beam induced charge microscopy. Nuclear Instrum. Methods Phys. Res. Sect. B Beam Interact. Mater. Atoms **264**(2), 345–360 (2007). https://doi.org/10.1016/j.nimb.2007.09.031

131. M. Jakšić et al., Ion microbeam studies of charge transport in semiconductor radiation detectors with three-dimensional structures: an example of LGAD. Front. Phys. (2022). https://doi.org/10.3389/fphy.2022.877577
132. The FAZIA. Collaboration, R. Bougault et al., The FAZIA project in Europe: R &D phase. Eur. Phys. J. A **50**(2), 47 (2014). https://doi.org/10.1140/epja/i2014-14047-4
133. C. Ciampi et al., First results from the indra-fazia apparatus on isospin diffusion in ^{58,64} Ni $+^{58,64}$ Ni systems at fermi energies. Phys. Rev. C **106**, 024603 (2022). https://doi.org/10.1103/PhysRevC.106.024603
134. C. Ciampi et al., Quasiprojectile breakup and isospin equilibration at fermi energies: potential indication of longer projectile-target contact times. Phys. Rev. C **108**, 054611 (2023). https://doi.org/10.1103/PhysRevC.108.054611
135. L. Bardelli, Developments of Sampling and Digital Signal Processing Techniques with Applications to Nuclear Physics Detectors. PhD Thesis, University of Florence (2005). https://pubblicazioni.dsi.infn.it/tesi/gettesi.php?filename=519-Bardelli-dottorato.pdf
136. M. Pârlog et al., Description of current pulses induced by heavy ions in silicon detectors. Nuclear Instrum. Methods Phys. Res. Sect. A Accel. Spectrom. Detect. Assoc. Equip. **613**(2), 290–294 (2010). https://doi.org/10.1016/j.nima.2009.12.010
137. Z. Sosin, Description of the plasma delay effect in silicon detectors. Nuclear Instrum. Methods. Phys. Res. Sect. A Accel. Spectrom. Detect. Assoc. Equip. **693**, 170–178 (2012). https://doi.org/10.1016/j.nima.2012.07.020
138. P. Kulig, Modeling of the signal induced by the charged particles in silicon detector. EPJ Web Conf. **66**, 03049 (2014). https://doi.org/10.1051/epjconf/20146603049
139. D. Tomasella, Simulation of Charged Particle Signals in Silicon Detectors with a Cluster Approach. Master Thesis, University of Padua (2021). https://hdl.handle.net/20.500.12608/38521
140. A. Stefanini et al., The heavy-ion magnetic spectrometer PRISMA. Nuclear Instrum. Methods A **701**, 217 (2002)
141. S. Szilner et al., Multinucleon transfer reactions in closed-shell nuclei. Phys. Rev. C **77**, 024604 (2007). https://doi.org/10.1103/PhysRevC.76.024604
142. M. Rejmund et al., Performance of the improved larger acceptance spectrometer: VAMOS++. Nuclear Instrum. Methods A **646**, 184 (2011). https://doi.org/10.1016/j.nima.2011.05.007
143. A. Cunsolo et al., Technique for 1st order design of a large-acceptance magnetic spectrometer. Nuclear Instrum. Methods Phys. Res. Sect. A Accel. Spectrom. Detect. Assoc. Equip. **481**(1–3), 48–56 (2002)
144. A. Cunsolo et al., Ion optics for large-acceptance magnetic spectrometers: application to the MAGNEX spectrometer. Nuclear Instrum. Methods Phys. Res. Sect. A Accel. Spectrom. Detect. Assoc. Equip. **484**(1–3), 56–83 (2002)
145. G. Montagnoli et al., The large-area micro-channel plate entrance detector of the heavy-ion magnetic spectrometer PRISMA. Nuclear Instrum. Methods Phys. Res. Sect. A Accel. Spectrom. Detect. Assoc. Equip. **547**(2–3), 455–463 (2005). https://doi.org/10.1016/j.nima.2005.03.158
146. C. Rodríguez-Tajes et al., Transfer reactions in inverse kinematics: an experimental approach for fission investigations. Phys. Rev. C **89**, 024614 (2014). https://doi.org/10.1103/PhysRevC.89.024614
147. E. Fioretto et al., A gas detection system for fragment identification in low-energy heavy-ion collisions. Nuclear Instrum. Methods Phys. Res. Sect. A Accel. Spectrom. Detect. Assoc. Equip. **899**, 73–79 (2018). https://doi.org/10.1016/j.nima.2018.05.011
148. F. Galtarossa et al., Mass correlation between light and heavy reaction products in multinucleon transfer ^{197}Au+^{130}Te collisions. Phys. Rev. C **97**(5), 054606 (2018). https://doi.org/10.1103/PhysRevC.97.054606
149. S. Akkoyun et al., AGATA: advanced gamma tracking array. Nuclear Instrum. Methods Phys. Res. Sect. A Accel. Spectrom. Detect. Assoc. Equip. **668**, 26–58 (2012). https://doi.org/10.1016/j.nima.2011.11.081
150. S. Beghini et al., The focal plane detector of the magnetic spectrometer PRISMA. Nuclear Instrum. Methods Phys. Res. Sect. A Accel. Spectrom. Detect. Assoc. Equip. **551**(2–3), 364–374 (2005). https://doi.org/10.1016/j.nima.2005.06.058
151. R.M. Pérez-Vidal et al., Nuclear structure advancements with multi-nucleon transfer reactions. Eur. Phys. J. A **59**(5), 114 (2023). https://doi.org/10.1140/epja/s10050-023-01027-2
152. E.M. Kozulin et al., The CORSET time-of-flight spectrometer for measuring binary products of nuclear reactions. Instrum. Exp. Technol. **51**, 44–58 (2008). https://doi.org/10.1134/S0020441208010041
153. E.M. Kozulin et al., Mass distributions of the system ^{136}Xe+^{208}Pb at laboratory energies around the coulomb barrier: a candidate reaction for the production of neutron-rich nuclei at $N = 126$. Phys. Rev. C **86**, 044611 (2012). https://doi.org/10.1103/PhysRevC.86.044611
154. E. Vardaci et al., Fission dynamics in systems of intermediate fissility. J. Phys. G: Nuclear Part. Phys **46**, 115111 (2019). https://doi.org/10.1088/1361-6471/ab445a
155. K.V. Novikov et al., Investigation of fusion probabilities in the reactions with ^{52,54}Cr, ^{64}Ni, and ^{68}Zn ions leading to the formation of $Z = 120$ superheavy composite systems. Phys. Rev. C **102**, 044605 (2020). https://doi.org/10.1103/PhysRevC.102.044605
156. E. Vardaci et al., Using γ rays to disentangle fusion-fission and quasifission near the coulomb barrier: A test of principle in the fusion-fission and quasielastic channels. Phys. Rev. C **101**, 064612 (2020). https://doi.org/10.1103/PhysRevC.101.064612
157. E. Vardaci et al., Fission dynamics of intermediate-fissility systems: a study within a stochastic three-dimensional approach. Phys. Rev. C **92**, 034610 (2015). https://doi.org/10.1103/PhysRevC.92.034610
158. M.G. Itkis et al., Fusion and fission of heavy and superheavy nuclei (experiment). Nuclear Phys. A **944**, 204 (2015). https://doi.org/10.1016/j.nuclphysa.2015.09.007. (**Special Issue on Superheavy Elements**)
159. A. Di Nitto et al., Clustering effects in ^{48}Cr composite nuclei produced via the ^{24}Mg+^{24}Mg reaction. Phys. Rev. C **93**, 044602 (2016). https://doi.org/10.1103/PhysRevC.93.044602
160. A. Di Nitto et al., Study of non-fusion products in the ^{50}Ti+^{249}Cf reaction. Phys. Lett. B **784**, 199–205 (2018). https://doi.org/10.1016/j.physletb.2018.07.058
161. A. Di Nitto et al., Evaporation and fission decay of ^{158}Er composite nuclei within the statistical model. Phys. Rev. C **102**, 024624 (2020). https://doi.org/10.1103/PhysRevC.102.024624
162. A. Di Nitto et al., Clustering effects in ^{36}Ar nuclei produced via the ^{24}Mg+^{12}C reaction. Phys. Rev. C **107**, 024615 (2023). https://doi.org/10.1103/PhysRevC.107.024615
163. E.M. Kozulin et al., Investigation of the reaction ^{64}Ni+^{238}U being an option of synthesizing element 120. Phys. Lett. B **686**(4), 227–232 (2010). https://doi.org/10.1016/j.physletb.2010.02.041
164. E.M. Kozulin et al., Challenging fission dynamics around the barrier: the case of ^{34}S+^{186}W. Eur. Phys. J. A **52**, 293 (2016). https://doi.org/10.1140/epja/i2016-16293-8
165. T. Banerjee et al., Systematic evidence for quasifission in ^{9}Be-, ^{12}C- and ^{16}O-induced reactions forming ^{258,260}No. Phys. Rev. C **102**, 024603 (2020). https://doi.org/10.1103/PhysRevC.102.024603
166. D.J. Hinde et al., Sub-barrier quasifission in heavy element formation reactions with deformed actinide target nuclei. Phys. Rev. C **97**, 024616 (2018). https://doi.org/10.1103/PhysRevC.97.024616

167. A. Di Nitto et al., Evaporation channel as a tool to study fission dynamics. Nucl. Phys. A **971**, 21–34 (2018). https://doi.org/10.1016/j.nuclphysa.2018.01.008
168. T. Banerjee et al., Search for possible fission modes at high excitation energies in ^{254}Fm. Phys. Rev. C **105**, 044614 (2022). https://doi.org/10.1103/PhysRevC.105.044614
169. T. Banerjee et al., Evolution of multimodal fission with energy in ^{238}Np populated by ^{6}Li+^{232}Th. Phys. Rev. C **108**(6), 064601 (2023). https://doi.org/10.1103/PhysRevC.108.064601
170. M. Ashaduzzaman et al., Search for ternary fission in the ^{40} Ar +^{208} Pb reaction. to be published
171. J.F. Liang et al., Fusion of radioactive ^{132}Sn with ^{64}Ni. Phys. Rev. C **75**(5), 054607 (2007). https://doi.org/10.1103/PhysRevC.75.054607
172. P.F.F. Carnelli et al., Multi-sampling ionization chamber (MUSIC) for measurements of fusion reactions with radioactive beams. Nuclear Instrum. Methods Phys. Res. Sect. A Accel. Spectrom. Detect. Assoc. Equip. **799**, 197–202 (2015). https://doi.org/10.1016/j.nima.2015.07.030
173. B.W. Asher et al., Experimental study of the ^{17}F+^{12}C fusion reaction and its implications for fusion of proton-halo systems. Phys. Rev. C **103**(4), 044615 (2021). https://doi.org/10.1103/PhysRevC.103.044615
174. M. Assié et al., The MUGAST-AGATA-VAMOS campaign: set-up and performances. Nuclear Instrum. Methods Phys. Res. Sect. A Accel. Spectrom. Detect. Assoc. Equip. **1014**, 165743 (2021). https://doi.org/10.1016/j.nima.2021.165743
175. F. Galtarossa et al., HeCTOr: the ^{3}He cryogenic target of orsay for direct nuclear reactions with radioactive ion beams. Nuclear Instrum. Methods Phys. Res. Sect. A Accel. Spectrom. Detect. Assoc. Equip. **1018**, 165830 (2021). https://doi.org/10.1016/j.nima.2021.165830
176. K.Y. Chae et al., Construction of a fast ionization chamber for high-counting rate particle identification. Nuclear Instrum. Methods Phys. Res. Sect. A Accel. Spectrom. Detect. Assoc. Equip. **751**, 6–10 (2014). https://doi.org/10.1016/j.nima.2014.03.016
177. G. Colucci et al., A fast ionization chamber for the study of fusion reactions induced by radioactive beams. Acta Physica Polonica B **50**, 573 (2019). https://doi.org/10.5506/APhysPolB.50.573
178. J. Lai et al., Position-sensitive, fast ionization chambers. Nuclear Instrum. Methods Phys. Res. Sect. A Accel. Spectrom. Detect. Assoc. Equip. **890**, 119–125 (2018). https://doi.org/10.1016/j.nima.2018.01.010
179. K. Wimmer, Nucleon transfer reactions with radioactive beams. J. Phys. G Nuclear Particle Phys. **45**(3), 033002 (2018). https://doi.org/10.1088/1361-6471/aaa2bf
180. M. Labiche et al., TIARA: a large solid angle silicon array for direct reaction studies with radioactive beams. Nuclear Instrum. Methods Phys. Res. Sect. A Accel. Spectrom. Detect. Assoc. Equip. **614**, 439 (2010). https://doi.org/10.1016/j.nima.2010.01.009
181. W.N. Catford et al., Transfer reaction studies with exotic nuclei. AIP Conf. Proc. **704**(1), 185–194 (2004). https://doi.org/10.1063/1.1737110
182. V. Bildstein et al., T-REX: a new setup for transfer experiments at REX-ISOLDE. Eur. Phys. J. A **48**, 85 (2012). https://doi.org/10.1140/epja/i2012-12085-6
183. E. Pollacco et al., MUST2: a new generation array for direct reaction studies. Eur. Phys. J A **25**, 287 (2005). https://doi.org/10.1140/epjad/i2005-06-162-5
184. C.A. Diget et al., SHARC: silicon highly-segmented array for reactions and Coulex used in conjunction with the TIGRESS γ-ray spectrometer. J. Instrum. **6**(02), 02005 (2011). https://doi.org/10.1088/1748-0221/6/02/P02005
185. J. Simpson et al., The EXOGAM array: a radioactive beam gamma-ray spectrometer. Acta Phys. Hungarica New Ser. Heavy ion **11**, 159 (2000)
186. M.A. Schumaker et al., Measured and simulated performance of Compton-suppressed TIGRESS HPGe clover detectors. NIMA **570**(3), 437–445 (2007). https://doi.org/10.1016/j.nima.2006.10.185
187. M. Assié et al., New methods to identify low energy ^{3}He with silicon-based detectors. Nuclear Instrum. Methods Phys. Res. Sect. A Accel. Spectrom. Detect. Assoc. Equip. **908**, 250–255 (2018). https://doi.org/10.1016/j.nima.2018.08.050
188. R.J. Aliaga et al., PLAS: A compact, self-triggered, dead time-less, high channel count analog memory ASIC for TRACE. 2015 IEEE Nuclear Science Symposium and Medical Imaging Conference, NSS/MIC 2015 (2016). https://doi.org/10.1109/NSSMIC.2015.7581779
189. R.J. Aliaga et al., Conceptual design of the TRACE detector readout using a compact, dead time-less analog memory ASIC. Nuclear Instrum. Methods Phys. Res. Sect. A Accel. Spectrom. Detect. Assoc. Equip. **800**, 34–39 (2015). https://doi.org/10.1016/j.nima.2015.07.067
190. A. Pullia, F. Zocca, S. Capra, A 102 dB dynamic-range charge-sampling readout for ionizing particle/radiation detectors based on an application-specific integrated circuit (ASIC). Rev. Sci. Instrum. **89**(2), 026107 (2018). https://doi.org/10.1063/1.5012081
191. S. Capra et al., Performance of the new integrated front-end electronics of the TRACE array commissioned with an early silicon detector prototype. Nucl. Instrum. Methods A **935**, 178–184 (2019). https://doi.org/10.1016/j.nima.2019.05.039
192. S. Capra, A. Pullia, Design and experimental validation of an integrated multichannel charge amplifier for solid-state detectors with innovative spectroscopic range booster. IEEE Trans. Nucl. Sci. **67**(8), 1877–1884 (2020). https://doi.org/10.1109/TNS.2020.3006892
193. S. Capra et al., Design of an integrated low-noise, low-power charge sensitive preamplifier for γ and particle spectroscopy with solid state detectors. 2014 IEEE NSS/MIC Conf. Rec. (2016). https://doi.org/10.1109/NSSMIC.2014.7431043
194. S. Capra et al., Experimental performance of the I^2C integrated multichannel charge-sensitive preamplifier of TRACE. 2015 IEEE NSS/MIC Conf. Rec. (2016). https://doi.org/10.1109/NSSMIC.2015.7581814
195. A. Pullia, S. Capra, Performance evaluation of an innovative integrated charge-sensitive preamplifier with dynamic range booster. 2015 IEEE NSS/MIC Conf. Rec. (2016). https://doi.org/10.1109/NSSMIC.2015.7581811
196. A. Pullia, S. Capra, Experimental performance of a highly-innovative low-noise charge-sensitive preamplifier with integrated range-booster. J. Instrum. **13**(12), 12004 (2018). https://doi.org/10.1088/1748-0221/13/12/C12004
197. S. Capra, G. Secci, A. Pullia, An innovative analog circuit to retrieve energy information from signals of deeply saturated preamplifiers connected to semiconductor detectors. IEEE Trans. Nucl. Sci. **69**(7), 1757–1764 (2022). https://doi.org/10.1109/TNS.2022.3178760
198. A. Pullia, S. Capra, Design of a resistorless ASIC preamplifier for hpge detectors with non-linear pole/zero cancellation and controlled fast-reset feature. 2012 IEEE NSS/MIC Conf. Rec., 86–90 (2012). https://doi.org/10.1109/NSSMIC.2012.6551066
199. S. Capra, A. Pullia, Measurement of the power spectral density of noise produced by a large integrated feedback resistor for charge-sensitive preamplifiers. 2016 IEEE NSS/MIC Conf. Rec. **2017-January** (2017). https://doi.org/10.1109/NSSMIC.2016.8069661
200. S. Capra, Impedance and noise closed-form model of large-area integrated resistors with high stray capacitance to be used as feedback discharge devices in charge-sensitive preamplifiers for nuclear spectroscopy. IEEE Trans. Nuclear Sci. **67**(4), 722–731 (2020). https://doi.org/10.1109/TNS.2020.2975311
201. S. Capra, G. Secci, A. Pullia, Equivalent noise charge contribution of the $\sqrt{f}$ parallel noise in nuclear spectroscopic measurements using different shaping amplifiers. IEEE Trans. Nuclear Sci. **70**(4), 730–736 (2023). https://doi.org/10.1109/TNS.2023.3259143
202. I.-Y. Lee, The GAMMASPHERE. Nuclear Phys. A **520**, 641–655 (1990)
203. C.L. Jiang et al., Reaction rate for carbon burning in massive stars. Phys. Rev. C **97**(1), 012801 (2018). https://doi.org/10.1103/PhysRevC.97.012801
204. T. Nakamura et al., The opera film: new nuclear emulsion for large-scale, high-precision experiments. Nuclear Instrum. Methods Phys. Res. Sect. A Accel. Spectrom. Detect. Assoc. Equip. **556**, 80–86 (2006). https://doi.org/10.1016/j.nima.2005.08.109

205. The SND@LHC Collaboration: SND@LHC: The Scattering and Neutrino Detector at the LHC (2022). https://doi.org/10.48550/arXiv.2210.02784
206. C. Ahdida et al., The SHiP experiment at the proposed CERN SPS beam dump facility. Eur. Phys. J. C (2022). https://doi.org/10.1140/epjc/s10052-022-10346-5
207. A. Alexandrov et al., Directionality preservation of nuclear recoils in an emulsion detector for directional dark matter search. J. Cosmol. Astropart. Phys. **2021**, 047 (2021). https://doi.org/10.1088/1475-7516/2021/04/047
208. A. Alexandrov et al., A new generation scanning system for the high-speed analysis of nuclear emulsions. J. Instrum. **11**, 06002 (2016). https://doi.org/10.1088/1748-0221/11/06/P06002
209. G. Battistoni et al., Measuring the impact of nuclear interaction in particle therapy and in radio protection in space: the foot experiment. Front. Phys. **8**(568242), 1–20 (2021). https://doi.org/10.3389/fphy.2020.568242
210. N. Agafonova et al., Momentum measurement by the multiple Coulomb scattering method in the OPERA lead-emulsion target. New J. Phys. **14**, 013026 (2012). https://doi.org/10.1088/1367-2630/14/1/013026
211. A. Alexandrov et al., The FOOT experiment: fragmentation measurements in particle therapy. Radiat. Appl. (2018). https://doi.org/10.21175/RadJ.2018.03.032
212. G. De Lellis et al., Emulsion cloud chamber technique to measure the fragmentation of a high-energy carbon beam. J. Instrum. (2007). https://doi.org/10.1088/1748-0221/2/06/P06004
213. G. De Lellis et al., Measurement of the fragmentation of carbon nuclei used in hadron-therapy. Nuclear Phys. A **853**(1), 124–134 (2011). https://doi.org/10.1016/j.nuclphysa.2011.01.019
214. M.C. Montesi, Ion charge separation with new generation of nuclear emulsion films. Open Phys. **17**(1), 233–240 (2019). https://doi.org/10.1515/phys-2019-0024
215. G. Galati et al., Charge identification of fragments with the emulsion spectrometer of the FOOT experiment. Open Phys. **19**(1), 383–394 (2021). https://doi.org/10.1515/phys-2021-0032
216. T. Asada, T. Naka, K.-I. Kuwabara, M. Yoshimoto, The development of super fine-grained nuclear emulsion. Prog. Theoret. Exp. Phys. (2017). https://doi.org/10.1093/ptep/ptx076
217. A. Alexandrov et al., Super-resolution high-speed optical microscopy for fully automated readout of metallic nanoparticles and nanostructures. Sci. Rep. **10**, 18773 (2020). https://doi.org/10.1038/s41598-020-75883-z
218. T. Shimaoka, S. Koizumi, J.H. Kaneko, Recent progress in diamond radiation detectors. Funct. Diam. **1**(1), 205–220 (2021). https://doi.org/10.1080/26941112.2021.2017758
219. G. Chiodini, M. Martino, Diamond Radiation Detectors, pp. 689–714. John Wiley & Sons, Ltd, (2022). Chap. 17. https://doi.org/10.1002/9781119579182.ch17. https://onlinelibrary.wiley.com/doi/abs/10.1002/9781119579182.ch17
220. H. Kagan, W. Trischuk, Development of Diamond Tracking Detectors for High Luminosity Experiments at the LHC, HL-LHC and Beyond. Technical Report CERN-LHCC-2018-015, LHCC-SR-005, CERN, Geneva (2018). https://cds.cern.ch/record/2320382
221. C. Talamonti, K. Kanxheri, S. Pallotta, L. Servoli, Diamond detectors for radiotherapy x-ray small beam dosimetry. Front. Phys. (2021). https://doi.org/10.3389/fphy.2021.632299
222. M. Angelone, C. Verona, Properties of diamond-based neutron detectors operated in harsh environments. J. Nuclear Eng. **2**(4), 422–470 (2021)
223. M. Liao, Progress in semiconductor diamond photodetectors and MEMS sensors. Funct. Diam. **1**(1), 29–46 (2021). https://doi.org/10.1080/26941112.2021.1877019
224. C. Xie et al., Recent progress in solar-blind deep-ultraviolet photodetectors based on inorganic ultrawide bandgap semiconductors. Adv. Funct. Mater. **29**(9), 1806006 (2019). https://doi.org/10.1002/adfm.201806006
225. E. Bossini, N. Minafra, Diamond detectors for timing measurements in high energy physics. Front. Phys. **8**, 248 (2020). https://doi.org/10.3389/fphy.2020.00248
226. A. Crnjac et al., Charge transport in single crystal CVD diamond studied at high temperatures. J. Phys. D Appl. Phys. **54**(46), 465103 (2021). https://doi.org/10.1088/1361-6463/ac1e4e
227. S. Lagomarsino et al., Radiation hardness of three-dimensional polycrystalline diamond detectors. Appl. Phys. Lett. **106**(19), 193509 (2015). https://doi.org/10.1063/1.4921116
228. L. Anderlini et al., A study of the radiation tolerance and timing properties of 3d diamond detectors. Sensors (2022). https://doi.org/10.3390/s22228722
229. T.V. Kononenko et al., Femtosecond laser microstructuring in the bulk of diamond. Diam. Relat. Mater. **18**(2), 196–199 (2009). https://doi.org/10.1016/j.diamond.2008.07.014. (**NDNC 2008 Proceedings of the International Conference on New Diamond and Nano Carbons 2008**)
230. A. Oh, B. Caylar, M. Pomorski, T. Wengler, A novel detector with graphitic electrodes in CVD diamond. Diam. Relat. Mater. **38**, 9–13 (2013). https://doi.org/10.1016/j.diamond.2013.06.003
231. B. Caylar, M. Pomorski, P. Bergonzo, Laser-processed three dimensional graphitic electrodes for diamond radiation detectors. Appl. Phys. Lett. **103**(4), 043504 (2013). https://doi.org/10.1063/1.4816328
232. B. Sun, P.S. Salter, M.J. Booth, High conductivity micro-wires in diamond following arbitrary paths. Appl. Phys. Lett. **105**(23), 231105 (2014). https://doi.org/10.1063/1.4902998
233. S. Lagomarsino et al., Three-dimensional diamond detectors: charge collection efficiency of graphitic electrodes. Appl. Phys. Lett. **103**(23), 233507 (2013). https://doi.org/10.1063/1.4839555
234. L. Anderlini et al., Fabrication and characterisation of 3D diamond pixel detectors with timing capabilities. Front. Phys. **8**, 589844 (2020). https://doi.org/10.3389/fphy.2020.589844
235. H.F.-W. Sadrozinski, A. Seiden, N. Cartiglia, 4D tracking with ultra-fast silicon detectors. Rep. Prog. Phys. **81**(2), 026101 (2017). https://doi.org/10.1088/1361-6633/aa94d3
236. J.J. Gracio, Q.H. Fan, J.C. Madaleno, Diamond growth by chemical vapour deposition. J. Phys. D Appl. Phys. **43**(37), 374017 (2010). https://doi.org/10.1088/0022-3727/43/37/374017
237. M. Schwander, K. Partes, A review of diamond synthesis by CVD processes. Diam. Relat. Mater. **20**(9), 1287–1301 (2011). https://doi.org/10.1016/j.diamond.2011.08.005
238. P.S. Salter et al., Exploring the depth range for three-dimensional laser machining with aberration correction. Opt. Express **22**(15), 17644–17656 (2014). https://doi.org/10.1364/OE.22.017644
239. P.S. Salter et al., High resolution structural characterisation of laser-induced defect clusters inside diamond. Appl. Phys. Lett. **111**(8), 081103 (2017). https://doi.org/10.1063/1.4993118
240. K.K. Ashikkalieva et al., Direct observation of graphenic nanostructures inside femtosecond-laser modified diamond. Carbon **102**, 383–389 (2016). https://doi.org/10.1016/j.carbon.2016.02.044
241. L. Anderlini et al., A 4D diamond detector for HL-LHC and beyond. Nuclear Instrum. Methods Phys. Res. Sect. A Accel. Spectrom. Detect. Assoc. Equip. **1040**, 167230 (2022). https://doi.org/10.1016/j.nima.2022.167230

242. L. Piccolo et al., The first ASIC prototype of a 28 nm time-space front-end electronics for real-time tracking. PoS TWEPP2019, 022 (2020). https://doi.org/10.22323/1.370.0022
243. L. Piccolo et al., First measurements on the Timespot1 ASIC: a fast-timing, high-rate pixel-matrix front-end. J. Instrum. **17**(03), 03022 (2022). https://doi.org/10.1088/1748-0221/17/03/C03022
244. L. Anderlini et al., Fabrication and first full characterisation of timing properties of 3d diamond detectors. Instruments **5**(4), 39 (2021)
245. L. Anderlini et al., Construction and characterisation of high time resolution 3D diamond pixel detectors. Nuclear Instrum. Methods Phys. Res. Sect. A Accel. Spectrom. Detect. Assoc. Equip. **1046**, 167692 (2023). https://doi.org/10.1016/j.nima.2022.167692
246. A. Morozzi et al., 3D diamond tracking detectors: numerical analysis for timing applications with TCAD tools. J. Instrum. **15**(01), 01048–01048 (2020). https://doi.org/10.1088/1748-0221/15/01/c01048
247. R. Street, *Technology and Applications of Amorphous Silicon* (Springer, Berlin, 2000)
248. A. Matsuda, *Amorphous and Microcrystalline Silicon* (Springer, Berlin, 2017)
249. M. Menichelli et al., Development of thin hydrogenated amorphous silicon detectors on a flexible substrate, 1–5 (2022).https://doi.org/10.48550/arXiv.2211.17114
250. A. Danilyuk et al., An enhanced charge carrier separation in a heterojunction solar cell with a metal oxide. Physica Status Solidi (2021). https://doi.org/10.1002/pssa.202100525
251. M. Large et al., Hydrogenated amorphous silicon high flux x-ray detectors for synchrotron microbeam radiation therapy. Phys. Med. Biol. (2023). https://doi.org/10.1088/1361-6560/acdb43
252. M. Menichelli et al., Testing of planar hydrogenated amorphous silicon sensors with charge selective contacts for the construction of 3D-detectors. J. Instrum. IOP SISSA J. **17**, 03033 (2022). https://doi.org/10.1088/1748-0221/17/03/C03033
253. M. Menichelli et al., Neutron irradiation of hydrogenated amorphous silicon p-i-n diodes and charge selective contacts detectors. Nuclear Instrum. Methods Phys. Res. Sect. A Accel. Spectrom. Detect. Assoc. Equip. **1032**, 168308 (2023). https://doi.org/10.1016/j.nima.2023.168308
254. E.V. Pagano et al., The NArCoS project. IL Nuovo Cimento C **5**, 181 (2018). https://doi.org/10.1393/ncc/i2018-18181-9
255. E.V. Pagano et al., The NArCoS project: the latest results. JPS Conf. Proc. (2020). https://doi.org/10.7566/JPSCP.32.010096
256. E.V. Pagano et al., NArCoS project for nuclear physics and applications. IL NUOVO CIMENTO C (2020). https://doi.org/10.1393/ncc/i2020-20012-9
257. E.V. Pagano et al., The NArCoS project: efficiency estimation and the cross talk problem studied through Monte Carlo simulations. J. Phys. Conf. Ser. **1643**, 012037 (2020). https://doi.org/10.1088/1742-6596/1643/1/012037
258. E.V. Pagano et al., Recent results on the construction of a new correlator for neutrons and charged particles and for FARCOS. IL NUOVO CIMENTO C (2022). https://doi.org/10.1393/ncc/i2022-22064-1
259. E.V. Pagano et al., NArCoS: the new hodoscope for neutrons and charged particles. Front. Phys. **10**, 1051058 (2023). https://doi.org/10.3389/fphy.2022.1051058
260. E.V. Pagano et al., Pulse shape discrimination of plastic scintillator EJ 299–33 with radioactive sources. Nuclear Instrum. Methods Phys. Res. Sect. A Accel. Spectrom. Detect. Assoc. Equip. **889**, 83–88 (2018). https://doi.org/10.1016/j.nima.2018.02.010
261. J.J. Valiente-Dobon et al., NEDA - NEutron detector array. Nuclear Instrum. Methods Phys. Res. Sect. A Accel. Spectrom. Detect. Assoc. Equip. **927**, 81–86 (2019). https://doi.org/10.1016/j.nima.2019.02.021
262. T. Hüyük et al., Conceptual design of the early implementation of the neutron detector array (NEDA) with AGATA. Eur. Phys. J. A **52**(3), 1–8 (2016)
263. E. Clément et al., Conceptual design of the AGATA 1π array at GANIL. Nuclear Instrum. Methods Phys. Res. Sect. A Accel. Spectrom. Detect. Assoc. Equip. **855**, 1–12 (2017)
264. B. Cederwall et al., Isospin properties of nuclear pair correlations from the level structure of the self-conjugate nucleus Ru88. Phys. Rev. Lett. **124**(6), 263 (2020). https://doi.org/10.1103/physrevlett.124.062501
265. Ö. Skeppstedt et al., The EUROBALL neutron wall-design and performance tests of neutron detectors. Nuclear Instrum. Methods Phys. Res. Sect. A Accel. Spectrom. Detect. Assoc. Equip. **421**(3), 531–541 (1999)
266. J. Ljungvall, M. Palacz, J. Nyberg, Monte Carlo simulations of the neutron wall detector system. Nuclear Instrum. Methods Phys. Res. Sect. A Accel. Spectrom. Detect. Assoc. Equip. **528**(3), 741–762 (2004)
267. D.G. Sarantites et al., Neutron shell: a high efficiency array of neutron detectors for γ-ray spectroscopic studies with gammasphere. Nuclear Instrum. Methods Phys. Res. Sect. A Accel. Spectrom. Detect. Assoc. Equip. **530**(3), 473–492 (2004)
268. P.E. Garrett, DESCANT – the deuterated scintillator array for neutron tagging. Hyperfine Interact. **225**(1–3), 137–141 (2013)
269. A. Best et al., Underground nuclear astrophysics: why and how. Eur. Phys. J. A **52**(4), 72 (2016). https://doi.org/10.1140/epja/i2016-16072-7
270. J. Tolosa-Delgado et al., Commissioning of the BRIKEN detector for the measurement of very exotic β-delayed neutron emitters. Nuclear Instrum. Methods Phys. Res. Sect. A Accel. Spectrom. Detect. Assoc. Equip. **925**, 133–147 (2019). https://doi.org/10.1016/j.nima.2019.02.004
271. P. Adsley et al., Reevaluation of the $^{22}\mathrm{Ne}(\alpha,\gamma)^{26}\mathrm{Mg}$ and $^{22}\mathrm{Ne}(\alpha,n)^{25}\mathrm{Mg}$ reaction rates. Phys. Rev. C **103**, 015805 (2021). https://doi.org/10.1103/PhysRevC.103.015805
272. D. Strickland, G. Mourou, Compression of amplified chirped optical pulses. Optics Commun. **55**(6), 447–449 (1985). https://doi.org/10.1016/0030-4018(85)90151-8
273. G.A. Mourou, T. Tajima, S.V. Bulanov, Optics in the relativistic regime. Rev. Mod. Phys. **78**(2), 309–371 (2006). https://doi.org/10.1103/RevModPhys.78.309
274. A.J. Kemp, S.C. Wilks, E.P. Hartouni, G. Grim, Generating keV ion distributions for nuclear reactions at near solid-density using intense short-pulse lasers. Nat. Commun. **10**(1), 4156 (2019)
275. W. Bang et al., Temperature measurements of fusion plasmas produced by petawatt-laser-irradiated $\mathbf{d}_2-^3\mathrm{He}$ or $\mathrm{cd}_4-^3\mathrm{He}$ clustering gases. Phys. Rev. Lett. **111**, 055002 (2013). https://doi.org/10.1103/PhysRevLett.111.055002
276. M. Barbui et al., Measurement of the plasma astrophysical s factor for the $^3\mathrm{He}(d,p)^4\mathrm{He}$ reaction in exploding molecular clusters. Phys. Rev. Lett. **111**, 082502 (2013). https://doi.org/10.1103/PhysRevLett.111.082502
277. D. Lattuada et al., Model-independent determination of the astrophysical s factor in laser-induced fusion plasmas. Phys. Rev. C **93**, 045808 (2016). https://doi.org/10.1103/PhysRevC.93.045808
278. C. Iliadis, *Nuclear Physics of Stars* (Wiley, Hoboken, 2007)
279. M.D. Cable, S.P. Hatchett, Neutron spectra from inertial confinement fusion targets for measurement of fuel areal density and charged particle stopping powers. J. Appl. Phys. **62**(6), 2233–2236 (1987). https://doi.org/10.1063/1.339850
280. W. Bang et al., Experimental study of fusion neutron and proton yields produced by petawatt-laser-irradiated d_2-^{3}he or cd_4-^{3}he clustering gases. Phys. Rev. E **88**, 033108 (2013). https://doi.org/10.1103/PhysRevE.88.033108
281. H.J. Quevedo et al., Neutron enhancement from laser interaction with a critical fluid. Phys. Lett. A **382**(2), 94–98 (2018). https://doi.org/10.1016/j.physleta.2017.11.002

282. S. Marrone et al., A low background neutron flux monitor for the n_TOF facility at CERN. Nuclear Instrum. Methods Phys. Res. Sect. A Accel. Spectrom. Detect. Assoc. Equip. **517**(1), 389–398 (2004). https://doi.org/10.1016/j.nima.2003.09.060
283. J.M. Rafí et al., Electron, neutron, and proton irradiation effects on sic radiation detectors. IEEE Trans. Nuclear Sci. **67**(12), 2481–2489 (2020). https://doi.org/10.1109/TNS.2020.3029730
284. S. Amaducci et al., Measurement of the 235u(n, f) cross section relative to the 6li(n, t) and 10b(n,α) standards from thermal to 170 keV neutron energy range at n_TOF. Eur. Phys. J. A **55**(7), 120 (2019). https://doi.org/10.1140/epja/i2019-12802-7
285. C. Paradela et al., Neutron-induced fission cross section of ^{234} U and ^{237} Np measured at the CERN neutron time-of-flight (n_TOF) facility. Phys. Rev. C **82**, 034601 (2010). https://doi.org/10.1103/PhysRevC.82.034601
286. A. Manna et al., Recoil proton telescopes and parallel plate avalanche counters for the 235u(n, f) cross section measurement relative to h(n, n)h between 10 and 450 mev neutron energy. J. Instrum. **18**(04), 04024 (2023). https://doi.org/10.1088/1748-0221/18/04/P04024
287. E. Pirovano et al., A detector system for 'absolute' measurements of fission cross sections at n_tof in the energy range below 200 mev. J. Instrum. **18**(11), 11011 (2023). https://doi.org/10.1088/1748-0221/18/11/P11011
288. G. Martín-Hernández et al., Excitation function shape and neutron spectrum of the ^{7} Li $(p, n)^{7}$ Be reaction near threshold. Phys. Rev. C **94**, 034620 (2016). https://doi.org/10.1103/PhysRevC.94.034620
289. T. Poikela et al., Timepix3: a 65k channel hybrid pixel readout chip with simultaneous ToA/ToT and sparse readout. J. Instrum. **9**(05), 05013 (2014). https://doi.org/10.1088/1748-0221/9/05/C05013
290. P. Burian, P. Broulím, M. Jára, V. Georgiev, B. Bergmann, Katherine: ethernet embedded readout interface for timepix3. J. Instrum. **12**(11), 11001 (2017). https://doi.org/10.1088/1748-0221/12/11/C11001
291. G. Claps et al., Diamondpix: a CVD diamond detector with timepix3 chip interface. IEEE Trans. Nuclear Sci. **65**(10), 2743–2753 (2018). https://doi.org/10.1109/TNS.2018.2871605
292. X. Llopart, R. Ballabriga, M. Campbell, L. Tlustos, W. Wong, Timepix, a 65k programmable pixel readout chip for arrival time, energy and/or photon counting measurements. Nuclear Instrum. Methods Phys. Res. Sect. A Accel. Spectrom. Detect. Assoc. Equip. **581**(1), 485–494 (2007). https://doi.org/10.1016/j.nima.2007.08.079. (**VCI 2007**)
293. G. Croci et al., Gem-based thermal neutron beam monitors for spallation sources. Nuclear Instrum. Methods Phys. Res. Sect. A Accel. Spectrom. Detect. Assoc. Equip. **732**, 217–220 (2013). https://doi.org/10.1016/j.nima.2013.05.111. (**Vienna Conference on Instrumentation 2013**)
294. G. Croci et al., I-band-gem: a new way for improving band-gem efficiency to thermal and cold neutrons. Eur. Phys. J. Plus **134**(4), 166 (2019). https://doi.org/10.1140/epjp/i2019-12522-5
295. A. Muraro et al., Mbgem: a stack of borated gem detector for high efficiency thermal neutron detection. Eur. Phys. J. Plus **136**(7), 742 (2021). https://doi.org/10.1140/epjp/s13360-021-01707-2
296. J.M. Gómez-Ros et al., The directional neutron spectrometer CYSP: further developments for measuring low intensity fields. Radiat. Measurem. **106**, 580–584 (2017). https://doi.org/10.1016/j.radmeas.2017.05.007. (**Proceedings of the 18th International Conference on Solid State Dosimetry (SSD18), Munich, Germany, 3 - 8 July 2016**)
297. R. Bedogni, J.M. Gomez-Ros, A. Scherillo, M. Costa, A. Pietropaolo, Thermal to GeV neutron spectrometry of the INES beam line at ISIS using the CYSP-BEAM spectrometer. Europhys. Lett. **127**(1), 12002 (2019). https://doi.org/10.1209/0295-5075/127/12002
298. R. Bedogni et al., Nct-wes: a new single moderator directional neutron spectrometer for neutron capture therapy. Experimental validation. Europhys. Lett. **134**(4), 42001 (2021). https://doi.org/10.1209/0295-5075/134/42001
299. R. Bedogni et al., Measuring the near-target neutron field of a d-d fusion facility with the novel NCT-WES spectrometer. Eur. Phys. J. Plus **137**(7), 773 (2022). https://doi.org/10.1140/epjp/s13360-022-02922-1
300. M. Cesaria et al., 10b-based films grown by pulsed laser deposition for neutron conversion applications. Appl. Phys. A (2020). https://doi.org/10.1007/s00339-020-03538-x
301. A.P. Caricato et al., Thermal neutron conversion by high purity 10b-enriched layers: PLD-growth, thickness-dependence and neutron-detection performances. Eur. Phys. J. Plus **137**(4), 431 (2022). https://doi.org/10.1140/epjp/s13360-022-02523-y
302. J.C. Delgado et al., Study of a metal-halide perovskite cspbbr3 thin film deposited on a 10b layer for neutron detection. J. Phys. D Appl. Phys. **57**(5), 055501 (2023). https://doi.org/10.1088/1361-6463/ad0569
303. A. Giaz et al., Fast neutron measurements with ^{7}Li and ^{6}Li enriched CLYC scintillators. Nuclear Instrum. Methods Phys. Res. Sect. A Accel. Spectrom. Detect. Assoc. Equip. **825**, 51–61 (2016). https://doi.org/10.1016/j.nima.2016.03.090
304. A. Giaz et al., The CLYC-6 and CLYC-7 response to γ-rays, fast and thermal neutrons. Nuclear Instrum. Methods Phys. Res. Sect. A Accel. Spectrom. Detect. Assoc. Equip. **810**, 132–139 (2016). https://doi.org/10.1016/j.nima.2015.11.119
305. A. Gottardo, G. Andreetta, R. Lombardi, The CLYC-7 scintillator as a fast neutron spectrometer: pulse-shape discrimination for different neutron-induced reaction channels. Nuclear Instrum. Methods Phys. Res. Sect. A Accel. Spectrom. Detect. Assoc. Equip. **1041**(167332), 1–6 (2022). https://doi.org/10.1016/j.nima.2022.167332
306. F. Ferrulli, M. Labalme, M. Silari, Investigation of CLYC-6 for thermal neutron detection and CLYC-7 for fast neutron spectrometry. Nuclear Instrum. Methods Phys. Res. Sect. A Accel. Spectrom. Detect. Assoc. Equip. **1029**(166460), 1–6 (2022). https://doi.org/10.1016/j.nima.2022.166460
307. M.B. Smith et al., Fast neutron spectroscopy using Cs_2 LiYCl_6: Ce (CLYC) scintillator. IEEE Trans. Nuclear Sci. **60**(13428776), 855–859 (2013). https://doi.org/10.1109/TNS.2012.2219068
308. A.R. Garcia et al., MONSTER: a time of flight spectrometer for β-delayed neutron emission measurements. J. Instrum. **7**(C05012), 855–859 (2012). https://doi.org/10.1088/1748-0221/7/05/C05012
309. W.A. Peters et al., Performance of the versatile array of neutron detectors at low energy (VANDLE). Nuclear Instrum. Methods Phys. Res. Sect. A Accel. Spectrom. Detect. Assoc. Equip. **836**, 122–133 (2016). https://doi.org/10.1016/j.nima.2016.08.054
310. M. Scheck et al., Investigating the pygmy dipole resonance using β decay. Phys. Rev. Lett. **116**(132501), 1–5 (2016). https://doi.org/10.1103/PhysRevLett.116.132501
311. A. Gottardo et al., Unexpected high-energy γ emission from decaying exotic nuclei. Phys. Lett. B **772**, 359–362 (2017). https://doi.org/10.1016/j.physletb.2017.06.050
312. J. Glodo et al., Selected properties of Cs_2 LiYCl_6, Cs_2 LiLaCl_6, and Cs_2 LiLaBr_6 scintillators. IEEE Trans. Nuclear Sci. **58**(1), 333–338 (2011). https://doi.org/10.1109/TNS.2010.2098045
313. J. Glodo, R. Hawrami, E. van Loef, U. Shirwadkar, K.S. Shah, Pulse shape discrimination with selected Elpasolite crystals. IEEE Trans. Nuclear Sci. **59**(5), 2328–2333 (2012). https://doi.org/10.1109/TNS.2012.2188646
314. G. Hull et al., Detection properties and internal activity of newly developed La-containing scintillator crystals. Nuclear Inst. Methods Phys. Res. A **925**, 70–75 (2019). https://doi.org/10.1016/j.nima.2019.01.094
315. G. Hawrami et al., Tl_2 LiYCl_6: large diameter, high performing dual mode scintillator. Cryst. Growth Des. **17**, 3960–3964 (2017). https://doi.org/10.1021/acs.cgd.7b00583

316. S.M. Carturan, A. Quaranta, In: Hamel, M. (ed.) Polysiloxane-Based Scintillators, pp. 169–199. Springer, Cham (2021). https://doi.org/10.1007/978-3-030-73488-6_5
317. S.M. Carturan et al., Temperature effects on light yield and pulse shape discrimination capability of siloxane based scintillators. Eur. Phys. J. C **80**(11), 1057 (2020). https://doi.org/10.1140/epjc/s10052-020-08640-1
318. T. Marchi et al., Optical properties and pulse shape discrimination in siloxane-based scintillation detectors. Sci. Rep. **9**(1), 9154 (2019). https://doi.org/10.1038/s41598-019-45307-8
319. F. Pino et al., Novel flexible and conformable composite neutron scintillator based on fully enriched lithium tetraborate. Sci. Rep. **13**, 4799 (2023)
320. I. Fratelli, *BEYOND (FlexiBlE hYbrid neutrON Detector)* (Young Researcher Grant, Vth Commission, INFN, 2023)
321. M. Toppi et al., Elemental fragmentation cross sections for a ^{16}O beam of 400 MeV/u kinetic energy interacting with a graphite target using the foot ΔE-ΔTOF detectors. Front. Phys. **10**(979229), 1–16 (2022). https://doi.org/10.3389/fphy.2022.979229
322. I. Mattei et al., Measurement of ^{12}C fragmentation cross sections on C, O and H in the energy range of interest for particle therapy applications. IEEE Trans. Radiat. Plasma Med. Sci. **4**(19547434), 269–282 (2020). https://doi.org/10.1109/TRPMS.2020.2972197
323. M. Durante, H. Paganetti, Nuclear physics in particle therapy: a review. Rep. Prog. Phys. **79**(9), 1–59 (2016). https://doi.org/10.1088/0034-4885/79/9/096702
324. J.W. Norbury et al., Are further cross section measurements necessary for space radiation protection or ion therapy applications? Helium projectiles. Front. Phys. **8**(565954), 1–30 (2020). https://doi.org/10.3389/fphy.2020.565954
325. M. Durante, Space radiation protection: destination Mars. Life Sci. Space Res. **1**, 2–9 (2014). https://doi.org/10.1016/j.lssr.2014.01.002
326. V. Patera et al., FOOTPRINT (Forward neutrOn prOducTion exPeRImeNT). PRIN: Progetti di Ricerca di Rilevante Interesse Nazionale - Bando 2020 Prot. 2020249XWA (2020)
327. T. Shiraishi et al., Environmental sub-MeV neutron measurement at the Gran Sasso surface laboratory with a super-fine-grained nuclear emulsion detector. Phys. Rev. C **107**, 014608 (2023). https://doi.org/10.1103/PhysRevC.107.014608
328. M. Durante, F.A. Cucinotta, Physical basis of radiation protection in space travel. Rev. Mod. Phys. **83**, 1245–1281 (2011). https://doi.org/10.1103/RevModPhys.83.1245
329. J.W. Norbury, J. Miller, Physical basis of radiation protection in space travel. Rev. Mod. Phys. **5**(103), 640–642 (2011). https://doi.org/10.1097/HP.0b013e318261fb7f
330. Y. Dong et al., The drift chamber detector of the foot experiment: performance analysis and external calibration. Nuclear Instrum. Methods Phys. Res. Sect. A **164756**, 1–8 (2021). https://doi.org/10.1016/j.nima.2020.164756
331. G. Traini et al., Performance of the TOF detectors in the foot experiment. IL NUOVO CIMENTO C **164756**, 1–8 (2020). https://doi.org/10.1016/j.nima.2020.164756
332. G. Silvestre et al., Characterization of 150 μ m thick silicon microstrip prototype for the FOOT experiment. IL NUOVO CIMENTO C **17**, 1–15 (2022). https://doi.org/10.1088/1748-0221/17/12/P12012
333. G.F. Knoll, *Radiation Detector and Measurements, 3rd Edition, Chapter 10, pp. 344–345, ISBN 978-0-470-13148-0* (Inc, J. Wiley & Sons, 2000)
334. N. Agafonova et al., Discovery of τ neutrino appearance in the CNGS neutrino beam with the OPERA experiment. Phys. Rev. Lett. **115**(121802), 1–7 (2015). https://doi.org/10.1103/PhysRevLett.115.121802
335. S. Alef, The BGOOD experimental setup at ELSA. Eur. Phys. J. A **56**(104), 27 (2020). https://doi.org/10.1140/epja/s10050-020-00107-x
336. W.P. Abfalterer et al., Measurement of neutron total cross sections up to 560 MeV. Phys. Rev. C **63**, 044608 (2001). https://doi.org/10.1103/PhysRevC.63.044608
337. R. Arndt, R.A. Workman, Nuclear Data Standards for Nuclear Measurements, H. Conde, Ed., NEANDC - 311 "U"/INDC(SEC)-101, (1992) 17 (1992)
338. R.A. Arndt et al., Nucleon-nucleon partial-wave analysis to 1.6 GeV. Phys. Rev. D **45**, 3995 (1992). https://doi.org/10.1103/PhysRevD.45.3995
339. R.A. Arndt et al., Updated analysis of NN elastic scattering data to 16 GeV. Phys. Rev. D **50**, 2731 (1994). https://doi.org/10.1103/PhysRevC.50.2731
340. J. Hu et al., Recoil-proton track imaging as a new way for neutron spectrometry measurements. Sci. Rep. **8**, 13363 (2018). https://doi.org/10.1038/s41598-018-31711-z
341. S.M. Valle et al., The MONDO project: a secondary neutron tracker detector for particle therapy. NIM A **845**, 556–559 (2017). https://doi.org/10.1016/j.nima.2016.05.001
342. E. Gioscio et al., Development of a novel neutron tracker for the characterisation of secondary neutrons emitted in particle therapy. NIM A **958**(162862), 1–4 (2020). https://doi.org/10.1016/j.nima.2019.162862
343. G. Wang et al., Optical method based on a gaseous scintillator for neutron energy spectrum measurements. J. Appl. Spectrosc. **87**, 911–918 (2020). https://doi.org/10.1007/s10812-020-01088-x
344. R.S. Miller et al., Sontrac: an imaging spectrometer for MeV neutrons. NIM A **505**, 36–40 (2003). https://doi.org/10.1016/S0168-9002(03)01015-5
345. G.A. De Nolfo et al., SOlar Neutron TRACking (SONTRAC) Concept. PoS (ICRC2019) **358** 1074, (2019). https://doi.org/10.22323/1.358.1074
346. J.G. Mitchell et al., Development of the Solar Neutron TRACking (SONTRAC) Concept. PoS (ICRC2021) **395**(1250) (2021). https://doi.org/10.22323/1.395.1250
347. M. Marafini et al., MONDO: a neutron tracker for particle therapy secondary emission characterisation. Phys. Med. Biol. **62**(8), 3299–3312 (2017). https://doi.org/10.1088/1361-6560/aa623a
348. Z. Wang, C.L. Morris, Tracking fast neutrons. NIM A **726**, 145–154 (2021). https://doi.org/10.1016/j.nima.2013.05.167
349. P. Console Camprini et al., A proton-recoil track imaging system for fast neutrons: the riptide detector. JINST **18**, C01054 (2023). https://doi.org/10.1088/1748-0221/18/01/C01054
350. C. Massimi et al., Riptide—an innovative recoil-proton track imaging detector. JINST **17**, C09026 (2023). https://doi.org/10.1088/1748-0221/17/09/C09026
351. A. Musumarra et al., Riptide: a novel recoil-proton track imaging detector for fast neutrons. JINST **16**, C12013 (2021). https://doi.org/10.1088/1748-0221/16/12/C12013
352. M. Filipenko et al., Three-dimensional photograph of electron tracks through a plastic scintillator. Eur. Phys. J. C **74**, 3131 (2014). https://doi.org/10.1140/epjc/s10052-014-3131-9
353. S. Agostinelli et al., Geant4-a simulation toolkit. NIM A (2003). https://doi.org/10.1016/S0168-9002(03)01368-8
354. N. Terranova et al., Monte Carlo simulations and n-p differential scattering data measured with Proton Recoil Telescopes. EPJ Web Conf. (2020). https://doi.org/10.1051/epjconf/202023901024
355. X. Llopart et al., Timepix4, a large area pixel detector readout chip which can be tiled on 4 sides providing sub-200 ps timestamp binning. JINST **17**, C01044 (2022). https://doi.org/10.1088/1748-0221/17/01/C01044
356. M. Deveaux et al., Observations on mimosis-0, the first dedicated cps prototype for the CBM MVD. NIM A **958**, 162653 (2020). https://doi.org/10.1016/j.nima.2019.162653

357. A.S. Tremsin, J.V. Vallerga, Unique capabilities and applications of microchannel plate (MCP) detectors with medipix/timepix readout. Radiat. Measurem. **130**, 106228 (2020). https://doi.org/10.1016/j.radmeas.2019.106228
358. M. Fiorini, J. Alozy, M. Bolognesi, M. Campbell, A.C. Ramusino, X. LLopart, T. Michel, S. Schifano, A. Tremsin, J. Vallerga, Single-photon imaging detector with $\mathcal{O}(10)$ ps timing and sub-10 μ m position resolutions. J. Instrum. **13**(12), 12005 (2018)
359. K. Gunzert-Marx, D. Schartd, R.S. Simon, Fast neutrons produced by nuclear fragmentation in treatment irradiations with 12C beam. Radiat. Prot. Dosim. **110**, 595 (2004). https://doi.org/10.1093/rpd/nch138
360. M. Hultqvist, I. Gudowska, Secondary absorbed doses from light ion irradiation in anthropomorphic phantoms representing an adult male and a 10 year old child. Phys. Med. Biol. **55**(22), 6633 (2010). https://doi.org/10.1088/0031-9155/55/22/004
361. M. Marafini et al., Mondo: a neutron tracker for particle therapy secondary emission fluxes measurements. Nuclear Instrum. Methods Phys. Res. Sect. A Accel. Spectrom. Detect. Assoc. Equip. **824**, 210–211 (2016). https://doi.org/10.1016/j.nima.2015.10.109
362. R. Mirabelli et al., The MONDO detector prototype development and test: steps toward an SPAD-CMOS-based integrated readout (SBAM sensor). IEEE Trans. Nuclear Sci. **65**(2), 744–751 (2018). https://doi.org/10.1109/TNS.2017.2785768
363. E. Manuzzato et al., A 16 x 8 Digital-SiPM array with distributed trigger generator for low SNR particle tracking. IEEE Int. Solid-State Circuits Conf. (ISSCC) Dig. Tech. Papers **2**(9), 75–78 (2019). https://doi.org/10.1109/LSSC.2019.2934598
364. M. Toppi et al., The MONDO tracker: characterisation and study of secondary ultrafast neutrons production in carbon ion radiotherapy. Front. Phys. **8**, 567990 (2020). https://doi.org/10.3389/fphy.2020.567990
365. F. Sauli, Gem: A new concept for electron amplification in gas detectors. Nuclear Instrum. Methods Phys. Res. Sect. A Accel. Spectrom. Detect. Assoc. Equip. **386**(2), 531–534 (1997). https://doi.org/10.1016/S0168-9002(96)01172-2
366. R. Bellazzini et al., A novel gaseus x-ray polarimeter: Data analysis and simulation, vol. 4843 (2002). https://doi.org/10.1117/12.459381
367. A.L. Peirson et al., Deep ensemble analysis for imaging x-ray polarimetry. Nuclear Instrum. Methods Phys. Res. Sect. A Accel. Spectrom. Detect. Assoc. Equip. **986**, 164740 (2021). https://doi.org/10.1016/j.nima.2020.164740
368. L. Baldini et al., Design, construction, and test of the gas pixel detectors for the IXPE mission. Astropart. Phys. **133**, 102628 (2021). https://doi.org/10.1016/j.astropartphys.2021.102628
369. R. Bellazzini et al., Direct reading of charge multipliers with a self-triggering CMOS analog chip with 105k pixels at 50 μ m pitch. Nucl. Instrum. Methods Phys. Res. A Accel. Spectrom. Detect. Assoc. Equip. **566**(2), 552–562 (2006). https://doi.org/10.1016/j.nima.2006.07.036
370. M. Minuti et al., XPOL-III: A new-generation VLSI CMOS ASIC for high-throughput X-ray polarimetry. Nuclear Instrum. Methods Phys. Res. Sect. A Accel. Spectrom. Detect. Assoc. Equip. **1046**, 167674 (2023). https://doi.org/10.1016/j.nima.2022.167674
371. S. Biri et al., Innovative experimental setup for X-ray imaging to study energetic magnetized plasmas. J. Instrum. **16**, P03003 (2021). https://doi.org/10.1088/1748-0221/16/03/P03003
372. D. Mascali et al., A novel approach to β-decay: PANDORA, a new experimental setup for future in-plasma measurements. Universe (2022). https://doi.org/10.3390/universe8020080
373. D. Mascali et al., *Nuclear Phys. Astrophys. Plasma Traps* (Frontiers Media SA, Lausanne, 2023). https://doi.org/10.3389/978-2-83251-062-9
374. B. Mishra et al., A novel numerical tool to study electron energy distribution functions of spatially-anisotropic and non-homogeneous ECR plasmas. Plasma Phys. **28**, 102509 (2021). https://doi.org/10.1063/5.0061368
375. Eugenia Naselli, Laboratory magnetoplasmas as an ideal experimental environment for nuclear astrophysics ay studies. EPJ Web Conf. **275**, 02008 (2023). https://doi.org/10.1051/epjconf/202327502008
376. G.Q. Zhao et al., Cyclotron maser emission from power-law electrons with strong pitch-angle anisotropy. APJ (2016). https://doi.org/10.3847/0004-637X/822/2/58
377. S. Vichi et al., An innovative gamma-ray spectrometry system using a compact and portable CZT detector for radionuclidic purity tests of pet radiopharmaceuticals. Radiat. Effects Defects Solids **171**(9–10), 726–735 (2016)
378. N. Auricchio et al., Evaluation of the spectroscopic performance of 3D CZT drift strip detectors. In: 2021 IEEE Nuclear Science Symposium and Medical Imaging Conference (NSS/MIC), pp. 1–8 (IEEE, 2021)
379. J. McEnery et al., All-sky medium energy gamma-ray observatory: exploring the extreme multimessenger universe. arXiv preprint arXiv:1907.07558 (2019)
380. L. Abbene et al., Recent advances in the development of high-resolution 3D cadmium-zinc-telluride drift strip detectors. J. Synchrotron Radiat. **27**(6), 1564–1576 (2020)
381. S. Del Sordo et al., The badg3r prototype on board of a stratospheric balloon flight in the framework of the hemera program. In: 25th ESA Symposium on Rocket & Balloon Programmes and Related Researchs, pp. 1–5 (2022)
382. J. Hong et al., Building large area CZT imaging detectors for a wide-field hard X-ray telescope-protoexist1. Nuclear Instrum. Methods Phys. Res. Sect. A Accel. Spectrom. Detect. Assoc. Equip. **605**(3), 364–373 (2009)
383. W. Duvall et al., Reduced isotope dose and imaging time with a high-efficiency CZT spect camera. J. Nuclear Cardiol. **18**, 847–857 (2011)
384. K. Iniewski, CZT detector technology for medical imaging. J. Instrum. **9**(11), 11001 (2014)
385. S. Fatemi et al., High performance 3d czt spectro-imager for bnct-spect: Preliminary characterization. In: 2018 IEEE Nuclear Science Symposium and Medical Imaging Conference Proceedings (NSS/MIC), pp. 1–3 (IEEE, 2018)
386. F. Rupcich, T. Gilat-Schmidt, Experimental study of optimal energy weighting in energy-resolved CT using a CZT detector. In: Medical Imaging 2013: Physics of Medical Imaging, vol. 8668, pp. 511–518 (SPIE, 2013)
387. S. Fatemi et al., High performance 3d czt spectro-imager for bnct-spect: Preliminary characterization. In: 2018 IEEE Nuclear Science Symposium and Medical Imaging Conference Proceedings (NSS/MIC), pp. 1–3 (IEEE, 2018)
388. L. Abbene et al., Potentialities of high-resolution 3-D CZT drift strip detectors for prompt gamma-ray measurements in BNCT. Sensors **22**(4), 1502 (2022)
389. N. Sarzi Amadè et al., Gamma-ray spectral unfolding of CDZNTE-based detectors using a genetic algorithm. Sensors **20**(24), 7316 (2020)
390. J. Aleotti et al., Detection of nuclear sources by UAV teleoperation using a VISUO-haptic augmented reality interface. Sensors **17**(10), 2234 (2017)
391. J. Aleotti et al., Haptic teleoperation of UAV equipped with gamma-ray spectrometer for detection and identification of radio-active materials in industrial plants. Factories of the Future: The Italian Flagship Initiative, pp. 197–214 (2019)
392. L. Menzio et al., Sicura: a new handheld radionuclide identification device with gamma and neutron response. J. Instrum. **16**(07), 07051 (2021). https://doi.org/10.1088/1748-0221/16/07/P07051
393. L. Abbene et al., Room-temperature X-ray response of cadmium-zinc-telluride pixel detectors grown by the vertical bridgman technique. J. Synchrotron Radiat. **27**(2), 319–328 (2020)
394. S. Tsigaridas et al., Fabrication of small-pixel CDZNTE sensors and characterization with X-rays. Sensors **21**(9), 2932 (2021)
395. O. Baussens et al., Characterization of high-flux CDZNTE with optimized electrodes for 4th generation synchrotrons. J. Instrum. **17**(11), 11008 (2022)

396. N. Sévelin-Radiguet, Towards a dynamic compression facility at the ESRF. J. Synchrotron Radiat. **29**(1), 167–169 (2022). https://doi.org/10.1107/S1600577521011632
397. O. Mathon et al., X-ray absorption and X-ray emission spectroscopy: theory and applications, Ch.8: Time-Resolved XAS Using an Energy Dispersive Spectrometer: Techniques and Applications. John Wiley & Sons, 185–212 (2016). https://doi.org/10.1002/9781118844243
398. R. Torchio et al., Probing local and electronic structure in Warm Dense Matter: single pulse synchrotron x-ray absorption spectroscopy on shocked Fe. Sci. Rep. **6**, 26402 (2016). https://doi.org/10.1038/srep26402
399. M. Borri et al., Customisation and verification tests of a LN2 cryostat for a cryogenic Compton camera. IEEE Nuclear Science Symposium and Medical Imaging Conference N-03-NSS-Posters-I(Poster NSS-03-103), 1019 (2022)
400. G. Maggioni et al., Pulsed laser diffusion of thin hole-barrier contacts in high purity germanium for gamma radiation detectors. Eur. Phys. J. A **54**(3), 34 (2018). https://doi.org/10.1140/epja/i2018-12471-0
401. D. Greiffenberg et al., Characterization of chromium compensated gaas sensors with the charge-integrating jungfrau readout chip by means of a highly collimated pencil beam. Sensors (2021). https://doi.org/10.3390/s21041550
402. M. Meyer et al., Observation of radiation damage in CDTE Schottky sensors created by 20 KeV photons. J. Instrum. **17**(06), 06035 (2022). https://doi.org/10.1088/1748-0221/17/06/P06035
403. M. Carulla et al., Study of the internal quantum efficiency of FBK sensors with optimized entrance windows. J. Instrum. **18**(01), 01073 (2023). https://doi.org/10.1088/1748-0221/18/01/C01073
404. J. Zhang et al., Development of LGAD sensors with a thin entrance window for soft x-ray detection. J. Instrum. **17**(11), 11011 (2022). https://doi.org/10.1088/1748-0221/17/11/C11011
405. A. Bergamaschi et al., The MYTHEN detector for X-ray powder diffraction experiments at the Swiss Light Source. J. Synchrotron Radiat. **17**(5), 653–668 (2010). https://doi.org/10.1107/S0909049510026051. (**Number: 5 Publisher: International Union of Crystallography. Accessed 2020-09-13**)
406. G. Tinti et al., Performance of the EIGER single photon counting detector. J. Instrum. **10**, 03011–03011 (2015). https://doi.org/10.1088/1748-0221/10/03/c03011. (**Publisher: IOP Publishing**)
407. J. Zhang et al., Design and first tests of the Gotthard-ii readout ASIC for the European X-ray free-electron laser. J. Instrum. **16**(04), 04015 (2021). https://doi.org/10.1088/1748-0221/16/04/P04015
408. A. Mozzanica et al., Characterization results of the Jungfrau full scale readout ASIC. J. Instrum. **11**(02), 02047 (2016). https://doi.org/10.1088/1748-0221/11/02/C02047
409. M. Ramilli et al., Measurements with MÖNCH, a 25 μ m pixel pitch hybrid pixel detector. J. Instrum. **12**(01), 01071–01071 (2017). https://doi.org/10.1088/1748-0221/12/01/c01071
410. S. Cartier et al., Micrometer-resolution imaging using MÖNCH: towards G_2-less grating interferometry. J. Synchrotron Radiat. **23**(6), 1462–1473 (2016). https://doi.org/10.1107/S1600577516014788
411. K.D. Irwin, G.C. Hilton, Transition-edge sensors. Top. Appl. Phys. **99**, 63–150 (2005). https://doi.org/10.1007/10933596_3
412. D.H. Andrews et al., Attenuated superconductors I for measuring infra-red radiation. Rev. Sci. Instrum. **13**(7), 281–292 (1942). https://doi.org/10.1063/1.1770037
413. L. Gottardi, K. Nagayashi, A Review of X-ray microcalorimeters based on superconducting transition edge sensors for astrophysics and particle physics. Appl. Sci. **11**(9), 3793 (2021). https://doi.org/10.3390/app11093793. arXiv:2210.06914 [astro-ph.IM]
414. S.J. Smith, Performance of a broad-band, high-resolution, transition-edge sensor spectrometer for x-ray astrophysics. IEEE Trans. Appl. Supercond. **31**(5), 1–6 (2021). https://doi.org/10.1109/TASC.2021.3061918
415. T. Okumura et al., Deexcitation dynamics of muonic atoms revealed by high-precision spectroscopy of electronic k x rays. Phys. Rev. Lett. **127**, 053001 (2021). https://doi.org/10.1103/PhysRevLett.127.053001
416. T. Hashimoto et al., Measurements of strong-interaction effects in kaonic-helium isotopes at sub-ev precision with x-ray microcalorimeters. Phys. Rev. Lett. **128**, 112503 (2022). https://doi.org/10.1103/PhysRevLett.128.112503
417. M.D. Yoho et al., Improved plutonium and americium photon branching ratios from microcalorimeter gamma spectroscopy. Nucl. Instrum. Meth. A **977**, 164307 (2020). https://doi.org/10.1016/j.nima.2020.164307. arXiv:2005.10304 [nucl-ex]
418. A.D. Tollefson et al., Measurement of ^{227}Ac impurity in ^{225}Ac using decay energy spectroscopy. Appl. Radiat. Isot. **172**, 109693 (2021). https://doi.org/10.1016/j.apradiso.2021.109693. arXiv:2102.02813 [physics.ins-det]
419. K. Nakamura et al., Development of a microcalorimeter with transition edge sensor for detection of LX rays emitted by transuranium elements. Radiat. Protect. Dosim. **146**(1–3), 88–91 (2011). https://doi.org/10.1093/rpd/ncr118
420. D.J. Mercer et al., Gamma and decay energy spectroscopy measurements of trinitite. Nuclear Technol. **207**(sup1), 309–320 (2021). https://doi.org/10.1080/00295450.2021.1922258
421. C. Curceanu, C. Guaraldo, M. Iliescu, M. Cargnelli, R. Hayano, J. Marton, J. Zmeskal, T. Ishiwatari, M. Iwasaki, S. Okada, D.L. Sirghi, H. Tatsuno, The modern era of light kaonic atom experiments. Rev. Mod. Phys. **91**, 025006 (2019). https://doi.org/10.1103/RevModPhys.91.025006
422. A. Scordo, V. De Leo, C. Curceanu, M. Miliucci, F. Sirghi, Efficiency measurements and simulations of a HAPG based Von Hamos spectrometer for large sources. J. Anal. At. Spectrom. **36**, 2485–2491 (2021). https://doi.org/10.1039/D1JA00214G
423. A. Scordo, C. Curceanu, M. Miliucci, F. Sirghi, J. Zmeskal, Pyrolitic graphite mosaic crystal thickness and mosaicity optimization for an extended source Von Hamos x-ray spectrometer. Cond. Matter (2019). https://doi.org/10.3390/condmat4020038
424. V. De Leo, A. Scordo, C. Curceanu, M. Miliucci, F. Sirghi, Reflection efficiency and spectra resolutions ray-tracing simulations for the VOXES HAPG crystal based Von Hamos spectrometer. Condens. Matter (2022). https://doi.org/10.3390/condmat7010001
425. R.L. Workman et al., Review of particle physics. PTEP (2022). https://doi.org/10.1093/ptep/ptac097
426. J.P. Lees et al., Measurement of the mass of the D^0 meson. Phys. Rev. D **88**, 071104 (2013). https://doi.org/10.1103/PhysRevD.88.071104
427. S. Wycech, B. Loiseau, An advantage of “upper levels”. Acta Phys. Polon. B **51**, 109 (2020). https://doi.org/10.5506/APhysPolB.51.109
428. C. Curceanu et al., Fundamental physics at the strangeness frontier at DAFNE. Outline of a proposal for future measurements (2021)
429. L. Anklamm, C. Schlesiger, W. Malzer, D. Grötzsch, M. Neitzel, B. Kanngießer, A novel Von Hamos spectrometer for efficient x-ray emission spectroscopy in the laboratory. Rev. Sci. Instrum. **85**, 053110 (2014)
430. A. Goasduff et al., The GALILEO γ-ray array at the Legnaro National Laboratories. Nuclear Instrum. Methods Phys. Res. Sect. A Accel. Spectrom. Detect. Assoc. Equip. **1015**, 165753 (2021). https://doi.org/10.1016/j.nima.2021.165753
431. A. Wiens et al., The AGATA triple cluster detector. Nuclear Instrum. Methods Phys. Res. Sect. A Accel. Spectrom. Detect. Assoc. Equip. **618**(1–3), 223–233 (2010). https://doi.org/10.1016/j.nima.2010.02.102
432. J. Eberth, J. Simpson, From GE (LI) detectors to gamma-ray tracking arrays-50 years of gamma spectroscopy with germanium detectors. Prog. Particle Nuclear Phys. **60**(2), 283–337 (2008). https://doi.org/10.1016/j.ppnp.2007.09.001
433. M. Berst, J. Eberth, H. Jäger, H. Kämmerling, R. Lieder, W. Renfile, Process for Producing an Encapsulated Detector. WO1995003556A1 (July 1993)

434. M. Berst, J. Eberth, H. Jäger, H. Kämmerling et al., Enclosure for a Detector Operating in an Ultra-high Vacuum. WO1995003555A1 (July 1993)
435. F. Crespi, F. Camera, B. Million, M. Sassi, O. Wieland, A. Bracco, A novel technique for the characterization of a HPGE detector response based on pulse shape comparison. Nuclear Instrum. Methods Phys. Res. Sect. A Accel. Spectrom. Detect. Assoc. Equip. **593**(3), 440–447 (2008). https://doi.org/10.1016/j.nima.2008.05.057
436. F. Cristiano, A. La Magna, Laser annealing processes in semiconductor technology: theory. In: Modeling and Applications in Nanoelectronics. Woodhead Publishing, United Kingdom (2021)
437. L. Darken, Role of disordered regions in fast-neutron damage of HPGE detectors. Nuclear Instrum. Methods Phys. Res. Sect. B Beam Interact. Mater. Atoms **74**(4), 523–526 (1993). https://doi.org/10.1016/0168-583X(93)95951-Z
438. D. De Salvador, G. Maggioni, E. Napolitani, D.R. Napoli, Patent: P+ or N+ type doping process for semiconductors. W02021214028A1 (October 2021)
439. W. Raniero, G. Maggioni, S. Bertoldo, S. Carturan, F. Sgarbossa, Segmented hyperpure germanium detector. Il Nuovo Cimento C **44**(4–5), 1–4 (2021). https://doi.org/10.1393/ncc/i2021-21154-x
440. S. Carturan, G. Maggioni, S. Rezvani, R. Gunnella, N. Pinto et al., Wet chemical treatments of high purity GE crystals for γ-ray detectors: surface structure, passivation capabilities and air stability. Mater. Chem. Phys. **161**, 116–122 (2015). https://doi.org/10.1016/j.matchemphys.2015.05.022
441. G. Maggioni, D. Napoli, J. Eberth, M. Gelain, S. Carturan et al., Characterization of different surface passivation routes applied to a planar HPGE detector. Eur. Phys. J. A **51**, 1–9 (2015). https://doi.org/10.1140/epja/i2015-15141-9
442. G. Maggioni, S. Carturan, L. Fiorese, N. Pinto et al., Germanium nitride and oxynitride films for surface passivation of GE radiation detectors. Appl. Surface Sci. **393**, 119–126 (2017). https://doi.org/10.1016/j.apsusc.2016.10.006
443. F. Sgarbossa, A. Levarato, S.M. Carturan, G.A. Rizzi, C. Tubaro et al., Phosphorus precursors reactivity versus hydrogenated GE surface: towards a reliable self-limited monolayer doping. Appl. Surface Sci. **541**, 148532 (2021). https://doi.org/10.1016/j.apsusc.2020.148532
444. F. Sgarbossa, G. Maggioni, G.A. Rizzi, S.M. Carturan et al., Self-limiting SB monolayer as a diffusion source for GE doping. Appl. Surface Sci. **496**, 143713 (2019). https://doi.org/10.1016/j.apsusc.2019.143713
445. G. Maggioni, F. Sgarbossa, E. Napolitani, W. Raniero et al., Diffusion doping of germanium by sputtered antimony sources. Mater. Sci. Semicond. Process. **75**, 118–123 (2018). https://doi.org/10.1016/j.mssp.2017.11.026
446. F. Sgarbossa, Germanium monolayer doping: successes and challenges for the next generation GE devices. Mater. Sci. Semicond. Process. **167**, 107795 (2023). https://doi.org/10.1016/j.mssp.2023.107795
447. S. Capra, A. Pullia, Design and experimental validation of an integrated multichannel charge amplifier for solid-state detectors with innovative spectroscopic range booster. IEEE Trans. Nuclear Sci. **67**(8), 1877–1884 (2020). https://doi.org/10.1109/TNS.2020.3006892
448. S. Capra, D. Mengoni, R. Aliaga, A. Gadea, V. Gonzalez, A. Pullia, Design of an integrated low-noise, low-power charge sensitive preamplifier for γ and particle spectroscopy with solid state detectors. In: 2014 IEEE Nuclear Science Symposium and Medical Imaging Conference (NSS/MIC), pp. 1–4 (IEEE, 2014). https://doi.org/10.1109/NSSMIC.2014.7431043
449. A. Beckers, F. Jazaeri, C. Enz, Cryogenic MOS transistor model. IEEE Trans. Electron Devices **65**(9), 3617–3625 (2018). https://doi.org/10.1109/TED.2018.2854701
450. A. Beckers, F. Jazaeri, C. Enz, Cryogenic mosfet threshold voltage model. In: ESSDERC 2019-49th European Solid-State Device Research Conference (ESSDERC), pp. 94–97 (IEEE, 2019). https://doi.org/10.1109/ESSDERC.2019.8901806
451. K. Takahashi, K. Yokoi, Beta-decay rates of highly ionized heavy atoms in stellar interiors. Atomic Data Nuclear Data Tables **36**(3), 375–409 (1987). https://doi.org/10.1016/0092-640X(87)90010-6
452. J.N. Bahcall, Theory of bound-state beta decay. Phys. Rev. **124**(2), 495 (1961). https://doi.org/10.1103/PhysRev.124.495
453. D. Mascali, S. Palmerini, G. Torrisi, G. De Angelis et al., Nuclear Physics and Astrophysics in Plasma Traps vol. 16648714. Frontiers Media SA, (2023)
454. E. Naselli, D. Santonocito, S. Amaducci, L. Celona et al., Design study of a HPGE detector array for β-decay investigation in laboratory ECR plasmas. Front. Phys. (2022). https://doi.org/10.3389/fphy.2022.935728
455. D. Di Vita, L. Buonanno, F. Canclini, G. Ticchi et al., A 144-SiPM 3" LaBr3 readout module for PMTs replacement in gamma spectroscopy. Nuclear Instrum. Methods Phys. Res. Sect. A Accel. Spectrom. Detect. Assoc. Equip. **1040**, 167179 (2022). https://doi.org/10.1016/j.nima.2022.167179
456. G. Montagnani, L. Buonanno, D. Di Vita, M. Carminati, F. Camera, A. Gola, V. Regazzoni, C. Fiorini, Spectroscopic performance of a Sr co-doped 3" LaBr3 scintillator read by a SIPM array. Nuclear Instrum. Methods Phys. Res. Sect. A Accel. Spectrom. Detect. Assoc. Equip. **931**, 158–161 (2019). https://doi.org/10.1016/j.nima.2019.03.067
457. A. Giaz, L. Pellegri, S. Riboldi, F. Camera, N. Blasi et al., Characterization of large volume $3.5'' \times 8'' labr_3{:}ce$ detectors. Nuclear Instrum. Methods Phys. Res. Sect. A Accel. Spectrom. Detect. Assoc. Equip. **729**, 910–921 (2013). https://doi.org/10.1016/j.nima.2013.07.084
458. D. Di Vita et al., To be submitted. IEEE Transactions on Nuclear Science -(-), (2023)
459. L. Bandiera, V. Tikhomirov, M. Romagnoni, N. Argiolas, E. Bagli, G. Ballerini et al., Strong reduction of the effective radiation length in an axially oriented scintillator crystal. Phys. Rev. Lett. **121**(2), 021603 (2018). https://doi.org/10.1103/PhysRevLett.121.021603
460. Particle Therapy Co-Operative Group; https://ptcog.site/ (2024)
461. S. Giordanengo, H. Palmans, Dose detectors, sensors, and their applications. Med. Phys. **45**, 1051 (2018)
462. O. Marti Villarreal et al., Characterization of thin LGAD sensors designed for beam monitoring in proton therapy. In: Nuclear Instruments and Methods in Physics Research, Section A (2023)
463. A. Vignati et al., A new detector for the beam energy measurement in proton therapy: a feasibility study. Phys. Med. Biol. **65**, 215030 (2020)
464. V. Ferrero et al., The MERLINO project: characterization of LaBr 3: Ce detectors for stopping power monitoring in proton therapy. J. Instrum. **17**, C11013 (2022)
465. G. Bisogni et al., INSIDE in-beam positron emission tomography system for particle range monitoring in hadrontherapy. J. Med. Imaging **4**, 011005 (2016)
466. V. Ferrero et al., Tonline proton therapy monitoring: clinical test of a silicon-photodetector-based in-beam pet. Sci. Rep. **8**, 4100 (2018)
467. V. Ferrero et al., Double-field hadrontherapy treatment monitoring with the inside in-beam pet scanner: proof of concept. IEEE Trans. Radiat. Plasma Med. Sci. **2**, 588 (2018)
468. G. Traini et al., Review and performance of the dose profiler, a particle therapy treatments online monitor. Physica Medica **65**, 84 (2017)
469. M. Moglioni et al., In-vivo range verification analysis with in-beam PET data for patients treated with proton therapy at CNAO. Front. Oncol. **12**, 929949 (2022)
470. M. Fischetti et al., Inter-fractional monitoring of 12 C ions treatments: results from a clinical trial at the CNAO facility. Sci. Rep. **10**, 20735 (2020)
471. E. Fiorina et al., Detection of interfractional morphological changes in proton therapy: A simulation and in vivo study with the inside in-beam pet. Front. Phys. **8**, 578388 (2021)
472. C. Golnik et al., Range assessment in particle therapy based on prompt γ-ray timing measurements. Phys. Med. Biol. **59**, 5399 (2014)

473. M. Toppi et al., PAPRICA: the pair production imaging chamber proof of principle. Front. Phys. **9**, 568139 (2021)
474. G. Calvi et al., PAPRICA: the pair production imaging chamber. Il Nuovo Cimento C **9**, 568139 (2021)
475. G. Aglieri Rinella et al., The Alpide pixel sensor chip for the upgrade of the Alice inner tracking system, Nuclear Instruments and Methods in Physics Research, Section A (2017)
476. S. Kushpil et al., Recent results from beam tests of the Alpide pixel chip for the upgrade of the Alice inner tracker. IEEE Trans. Nuclear Sci. **66**, 2319 (2019)
477. H. Dong Li et al., Toward a better understanding of the gamma index: investigation of parameters with a surface-based distance method. Med. Phys. **38**, 6730 (2011)
478. V. Ferrero et al., Estimating the stopping power distribution during proton therapy: a proof of concept. Front. Phys. **10**, 971767 (2022)
479. V. Ferrero et al., The merlino project:characterization of LaBr3:Ce detectors for stopping power monitoring in proton therapy. J. Instrum. **10**, 971767 (2022)
480. V. Ferrero, In-vivo treatment verification in particle therapy: from the inside clinical trial to new monitoring approaches. In: Mini- Micro- Nano-Dosimetry and Innovation Technologies in Radiation Oncology Conference (2023)
481. J. Esposito et al., Be target development for the accelerator-based SPES-BNCT facility at INFN Legnaro. Appl. Radiat. Isot. **67**, S270 (2009)
482. I. Postuma et al., A novel approach to design and evaluate BNCT neutron beams combining physical, radiobiological, and dosimetric figures of merit. Biology **10**, 174 (2021)
483. M. Durante, H. Paganetti, Nuclear physics in particle therapy: a review. Rep. Prog. Phys. **79**, 096702 (2016)
484. D. Schardt, T. Elsasser, D. Schulz-Ertner, Heavy-ion tumor therapy: physical and radiobiological benefits. Rev. Mod. Phys. **82**, 383 (2010)
485. G. Battistoni et al., Measuring the impact of nuclear interaction in particle therapy and in radio protection in space: the FOOT experiment. Front. Phys. **8**, 568242 (2021)
486. R. Cirio et al., A simple method to increase the current range of the tera chip in charged particle therapy applications. In: Nuclear Instruments and Methods in Physics Research, Section A (2015)
487. F. Di Martino et al., FLASH radiotherapy with electrons: issues related to the production, monitoring, and dosimetric characterization of the beam. Front. Phys. **8**, 570697 (2020)
488. M. Marinelli et al., Design, realization, and characterization of a novel diamond detector prototype for FLASH radiotherapy dosimetry. Med. Phys. **49**(3), 1902–1910 (2022)
489. F. Gómez et al., Development of an ultra-thin parallel plate ionization chamber for dosimetry in FLASH radiotherapy. Med. Phys. **49**(7), 4705–4714 (2022)
490. R. Bedogni et al., Epd057—a direct-reading dosemeter for FLASH radiotherapy with linear response up to 25 gy/pulse. Physica Medica **94**, 85 (2022). https://doi.org/10.1016/S1120-1797(22)01628-3. (**Abstracts of the FLASH Radiotherapy and Particle Therapy Conference**)
491. C. Verona et al., Toward the use of single crystal diamond based detector for ion-beam therapy microdosimetry. Radiat. Meas. **110**, 25–31 (2018)
492. G. Magrin, C. Verona, M. Ciocca, M. Marinelli, E. Mastella, M. Stock, G.V. Rinati, Microdosimetric characterization of clinical carbon-ion beams using synthetic diamond detectors and spectral conversion methods. Med. Phys. **47**, 713–721 (2020)
493. C. Verona, G.A.P. Cirrone, G. Magrin, M. Marinelli, S. Palomba, G. Petringa, G.V. Rinati, Microdosimetric measurements of a monoenergetic and modulated Bragg peaks of 62 MeV therapeutic proton beam with a synthetic single crystal diamond microdosimeter. Med. Phys. **47**, 5791 (2020)
494. C. Meouchi et al., On the measurement uncertainty of microdosimetric quantities pusing diamond and silicon microdosimeters in carbon-ion beams. Med. Phys. **49**, 6699 (2022)
495. L. De Nardo, V. Cesari, G. Doná, G. Magrin, P. Colautti, V. Conte, G. Tornielli, Mini-tepcs for radiation therapy. Radiat. Prot. Dosim. **108**, 345 (2004)
496. A. Bianchi et al., Repeatability and reproducibility of microdosimetry with a mini-TEPC. Front. Phys. **9**, 727816 (2021)
497. A. Selva et al., Microdosimetry of an accelerator based thermal neutron field for boron neutron capture therapy. Appl. Radiat. Isot. **182**, 110144 (2022)
498. D. Mazzucconi et al., Microdosimetry at nanometric scale with an avalanche-confinemente tepc: response against a helium ion beam. Radiat. Prot. Dosim. **183**, 177–181 (2019)
499. M. Guarrera, G. Petringa, S. Tudisco, G.A.P. Cirrone, Characterization of a sic detector for dosimetric application. IL NUOVO CIMENTO C **100**, 45 (2022)
500. H. Caracciolo et al., Beam diagnostics commissioning at CNAO (2011)
501. M. Large, C. Haspide, Hydrogenated amorphous silicon high flux x-ray detectors for synchrotron microbeam radiation therapy. Phys. Med. Biol. (2023). https://doi.org/10.1088/0031-9155/53/5/017
502. M. Menichelli, C. Haspide, Neutron irradiation of hydrogenated amorphous silicon p-i-n diodes and charge selective contacts detectors. Nuclear Instrum. Methods Phys. Res. Sect. A Accel. Spectrom. Detect. Assoc. Equip. **1052**, 168308 (2023). https://doi.org/10.1016/j.nima.2023.168308
503. S. Lagomarsino et al., Polycrystalline diamond detectors with three-dimensional electrodes. Nuclear Instrum. Methods Phys. Res. Sect. A Accel. Spectrom. Detect. Assoc. Equip. **796**, 42–46 (2015). https://doi.org/10.1016/j.nima.2015.03.041
504. K. Kanxheri et al., Investigation of 3d diamond detector dosimetric characteristics. J. Instrum. **13**, 06006–06006 (2018)
505. A. Porter, K. Kanxheri, I. Lopez Paz, A. Oh, L. Servoli, C. Talamonti, A 3D diamond dosimeter with graphitic surface connections. Diam. Relat. Mater. (2023). https://doi.org/10.1016/j.diamond.2023.109692
506. K. Kanxheri et al., Performance of 3D diamond detectors in small field dosimetry: the impact of pixel size. Physica Medica **102**, 73–78 (2022). https://doi.org/10.1016/j.ejmp.2022.09.006
507. R. Ballabriga, M. Campbell, X. Llopart, An introduction to the Medipix family ASICS. Radiat. Measurem. **136**, 106271 (2020)
508. X. Llopart, J. Alozy, R. Ballabriga, M. Campbell, R. Casanova, V. Gromov, E. Heijne, T. Poikela, E. Santin, V. Sriskaran et al., Timepix4, a large area pixel detector readout chip which can be tiled on 4 sides providing sub-200 ps timestamp binning. J. Instrum. **17**(01), 01044 (2022)
509. R. Longo et al., Advancements towards the implementation of clinical phase-contrast breast computed tomography at Elettra. J. Synchrotron Radiat. **26**(4), 1343–1353 (2019)
510. L. Brombal et al., Image quality comparison between a phase-contrast synchrotron radiation breast CT and a clinical breast CT: a phantom based study. Sci. Rep. **9**(1), 17778 (2019)
511. F. Brun et al., Single-shot k-edge subtraction x-ray discrete computed tomography with a polychromatic source and the Pixie-III detector. Phys. Med. Biol. **65**(5), 055016 (2020)
512. L. Brombal, F. Arfelli, R.H. Menk, L. Rigon, F. Brun, Pepi lab: a flexible compact multi-modal setup for x-ray phase-contrast and spectral imaging. Sci. Rep. **13**(1), 4206 (2023)
513. V. Di Trapani, L. Brombal, F. Brun, Multi-material spectral photon-counting micro-CT with minimum residual decomposition and self-supervised deep denoising. Opt. Express **30**(24), 42995–43011 (2022)
514. R. Ballabriga, J. Alozy, F. Bandi, M. Campbell, N. Egidos, J. Fernandez-Tenllado, E. Heijne, I. Kremastiotis, X. Llopart, B. Madsen et al., Photon counting detectors for x-ray imaging with emphasis on CT. IEEE Trans. Radiat. Plasma Medic. Sci. **5**(4), 422–440 (2020)

515. H. Wei, J. Huang, Halide lead perovskites for ionizing radiation detection. Nat. Commun. **10**(1), 1066 (2019)
516. I. Viola et al., Microfluidic-assisted growth of perovskite single crystals for photodetectors. Adv. Mater. Technol. **8**, 2300023 (2023)
517. X. Zhao et al., Interface engineering for gain perovskite photodetectors with extremely high external quantum efficiency. RSC Adv. **10**(54), 32976–32983 (2020)
518. S. Morganti et al., A wearable radiation measurement system for collection of patient-specific time-activity data in radiopharmaceutical therapy: system design and monte carlo simulation results. Med. Phys. **48**(12), 8117–8126 (2021)
519. E. Solfaroli Camillocci et al., A novel radioguided surgery technique exploiting β^- decays. Sci. Rep. **4**(1), 4401 (2014)
520. F. Collamati et al., Radioguided surgery with β radiation: a novel application with Ga^{6}8. Sci. Rep. **8**(1), 16171 (2018)
521. A. Andrighetto et al., The ISOLPHARM project: ISOL-based production of radionuclides for medical applications. J. Radioanal. Nuclear Chem. **322**(1), 73–77 (2019)
522. Target Lab, Laboratori Nazionali del Sud, INFN: https://www.lns.infn.it/en/targets.html
523. A. Guglielmetti, Studying stars by going underground: the LUNA experiment at Gran Sasso laboratory. EPJ Web Conf. **66**, 07007 (2014)
524. C. Broggini, D. Bemmerer, A. Caciolli, D. Trezzi, Luna: status and prospects. Prog. Particle Nuclear Phys. **98**, 55–84 (2018)
525. A.H.F. Muggleton, Deposition techniques for the preparation of thin film nuclear targets. Vacuum **37**, 785–817 (1987)
526. J.R. Tesmer, M. Nastasi, Handbook of Modern Ion Beam Materials Analysis, (1995)
527. C. Spitaleri, C.A. Bertulani, L. Fortunato, A. Vitturi, The electron screening puzzle and nuclear clustering. Phys. Lett. B **755**, 275–278 (2016)
528. H.J. Assenbaum, K. Langanke, C. Rolfs, Effects of electron screening on low-energy fusion cross sections. Z. Phys. A Atomic Nuclei **327**, 461–468 (1987)
529. F. Strieder, C. Rolfs, C. Spitaleri, P. Corvisiero, Electron-screening effects on fusion reaction. Naturwissenschaften **88**, 461–467 (2001)
530. L. Bracci, G. Fiorentini, V.S. Melezhik, G. Mezzorani, P. Quarati, Atomic effects in the determination of nuclear cross sections of astrophysical interest. Nuclear Phys. A **513**(2), 316–343 (1990)
531. F. Schümann, S. Zavatarelli, L. Giallanella et al., Electron screening in backward elastic scattering. EPJA **2**, 337–342 (1998)
532. G. Arpesella et al., Measurement of the 3He(3He,2p)4He cross section within the solar Gamow peak. Phys. Lett. B **389**(3), 452–456 (1996). https://doi.org/10.1016/S0370-2693(96)01326-3
533. D. Rapagnani et al., A supersonic jet target for the cross section measurement of the $^{12}C(\alpha,\gamma)^{16}$O reaction with the recoil mass separator ERNA. Nucl. Instr. Meth. Phys. Res. B **407**, 217 (2017)
534. C. Purpura, F.D. Filippis, E. Graps, E. Trifoni, R. Savino, The Ghibli plasma wind tunnel: description of the new CIRA-PWT facility. Acta Astronaut. **61**, 331–340 (2007)
535. F. Brandi, L. Lbate, D. Rapagnani, R. Buompane, A. di Leva, L. Gialanella, L.A. Gizzi, Optical and spectroscopic study of a supersonic flowing helium plasma: energy transport in the afterglow. Sci. Rep. **10**, 5087 (2022). https://doi.org/10.1038/s41598-020-61988-y
536. D. Rapagnani et al., Feasibility study of a compact and multi-gas supersonic plasma jet for nuclear astrophysics and space research. Nuclear Instrum. Methods Phys. Res. Sect. A Accel. Spectrom. Detect. Assoc. Equip. **1056**, 168536 (2023). https://doi.org/10.1016/j.nima.2023.168536
537. M. Sedlak et al., The cryogenic targets for direct reactions (ctadir) project. Il Nuovo Cimento C **45**, 108 (2022). https://doi.org/10.1393/ncc/i2022-22108-6
538. A. Goasduff et al., LNL Annual Report **262**(262), 41 (2022)
539. J.-J. Dormard et al., Pulse shape discrimination for grit: beam test of a new integrated charge and current preamplifier coupled with high granularity silicon detectors. Nuclear Instrum. Methods Phys. Res. Sect. A Accel. Spectrom. Detect. Assoc. Equip. **1013**, 165641 (2021). https://doi.org/10.1016/j.nima.2021.165641
540. F. Cappuzzello et al., Shedding light on nuclear aspects of neutrinoless double beta decay by heavy-ion double charge exchange reactions. Prog. Particle Nuclear Phys. **128**, 103999 (2023). https://doi.org/10.1016/j.ppnp.2022.103999
541. S. Calabrese et al., First measurement of the ^{116} Cd (^{20} Ne ,^{20} O)^{116} Sn reaction at 15 A MeV . Acta Phys. Pol. B **49**, 275 (2018)
542. M. Cavallaro et al., A constrained analysis of the 40ca(18o,18f)40k direct charge exchange reaction mechanism at 275 MeV . Front. Astron. Space Sci. **8**, 61 (2021). https://doi.org/10.3389/fspas.2021.659815
543. V. Soukeras et al., Measurement of the double charge exchange reaction for the ^{20} Ne +^{130} Te system at 306 MeV . Res. Phys. **28**, 104691 (2021)
544. M. Cavallaro et al., The MAGNEX magnetic spectrometer for double charge exchange reactions. Nuclear Instrum. Methods Phys. Res. Sect. B Beam Interact. Mater. Atoms **463**, 334–338 (2020). https://doi.org/10.1016/j.nimb.2019.04.069
545. C. Agodi et al., The numen project: toward new experiments with high-intensity beams. Universe **7**, 72 (2021). https://doi.org/10.3390/universe7030072
546. D. Calvo et al., Present outcome from the numen r &d phase. Nuclear Instrum. Methods Phys. Res. Sect. A Accel. Spectrom. Detect. Assoc. Equip. **1041**, 167336 (2022). https://doi.org/10.1016/j.nima.2022.167336
547. F. Iazzi et al., A new cooling technique for targets operating under very intense beams. WIT Trans. Eng. Sci. **116**, 61–70 (2017). https://doi.org/10.2495/MC170071
548. F. Pinna et al., Tests of a cooling system for thin targets submitted to intense ion beams for the numen experiment. Acta Phys. Pol. B **51**, 655 (2020)
549. A. Massara et al., Preparation and characterisation of high oriented pyrolytic graphite backed targets for the numen project. EPJ Web Conf. **285**, 06003 (2023). https://doi.org/10.1051/epjconf/202328506003
550. M. Fisichella et al., Sub-barrier radioactive ion beam investigations using a new methodology and analysis for the stacked target technique. Phys. Rev. C **92**, 064611 (2015). https://doi.org/10.1103/PhysRevC.92.064611
551. J.F. Ziegler, M.D. Ziegler, J.P. Biersack, SRIM—the stopping and range of ions in matter (2010). Nuclear Instrum. Methods Phys. Res. Sect. B Beam Interact. Mater. Atoms **268**(11), 1818–1823 (2010). https://doi.org/10.1016/j.nimb.2010.02.091. (**19th International Conference on Ion Beam Analysis**)
552. A. Andrighetto et al., Spes: an intense source of Neutron-Rich Radioactive Beams at Legnaro. J. Phys. Conf. Ser. **966**(1), 012028 (2018). https://doi.org/10.1088/1742-6596/966/1/012028. (**Publisher: IOP Publishing. Accessed 2023-02-22**)
553. S. Corradetti et al., Effect of graphite and graphene oxide on thorium carbide microstructural and thermal properties. Sci. Rep. **11**(1), 9058 (2021). https://doi.org/10.1038/s41598-021-87621-0
554. S. Corradetti et al., Research and development on materials for the SPES target. EPJ Web Conf. **66**, 11009 (2014). https://doi.org/10.1051/epjconf/20146611009
555. S. Corradetti et al., Nanocrystalline titanium carbide/carbon composites as irradiation targets for isotopes production. Ceram. Int. **46**(7), 9596–9605 (2020). https://doi.org/10.1016/j.ceramint.2019.12.225
556. A. Zanini et al., Sucrose-based sol-gel synthesis of microporous titanium carbide as target material for the production of radioisotopes. Microporous Mesoporous Mater. **337**, 111917 (2022). https://doi.org/10.1016/j.micromeso.2022.111917
557. L. Biasetto et al., Morphological and functional effects of graphene on the synthesis of uranium carbide for isotopes production targets. Sci. Rep. **8**(1), 8272 (2018). https://doi.org/10.1038/s41598-018-26572-5

558. M. Manzolaro et al., Thermal and mechanical characterization of carbides for high temperature nuclear applications. Materials **14**(10), 2689 (2021). https://doi.org/10.3390/ma14102689. (**Accessed 2023-02-23**)
559. L. Silvestroni et al., Novel SiC/C composite targets for the production of radioisotopes for nuclear applications. J. Eur. Ceram. Soc. **42**(14), 6750–6756 (2022). https://doi.org/10.1016/j.jeurceramsoc.2022.07.017. (**Accessed 2023-02-23**)
560. M. Deicher, G. Weyer, T. Wichert, The ISOLDE collaboration: solid state physics at ISOLDE. Hyperfine Interact. **151**(1), 105–123 (2003). https://doi.org/10.1023/B:HYPE.0000020422.39876.97. (**Accessed 2023-02-22**)
561. R. Formento-Cavaier et al., Very high specific activity erbium 169Er production for potential receptor-targeted radiotherapy. Nuclear Instrum. Methods Phys. Res. Sect. B Beam Interact. Mater. Atoms **463**, 468–471 (2020). https://doi.org/10.1016/j.nimb.2019.04.022. (**Accessed 2023-02-22**)
562. C. Müller et al., A unique matched quadruplet of terbium radioisotopes for PET and SPECT and for α- and β-radionuclide therapy: An in vivo proof-of-concept study with a new receptor-targeted folate derivative. J. Nuclear Med. **53**(12), 1951–1959 (2012)
563. C. Müller et al., Future prospects for SPECT imaging using the radiolanthanide terbium-155—production and preclinical evaluation in tumor-bearing mice. Nuclear Med. Biol. **41**, 58–65 (2014). https://doi.org/10.1016/j.nucmedbio.2013.11.002. (**Accessed 2023-02-22**)
564. C. Hoehr et al., Medical Isotope Production at TRIUMF—from Imaging to Treatment. Phys. Procedia **90**, 200–208 (2017). https://doi.org/10.1016/j.phpro.2017.09.059. (**Accessed 2023-02-22**)
565. C. Ramogida et al., Evaluation of polydentate picolinic acid chelating ligands and an α-melanocyte-stimulating hormone derivative for targeted alpha therapy using ISOL-produced 225Ac. EJNMMI Radiopharm. Chem. **4**(1), 21 (2019). https://doi.org/10.1186/s41181-019-0072-5. (**Accessed 2023-02-22**)
566. D.E. Fiaccabrino, P. Kunz, V. Radchenko, Potential for production of medical radionuclides with on-line isotope separation at the ISAC facility at TRIUMF and particular discussion of the examples of 165Er and 155Tb. Nuclear Med. Biol. **94–95**, 81–91 (2021). https://doi.org/10.1016/j.nucmedbio.2021.01.003. (**Accessed 2023-02-22**)
567. F. Borgna et al., A preliminary study for the production of high specific activity radionuclides for nuclear medicine obtained with the isotope separation on line technique. Appl. Radiat. Isot. **127**, 214–226 (2017). https://doi.org/10.1016/j.apradiso.2017.06.022. (**Accessed 2023-02-22**)
568. M. Ballan et al., Preliminary evaluation of the production of non-carrier added 111Ag as core of a therapeutic radiopharmaceutical in the framework of ISOLPHARM_ag experiment. Appl. Radiat. Isot. **164**, 109258 (2020). https://doi.org/10.1016/j.apradiso.2020.109258. (**Accessed 2023-02-22**)
569. M. Ballan et al., Development of implantation substrates for the collection of radionuclides of medical interest produced via ISOL technique at INFN-LNL. Appl. Radiat. Isot. **175**, 109795 (2021). https://doi.org/10.1016/j.apradiso.2021.109795. (**Accessed 2023-02-22**)
570. J. Esposito et al., LARAMED: a laboratory for radioisotopes of medical interest. Molecules **24**(1), 20 (2019). https://doi.org/10.3390/molecules24010020
571. T. Marchi et al., The Spes facility at Legnaro national laboratories. J. Phys. Conf. Ser. **1643**(1), 012036 (2020). https://doi.org/10.1088/1742-6596/1643/1/012036
572. A. Boschi, P. Martini, V. Costa, A. Pagnoni, L. Uccelli, Interdisciplinary tasks in the cyclotron production of radiometals for medical applications. The case of 47sc as example. Molecules (2019). https://doi.org/10.3390/molecules24030444
573. G. Pupillo et al., Nuclear data for light charged particle induced production of emerging medical radionuclides. Radiochimica Acta **110**(6–9), 689–706 (2022). https://doi.org/10.1515/ract-2022-0011
574. H. Skliarova et al., Cyclotron solid targets preparation for medical radionuclides production in the framework of LARAMED project. J. Phys. Conf. Ser. **1548**(1), 012022 (2020). https://doi.org/10.1088/1742-6596/1548/1/012022
575. S. Cisternino et al., Upgrade of the HIVIPP deposition apparatus for nuclear physics thin targets manufacturing. Instruments **6**(3), 23 (2022). https://doi.org/10.3390/instruments6030023
576. G. Pupillo et al., Production of 47Sc with natural vanadium targets: results of the PASTA project. J. Radioanal. Nuclear Chem. **322**(3), 1711–1718 (2019). https://doi.org/10.1007/s10967-019-06844-8
577. G. Pupillo et al., Preliminary results of the PASTA project. Il Nuovo Cimento C **42**(203), 1–4 (2019). https://doi.org/10.1393/ncc/i2019-19139-1. (**Accessed 2023-02-16**)
578. F. Barbaro et al., New results on proton-induced reactions on vanadium for ^{47}Sc production and the impact of level densities on theoretical cross sections. Phys. Rev. C **104**(4), 044619 (2021). https://doi.org/10.1103/PhysRevC.104.044619
579. F. Haddad et al., ARRONAX, a high-energy and high-intensity cyclotron for nuclear medicine. Eur. J. Nuclear Med. Mol. Imaging **35**(7), 1377–1387 (2008). https://doi.org/10.1007/s00259-008-0802-5
580. U. Anselmi-Tamburini, S. Gennari, J.E. Garay, Z.A. Munir, Fundamental investigations on the spark plasma sintering/synthesis process: II. Modeling of current and temperature distributions. Mater. Sci. Eng. A **394**(1), 139–148 (2005). https://doi.org/10.1016/j.msea.2004.11.019
581. S. Cisternino et al., Target manufacturing by Spark Plasma Sintering for efficient 89Zr production. Nuclear Med. Biol. **104–105**, 38–46 (2022). https://doi.org/10.1016/j.nucmedbio.2021.11.004
582. G. Sciacca et al., A universal cassette-based system for the dissolution of solid targets. Molecules **26**(20), 6255 (2021). https://doi.org/10.3390/molecules26206255
583. H. Skliarova et al., Innovative target for production of technetium-99m by biomedical cyclotron. Molecules **24**(1), 25 (2019). https://doi.org/10.3390/molecules24010025
584. H. Skliarova et al., Medical cyclotron solid target preparation by Ultrathick film magnetron sputtering deposition. Instruments **3**(1), 21 (2019). https://doi.org/10.3390/instruments3010021
585. A. Kotliarenko, O. Azzolini, G. Keppel, C. Pira, J. Esposito, Investigation of a possible material-saving approach of sputtering techniques for radiopharmaceutical target production. Appl. Sci. **11**(19), 9219 (2021). https://doi.org/10.3390/app11199219
586. H. Skliarova et al., Recovery of molybdenum precursor material in the cyclotron-based technetium-99m production cycle. Instruments **3**(1), 17 (2019). https://doi.org/10.3390/instruments3010017
587. G. Sciacca et al., Experimental and numerical characterization of pure copper heat sinks produced by laser powder bed fusion. Mater. Des. **214**, 110415 (2022). https://doi.org/10.1016/j.matdes.2022.110415
588. P. Mastinu et al., Status of the LEgnaro NeutrOn Source facility (LENOS). Physics Procedia **26**, 261–273 (2012). https://doi.org/10.1016/j.phpro.2012.03.034
589. P. Mastinu et al., Fast neutrons at LNL Legnaro. J. Neutron Res. **22**(2–3), 233–247 (2020). https://doi.org/10.3233/JNR-200156
590. G. Acosta et al., ANEM: a rotating composite target to produce an atmospheric-like neutron beam at the LNL SPES facility. Int. J. Mod. Phys. Conf. Ser. **44**, 1660207 (2016). https://doi.org/10.1142/S2010194516602076
591. R. Alfonso Barrera et al., CoolGAL: a Galinstan bathed Be fast neutron production target at the NEPIR facility. EPJ Web Conf. **231**, 03002 (2020). https://doi.org/10.1051/epjconf/202023103002

592. G. D'Agostino, L. Calabretta, W. Kleeven, D. Rifuggiato, Upgrade of the Central Region of the Superconducting Cyclotron at INFN-LNS. Proceedings of the 22nd International Conference on Cyclotrons and their Applications Cyclotrons2019, 177–180 (2020). https://doi.org/10.18429/JACOW-CYCLOTRONS2019-TUP011
593. P. Russotto et al., Status and Perspectives of the INFN-LNS In-Flight Fragment Separator. J. Phys. Conf. Ser. **1014**(1), 012016 (2018). https://doi.org/10.1088/1742-6596/1014/1/012016
594. Nuclear Physics Mid Term Plan in Italy Workshop - LNS Session: https://agenda.infn.it/event/28717/
595. N. Martorana et al., Radioactive ion beam opportunities at the new FRAISE facility of INFN-LNS. Front. Phys. **10**, 1058419 (2022)
596. N.S. Martorana, Status of the FraISe facility and diagnostics system. Il Nuovo Cimento C **44**(1), 1–10 (2021). https://doi.org/10.1393/ncc/i2021-21001-2
597. N. Martorana et al., The new fragment in-flight separator at INFN-LNS. Il Nuovo Cimento C **45**(3), 1–7 (2022). https://doi.org/10.1393/ncc/i2022-22063-2
598. F. Risitano, Simulation study of radioactive ion beams production at FRAISE (INFN-LNS). Il Nuovo Cimento C **45**(4), 1–10 (2022). https://doi.org/10.1393/ncc/i2022-22068-9
599. D.J. Morrissey, B.M. Sherrill, In-Flight Separation of Projectile Fragments. In: Al-Khalili, J., Roeckl, E. (eds), The Euroschool Lectures on Physics with Exotic Beams, Vol. I vol. 651, pp. 113–135. Springer, Berlin, Heidelberg (2004). https://doi.org/10.1007/978-3-540-44490-9_4
600. G. Raciti et al., Intermediate energies tagged RIBs. Nuclear Instrum. Methods Phys. Res. Sect. B Beam Interact. Mater. Atoms **266**(19), 4632–4636 (2008). https://doi.org/10.1016/j.nimb.2008.05.153
601. S. Grévy, R. Hue, CLIM : the new rotating target for exotic nuclei production at LISE spectrometer. (2008). https://hal.in2p3.fr/in2p3-00326196
602. R. Anne, M. Alex, LISE 3: A magnetic spectrometer—Wien filter combination for secondary radioactive beam production. Nuclear Instrum. Methods Phys. Res. Sect. B Beam Interact. Mater. Atoms **70**(1), 276–85 (1992). https://doi.org/10.1016/0168-583X(92)95943-L
603. SPES project website: https://web.infn.it/spes/
604. F. Herfurth et al., A linear radiofrequency ion trap for accumulation, bunching, and emittance improvement of radioactive ion beams. Nuclear Instrum. Methods Phys. Res. Sect. A Accel. Spectrom. Detect. Assoc. Equip. **469**(2), 254–275 (2001). https://doi.org/10.1016/S0168-9002(01)00168-1
605. M. Smith, L. Blomeley, P. Delheij, J. Dilling, First tests of the TITAN digital RFQ beam cooler and buncher. Hyperfine Interact. **173**(1), 171–180 (2006). https://doi.org/10.1007/s10751-007-9554-z
606. T. Eronen, A. Kankainen, J. Äystö, Ion traps in nuclear physics-recent results and achievements. Prog. Particle Nuclear Phys. **91**, 259–293 (2016). https://doi.org/10.1016/j.ppnp.2016.08.001
607. B. Cheal, D.H. Forest, Collinear laser spectroscopy techniques at JYFL. Hyperfine Interact. **223**(1), 63–71 (2014). https://doi.org/10.1007/s10751-012-0608-5
608. P. Delahaye et al., The mora project. Hyperfine Interact. **240**(1), 63 (2019). https://doi.org/10.1007/s10751-019-1611-x
609. G. Arrowsmith-Kron et al., Opportunities for fundamental physics research with radioactive molecules (2023). arXiv:2302.02165 [nucl-ex]
610. G. Sikler, J.R. Crespo López-Urrutia, J. Dilling, S. Epp, C.J. Osborne, J. Ullrich, A high-current EBIT for charge-breeding of radionuclides for the TITAN spectrometer. Eur. Phys. J. A Hadrons Nuclei **25**(1), 63–64 (2005)
611. B. Seiferle et al., Extending our knowledge about the 229th nuclear isomer. Atoms (2022). https://doi.org/10.3390/atoms10010024
612. Spectrometers Accelerators, A versatile triple radiofrequency quadrupole system for cooling, mass separation and bunching of exotic nuclei. Nuclear Instrum. Methods Phys. Res. Sect. A Detect. Assoc. Equip. **880**, 138–151 (2018). https://doi.org/10.1016/j.nima.2017.10.003
613. F. Greiner et al., Removal of molecular contamination in low-energy ribs by the isolation-dissociation-isolation method. Nuclear Instrum. Methods Phys. Res. Sect. B Beam Interact. Mater. Atoms **463**, 324–326 (2020). https://doi.org/10.1016/j.nimb.2019.04.072
614. R.J. Chris et al., Production of radioactive molecular ions in radiofrequency quadrupole gas-reaction cells. J. Phys. Conf. Ser. **2244**(1), 012100 (2022). https://doi.org/10.1088/1742-6596/2244/1/012100
615. R.N. Wolf et al., Isoltrap's multi-reflection time-of-flight mass separator/spectrometer. Int. J. Mass Spectrom. **349–350**, 123–133 (2013). https://doi.org/10.1016/j.ijms.2013.03.020. (**100 years of Mass Spectrometry**)
616. C. Jesch et al., The MR-TOF-MS isobar separator for the TITAN facility at TRIUMF. Hyperfine Interact. **235**(1), 97–106 (2015). https://doi.org/10.1007/s10751-015-1184-2
617. M.P. Reiter et al., Improved beam diagnostics and optimization at ISAC via titan's MR-TOF-MS. Nuclear Instrum. Methods Phys. Res. Sect. B Beam Interact. Mater. Atoms **463**, 431–436 (2020). https://doi.org/10.1016/j.nimb.2019.04.034
618. M. Mougeot et al., Mass measurements of 99–101in challenge ab initio nuclear theory of the nuclide 100sn. Nat. Phys. **17**(10), 1099–1103 (2021). https://doi.org/10.1038/s41567-021-01326-9
619. B. Sönke et al., Mass measurements of neutron-deficient YB isotopes and nuclear structure at the extreme proton-rich side of the $n = 82$ shell. Phys. Rev. Lett. **127**, 112501 (2021). https://doi.org/10.1103/PhysRevLett.127.112501
620. E. Leistenschneider et al., Dawning of the $n = 32$ shell closure seen through precision mass measurements of neutron-rich titanium isotopes. Phys. Rev. Lett. **120**, 062503 (2018). https://doi.org/10.1103/PhysRevLett.120.062503
621. T. Dickel et al., First spatial separation of a heavy ion isomeric beam with a multiple-reflection time-of-flight mass spectrometer. Phys. Lett. B **744**, 137–141 (2015). https://doi.org/10.1016/j.physletb.2015.03.047
622. A. Galatà et al., Towards the first beams from the ADIGE injector for the SPES project. J. Phys. Conf. Ser. **1350**(1), 12090 (2019)
623. A. Maj et al., The Paris project. Acta Physics Polonica B **40**, 565 (2009)
624. J. Diklić et al., Transfer reactions in ^{206}Pb $+^{118}$ Sn : from quasielastic to deep-inelastic processes. Phys. Rev. C **107**, 014619 (2023). https://doi.org/10.1103/PhysRevC.107.014619
625. K. Rudolph, D. Evers, P. Konrad, K.E.G. Löbner, U. Quade, S.J. Skorka, I. Weidl, The Munich RF-recoil spectrometer for the observation of heavy-ion reaction products at zero degree. Nuclear Instrum. Methods Phys. Res. **204**(2), 407–418 (1983). https://doi.org/10.1016/0167-5087(83)90069-8
626. J.M. Figueira et al., The use of the gas-filled magnet technique for the detection of medium mass ions. Nuclear Instrum. Methods Phys. Res. Sect. A Accel. Spectrom. Detect. Assoc. Equip. **670**, 32–39 (2012). https://doi.org/10.1016/j.nima.2011.12.048
627. C. Schmitt et al., New gas-filled mode of the large-acceptance spectrometer VAMOS. Nuclear Instrum. Methods Phys. Res. Sect. A Accel. Spectrom. Detect. Assoc. Equip. **621**(1), 558–565 (2010). https://doi.org/10.1016/j.nima.2010.03.146
628. B.B. Back, The AGFA and AIRIS separators at ATLAS. EPJ Web Conf. **163**, 00003 (2017). https://doi.org/10.1051/epjconf/201716300003
629. J.C. Lighthall et al., Commissioning of the Helios spectrometer. Nucl. Instrum. Meth. A **622**, 97 (2010)
630. P.T. MacGregor et al., Phys. Rev. C **104**, (2021)
631. J. Bradt et al., Commissioning of the active-target time projection chamber. Nucl. Instrum. Meth. A **875**, 65–79 (2017)
632. A.H. Wuosmaa et al., $^{15}\mathbf{C}(d, p)^{16}\mathbf{C}$ reaction and exotic behavior in $^{16}\mathbf{C}$. Phys. Rev. Lett **105**(13250), 1 (2010)
633. B.P. Kay et al., Single-neutron energies outside ^{136}Xe. Phys. Rev. C **84**, 024325 (2011)
634. T.L. Tang et al., First exploration of neutron shell structure below lead and beyond $n = 126$. Phys. Rev. Lett. **124**, 062502 (2020)

635. S. Bedoor et al., Structure of ^{14} C and ^{14} B from the ^{14,15} C (d, ^{3} He)^{13,14} B reactions. Phys. Rev. C **93**, 044323 (2016)
636. D.G. McNeel et al., Configuration mixing in ^{28} Mg and the ^{26} Mg (t, p)^{28} Mg reaction. Phys. Rev. C **103**, 064320 (2021)
637. J. Chen et al., Probing the quadrupole transition strength of ^{15} C via deuteron inelastic scattering. Phys. Rev. C **106**, 064312 (2022)
638. C. Bontoiu, I. Martel, J. Resta-López, V. Rodin, C.P. Welsch, Conceptual design of a novel and compact superconducting recoil separator for radioactive isotopes. Nuclear Instrum. Methods Phys. Res. Sect. A Accel. Spectrom. Detect. Assoc. Equip. **969**, 164048 (2020). https://doi.org/10.1016/j.nima.2020.164048
639. I. Martel et al., An innovative superconducting recoil separator for HIE-ISOLDE. Nuclear Instrum. Methods Phys. Res. Sect. B Beam Interact. Mater. Atoms **541**, 176–179 (2023). https://doi.org/10.1016/j.nimb.2023.05.052
640. Pulse-shape analysis of clyc for thermal neutrons, Fast neutrons, and gamma-rays. Nuclear Instrum. Methods Phys. Res. Sect. A Accel. Spectrom. Detect. Assoc. Equip. **714**, 121–127 (2013). https://doi.org/10.1016/j.nima.2013.02.043
641. A. Giaz, N. Blasi, C. Boiano, S. Brambilla, F. Camera, C. Cattadori, S. Ceruti, F. Gramegna, T. Marchi, I. Mattei, A. Mentana, B. Million, L. Pellegri, M. Rebai, S. Riboldi, F. Salamida, M. Tardocchi, Fast neutron measurements with 7Li and 6Li enriched CLYC scintillators. Nuclear Instrum. Methods Phys. Res. Sect. A Accel. Spectrom. Detect. Assoc. Equip. **825**, 51–61 (2016). https://doi.org/10.1016/j.nima.2016.03.090
642. A. Gottardo, G. Andreetta, R. Lombardi, The CLYC-7 scintillator as a fast neutron spectrometer: pulse-shape discrimination for different neutron-induced reaction channels. Nuclear Instrum. Methods Phys. Res. Sect. A Accel. Spectrom. Detect. Assoc. Equip. **1041**, 167332 (2022). https://doi.org/10.1016/j.nima.2022.167332
643. D. Testov et al., The 3He long-counter TETRA at the ALTO ISOL facility. Nuclear Instrum. Methods Phys. Res. Sect. A Accel. Spectrom. Detect. Assoc. Equip. **815**, 96–103 (2016). https://doi.org/10.1016/j.nima.2015.11.150
644. T. Martínez et al., Monster: a ToF spectrometer for β-delayed neutron spectroscopy. Nuclear Data Sheets **120**, 78–80 (2014). https://doi.org/10.1016/j.nds.2014.07.011
645. W.A. Peters et al., Performance of the versatile array of neutron detectors at low energy (VANDLE). Nuclear Instrum. Methods Phys. Res. Sect. A Accel. Spectrom. Detect. Assoc. Equip. **836**, 122–133 (2016). https://doi.org/10.1016/j.nima.2016.08.054
646. S. Neupane et al., Neutron detection efficiency of the neutron detector with Xn tracking (NEXT). Nuclear Instrum. Methods Phys. Res. Sect. A Accel. Spectrom. Detect. Assoc. Equip. **1020**, 165881 (2021). https://doi.org/10.1016/j.nima.2021.165881
647. C. Delafosse et al., First trap-assisted decay spectroscopy of the ^{81}Ge ground state. Eur. Phys. J. A **58**(3), 51 (2022). https://doi.org/10.1140/epja/s10050-022-00698-7
648. J. Esposito et al., LARAMED: a laboratory for radioisotopes of medical interest. Molecules (2019). https://doi.org/10.3390/molecules24010020
649. G. Pupillo et al., The Laramed project at LNL: 67Cu and 47Sc production for theranostic applications. AIP Conference Proceedings **2295**(1), 020001 (2020) https://doi.org/10.1063/5.0032898https://pubs.aip.org/aip/acp/article-pdf/doi/10.1063/5.0032898/13551685/020001_1_online.pdf
650. F. Borgna et al., Early evaluation of copper radioisotope production at ISOLPHARM. Molecules (2018). https://doi.org/10.3390/molecules23102437
651. PRISMAP website: https://www.prismap.eu/
652. F. Cappuzzello et al., Signatures of the giant pairing vibration in the 14C and 15C atomic nuclei. Nat. Commun. (2015). https://doi.org/10.1038/ncomms7743
653. D. Pereira et al., Nuclear rainbow in the ^{16} O +^{27} Al system: the role of couplings at energies far above the barrier. Phys. Lett. B **710**(3), 426–429 (2012). https://doi.org/10.1016/j.physletb.2012.03.032
654. F. Cappuzzello, D. Carbone, M. Cavallaro, Measuring the ions momentum vector with a large acceptance magnetic spectrometer. Nuclear Instrum. Methods Phys. Res. Sect. A Accel. Spectrom. Detect. Assoc. Equip. **638**(1), 74–82 (2011). https://doi.org/10.1016/j.nima.2011.02.045
655. F. Cappuzzello et al., The NUMEN project: an update of the facility toward the future experimental campaigns. Front. Astron. Space Sci. **8**, 668587 (2021). https://doi.org/10.3389/fspas.2021.668587
656. P. Finocchiaro et al., The NUMEN heavy ion multidetector for a complementary approach to the neutrinoless double beta decay. Universe **6**, 129 (2020). https://doi.org/10.3390/universe6090129
657. C. Grupen, B.A. Shwartz, H. Spieler, S. Eidelman, T. Stroh, *Particle Detectors*, vol. 10 (Cambridge University Press, Cambridge, 2008)
658. I. Ciraldo et al., Characterization of a gas detector prototype based on Thick-GEM for the MAGNEX focal plane detector. Nucl. Instrum. Meth. A **1048**, 167893 (2022)
659. D. Torresi et al., An upgraded focal plane detector for the MAGNEX spectrometer. Nucl. Inst. Meth. A **989**, 164918 (2021)
660. F. Cappuzzello, M. Cavallaro, A. Cunsolo, A. Foti, D. Carbone, S.E.A. Orrigo, M.R.D. Rodrigues, A particle identification technique for large acceptance spectrometers. Nuclear Instrum. Methods Phys. Res. Sect. A Accel. Spectrom. Detect. Assoc. Equip. **621**(1), 419–423 (2010). https://doi.org/10.1016/j.nima.2010.05.027
661. A. Pagano, Studies of nuclear reactions and time scale with the 4π detector CHIMERA. Nuclear Phys. News **22**(1), 28 (2012)
662. S. Pirrone et al., Isospin influence on fragments production in ^{78}Kr + ^{40}Ca and ^{86}Kr + ^{48}Ca collisions at 10 MeV/nucleon. Eur. Phys. J. A **55**(2), 22 (2019). https://doi.org/10.1140/epja/i2019-12695-4
663. B. Gnoffo, S. Pirrone, G. Politi et al., Isospin influence on the thermal characteristics in the reactions ^{78,86}Kr + ^{40,48}Ca at 10 AMeV. Il Nuovo Cimento C (2022). https://doi.org/10.1393/ncc/i2022-22052-5
664. E.V. Pagano et al., Status and perspective of FARCOS: a new correlator array for nuclear reaction studies. EPJ Web Conf. **117**, 10008 (2016). https://doi.org/10.1051/epjconf/201611710008
665. G. Baiocco et al., α-clustering effects in dissipative ^{12}C+^{12}C reactions at 95 MeV. Phys. Rev. C **87**, 054614 (2013). https://doi.org/10.1103/PhysRevC.87.054614
666. A. Camaiani et al., Experimental study of precisely selected evaporation chains in the decay of excited ^{25} Mg . Phys. Rev. C **97**, 044607 (2018). https://doi.org/10.1103/PhysRevC.97.044607
667. L. Morelli et al., Non-statistical decay and α-correlations in the 12C+ 12C fusion–evaporation reaction at 95 MeV. J. Phys. G Nuclear Particle Phys. **41**(7), 075108 (2014). https://doi.org/10.1088/0954-3899/41/7/075108
668. S. Bailey et al., Extracting the spectral signature of α clustering in ^{44,48,52} Ti using a continuous wavelet transform. Phys. Rev. C **100**, 051302 (2019). https://doi.org/10.1103/PhysRevC.100.051302
669. B. Borderie et al., Phys. Lett. B **755**, 475 (2016)
670. B. Borderie et al., Symmetry **13**, 1562 (2021)
671. S.A. Gillespie et al., Proton decay spectroscopy of ^{28} S and ^{30} Cl . Phys. Rev. C **105**, 044321 (2022). https://doi.org/10.1103/PhysRevC.105.044321
672. J. Bishop et al., Experimental investigation of α condensation in light nuclei. Phys. Rev. C **100**, 034320 (2019). https://doi.org/10.1103/PhysRevC.100.034320
673. D.T. Tran et al., Charge-changing cross-section measurements of $^{12-16}$ C at around 45 AMeV and development of a Glauber model for incident energies 10A–2100A MeV. Phys. Rev. C **94**, 064604 (2016). https://doi.org/10.1103/PhysRevC.94.064604

674. M. Tanaka et al., Charge-changing cross sections for $^{42-51}$ Ca and effect of charged-particle evaporation induced by neutron-removal reactions. Phys. Rev. C **106**, 014617 (2022). https://doi.org/10.1103/PhysRevC.106.014617
675. D. Santonocito et al., Onset of quenching of the giant dipole resonance at high excitation energies. Phys. Rev. C **90**, 054603 (2014). https://doi.org/10.1103/PhysRevC.90.054603
676. S. Valdré et al., The FAZIA setup: a review on the electronics and the mechanical mounting. Nuclear Instrum. Methods Phys. Res. Sect. A Accel. Spectrom. Detect. Assoc. Equip. **930**, 27–36 (2019). https://doi.org/10.1016/j.nima.2019.03.082
677. P. Figuera, E.A. Maugeri, R. Buompane, L. Cosentino, A. Di Leva, A. Di Pietro, M. Fisichella, L. Gialanella, S. Heinitz, N. Kivel, M. Lattuada, C. Marchetta, S. Marletta, D. Mascali, A. Massara, D. Schumann, F. Tudisco, Development of an intense ^{10} Be radioactive beam in 'off-line mode' at the Catania tandem accelerator. Nuclear Instrum. Methods Phys. Res. Sect. A Accel. Spectromet. Detect. Assoc. Equip. **972**, 164120 (2020). https://doi.org/10.1016/j.nima.2020.164120
678. C.E. Rolfs, W.S. Rodney, *Cauldrons in the Cosmos: Nuclear Astrophysics* (University of Chicago press, Chicago, 1988)
679. C. Spitaleri, M. La Cognata, L. Lamia, R.G. Pizzone, A. Tumino, Astrophysics studies with the Trojan Horse Method. Eur. Phys. J. A **55**(9), 161 (2019). https://doi.org/10.1140/epja/i2019-12833-0
680. A. Tumino, C.A. Bertulani, M. La Cognata, L. Lamia, R.G. Pizzone, S. Romano, S. Typel, The Trojan horse method: a nuclear physics tool for astrophysics. Ann. Rev. Nuclear Particle Sci. **71**, 345–376 (2021). https://doi.org/10.1146/annurev-nucl-102419-033642
681. M. La Cognata, S. Palmerini, P. Adsley, F. Hammache, A. Di Pietro, P. Figuera, R. Alba, S. Cherubini, F. Dell'Agli, G.L. Guardo, M. Gulino, L. Lamia, D. Lattuada, C. Maiolino, A. Oliva, R.G. Pizzone, P.M. Prajapati, S. Romano, D. Santonocito, R. Spartá, M.L. Sergi, A. Tumino, Exploring the astrophysical energy range of the ^{27} Al (p , α)2^{4} Mg reaction: a new recommended reaction rate. Phys. Lett. B **826**, 136917 (2022). https://doi.org/10.1016/j.physletb.2022.136917
682. M. La Cognata, S. Palmerini, P. Adsley, F. Hammache, A. Di Pietro, P. Figuera, F. Dell'Agli, R. Alba, S. Cherubini, G.L. Guardo, M. Gulino, L. Lamia, D. Lattuada, C. Maiolino, A. Oliva, R.G. Pizzone, P.M. Prajapati, G.G. Rapisarda, S. Romano, D. Santonocito, R. Spartá, M.L. Sergi, A. Tumino, P. Ventura, A new reaction rate of the ^{27} Al (p /α)^{24} Mg reaction based on indirect measurements at astrophysical energies and implications for ^{27} Al yields of intermediate-mass stars. Astrophys. J. **941**(1), 96 (2022). https://doi.org/10.3847/1538-4357/ac9c5e
683. Guardo, G.L., et al.: Direct measurement of the ^{19}F(p,α)^{16} O reaction at E$_{cm}$=0.6-0.8 MeV using the LHASA detector array. EPJ A **accepted for publication** (2023)
684. M. La Cognata et al., Proposal approved by TRUMF (2020)
685. G.L. Guardo, D. Balabanski, S. Chesneyskaya, M. La Cognata, D. Lattuada, C. Matei, T. Petruse, R.G. Pizzone, G.G. Rapisarda, S. Romano, C. Spitaleri, A. Tumino, Y. Xu, Nuclear astrophysics at ELI-NP: Preliminary experiments with ELISSA detector, in *Nuclei in the Cosmos XV*. ed. by A. Formicola, M. Junker, L. Gialanella, G. Imbriani (Springer, Cham, 2019), pp.219–223
686. Micron Semiconductors Ltd Catalogue. http://www.micronsemiconductor.co.uk/wp-content/uploads/2024/03/2024-MSL-Catalogue.pdf
687. D. Watson et al., Identification of strontium in the merger of two neutron stars. Nature (2019). https://doi.org/10.1038/s41586-019-1676-3
688. M.R. Mumpower, R. Surman, G.C. McLaughlin, A. Aprahamian, The impact of individual nuclear properties on r-process nucleosynthesis. Prog. Particle Nuclear Phys. **86**, 86–126 (2016). https://doi.org/10.1016/j.ppnp.2015.09.001
689. M. La Cognata et al., LNS activity report (2019)
690. A. Del Zoppo, P. Figuera, A. Musumarra, N. Colonna, R. Alba, C. Bonomo, S. Cherubini, L. Cosentino, A. Di Pietro, M. Gulino, M. La Cognata, L. Lamia, M.G. Pellegriti, R.G. Pizzone, C. Rolfs, S. Romano, C. Spitaleri, S. Tudisco, A. Tumino, 4π neutron detection with low-intensity radioactive beams. Nuclear Instrum. Methods Phys. Res. Sect. A Accel. Spectrom. Detect. Assoc. Equip. **581**(3), 783–790 (2007). https://doi.org/10.1016/j.nima.2007.08.069
691. L.M.S. Margato, A. Morozov, A. Blanco, P. Fonte, F.A.F. Fraga, B. Guerard, R. Hall-Wilton, C. Höglund, A. Mangiarotti, L. Robinson, S. Schmidt, K. Zeitelhack, Boron-10 lined RPCS for sub-millimeter resolution thermal neutron detectors: Feasibility study in a thermal neutron beam. J. Instrum. **14**(01), 01017 (2019). https://doi.org/10.1088/1748-0221/14/01/P01017
692. D. Mascali et al., A Novel Approach to β-Decay: PANDORA, a New Experimental Setup for Future In-Plasma Measurements. Universe **80**, 8 (2022)
693. M. Busso et al., Production of solar abundances for nuclei beyond Sr: The s- and r-process perspectives. Front. Astron. Space Sci **9**, 956633 (2022)
694. Pandora technical design report: https://pandora.infn.it/public/pandora-tdr
695. G. Mauro et al., An Innovative Superconducting Magnetic Trap for Probing β-decay in Plasmas. Front. Phys. **10**, 931953 (2022).
696. E. Naselli et al., Multidiagnostics setups for magnetoplasmas devoted to astrophysics and nuclear astrophysics research in compact traps. JINST **14**, C10008 (2019)
697. E. Naselli et al., Design study of a HPGe detector array for β-decay investigation in laboratory ECR plasmas. Front. Phys. **10**, 935728 (2022)
698. A. Goasduff et al., A high resolution γ-ray array for the pandora plasma trap. Front. Phys. **10**, 936081 (2022)
699. E. Naselli et al., The first measurement of plasma density by means of an interfero-polarimetric setup in a compact ECR-plasma trap, JINST **13**, C12020 (2018)
700. G. Torrisi et al., Mm-wave polarimeter and profilometry design study for retrieving plasma density in the PANDORA experiment. Front. Astron. Space Sci. **9**, 949920 (2022)
701. L. Di Donato et al., A Finite-Difference Approach for Plasma Microwave Imaging Profilometry. J. Imaging **5**(8), 70 (2019)
702. D. Mascali et al., Preliminary evaluation of inverse scattering-based plasma-profilometry application to fusion plasmas. JINST **17**, C06006 (2022)
703. S. Biri et al., Innovative experimental setup for X-ray imaging to study energetic magnetized plasmas. JINST **16**, P03003 (2021)
704. E. Naselli et al., Innovative Analytical Method for X-ray Imaging and Space-Resolved Spectroscopy of ECR Plasmas. Condens. Matter **7**(1), 5 (2021)
705. E. Naselli et al., Quantitative analysis of an ECR Ar plasma structure by X-ray spectroscopy at high spatial resolution. JINST **17**, C01009 (2022)
706. D. Mascali et al., Experimental study of single- vs two-close-frequency heating impact on confinement and loss dynamics in ECR ion source plasmas by means of x-ray spectroscopy and imaging. Plasma Phys. Control. Fusion **64**, 035020 (2022)
707. B. Mishra et al., A novel numerical tool to study electron energy distribution functions of spatially anisotropic and non-homogeneous ECR plasmas. Phys. Plasmas **28**, 102509 (2021)
708. A. Galata et al., On the Numerical Determination of the Density and Energy Spatial Distributions relevant for in-Plasma β-Decay Emission Estimation. Front. Phys. **10**, 947194 (2022)
709. T. Sasaya et al., Multi-pinhole fluorescent x-ray computed tomography for molecular imaging. Sci. Rep. **7**, 5742 (2017)
710. D. Mascali et al., Microwave techniques for electron cyclotron resonance plasma diagnostics. Rev. Sci. Instrum. **93**, 033302 (2022)
711. G.Q. Zhao, Cyclotron maser emission from power-law electrons with strong pitch-angle anisotropy. Astrophys. J. **822**, 58 (2016)
712. U. Greife, Laboratory for underground nuclear astrophysics. Nuclear Instrum. Methods Phys. Res. Sect. A Accel. Spectrom. Detect. Assoc. Equip. **350**(1–2), 327–337 (1994). https://doi.org/10.1016/0168-9002(94)91182-7
713. L. WeiPing, Underground nuclear astrophysics experiment Juna in China. Proc. Int. Astronom. Union **15**(S350), 313–320 (2019). https://doi.org/10.1017/S1743921320000733

714. R.E. Tribble, C.A. Bertulani, M. Cognata, A.M. Mukhamedzhanov, C. Spitaleri, Indirect techniques in nuclear astrophysics: a review. Rep. Prog. Phys. **77**(10), 106901 (2014). https://doi.org/10.1088/0034-4885/77/10/106901
715. E.E. Salpeter, H.M. Horn, Nuclear reaction rates at high densities. Astrophys. J. (1969). https://doi.org/10.1086/149858
716. G.A. Mourou, T. Tajima, S. Bulanov, Optics in the relativistic regime. Rev. Mod. Phys. **78**(2), 309–371 (2006). https://doi.org/10.1103/RevModPhys.78.309
717. T. Tajima, Y. Kishimoto, M.C. Downer, Optical properties of cluster plasma. Phys. Plasmas **6**(10), 3759–3764 (1999). https://doi.org/10.1063/1.873638
718. T. Ditmire, J. Zweiback, V.P. Yanovsky, T.E. Cowan, G. Hays, K.B. Wharton, Nuclear fusion from explosions of femtosecond laser-heated deuterium clusters. Nature **398**(6727), 489–492 (1999). https://doi.org/10.1038/19037
719. K.W. Madison et al., Role of laser-pulse duration in the neutron yield of deuterium cluster targets. Phys. Rev. A **70**(5), 053201 (2004). https://doi.org/10.1103/PhysRevA.70.053201
720. W. Bang, Disassembly time of deuterium-cluster-fusion plasma irradiated by an intense laser pulse. Phys. Rev. E **92**(1), 013102 (2015). https://doi.org/10.1103/PhysRevE.92.013102
721. H.J. Quevedo, Neutron enhancement from laser interaction with a critical fluid. Phys. Lett. A **382**(2–3), 94–98 (2018). https://doi.org/10.1016/j.physleta.2017.11.002
722. F. Consoli, Laser produced electromagnetic pulses: generation, detection and mitigation. High Power Laser Sci. Eng. **8**, 22 (2020). https://doi.org/10.1017/hpl.2020.13
723. S. Tudisco, Sicilia-silicon carbide detectors for intense luminosity investigations and applications. Sensors **18**(7), 2289 (2018). https://doi.org/10.3390/s18072289
724. M. Roth et al., *Ion Acceleration: TNSA* (Springer, Heidelberg, 2013), pp.303–350